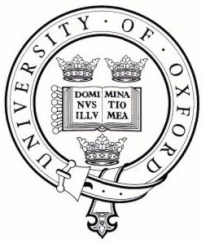
Surface Attachment Behaviour in *Rhodobacter sphaeroides*

Sarah Jane Chacko

A thesis submitted in partial fulfilment of

the requirements for the degree of

Doctor of Philosophy at the University of Oxford



Lincoln College

University of Oxford

Trinity Term 2013

Abstract

Surface Attachment Behaviour in *R. sphaeroides*

Sarah Jane Chacko

Lincoln College, University of Oxford

Submitted for the degree of Doctor of Philosophy, Trinity Term 2013

Motility and chemotaxis have been implicated in the process of biofilm formation in a wide range of species. Using a combination of microscopy and image analysis, genetics, microbiology and biochemistry, the initial approach of *Rhodobacter sphaeroides* cells to a solid surface has been characterised. Interestingly, these data suggest that for *R. sphaeroides* alterations in motility and swimming behaviour may result in differences in biofilm formation simply by changing the number of cells which reach the surface. This is in contrast to a few other well-studied species where the motility apparatus, the flagellum, has been shown to play an active role in surface sensing and the transition to biofilm growth.

Tracking swimming cells and measuring surface attachment revealed that changes in motility affect the ability of cells to attach to a surface, with non-motile cells attaching least and mutants with frequent stops attaching less than smooth swimming cells with few stops. Tracking attaching cells and classifying their method of attachment revealed that flagellar tethering is not essential for *R. sphaeroides* attachment.

Competition assays with fluorescently labelled strains showed that the initial imbalance between motile and non-motile cells remains as microcolonies develop over 48 hours,and the proportion of non-motile cells remains fairly constant. Development on a surface over 48 hours was similar for motile and non-motile strains, includeing aflagellate strains, once attached.

Using parameters calculated by tracking swimming cells to calculate the effective diffusion coefficient in a simple model of cell movement suggested that motion alone could explain the differences in attachment without assuming different cell properties. In particular, aflagellate strains might be hindered from surface attachment by their reduced motility alone. This is interesting since some other bacterial species use the flagellum as a surface sensor.

Declaration

The work in this thesis was performed in the department of Biochemistry at the University of Oxford from October 2009 to October 2013, under the supervision of Dr. G. Wadhams. All work in this thesis is my own unless otherwise stated and has not been submitted for a degree at this or any other university.

Acknowledgements

I would like to thank Dr. George Wadhams for supervising this project, and Professor Judy Armitage and everyone in the Armitage and Wadhams labs for help and support and for making the experience enjoyable, and the EPSRC and BBSRC for funding. I also thank Dr. Helen Packer for helpful discussions and the gift of strains, Dr. Anja Paulick and her colleagues at Marburg for showing me how to make and use flowcells and for the gift of flowcells for the inverted microscope, Gabriel Rosser, David Wilkinson and Jennifer de Beyer for their enthusiasm and thoroughness in writing, using, discussing and adapting the tracking analysis software, Wilson Kong Tang for help with the work on viscosity and Michael Shaw for help with electron microscopy.

Publications

Wilkinson, D. A., **Chacko, S. J.**, Venien-Bryan, C., Wadhams, G. H., and Armitage, J. P. (2011). Regulation of flagellum number by FliA and FlgM and role in biofilm formation by *Rhodobacter sphaeroides*. Journal of Bacteriology, 193(15), 4010-4014.

Abbreviations

A	Absorbance
Amp^R	ampicillin resistant
ANOVA	analysis of variance
CCW	counter clockwise
CFP	cyan fluorescent protein
CheY-P	phosphorylated CheY
CW	clockwise
cyclic-di-GMP	3',5'-Cyclic diguanylic acid
delta	deletion (of gene)
DIC	differential interference contrast
DMSO	Dimethyl sulfoxide
DNA	deoxyribonucleic acid
DTU	Technical University of Denmark
EDTA	ethylenediaminetetraacetic acid
EM	electron microscopy
EMS	Effective Mean Speed
EPS	Extracellular polymeric substances, which form the biofilm matrix
GC content	guanine-cytosine content, percentage of guanine or cytosine bases in the DNA
GFP	green fluorescent protein
HEPES	sodium N-2-hydroxyethylpiperazine-N'-2-ethanesulphonic acid
IBM	individual based modelling
IPTG	isopropyl β-D-thiogalactoside
Kan, Kn	kanamycin
Kn^R	kanamycin resistant
LB	Luria-Bertani
MAC	Mean absolute framewise angle change
MCP	methyl accepting chemotaxis protein
Min	minimum
NA	numerical aperture
Nal	nalidixic acid
Nal^R	nalidixic acid resistant
NEMS	Normalised effective mean speed

Abbreviations

OD	optical density
PAGE	polyacrilamide gel electrophoresis
PBS	phosphate buffered saline
PCR	polymerase chain reaction
PDMS	Polydimethylsiloxane
RNA	ribonucleic acid
TP	tryptone broth
TBE	tris-borate-EDTA buffer
TLP	transducer-like protein
UV	ultraviolet
YFP	yellow fluorescent protein
2D	two dimensional
3D	three dimensional
w.t.	wild type
v/v	percentage volume per volume
w/v	percentage weight by volume
η	viscosity
k_B	Boltzmann's constant

Contents

1 Introduction **1**

1.1 Why study bacterial biofilms? 1
1.2 Bacterial motility 4
1.2.1 Swimming through fluids, the flagella and flagellar motor 4
1.2.2 Movement on surfaces 6
1.2.3 Uses of motility apparatus in surface attachment . . . 10
1.3 Bacterial biofilm formation 12
1.4 Biofilm modelling 15
1.5 Attachment of individual cells 18
1.5.1 Attachment structures 18
1.6 Bacterial signalling and decision making 22
1.6.1 Two component signalling and phosphorelay systems . 22
1.6.2 Quorum sensing systems 25
1.6.3 Cyclic-di-GMP 26
1.7 Chemotaxis and motility 28
1.8 Motility, chemotaxis and biofilm formation 33
1.8.1 Chemotaxis and surface attachment 35
1.9 Brownian motion - passive movement in fluids 36
1.10 Surface behaviour and swimming at low Reynolds number . . 37
1.11 *Rhodobacter sphaeroides* 39
1.12 Chemotaxis in *R. sphaeroides* 41
1.12.1 The *R. sphaeroides* flagellum and flagellar motor . . . 45
1.13 *R. sphaeroides* biofilms 46
1.14 Aims of this study 47

2 Materials and Methods **49**
2.1 Plasmids and strains 49
2.2 Standard methods 52
2.2.1 Media and growth conditions 52
2.2.2 *R. sphaeroides* liquid cultures 52
2.2.3 *R. sphaeroides* agar plates 52
2.2.4 *E. coli* liquid cultures 52
2.2.5 *E. coli* agar plates 53
2.2.6 Preparation of *R. sphaeroides* chromosomal DNA from colonies 53
2.2.7 Preparation of *R. sphaeroides* chromosomal DNA from cultures 53
2.2.8 Preparation of *E. coli* plasmid DNA 53
2.2.9 Restriction Digest 54
2.2.10 Ligation 54
2.2.11 Agarose Gel Electrophoresis 54
2.2.12 Gel Extraction 54
2.2.13 Polymerase Chain Reaction (PCR) 55
2.2.14 Overlap extension PCR 55
2.2.15 DNA purification 57
2.2.16 Preparing *E. coli* competent cells (Rubidium Chloride protocol) 57
2.2.17 Transforming plasmids into *E. coli* competent cells . . 57
2.2.18 Transferring plasmids to *R. sphaeroides* from *E. coli* donor strain by conjugation 58
2.2.19 DNA insertion into the *R. sphaeroides* chromosome . . 58
2.2.20 DNA sequencing 61
2.2.21 Frozen stocks 61
2.2.22 Soft agar swim plates 61
2.2.23 Growth Curves 62
2.3 Staining Techniques 62
2.3.1 Crystal violet staining to measure attachment 62

2.3.2 Ryu staining to visualise flagella using brightfield, phase contrast or DIC microscopy . . . 63
2.3.3 Cy3 staining for *E. coli* and *R. sphaeroides* to visualise flagella using fluorescence . . . 63
2.3.4 Calcofluor plates to assess cellulose-like exopolysaccharide (EPS) production . . . 64
2.4 Microscopy techniques . . . 65
2.4.1 Microscopes and filters . . . 65
2.4.2 Cleaning slides and coverslips . . . 65
2.4.3 Agarose pad preparation . . . 66
2.4.4 Tunnel slide preparation . . . 66
2.4.5 Single channel flowcell preparation . . . 66
2.5 Methods adapted for this study . . . 69
2.5.1 Competitive assays in static conditions . . . 69
2.5.2 Three channel flowcells and bubbletraps (DTU) . . . 72
2.5.3 Free swimming assay for *R. sphaeroides* . . . 72
2.6 Characterising swimming patterns by analysing video data . . . 74
2.7 Free swimming analysis . . . 74
2.7.1 Identifying swimming cells . . . 74
2.7.2 Tracking paths of swimming cells . . . 76
2.7.3 Censoring tracks - detecting and removing spurious tracks . . . 79
2.7.4 Analysing tracks - velocity, angles, runs and stops . . . 80
2.7.5 MAC/NEMS plot . . . 82
2.7.6 Noise and smoothing . . . 83
2.8 Analysing Confocal Images . . . 87
2.8.1 Image Formats . . . 87
2.8.2 Image Channels . . . 88
2.8.3 Image Analysis . . . 89
2.9 Statistical Analysis . . . 91
2.9.1 Comparing two datasets . . . 91
2.9.2 Comparing several datasets . . . 92
2.10 Modelling . . . 92

3 Attachment of motility and chemotaxis mutants of *Rhodobacter sphaeroides* 93
3.1 Introduction . . . 93
3.2 Aims . . . 94
3.3 Strains used for motility experiments . . . 94
3.4 Attachment in motility mutants . . . 102
3.4.1 In static assays do *R. sphaeroides* motile strains attach more in 30 minutes than non-motile strains? . . . 102
3.4.2 Non motile strains - does having a flagellum help or hinder attachment in static conditions? . . . 105
3.4.3 In stationary phase cultures, motile strains no longer swim. Does this affect attachment? . . . 105
3.4.4 In many species non-motile cells attach more in moving than in static conditions, does shaking the culture change the relationship between motility and attachment? . . . 110
3.5 Attachment of chemotaxis mutants . . . 114
3.5.1 Strains used for chemotaxis experiments . . . 115
3.5.2 Comparison between attachment of photoheterotrophically grown chemotaxis mutants over 30 minutes . . . 116
3.5.3 Comparison between attachment of photoheterotrophically grown chemotaxis mutants over 6 hours . . . 121
3.6 Does changing swimming patterns by deleting single chemotaxis genes affect attachment? . . . 123
3.7 *R. sphaeroides* produces cellulose-like extracellular polysaccharide that binds calcofluor. Does the over or under-production of this EPS affect initial attachment? . . . 126
3.8 Discussion of initial attachment data . . . 131

4 *Rhodobacter sphaeroides* swimming at and away from surfaces 133
4.1 Introduction . . . 133
4.2 Aims . . . 136

4.2.1 Tracking swimming bacteria 136
4.3 Optimal speed cutoff to remove non-motile cells 138
4.3.1 The expected movement in one frame transition due to Brownian motion 138
4.3.2 Determining the movement due to Brownian motion by experiment 139
4.4 Angle speed data after removing non-motile cells 142
4.5 Calculating *R. sphaeroides* swimming speed 145
4.5.1 Published data on *R. sphaeroides* swimming speed . . 145
4.5.2 Estimating velocity during runs and stops using data on all transitions 145
4.5.3 Estimating velocity during runs using run/stop analysis 147
4.6 Changes of direction 150
4.6.1 Angle changes between transitions, at and away from a surface 150
4.6.2 The angle change between two runs is related to stop length for short stops, but becomes random for longer stops 152
4.6.3 Counts of bacteria at and away from the surface 156
4.6.4 Lengths of stops at and away from a surface 159
4.7 Swimming behaviour of chemotaxis mutant strains compared to *R. sphaeroides* WS8N 161
4.7.1 Swimming behaviour of strain *R. sphaeroides* JPA117 (Δ*che*Op1) 161
4.7.2 Swimming behaviour of the smooth swimming strains, *R. sphaeroides* JPA1353 and *R. sphaeroides* JPA1419 (Δ*che*Op3) 164
4.7.3 Swimming behaviour of the frequently stopping strain *R. sphaeroides* JPA403 (Δ*che*Op2) 169
4.7.4 Speeds of wild-type, smooth and stoppy strains 172
4.8 Measuring the proportion of tracks which correspond to stops 174
4.9 Discussion of free swimming results 177

5 Modelling attachment **179**
5.1 Introduction . . . 179
5.2 Aims . . . 181
5.3 Effect of motility on attachment . . . 181
5.4 Estimating the diffusion coefficients for the *R. sphaeroides* experimental strains . . . 184
5.5 Partial differential equation model based on motility only . . . 186
5.6 Diffusion and attachment in three dimensions . . . 190
5.7 Discussion of 'motility only' model and assumptions . . . 195

6 *Rhodobacter sphaeroides* attachment of single cells to a surface. **197**
6.1 Introduction . . . 197
6.2 Aims . . . 198
6.3 Initial attachment to a glass surface . . . 198
6.3.1 The attachment process in *R. sphaeroides* WS8N . . . 198
6.3.2 Recording the first exposure of cells to a surface . . . 201
6.3.3 Time the first cell attached . . . 203
6.3.4 Type of initial attachment . . . 203
6.4 Build up of attached cells over 6 hours in a static microcosm . 206
6.4.1 Discussion of single cell attachment experiments . . . 208

7 Viscosity **210**
7.1 Introduction . . . 210
7.2 Aims . . . 213
7.3 Ficoll_{400} . . . 213
7.4 How does *R. sphaeroides* react to Ficoll? . . . 214
7.5 How does swimming change with increased viscosity for *R. sphaeroides* ? . . . 215
7.6 Does increased viscosity have an effect on attachment? . . . 225
7.7 Discussion . . . 227

8 Fluorescence and Flowcells **228**
8.1 Introduction . . . 228

8.2 Aims . . . 228
8.3 Fluorescence using plasmids . . . 229
8.4 Expressing fluorescent protein from the chromosome . . . 229
8.4.1 Selection of promoter . . . 230
8.4.2 Selection of genomic region . . . 230
8.4.3 Phenotypic analysis of genomic reporter strains of *R. sphaeroides* WS8N . . . 231
8.5 Flowcells . . . 233
8.5.1 Flowcell Experiments . . . 233
8.6 Discussion . . . 236

9 *Rhodobacter sphaeroides* surface attachment. 237
9.1 Introduction . . . 237
9.2 Aims . . . 238
9.3 Do the initial differences in attachment for motile and non-motile strains persist in 48 hour microcolonies? . . . 238
9.3.1 The non-motile, aflagellate strain *R. sphaeroides* JPA467 contributed fewer cells to 48 hour microcolonies than *R. sphaeroides* WS8N. . . . 241
9.3.2 The non-motile, flagellate strain *R. sphaeroides* JPA452 contributed fewer cells to 48 hour microcolonies than *R. sphaeroides* WS8N. . . . 245
9.3.3 *R. sphaeroides* WS8N and the smooth swimming *R. sphaeroides* JPA1353 show similar levels of attachment in microcolonies after 48 hours. . . . 249
9.3.4 Discussion of 48 hour colony results . . . 253
9.4 Random fields of view with wild-type and non-motile strains . 254
9.4.1 *R. sphaeroides* WS8N/*R. sphaeroides* JPA1213 24 hours random choice of fields . . . 255
9.4.2 *R. sphaeroides* WS8N/*R. sphaeroides* JPA1213 48 hours random choice of fields . . . 259
9.5 Discussion of attachment assays for random fields of view. . . 263
9.6 Flowcell data . . . 263

9.6.1 Attachment in Flowcells . . . 264
9.6.2 The development of chained cells . . . 266
9.6.3 Do non motile cells form chained cells following surface attachment? . . . 270
9.6.4 Electron microscopy of cells attached to a glass surface after one hour . . . 271
9.7 Discussion . . . 272

10 Discussion **274**
10.1 Future Work . . . 277

Bibliography **279**

11 Appendix A - Media recipes and reagents **307**
11.0.1 LB Medium . . . 307
11.0.2 M22 Minimal Medium . . . 307
11.0.3 Succinate medium . . . 308
11.0.4 Concentrated Base . . . 308
11.0.5 Metals 44 Solution . . . 308
11.0.6 Growth Factors . . . 309
11.0.7 1M Phosphate Buffer . . . 309
11.0.8 HEPES Motility Buffer . . . 309

12 Appendix B - Primers **310**

13 Appendix C - Software **312**
13.1 CountCells MATLAB code . . . 312
13.2 3D cylinder PDE code . . . 329

Chapter 1

Introduction

1.1 Why study bacterial biofilms?

Bacteria were first seen as tiny moving creatures in 1676, by Antony van Leeuwenhoek, using one of the first microscopes.

> '... no greater pleasure has yet come to my eye than these spectacles of so many thousands of living creatures in a small drop of water moving among one another, each individual creature with its particular movement.'

(Antony van Leeuwenhoek, quoted in Porter (1976))

By the end of the 19th century Robert Koch had isolated the bacteria causing cholera, anthrax and tuberculosis. Harmless and essential bacteria were discovered as well, for example nitrogen fixing rhizobia in 1888 (Galloway et al., 2004). Bacteria were isolated using enrichment cultures and studied in the free-floating 'planktonic' state, and it was not until the late 20th century that bacterial communities attached to submerged surfaces, or at liquid-air interfaces, began to be studied in microbiology labs, though attached communities of bacteria encased in slime had been reported much earlier. Henrici (1933) states that

> 'It is quite evident that for the most part the water bacteria are not free floating organisms, but grow upon submerged surfaces.'

He also describes microcolonies growing on a glass slide submerged in a lake as follows

> 'The deposit of bacteria becomes apparent in a few days and increases progressively, eventually becoming so thick that individual cells may be distinguished with difficulty. That the cells are actually growing upon the glass is indicated by their occurrence in microcolonies of steadily increasing size. They are fairly firmly adherent to the glass, not removed by washing under a tap.'

It is now known that bacteria can live in two distinct ways, as separate cells and as biofilms, mixed colonies of cells surrounded by a matrix of biopolymers. These colonies may be formed on surfaces or at an air/fluid interface, or may be unattached aggregates of cells. The lifestyle of motile separate cells is called planktonic, colonies of cells attached to surfaces or at interfaces are known as biofilms. Unattached aggregates are not always classed with biofilms but there is some evidence that they share the same characteristics (Alhede et al., 2011).

Most, maybe all, bacteria can form biofilms and for many it may be the main lifestyle (Hall-Stoodley et al., 2004). Bacteria (and archaea) are essential for life, and are so numerous that in spite of their size they probably contain as much carbon as plants, and more nitrogen and phosphorus (Whitman et al., 1998).

The interactions of microbial communities forming biofilms in the gut affects the health of animals including humans, and bacterial biofilms in the mouth cause gum disease and tooth decay. Changes to microbial behaviour or the balance of communities could have serious consequences for the health of organisms or ecosystems. The rise of resistance to antibiotics and the unknown long term ecological effects of global warming and pollution make understanding the behaviour of bacteria and bacterial biofilms vitally important. Biofilms form protected reservoirs of infection in the human body, complicate

wound healing, and can contaminate hospital equipment and medical devices (Costerton et al., 1999; Hall-Stoodley et al., 2004). It has been claimed that 'biofilm disease kills more people than cancer' (Monroe, 2007) . Biofilms in and on living organisms such as sponges, coral and plants can be pathogenic or beneficial, the biofilm providing protection from predators and resistance to stress (Rosenberg and Ben-Haim, 2002; Danhorn and Fuqua, 2007; Webster and Taylor, 2012).

Biofilms may be useful in bioremediation, forming colonies of bacteria that can metabolise toxic substances (Singh et al., 2006). They are a major cause of biofouling, for example blocking pipes and contaminating drinking water (Hallam et al., 2001), corroding metals (Coetser and Cloete, 2005) or protecting metals from corrosion (Zuo, 2007), and contaminating food processing equipment (Zottola and Sasahara, 1994; Wong, 1998; Valderrama and Cutter, 2013).

New biofilms are initiated when bacteria attach to a surface. Understanding this process better could help encourage beneficial colonisers and discourage harmful ones in a huge range of situations.

Examples of 'bad' and 'good' biofilms are shown in Figs. 1.1 - a pathogen attached to a catheter and 1.2 - a beneficial bacterium recruited to the plant roots in response to infection.

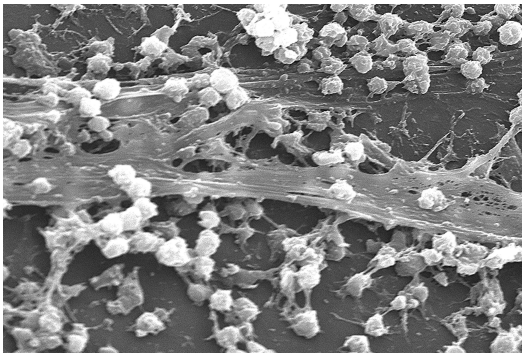


Figure 1.1: Scanning Electron Microscopy image of a *Staphylococcus aureus* biofilm growing on a catheter. Electron micrograph magnified 2363x, from Monroe (2007).

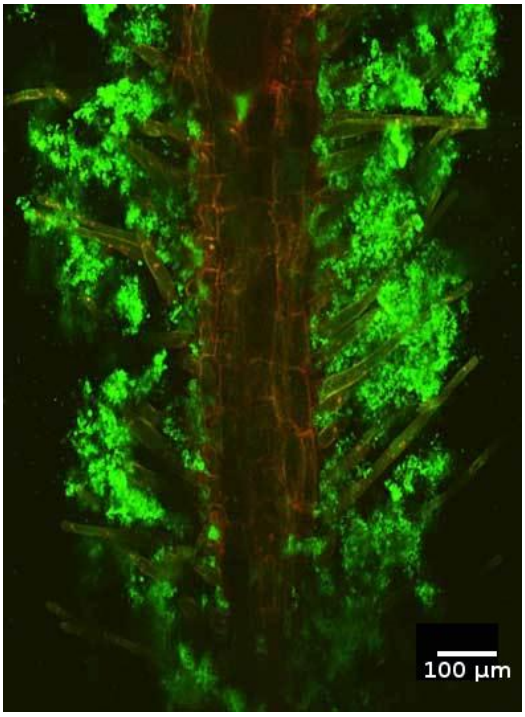


Figure 1.2: *Bacillus subtilis*, stained with the nucleic acid stain SYTO13 (Invitrogen), forming a beneficial biofilm on the roots of *Arabidopsis thaliana*. Confocal laser scanning micrograph by Thimmaraju Rudrappa (Rudrappa et al., 2008)

1.2 Bacterial motility

1.2.1 Swimming through fluids, the flagella and flagellar motor

Biofilm formation is affected by motility in many species of bacteria, discussed in Section 1.8, so an outline of the different types of bacterial motility is relevant here. The motor itself has been found to affect attachment to surfaces in some bacteria and it is thought that in some flagellated bacteria the flagellum and motor may act as a mechanosensor detecting a surface. This is discussed further in Section 1.2.3. Many bacteria swim through fluids using one or more flagella, long (several microns), thin (around 20nm) semi-rigid helical structures that are turned by a molecular motor, the bacteria flagellar

motor (Turner et al., 2000). This was first studied in *Escherichia coli* but is very similar in all flagellated swimming bacteria.

To create the flagella around 40 genes are expressed in a carefully controlled sequence (Chilcott and Hughes, 2000). There are three main sections of the flagellum, the basal body with the motor and switch complex, the hook which links the basal body to the filament, and the filament itself (Fig. 1.3). The flagellar motor is driven by the proton gradient across the inner membrane, protons flow through channels formed by the MotA/MotB stator complexes. The switch complex is in the C ring which is formed of FliG, FliM and FliN proteins, the switch complex is responsible for changing the direction of rotation. The flagellar motor is reviewed in Sowa and Berry (2008).

The flagellar filament is many times the length of the cell body and made up of 11 protofilaments each of which is a polymer of the flagellin protein FliC. The two ends of the FliC monomer are highly conserved, but the middle region varies in different species, and even in different strains of the same species (Tasteyre et al., 2000). The monomers are made in the cytoplasm, are exported through the hollow channel in the middle of the growing filament. They self assemble at the end of the filament furthest from the cell body. Each FliC monomer can polymerise in two different conformations, long and short. Each protofilament is either long or short depending on the conformation of the monomers. The shape of the flagellum depends on the state of the protofilaments, possible shapes are shown in Fig. 1.4.

Swimming speeds differ greatly between species, *E. coli* swims at a rate of 25–35 μm per second, *Bdellovibrio bacteriovorus* can swim at 160 μm per second (Jarrell and McBride, 2008). The patterns of swimming also vary between species, with different run and tumble lengths, reversals of direction, and characteristic turning angles (Taktikos et al., 2013).

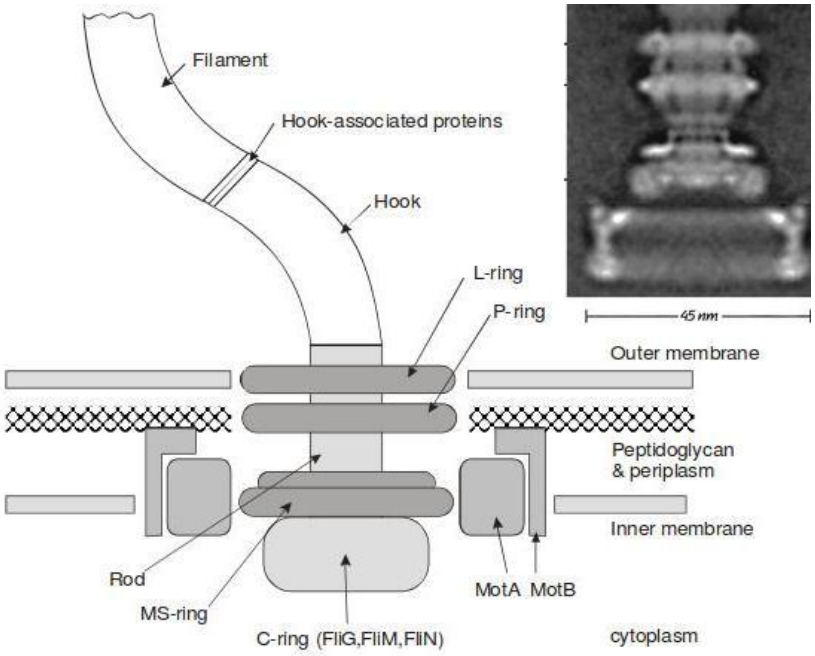


Figure 1.3: Diagram of the bacterial flagellum. The hook connects the basal body to the filament. The basal body consists of the C, MS, P and L rings, the rod, and the MotA and MotB stator unit proteins. The motor is driven by the flow of protons across the inner membrane through channels made by the MotA/MotB complex. The inset image shows an averaged image of the basal body from cryo-electron microscopy images. Image adapted from Porter (2002) and Berg (2003).

1.2.2 Movement on surfaces

Some species of bacteria move across surfaces using twitching motility, gliding motility or swarming motility (Fig. 1.5) (Jarrell and McBride, 2008; Kearns, 2010).

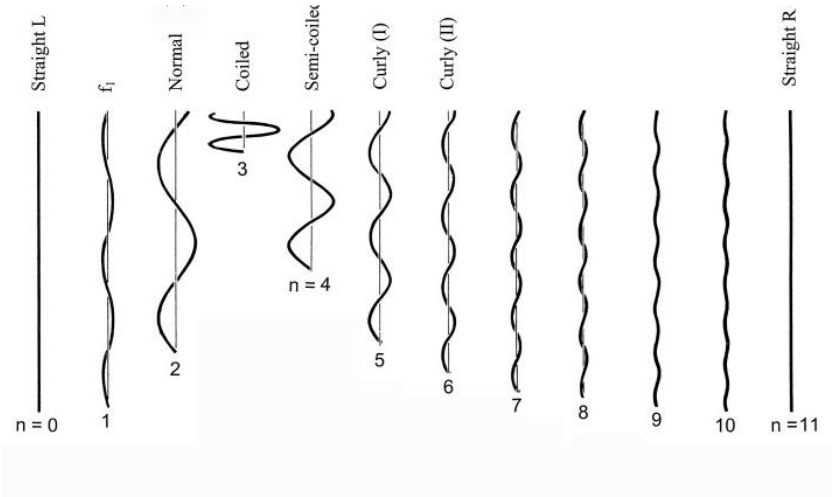


Figure 1.4: Possible shapes of the flagellar filament, which depend on the conformation (long or short forms) of FliC subunits in each of the 11 protofilaments. The shape of the flagellar filament of a cell can change, for example the *R. sphaeroides* filament is helical when swimming and coiled when stopped, and straight forms have been observed (Shah et al., 2000). n is the number of long protofilaments. The annotation above each filament shape is descriptive. Image adapted from Friedrich (2006).

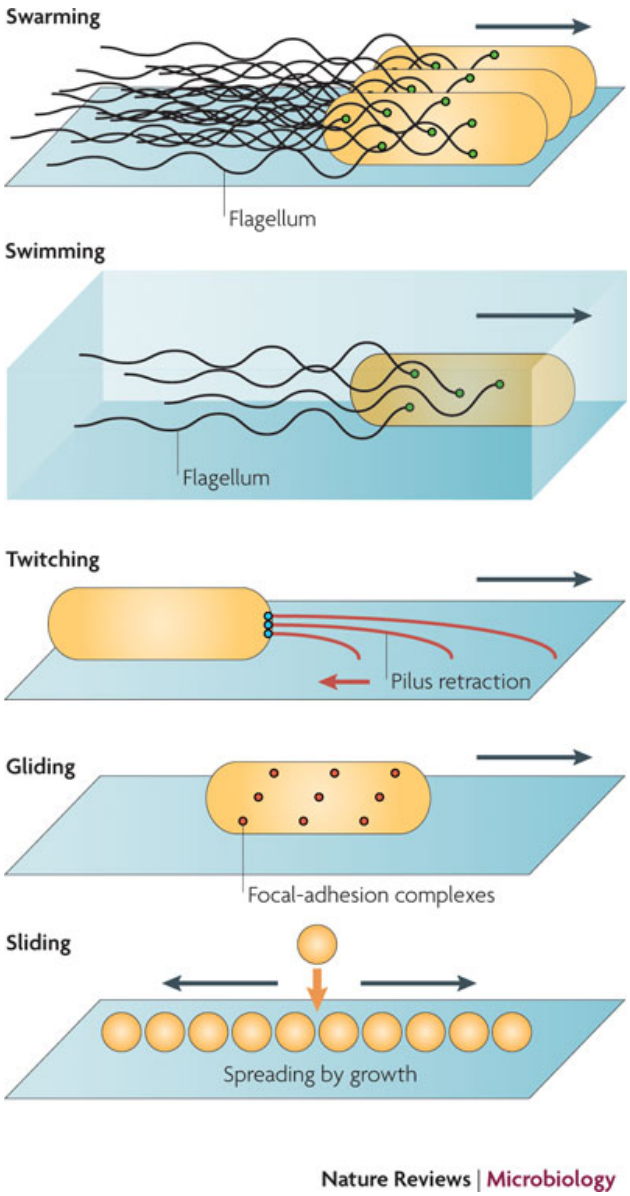


Figure 1.5: Diagram of the ways bacteria can move. Swarming over surfaces, swimming in fluid, twitching by extending and retracting pili, gliding and sliding. Image from Kearns (2010).

Swarming motility

Swarming motility uses flagella to move the cell over a surface (Kearns, 2010). Bacteria that swarm often change flagellar expression at a surface, changing from few polar flagella to many lateral flagella. They also secrete surfactants and move as a group. This change in flagellar expression implies that they detect and respond to the surface. *Proteus mirabilis* swarms with the same peretricious flagella as it swims with. *Vibrio parahaemolyticus* changes from swimming with sodium ion driven polar flagella to swarming with proton driven lateral flagella. *Rhodospirillum centenum* and *Aeromonas* spp. swim with a single polar flagellum and induce lateral flagella to swarm over surfaces (Kearns, 2010; Xu et al., 2012). *Pseudomonas aeruginosa* swims with one polar flagellum which it keeps during swarming, but it changes the stator units on the motor (Toutain et al., 2005). Swarming motility is inversely regulated with biofilm formation in *P. aeruginosa* (Caiazza et al., 2007).

Twitching motility

Bacteria that use twitching motility extend a type IV pilus that attaches to the surface at its tip and then retract the pilus, dragging the cell along (Fig. 1.5). This often leads to jerky movement, which has been directly observed (Skerker and Berg, 2001). Bacteria that use twitching motility are mainly β, γ and δ proteobacteria, some of the best characterised are *P. aeruginosa*, *Neisseria gonorrhoeae*, and *Myxococcus xanthus* (Mattick, 2002). In *P. aeruginosa*, twitching motility is controlled by a chemosensory system and is involved in biofilm formation, with cells moving over surfaces to join microcolonies. (Sun et al., 2000; Mattick, 2002; Whitchurch et al., 2004; Shrout et al., 2011). O'Toole and Kolter (1998) found that flagellar and twitching motility were both needed for biofilm formation in *P. aeruginosa*.

Gliding motility

Gliding motility covers several types of smooth movement across surfaces. The term has been used for smooth bacterial movement without a known mechanism and may include different types of movement. Recent work has suggested some mechanisms, for example production of slime (Ducret et al., 2012) and movement of cell surface adhesins. *Flavobacterium johnsoniae* has cell surface adhesins that move across the surface of the cell on helical tracks and are thought to move the cell along on surfaces. This happens whether or not there is a nearby external surface, since in bulk fluid latex spheres attached to the adhesins move around the cell surface, so may not depend on detecting the surface (Shrivastava et al., 2013). In *Flavobacterium psychrophilum* gliding motility was reduced in a mutant with increased biofilm formation (Alvarez et al., 2006).

Sliding

Some bacteria do not move actively on surfaces but spread by growing, so that cells are passively pushed apart, this movement is often facilitated by secreting surfactants (Jarrell and McBride, 2008).

1.2.3 Uses of motility apparatus in surface attachment

The motor and flagellum may have roles in biofilm formation apart from allowing motility. Flagella can attach to surfaces and the motor complex can be used for secretion (both FliC monomers and the anti-sigma factor FlgM are exported through the motor complex during flagellar synthesis).

Toutain et al. (2007) showed that in *P. aeruginosa*, mutations in the MotAB or MotCD stator units which did not affect motility affected biofilm formation. They suggest that the cause is misregulation of flagellar reversal rates and that this has worse consequences for biofilm formation than the inability to rotate the flagellum at all.

In *Vibrio cholerae* and *Bacillus subtilis* the flagellum is used as a mechanosensor and is involved in signalling and in EPS production (Kawagishi et al., 1996; Lauriano et al., 2004; Cairns et al., 2013).

Caulobacter crescentus produces a sticky holdfast which attaches a cell to a surface. The formation of the holdfast can be detected by a specific stain, and it has been shown that it is produced in response to increased load on the flagellar motor. *C. crescentus* has pili which attach to a surface and prevent the flagellum from rotating freely, triggering holdfast production, and holdfast production can be induced away from a surface by using high viscosity to increase flagellar load (Li et al., 2012).

Electron microscopy has shown tangled flagella in early *E. coli* microcolonies, which form a supportive framework and strengthen the colonies (Serra et al., 2013).

1.3 Bacterial biofilm formation

When bacteria attach to a surface they change their behaviour, so they must detect and respond to the surface in some way.

For many species attachment to surfaces has been shown to take place in two stages, initial transient attachment followed by either detachment or permanent attachment (Watnick and Kolter, 2000; Lemon et al., 2008). This may allow the bacterium to sample and reject unsuitable environments (Hinsa et al., 2003; Rodriguez-Navarro et al., 2007; Dellen et al., 2008). Cells attaching permanently produce polymers (EPS, or extracellular polymeric substances) which form an extracellular matrix, holding the cells together (Branda et al., 2005; Lopez et al., 2010; Flemming, 2011).

After attaching to a surface many bacteria first form small aggregates of attached cells called microcolonies, and later mature biofilm (Fig. 1.6,1.7). The mature biofilm in many species can have a complex structure, with 'towers' and 'channels' which allow nutrients to reach the cells, and wastes to leave (Branda et al., 2005; Karatan and Watnick, 2009). This complexity, as well as the fact that the pattern of gene expression in biofilm cells is different from that in planktonic cells of the same type (Schembri et al., 2003; Whiteley et al., 2001), has led to the suggestion that biofilms form a simple type of multicellularity, with bacterial cells differentiating to fill different roles (O'Toole et al., 2000). It is has also been suggested that as cell aggregates become larger, different microenvironments may lead to different behaviour without the need for a developmental program (Monds and O'Toole, 2009).

The details of behaviour after attachment vary. *P. aeruginosa* moves across surfaces to gather together into structures (Klausen et al., 2003), and has been shown to follow trails (Zhao et al., 2013). The form taken by *P. aeruginosa* biofilms depends on motility and on external conditions and may be flat or contain mushroom shaped microcolonies (Shrout et al., 2006). *C. crescentus* produces a holdfast which attaches to surfaces and which is synthesised in response to the additional load on the flagella when attached to

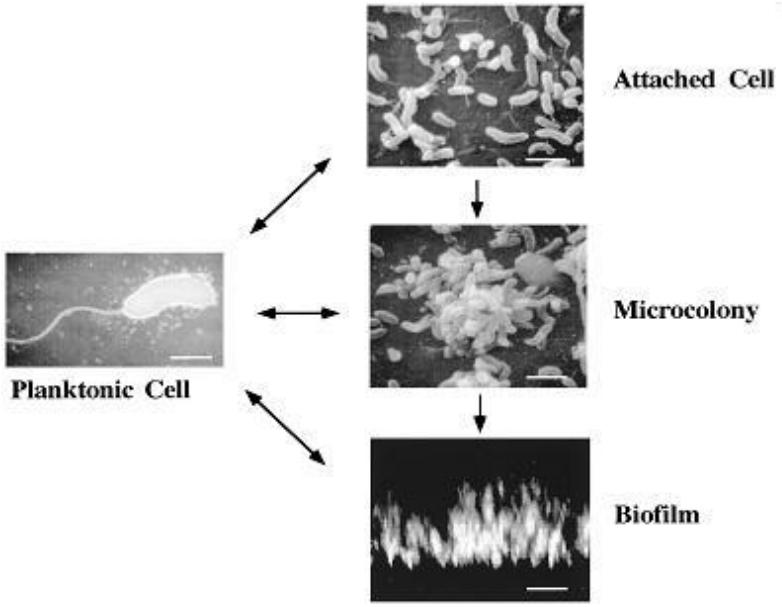


Figure 1.6: Biofilm development stages in *Vibrio cholerae*. Single attached cells, then microcolonies, then mature biofilm structures. For the planktonic bacterium bar = 1 μm, for the attached cells and microcolony bar = 2 μm, and the biofilm image is a section through a 20μm biofilm taken by confocal scanning laser microscopy. Image from Watnick and Kolter (2000).

the surface (Li et al., 2012). *C. crescentus* often attaches to surfaces in a single cell layer but can also form multicellular mushroom shaped structures (Entcheva-Dimitrov and Spormann, 2004). *E. coli* can form different structures, including clonal microcolonies and mushroom structures, sometimes depending on the surface properties of the individual cells (Reisner et al., 2003). *E. coli* can also form chained cells (Vejborg and Klemm, 2009).

Different surfaces affect attachment and surface coatings may attract or repel bacteria or increase the probability of attachment. This is an active area of research since biofilms on medical devices and food preparation equipment cause infections and contamination and are hard to remove (Gorth et al., 2012; Puckett et al., 2010). Some bacteria that form biofilms may not attach directly to abiotic surfaces like glass or sand but may attach to living cells or to preexisting biofilms. In some circumstances, such as bioremediation,

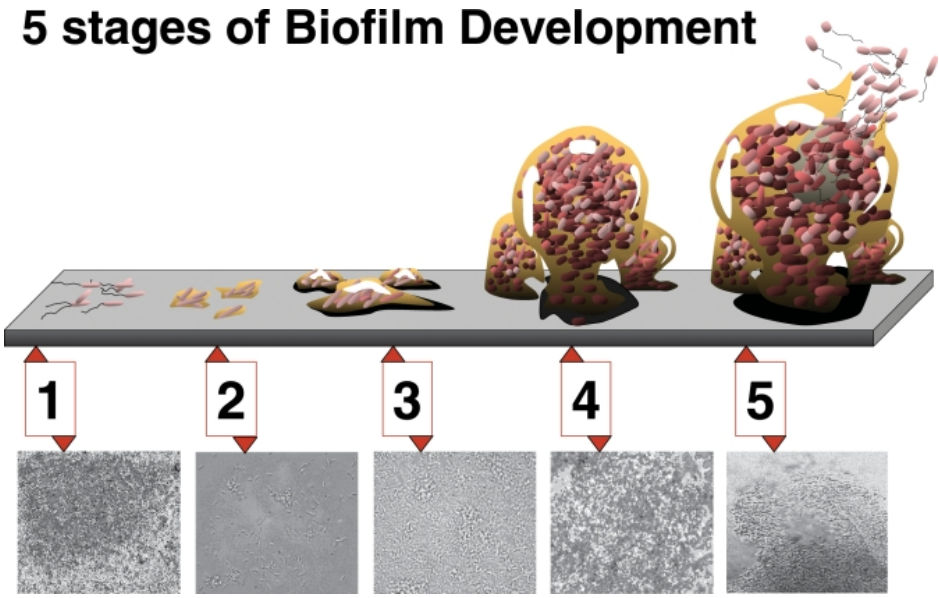


Figure 1.7: Biofilm development stages. Reversibly attached cells (1), then irreversibly attached cells (2), then microcolonies (3), then mature biofilm structures (4), followed by dispersal (5). Each stage in the schematic diagram also shows a micrograph of a *P. aeruginosa* biofilm at the same stage. Image from Monroe (2007).

biofilms are wanted, and surfaces that encourage attachment and growth of the right type of bacteria are needed.

Natural biofilms usually consist of multiple species. These species may co-operate, for example when one produces waste that is used by another, or they may compete, for example when they use the same nutrients. There may be cross species communication, as when quorum sensing signals indicate the presence of bacteria other than those of the same species. Two recent reviews summarise current knowledge of 'friendly' and 'unfriendly' interactions in biofilms (Elias and Banin, 2012; Rendueles and Ghigo, 2012). Multi species biofilms are important medically and environmentally, antibiotic resistance plasmids may transfer easily between species in a biofilm (Madsen et al., 2012), and waste treatment biofilms depend on a combination of species (Bastida et al., 2010; McGenity et al., 2012). Pure cultures may not reflect natural behaviour, since environmental biofilms usually contain a mixture of

species. However, Burmolle et al. (2007), looking at soil bacteria, deduced that behaviour in multispecies biofilms is related to the individual biofilm forming behaviour of each strain

Over the last 20 years of biofilm research, many pathways and regulators specific to certain species have been found, and it has also become clear that the environment has a major effect on biofilm formation and structure (Karatan and Watnick, 2009).

Biofilm formation could be a useful strategy to preserve cells in hostile conditions, or a strategy for keeping cells together in a favourable environment. For some species, the reports of increased biofilm formation in the presence of antibiotics (Bruchmann et al., 2013; Hoffman et al., 2005) suggests the former, while examples like *P. fluorescens* detaching from surfaces when phosphorus is limiting (Section 1.6.3) suggest the latter.

Recently, high throughput and bioinformatic studies have made new connections between genetics, metabolism, environment and biofilm, but the field remains complex, with large volumes of data but without a coherent synthesis (Pruss et al., 2010; Siggins, 2012).

1.4 Biofilm modelling

Mathematical modelling is useful for exploring the consequences of assumptions in systems that are too complex to predict otherwise. There are many different factors influencing the behaviour of a bacterial cell, including the physical and chemical environment, and bacterial sensors and intracellular signalling pathways. Understanding how these factors are integrated to produce a response may need mathematical or computational modelling to explore possible interactions and suggest consequences.

Some existing models for computational biofilm modelling are briefly described here. They follow the development of a biofilm after the initial attachment stage, and would require further development to include the earliest

stages. For that reason these frameworks were not used in this work, but they could be used to explore the consequences of attachment behaviour.

The growth of biofilms has been modelled mathematically since the 1970s, both for practical reasons, to assess likely contamination, antibiotic resistance, or potential for blocking pipes, and also to achieve greater understanding of processes such as detachment, nutrient starvation and competition or co-operation between species (Wimpenny and Colasanti, 1997; Gottenbos et al., 1999; Picioreanu et al., 2001; Pizarro et al., 2001; Kreft et al., 2001; van Loosdrecht et al., 2002; Chang et al., 2003; Hunt et al., 2003, 2004; Chambless et al., 2006).

These models are based on experimental data. They may use differential equations to model biofilm biomass growth as a continuous and deterministic process, or they may use individual based modelling (IBM) (Kreft et al., 2001) to treat cells as individuals, while still using deterministic rules, or they may allow some stochasticity in bacterial behaviour. Current models are often hybrid, with nutrients and wastes modelled as continuous fields, using reaction-diffusion equations, and bacteria as individuals.

In the earliest models (Wimpenny and Colasanti, 1997; Gottenbos et al., 1999; Picioreanu et al., 2001) the biofilm structure was the starting point of the model and the model looked at the consequences for nutrient transport, in later models the structure emerged as the biofilm developed, and could be compared to experimental data, but the initial arrangement of cells on the surface was either random or set at the start, and this could have important consequences for development (Kreft et al., 2001). Biofilm structures found in experimental work were shown to be able to develop simply from variations in nutrient availability (Nadell et al., 2009), an example is mushroom shaped colonies, which have been reported for many biofilms. They can be explained by small projections from a biofilm surface accessing more nutrients and growing faster, then using more nutrients and depriving cells immediately below them, leading to a faster growing top and slower growing stalk. A more complex model of the development of mushroom shaped structures in *P. aeruginosa* is given in Picioreanu et al. (2007).

There is an individual based modelling environment designed for biofilm studies, iDynomics, which allows metabolic properties to be set for mixtures of bacteria and calculates growth and death based on nutrient gradients (Kreft et al., 2001). Individual based modelling has been used to investigate plasmid spread in biofilms (Merkey et al., 2011), switching between aerobic and anaerobic growth, (Lardon et al., 2011), and the gut biota (Schluter and Foster, 2012) among many other things.

Most current biofilm software and mathematical models start from attached cells and do not include the attachment process.

The interaction of a bacterium with a surface is often studied using the Derjaguin Landau Verwey Overbeek (DLVO) theory, developed for colloids (Hermansson, 1999), which explains adhesion using forces at a surface, including attractive van der Waals forces and replusions due to elecrostatics (Fig. 1.8). DLVO theory predicts a repulsive barrier and a local energy minimum near surfaces, and suggests an explanation for transient attachment and a role for thin appendages such as pili and flagella in reaching the surface with less repulsion, and also for the polar initial attachment reported for many bacteria (Li et al., 2012). It treats bacteria as inert objects responding to physical forces.

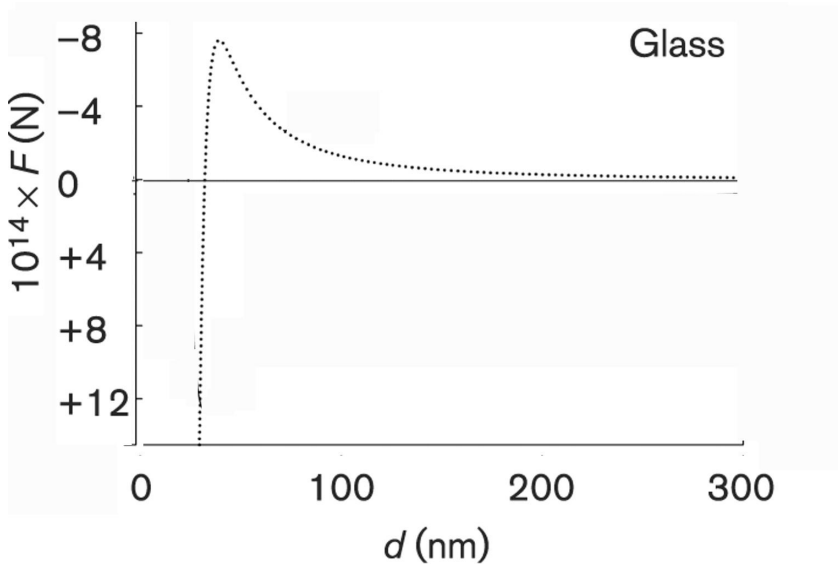


Figure 1.8: The approximate distances at which van der Waals and electrostatic forces operate between a surface and a bacterial cell. The force related to distance from a glass surface for *P. aeruginosa* KEI 1025, predicted using DLVO theory and surface properties (negative forces are attractive). Electrostatic forces may be repulsive or attractive, a bacterial cell surface is negatively charged overall, but a double layer is formed with positive ions around it so that it may be attracted even to a negatively charged surface. Specific interactions can be due to surface detail such as charged groups or hydrogen bonding and are only relevant a few nanometers from the surface. Image adapted from Boks et al. (2008).

1.5 Attachment of individual cells

Biofilms start with cells attaching to a surface. This may involve structures or adhesins on the cell surface.

1.5.1 Attachment structures

Flagella

Bacterial flagella sometimes stick to surfaces (Kamiya and Asakura, 1976; Darnton and Berg, 2007). This can lead to to the cell spinning around the

point of attachment as the motor continues to turn while the flagellum is fixed, a process called tethering. Tethering may be a precursor to attachment (Li et al., 2012), and in *P. aeruginosa* it has been seen as a precursor to detachment (Conrad et al., 2011).

Pili and fimbriae

Pili and fimbriae are thin protein structures extending from the cell surface, reviewed in Proft and Baker (2009). They are classified into several types, based on structure and assembly (Fig. 1.9). Type IV pili are needed for twitching motility (section 1.2.2). Conjugative pili pull cells together and allow DNA transfer (Fig. 1.10) (Clarke et al., 2008). Pili are virulence factors for many pathogens, they can have specific adhesins that allow them to bind to cell surface molecules (Proft and Baker, 2009).

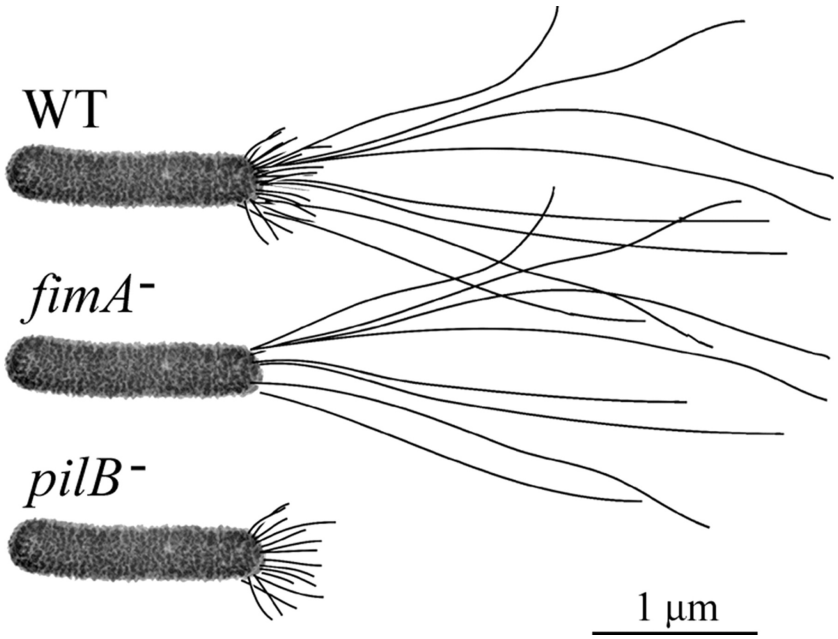


Figure 1.9: Drawing showing two types of pili in *Xylella fastidiosa*, type I pili (short) and type IV pili (long). The wild-type has both types of pili, the *fimA* deletion can only produce the longer type IV pili, and the *pilB* deletion can only produce the shorter type 1 pili. Image from Fuente et al. (2007).

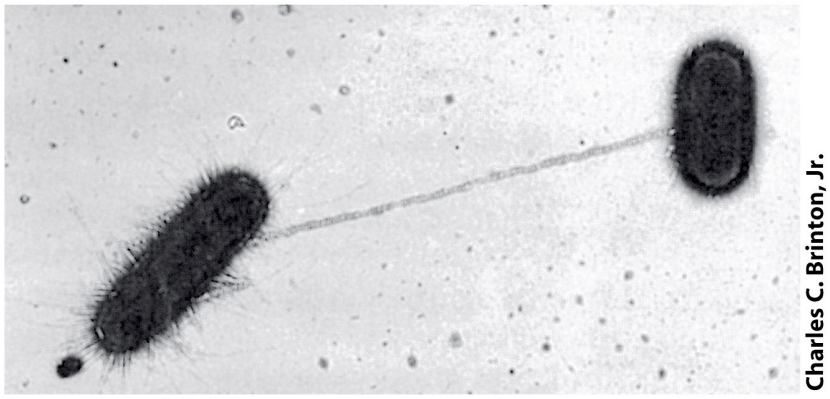


Figure 4-38 Brock Biology of Microorganisms 11/e
© 2006 Pearson Prentice Hall, Inc.

Figure 1.10: Electron micrograph showing two types of pili in *E. coli*, a surface layer of short pili and a conjugative pilus linking two cells. Image from Madigan and Martinko (2006).

In some cases pili cover the bacterium in a fuzzy layer which helps it to attach to a surface, as in Fig. 1.10. Some pili have adhesive structures at the end which are responsible for attachment (Lindberg et al., 1987). Pili affect biofilm formation in several species (Karatan and Watnick, 2009).

Adhesins

Many bacteria express protein adhesins which stick the cell to surfaces, for pathogenic bacteria these are often specific to structures on the cell type they attach to. Different adhesins may be used in different circumstances. Well studied adhesive proteins include *P. aeruginosa* LapA, which anchors a cell to a surface and can be cleaved to release the cell in response to phosphorus limitation (Newell et al., 2011), and the *E. coli* autotransporter Ag43, which is involved in cell aggregation and biofilm formation (van der Woude and Henderson, 2008). Recent reviews are Klemm and Schembri (2000); Kline et al. (2009).

Carbohydrate adhesins also exist, for example the *C. crescentus* holdfast. Li et al. (2012) showed how individual *C. crescentus* cells attach to a surface, stop rotating the flagellum and produce the holdfast adhesin. This is a rare

case where the mechanism of surface detection is known. They also show that many other α-proteobacteria attach to surfaces by their poles initially, suggesting a general use of polar adhesins.

Adhesins may be located in specific regions of the cell, Jones and Velegol (2006) used an optical trap to manipulate individual cells of *E. coli* and found that cells presented to a surface pole first either attached in seconds or not at all, and that while one or neither pole might be 'sticky', the two poles of the same cell were never both sticky.

1.6 Bacterial signalling and decision making

In bacterial signalling, inputs from the cell or the environment are detected and processed chemically, often using phosphorylation or methylation to alter the behaviour of other molecules (Stock et al., 1989, 1990). The output of such a signalling system may be changes in transcription leading to the production of new proteins, or changes in the behaviour of existing components of the cell. Several different types of signalling systems have been discovered in bacteria (Marijuan et al., 2010).

1.6.1 Two component signalling and phosphorelay systems

A very common bacterial signalling system is two component signalling (Stock et al., 2000; Galperin and Nikolskaya, 2007; Yamada and Shiro, 2008), where a histidine kinase sensor dimer autophosphorylates in response to a signal, and passes the phosphate to a conserved residue on a response regulator (Fig. 1.11). There may be tens to hundreds of two component systems in one bacterial cell, the majority of which are not characterised. How these systems avoid crosstalk between the many very similar proteins involved is an area of active research (Laub and Goulian, 2007).

Often the sensor kinase is bound to the membrane while the response regulator is free to diffuse through the cell. The response regulator may be a transcription factor (Wolanin et al., 2002). Some two component systems are involved in biofilm development. For example, in *Caulobacter crescentus* Purcell et al. (2007) found that a light activated two component system LovK/LovR increased biofilm formation in the presence of blue light.

In *Pseudomonas aeruginosa* PAO1 Petrova and Sauer (2009) found that the stages of biofilm formation are co-ordinated by a series of three two component systems, BfiSR (active during biofilm initiation), MifSR (active during microcolony formation) and BfmSR (active during biofilm maturation). If

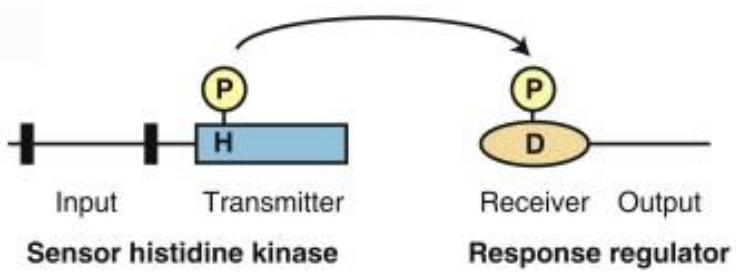


Figure 1.11: Canonical two-component signaling system. Black bars show transmembrane domains. Sites of phosphorylation are shown, on histidine (H) and aspartate (D) residues. Adapted from Schaller et al. (2011).

the genes for any one of these is deleted the biofilm stops developing at the stage where it would become active (Fig. 1.12) (Petrova and Sauer, 2009, 2010, 2011; Mikkelsen et al., 2011).

An extension of two component signalling is the phosphorelay system (Fig. 1.13), As well as a histidine kinase and a response regulator, a phosphorelay system passes phosphates along between histidine and aspartate residues on intermediate domains or proteins. The greater complexity gives more control and allows signals from different sources to be integrated (Hoch and Varughese, 2001).

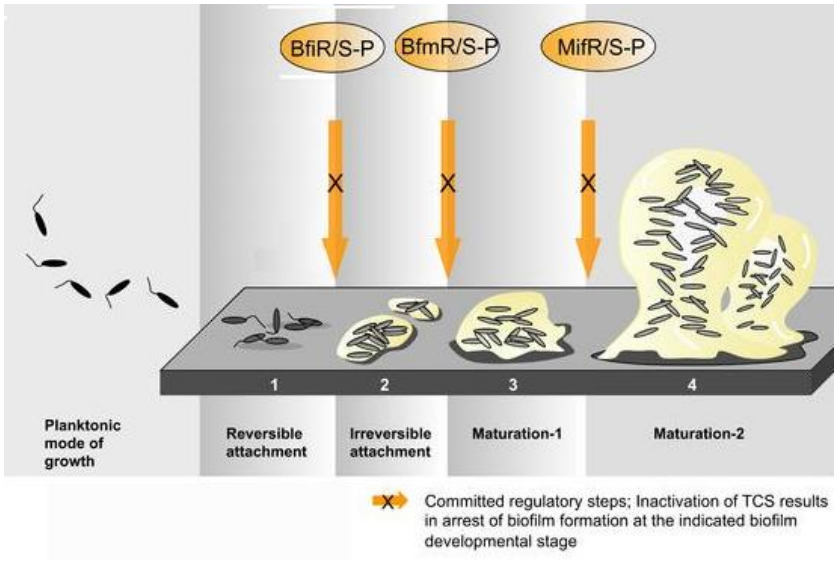


Figure 1.12: Sequentially active two component systems in *P. aeruginosa* PAO1 biofilm development. *P. aeruginosa* biofilms develop in stages, initial reversible attachment, irreversible attachment and microcolony formation with EPS production and development into mature structures. Two component systems phosphorylated at each stage, BfiSR (initiation), MifSR (microcolony formation) and BfmSR (maturation). Image adapted from Petrova and Sauer (2009)

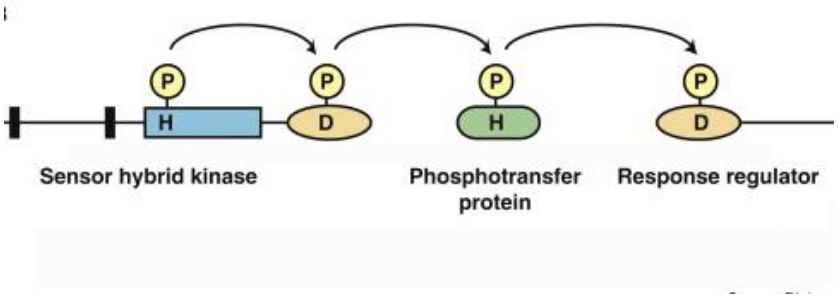


Figure 1.13: Canonical phosphorelay system. Black bars show transmembrane domains. Sites of phosphorylation are shown, on histidine (H) and aspartate (D) residues. Adapted from Schaller et al. (2011).

1.6.2 Quorum sensing systems

In quorum sensing systems bacteria both produce and detect a signal molecule. For gram negative bacteria this is a homoserine lactone, for gram-positive bacteria it is a peptide, the exact molecule depends on the species. When bacteria detect a high level of the quorum sensing signal molecule, they change behaviour. This allows bacteria to sense each other and co-ordinate their behaviour (Fuqua et al., 2001).

This system was first discovered in the light producing bacterium *Vibrio harveyi*, which only produce light when populations reach a high density and which use quorum sensing to detect the presence of others (Bassler et al., 1993). Quorum sensing is also used in virulence, so that toxins are not produced by isolated and vulnerable bacteria but only when enough are present to cause a serious infection (Miller and Bassler, 2001; Reading and Sperandio, 2006). It has been suggested that quorum sensing may not only be a method of assessing local populations but could measure local diffusion. If the quorum sensing signal is immediately swept away then other products such as siderophores or extracellular enzymes would not be worth producing (Redfield, 2002).

Bacteria can sometimes respond to quorum sensing signals from different strains of bacteria (Xavier and Bassler, 2005; Fernandez-Pinar et al., 2011). Because quorum sensing is related to numbers of bacteria in a region, it is likely to be relevant in the crowded conditions in biofilms. *P. aeruginosa* biofilms are known to use quorum sensing signals, and quorum sensing molecules have been suggested for environmental control of biofilms (Kim et al., 2012; Roy et al., 2013).

A marine α-proteobacterium roseobacterial sponge symbiont uses quorum sensing to activate motility when it becomes crowded, and thus to limit the size of biofilms (Zan et al., 2012).

1.6.3 Cyclic-di-GMP

Cyclic-di-GMP is an important signalling molecule in bacteria. It has been found to be involved in biofilm formation, virulence, motility and EPS production in several bacterial species. A recent review is Sondermann et al. (2012).

Many bacteria have several proteins with domains for creating and destroying cyclic-di-GMP, the GGDEF domain of diguanylate cyclases and the EAL or HD-GYP domain of phosphodiesterases. These are often combined with signalling and response domains such as PAS, BLUF and CACHE, indicating their use in signalling pathways. Some proteins have both GGDEF and EAL domains.

Knowledge of effectors responding to the cyclic-di-GMP levels has been slower to develop than of the cyclases and phosphodiesterases. A cyclic-di-GMP binding site, PilZ, has been identified and some of the GGDEF, EAL and HD-GYP domains are thought to be degenerate and to bind cyclic-di-GMP rather than creating or destroying it (Sondermann et al., 2012). There are also riboswitches that respond to cyclic-di-GMP levels (Sondermann et al., 2012). Cyclic di-GMP binding to the PilZ domain has been shown to cause conformational change. An example of a PilZ domain protein with a known function is YcgR in *Escherichia coli*, which slows flagellar rotation in response to the level of cyclic-di-GMP, by binding to motor proteins (Fig. 1.14) (Boehm et al., 2010).

In *Pseudomonas fluorescens* LapA is a large adhesin protein needed for surface attachment. An example of a effector protein with a non enzymatic EAL domain is *P. fluorescens* LapD, a membrane-associated GGDEF–EAL domain protein in which neither domain has enzymatic activity. When cyclic-di-GMP levels are high LapD binds cyclic-di-GMP at the EAL site, and represses LapG. When cyclic-di-GMP levels are low LapG is derepressed and cleaves the adhesin LapA, releasing attached cells from a surface. The levels of cyclic-di-GMP are regulated by proteins responding to external phosphate levels (Fig. 1.15) (Monds et al., 2007).

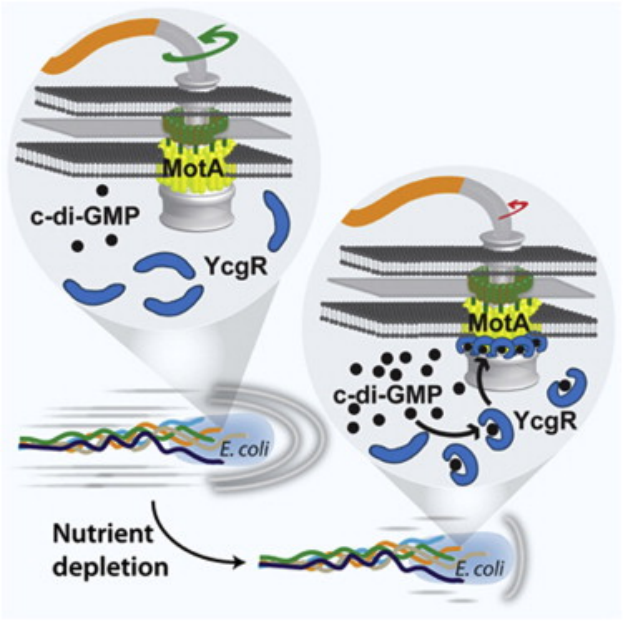


Figure 1.14: The action of YcgR in *E. coli* . When nutrient levels are low, cyclic-di-GMP levels increase and more YcgR binds cyclic-di-GMP. YcgR with cyclic-di-GMP bound attaches to the motor and slows flagellar rotation and thus swimming speed, saving energy. Image from Boehm et al. (2010).

Riboswitches are in the 5′ untranslated region of messenger RNAs. They are RNA sequences that bind different metabolites and repress or activate gene expression at the transcriptional or translational levels, often affecting synthesis or uptake of that metabolite. Recently several riboswitches that respond to cyclic-di-GMP have been identified (Sudarsan et al., 2008). One of these is on the Cd1 RNA in *V. cholerae*, in the 5′ untranslated region of the operon that encodes the proteins required to construct the flagellar apparatus, suggesting that changes in cyclic-di-GMP concentration regulate flagellar biosynthesis (Sudarsan et al., 2008).

Current knowledge of effectors responding to cyclic-di-GMP levels is reviewed in Ryan et al. (2012).

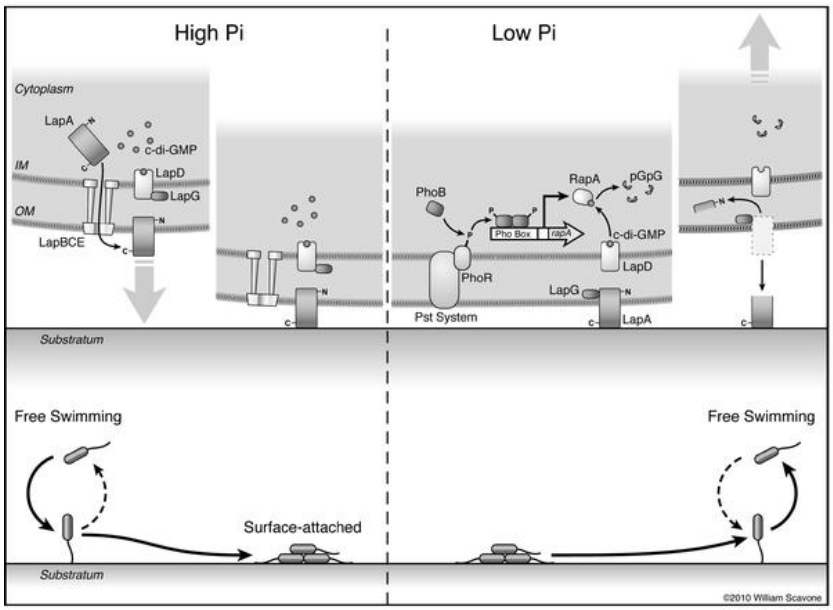


Figure 1.15: The *P. fluorescens* response to phosphate limitation uses cyclic-di-GMP signalling to regulate attachment to surfaces. Phosphate levels regulate cyclic-di-GMP levels which regulate LapG, which can cleave the adhesin LapA releasing the cell from the surface. This leads to attachment in high phosphate conditions and detachment in low phosphate conditions. Image from Newell et al. (2011).

1.7 Chemotaxis and motility

Swimming bacteria move through fluid by rotating one or more flagella. They can bias their swimming direction so that they accumulate near beneficial substances (attractants), and move further from toxic chemicals (repellents). They do this by sensing gradients of chemicals in the fluid. Most bacteria are considered too small to sense a gradient directly (Wadhams and Armitage, 2004), so they sense it over time as they swim, detecting whether concentrations are increasing or decreasing over 3 to 4 seconds. They can not steer in a particular direction, but they can change the frequency with which they change direction. This leads to a biased random walk, swimming for longer if conditions are improving, stopping and randomly reorienting more frequently if conditions are deteriorating (Fig. 1.16).

To do this they need to detect levels of chemicals and signal to the flagellar motor.

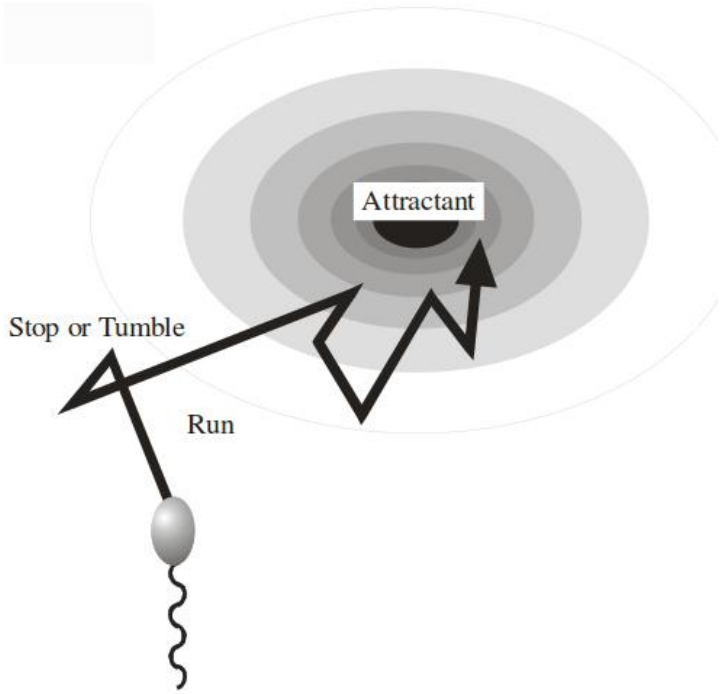


Figure 1.16: *E. coli* swims in a sequence of runs and tumbles. In a gradient of chemoattractants the runs are longer if the concentration is increasing, and shorter if it is decreasing. This motion, called a biased random walk, leads to overall movement towards highter concentrations. Image from Porter (2002).

The best understood and longest studied chemotaxis system is that in *E. coli*, shown in Fig. 1.17 and reviewed in detail in Sourjik and Wingreen (2012). *E. coli* has five to eight flagella and when the flagellar motors are all rotating counterclockwise the flagella form a bundle and the cell swims smoothly in a 'run'. When one or more motors rotate clockwise, the flagellar bundle separates and the cell stops swimming and 'tumbles', changing orientation so the the next run is in a new direction (Fig. 1.18).

E. coli has four types of Methyl Accepting Chemotaxis Proteins (MCPs) which are sensors. Each MCP detects several specific chemoeffectors, which

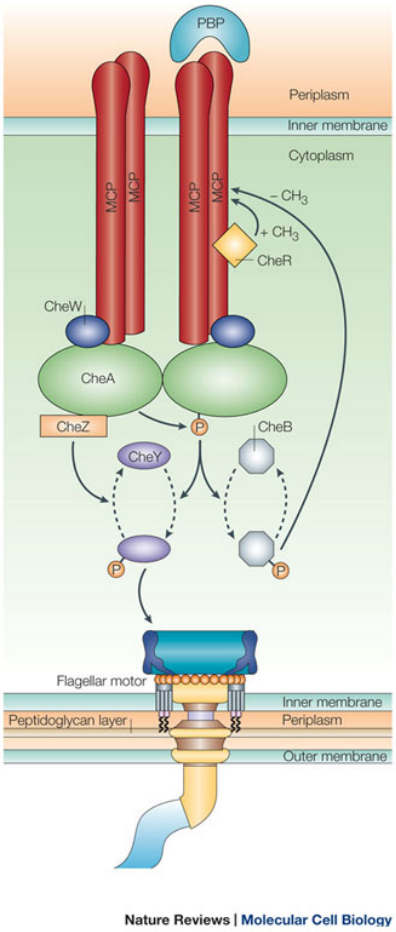


Figure 1.17: The chemotaxis system in *E. coli* . CheA, CheY and CheB form a two component system with two response regulators. The transmembrane MCP receptors bind chemoeffectors, either directly or using an intermediary periplasmic binding protein (shown here as PBP), and change conformation, passing phosphates to CheY and CheB. Phosphorylated CheY binds to the motor complex and increases the likelihood that the motor will switch to clockwise rotation. When motors rotate counterclockwise the flagella form a bundle and the cell swims smoothly forwards, in a run. When motors rotate clockwise the flagellar bundle separates and the cell stops swimming, a state called a tumble. During a tumble the cell reorients, so the next run is in a new direction. Image from Wadhams and Armitage (2004).

may be attractants or repellents. If attractant levels decrease, or repellent levels increase, there is a conformational change in the MCP which is trans-

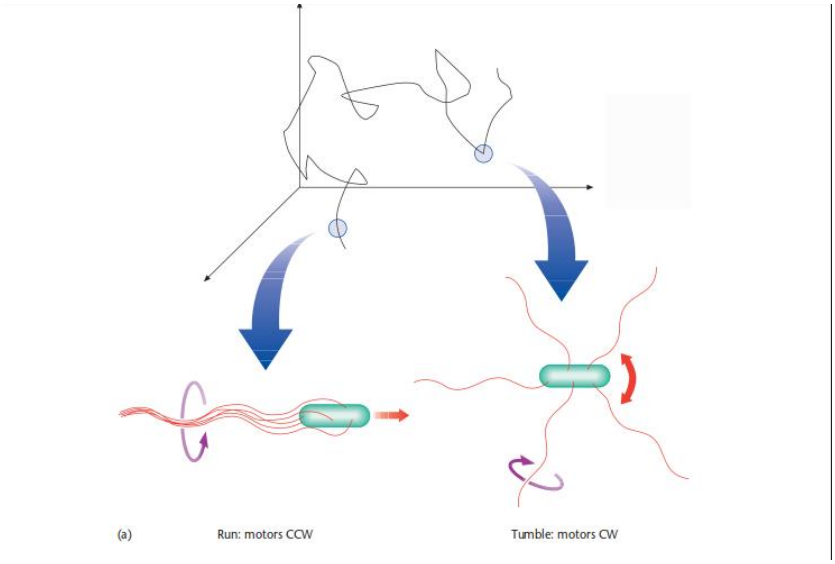


Figure 1.18: *E. coli* swims in a sequence of runs and tumbles. *E. coli* has several flagella and during runs, the flagella form a bundle, and the bacterium swims. During tumbles, the flagella separate and the bacterium stops swimming and reorients. When it starts swimming again it has changed direction. The frequency of tumbles is co-ordinated by the chemotaxis system. Image from Wadhams and Sowa (2001).

mitted through the adaptor protein CheW and activates a CheA histidine kinase, which can then phosphorylate a response regulator, CheY or CheB. Phosphorylated CheY interacts with the motor, making a switch in the direction of rotation more likely. CheY dephosphorylates automatically in around 10s, but in *E. coli* a phosphatase CheZ speeds up this reaction, allowing rapid responses to new signals (Lukat and Stock, 1993). Phosphorylated CheB demethylates the MCP and decreases its sensitivity for the chemoeffector. Another protein CheR constitutively increases the sensitivity of the MCP chemosensors by methylation (Fig. 1.17). The adjustment of the sensitivity of the MCPs means that they can adapt to the current chemoeffector conditions and can detect small changes in the concentration of a substance whatever the background concentrations, for a range of background concentrations of over five orders of magnitude (Wadhams and Armitage, 2004).

All flagellated swimming bacteria studied so far use similar flagellar motors

to swim and use similar chemotaxis proteins to bias their swimming direction, though there are many differences in details. The substances detected by the MCPs, the type of motor response, the adaption system and the number of homologues of the chemotaxis proteins all differ between species, with many bacteria having more complex chemotaxis systems than *E. coli* (Wadhams and Armitage, 2004).

1.8 Motility, chemotaxis and biofilm formation

Motility and/or chemotaxis have been found to be important in biofilm formation in many species of bacteria including:

- *Escherichia coli* - Pratt and Kolter (1998) found that motility but not chemotaxis was essential for biofilm formation in static conditions. More recently Wood et al. (2006) found, comparing several *E. coli* strains in flowcells, that the most motile cells formed the most extensive biofilms, and the worst biofilm forming strain had reduced motility. They related the differences in motility to differences in flagellar gene expression, and more recently still, Serra et al. (2013) found that flagella are used to form a strengthening framework in developing *E. coli* biofilms.

- *Agrobacterium tumefaciens* - aflagellate mutants attached very little in static conditions but attached rapidly in flow, while non-motile mutants which had non-functional flagella failed to attach in both static and flowing conditions (Merritt et al., 2007).

- *Pseudomonas aeruginosa* - O'Toole and Kolter (1998) showed that in static conditions motility due to both pili and flagella are necessary for attachment and biofilm development, however Klausen et al. (2003) showed that neither pili nor flagella were needed for *P. aeruginosa* attachment in flowcells, though the biofilm structure changed when either was missing. Klausen et al. (2003) suggest a model of *P. aeruginosa* biofilm growth where flagella are not involved in attachment, initial growth is clonal, and pili are used to spread across the surface. The previously accepted model was that flagella are involved in attachment and microcolonies are formed by pili mediated movement, followed by growth.

- *Bacillus cereus* - Houry et al. (2010) found that motility is important for biofilm formation in glass tubes and in microtitre plates, but not in

flow cells. A non-motile mutant with a flagellum produced more biofilm than an aflagellate mutant under static conditions, but neither flagella nor motility are required for biofilm formation under flow conditions, and the aflagellate mutant was the fastest to attach in flowcells.

- *Bacillus subtilis* - biofilms called pellicles are formed at the air-liquid interface as well as at surfaces, and motility was shown to be unnecessary for pellicle formation, but aflagellate and flagellated but non-motile mutants were slower to form pellicles so motility has a role in the process (Kobayashi, 2007).

- *Listeria monocytogenes* - Vatanyoopaisarn et al. (2000) found that a flagellin mutant attached to stainless steel at levels 10 times lower than wild-type cells at 22^oC, even under nutrient limited conditions which prevented active motility. *L. monocytogenes* does not produce flagella at 37^oC, and at 37^oC attachment of both strains was the same. The authors conclude that flagella are important for surface attachment independently of motility, probably as adhesins. O'Neil and Marquis (2006) found that flagella were not used as adhesins when attaching to human epithelial cells, though motility was important.

- *Aeromonas caviae* has two types of flagella, polar and lateral. Kirov et al. (2004) showed both to be important for adhesion to enterocytes and to glass. They also found an 80% reduction in attachment for a chemotaxis *cheA* mutant, which was non motile. Kirov et al. (2004) report differing results from previous studies, and suggest that different experimental procedures are the reason. More recently, in 76 strains of *A. caviae* isolated from the environment, there was a strong association between posessing both polar and lateral flagellin genes and forming biofilms in a static assay, all strains with neither gene and 76% of strains with one only could not form biofilms, and 94% of strains with both flagellins could form biofilms. However, motility was not assessed directly in these strains (Santos et al., 2011).

- *Vibrio cholerae* - Watnick et al. (2001) found that absence of the flag-

ellum altered the colony structure, and Dellen et al. (2008) found that the membrane potential had a role in biofilm formation and that the flagellum may be involved in sensing surfaces as well as in motility.

- *Shewanella oneidensis* seems to need the flagellum and flagellar motility more for biofilm development than for initial attachment (Thormann et al., 2004)

The work cited above, as well as many other studies, shows that motility and flagella affect biofilm formation in many species, but that the effects vary between species and for the same species in different conditions, and different experiments can give apparently contradictory results.

1.8.1 Chemotaxis and surface attachment

Chemotaxis is likely to affect surface attachment when surfaces are sources of chemoattractants, for example plant roots, animal cells, or abiotic surfaces coated with nutrient molecules. Chemotaxis will then increase the concentration of bacteria near the surface which is likely to affect attachment. As biofilms develop the biofilm itself will develop concentration gradients of nutrients and wastes and chemotaxis will lead other bacteria to approach or to avoid it, and may affect movement within the biofilm.

There are also chemotaxis-like pathways in some species which use the same adaptable sensory apparatus for purposes other than directed motility. Species where a chemotaxis-like pathway has a role other than chemotaxis include:

- *Azospirillum brasilense* - swimming speed and clumping (Siuti et al., 2011; Edwards et al., 2011; Bible et al., 2012)
- *Pseudomonas spp.* - biofilm formation through cyclic-di-GMP levels - (Hickman et al., 2005; Goymer et al., 2006; Spiers and Rainey, 2005)
- *Rhodospirillum centenum* - cyst development, flagellar synthesis - (Berleman and Bauer, 2005a,b)

- *Myxococcus xanthus* - polysaccharide production, development cycle - (Bellenger et al., 2002; Black and Yang, 2004; Zusman et al., 2007; Black et al., 2010)

1.9 Brownian motion - passive movement in fluids

Bacterial movement is linked to surface attachment and biofilm formation in many species, but not all bacterial movement is under the control of the organism. Passive responses to the surroundings may also be relevant and should be considered in an attempt to understand bacterial behaviour. An organism as small as a bacterium will be moved by any fluid flow, and even in still fluids will be moved by Brownian motion, which limits its ability to maintain a swimming direction and adds random jumps in position which may help or hinder the approach to a surface (Berg, 1993; Li et al., 2008; Li and Tang, 2009).

Brownian motion is the irregular movements made by very small objects due to random bombardment by even smaller objects such as molecules of water. It was first observed for dust and pollen grains and was explained mathematcially by Einstein in 1905. Brownian motion is the underlying cause of diffusion. The instantaneous speeds due to Brownian motion can be high, and diffusion is fast over very short distances.

These facts mean that a non-motile bacteria is still moving, but the random direction means that effective progress is slow. Analysis of diffusion in one dimension gives mean displacement at time t of zero, but mean square displacement proportional to t. Extending this to two and three dimensions, the distance travelled during time t by a diffusing particle is proportional to the square root of t, so that it takes 100 times as long to go 10 times as far. This keeps diffusion signals and diffusing bacteria local (Berg, 1993).

The other important factor is the diffusion coefficient, which depends on the

size and shape of the particle and the viscosity and temperature of the fluid.

If a bacterium is modelled as a sphere of radius 1 micron (reasonable for *R. sphaeroides*) the diffusion coefficient of a non-motile cell is roughly 2.2 x 10^{-13} m^2s^{-1} (Berg, 1993). Experimentally determined values of the diffusion coefficients of various non-motile bacteria in water given in Rijnaarts et al. (1993) agree with this value, coming between 1 and 6 x $10^{-13}m^2$ s^{-1}.

Berg (1993) states that in the absence of a chemosensory gradient, motile bacteria perform a random walk and can be regarded as diffusing with a diffusion coefficient related to the swim speed and angles of turns from one run to the next. Brownian motion is a cause of the change in direction of a swimmer during tumbles.

1.10 Surface behaviour and swimming at low Reynolds number

The behaviour of nanoscale moving objects at surfaces and in flow is different from the behaviour of larger objects. The dimensionless Reynolds number is the ratio of inertial forces to viscous forces, and gives a measure of whether momentum or fluid resistance is the most important factor. The Reynolds number depends on the size of the object, and the velocity of flow around the object, as well as the viscosity of the fluid.

$$Re = \frac{\rho U L}{\mu} \tag{1.1}$$

where ρ is the density of the fluid, U is the characteristic velocity, L is the characteristic length and μ is the viscosity of the fluid.

For a bacterium of around 1 micron length, swimming at .001 mms^{-1} the Reynolds number is 0.00001, which is very low and means that viscous forces are important and inertial forces are almost irrelevant.

The non intuitive nature of swimming at low Reynolds number (Purcell, 1977) means that it is useful to compare observed behaviour to mathematical predictions. Otherwise, behaviour due to physical forces could be thought to be a sign of signalling and decision making. An example is that swimming bacteria may turn towards a nearby surface due to hydrodynamic forces (Shum et al., 2010) without the need for surface detection and signal transduction.

The effect of a nearby surface on a swimming bacterium is not obvious. Many bacteria have been observed to swim in looping, almost circular paths when near a surface (Lauga et al., 2006; Li et al., 2008; Conrad et al., 2011), and some bacteria gather at surfaces as though trapped (Li and Tang, 2009; Li et al., 2011). These effects are thought to be due to interactions between the swimming cell and increased drag near a solid surface. In the study reported in Li et al. (2008), the distance from the surface was measured using TIRF microscopy, and this was found to be correlated with the radius of curvature of the path, bacteria near the surface moved in smaller circles. The speed was also affected by distance from the surface, being slightly slower near the surface. Previous studies (Frymier et al., 1995; Frymier and Ford, 1997) showed that the effect of a nearby surface on bacterial swimming speed depended on the swimming direction, with little effect for bacteria swimming parallel to the surface and slower speeds for bacteria approaching the surface.

1.11 *Rhodobacter sphaeroides*

R. sphaeroides (Fig. 1.19) is a photosynthetic α-proteobacterium in the purple non-sulfur group. It is metabolically diverse and can grow photosynthetically, aerobically, and anaerobically in the dark, and can fix nitrogen and carbon dioxide (Porter et al., 2011).

The original strains studied were collected in Delft, Holland, and California, USA (Choudhary et al., 2007). Strains of *R. sphaeroides* have been isolated from soil in China (He et al., 2010), marine mud in South Korea (Lim et al., 2009) and fresh water in New York, USA (Porter et al., 2011), and *R. sphaeroides* is believed to be ubiquitous in freshwater and soil. It is genetically very similar to the marine *Roseobacter* clade and it has been suggested that ancestors of *R. sphaeroides* were left in saline lakes as ancient seas withdrew, gradually adapting to fresh water as salinity reduced (Mackenzie et al., 2007). *R. sphaeroides* is found in low nutrient environments. It is known to be related to environmental primary colonisers (Dang et al., 2008).

R. sphaeroides is a model organism for photosynthesis (Tavano and Donohue, 2006) and chemotaxis (Porter et al., 2008), and is of interest for bioremediation (Bai et al., 2008; Madukasi et al., 2010). It is known to have a quorum sensing system, the CerI/CerR system (Puskas et al., 1997) and to use it in biofilm formation and dispersal (Hale, 2009). The positive control for calcofluor tests of EPS production used in this work is a CerI deletion mutant of WS8N which overproduces EPS. The *R. sphaeroides* WS8N EPS has not been characterised but it binds calcofluor and is similar to cellulose (Hale, 2009).

The *R. sphaeroides* genome consists of two chromosomes CI and CII of around 3 and 1 Mb and several endogenous plasmids, which vary in different strains. The genomes of five strains of *R. sphaeroides* have been sequenced, most recently the WS8N strain used in this work (Porter et al., 2011).

R. sphaeroides swims using a single subpolar flagellum (Fig. 1.20) with a unidirectional motor (Armitage and Macnab, 1987). Its swimming be-

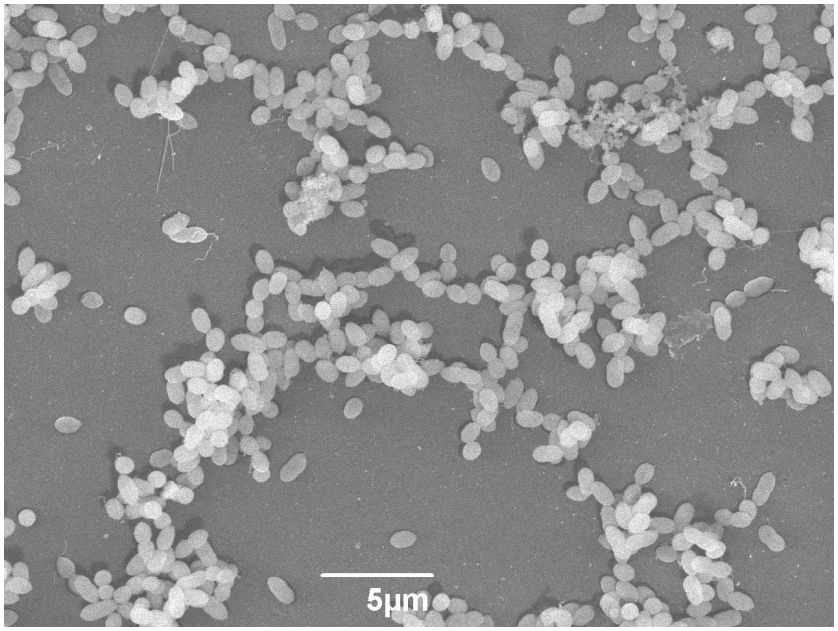


Figure 1.19: Scanning Electron micrograph of *R. sphaeroides* cells attached to a glass surface. Sarah Chacko/Michael Shaw (The Dunn School Bioimaging Facility, Oxford)

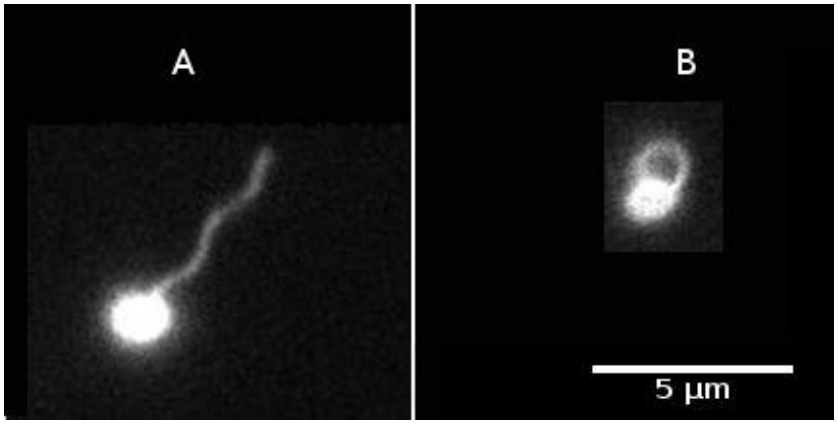


Figure 1.20: Swimming *R. sphaeroides* stained with Cy3 fluorescent dye, a) swimming and b) stopped. Image taken using the staining protocol in section 2.3.3. Sarah Chacko).

haviour and chemosensory systems are well characterised. It shows taxis towards many substances, such as propionate, succinate, acetate, sugars, oxygen and light. Cells growing aerobically are attracted to oxygen, cells

growing photoheterotrophically are repelled by oxygen. Some substances must be metabolised for taxis to occur (Porter et al., 2008). Existing knowledge of its swimming and chemotactic behaviour may help us understand why and when it stops swimming and forms a static colony.

1.12 Chemotaxis in *R. sphaeroides*

The *R. sphaeroides* chemotaxis sytem is more complex than that of *E. coli* (described in Section 1.7), though it is composed of similar proteins with similar roles. While *E. coli* has several motors and one chemotaxis cluster, with one homologue of each of CheA, CheY, CheB and CheR, *R. sphaeroides* has one motor controlled by two separate clusters of chemotaxis proteins, one polar and one cytoplasmic, both of which are necessary for chemotaxis.

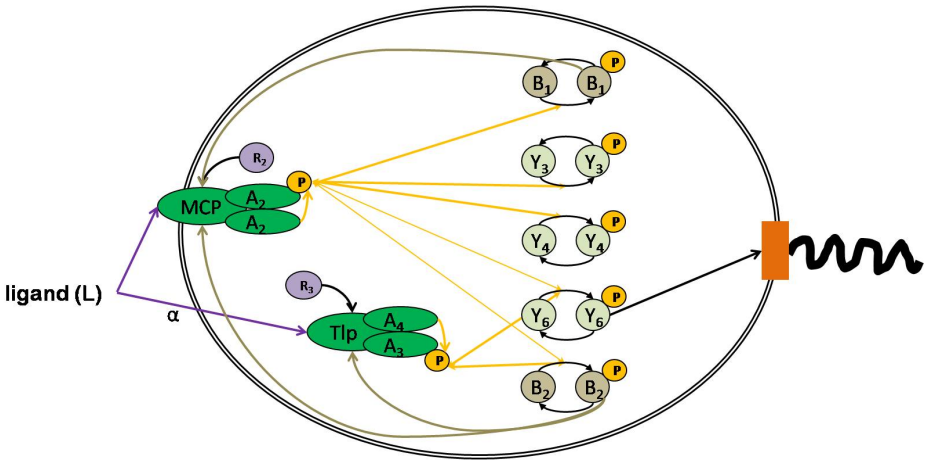


Figure 1.21: The chemotaxis system in *R. sphaeroides* . *R. sphaeroides* has one motor but two clusters of chemotaxis proteins. The two clusters are both required for *R. sphaeroides* chemotaxis and must co-ordinate signals, exactly how they do this is not known. The motor is running by default (Brown, 2009) and binding phosphorylated CheY6 stops it. As well as CheY6, either CheY3 or CheY4 is also needed for normal chemotaxis (Porter et al., 2006). Image from Roberts et al. (2009).

The *R. sphaeroides* genome encodes four CheA histidine kinases, three of which (CheA2, CheA3 and CheA4) are known to be expressed and used

in chemotaxis, and six CheY response regulators, three of which (CheY3, CheY4 and CheY6) are known to be expressed and used in chemotaxis. There are also multiple CheR methyltranferases and CheB methylesterases. Only CheY6 is known to bind to the flagellar motor and stop it, but either CheY3 or CheY4 must also be present for chemotaxis. The role of CheY3/CheY4 is not yet understood (Porter et al., 2006).

The *R. sphaeroides* transmembrane MCP sensor proteins in the polar chemotaxis cluster are similar to those in *E. coli* , though it is not known what each one senses. The polar cluster contains the histidine kinase CheA2, which phosphorylates the response regulators CheY3, CheY4, CheY6 and CheB1.

The cytoplasmic chemotaxis cluster contains sensor proteins without transmembrane regions, called TLPs (transducer like proteins) which are thought to sense metabolites, together with the CheA3 and CheA4 histidine kinases, which phosphorylate the response regulators CheY6 and CheB2. The *R. sphaeroides* chemotaxis system is outlined in Fig. 1.21.

Most of the chemotaxis proteins are encoded in three chemotaxis operons (Fig. 1.22). Both operons 2 and 3 encode proteins which are necessary for chemotaxis (Porter et al., 2002) and which form the polar and cytoplasmic chemotaxis clusters (Fig. 1.23).

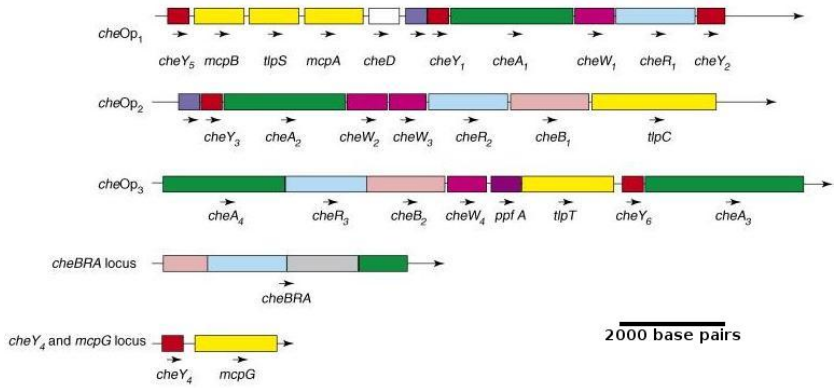


Figure 1.22: The chemotaxis operons and gene clusters in *R. sphaeroides*. The first operon (cheOp1) is not known to be expressed in laboratory conditions, cheOp2 encodes mainly the proteins in the polar cluster, and cheOp3 encodes proteins in the cytoplasmic cluster. Both cheOp2 and cheOp3 are essential for chemotaxis in all conditions studied so far. Image adapted from Porter et al. (2008)

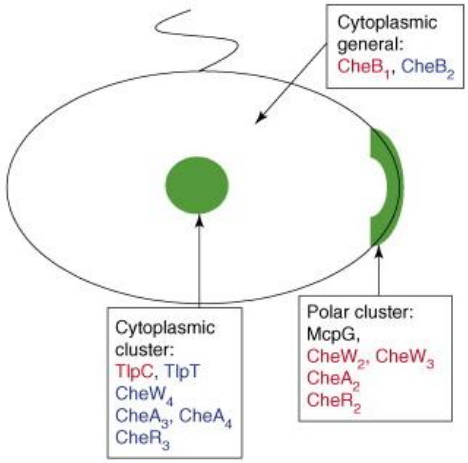


Figure 1.23: The location of chemotaxis proteins in the *R. sphaeroides* cell. Proteins labelled in red are encoded by chemotaxis operon 2, proteins labelled in blue by chemotaxis operon 3. Image adapted from Porter et al. (2008)

R. sphaeroides has two sets of flagellar genes, one set (*fla2*) has not been seen to be used under lab conditions, but forms a polar tuft if expressed (Poggio et al., 2007). Chemotaxis operon 1 (Fig. 1.22) has not been found to be expressed in any conditions studied so far, but has been shown to interact with the second (unused) flagella Fla2 when expressed in mutants (del Campo et al., 2011). Deletion of chemotaxis operon 1 has no apparent effect on *R. sphaeroides* WS8N in all conditions studied so far, but the fact that these genes are conserved and complete argues that there may be natural conditions in which they are used. In several other bacteria chemotaxis-like operons are used for different purposes from chemotaxis (Section 1.7), but there is no evidence for this in *R. sphaeroides*, all three *R. sphaeroides* chemotaxis operons are thought to be used for chemotaxis.

R. sphaeroides has MCP sensors similar to those in *E. coli*, and also cytoplasmic TLP (Transducer Like Protein) sensors which are similar to MCPs without the transmembrane regions. Unlike *E. coli*, specific substances sensed by the various MCPs and TLPs have not been identified. The co-ordination of signals from the two clusters is an area of current research (Scott et al., 2010; Sourjik and Armitage, 2010). In *R. sphaeroides* aerotaxis (movement up oxygen gradients) and phototaxis (movement towards or away from light) also use the chemotaxis system, since non chemotactic mutants lack these behaviours (Armitage and Hellingwerf, 2003). It is not known how light and oxygen are sensed by *R. sphaeroides*, though some of the proteins regulating responses to oxygen levels and light levels are known. It may be that what is sensed is changes in electron transport, rather than light and oxygen levels, so that deteriorating conditions are detected by the internal state of the cell, and motor stops are biased to improve things (Armitage, 1997; Porter et al., 2008). It is not known how this information is integrated into the chemotaxis system.

The metabolic versatility and fluctuating environments that *R. sphaeroides* inhabits may require more complex sensory apparatus than is needed by enteric bacteria such as *E. coli*.

Recent work suggests that complexity is common, with many species having

more than one predicted set of chemosensory genes (Hamer et al., 2010).

1.12.1 The *R. sphaeroides* flagellum and flagellar motor

The overall structure of the *R. sphaeroides* flagellar motor is similar to that of *E. coli* (Fig. 1.3). It is powered by the proton motive force and though the speed can change in discrete steps it is not thought that the bacteria has any active control over the motor speed. Unlike the *E. coli* motor, the *R. sphaeroides* motor is unidirectional, so swimming is run and stop rather than run and tumble. Phosphorylated CheY6 bound to the motor switch complex is responsible for stopping the motor (Porter et al., 2006). The motor speed does not vary much from cell to cell in given conditions, but a culture will include cells of different ages and sizes, and thus a range of swimming speeds. After the motor stops the swimming speed returns to its original value when the next run starts. As usual for motile bacteria, adjustment of run and stop length is used to bias the cell's path in a favourable direction towards some substances and conditions and away from others.

The mean stop duration and stop frequency and run bias in the absence of a chemical gradient were established in Brown (2009) by attaching beads to sheared flagella (which gives a load similar to that during normal swimming) and observing their rotation, the values were

- Mean Stop Duration 0.66 $\pm$ 1.01 s
- Mean Stop Frequency 0.31 $\pm$ 0.19 s^{-1}
- Run Bias 0.80 $\pm$ 0.20

Of the six CheY proteins in *R. sphaeroides*, CheY6 and either CheY3 or CheY4 are needed for wild-type chemotaxis. Their function has been studied by mutagenesis (Porter et al., 2006). If the aspartate phosphorylation site is changed to alanine the CheY proteins do not function. This is the same as *E. coli* . However, the CheY6 aspartate phosphorylation site is changed

to asparagine, mimicking the phosphorylated state, the flagellar motor stops completely and the cell is non-motile.

R. sphaeroides flagella attach to glass surfaces and spinning tethered cells are common on microscope slides. *R. sphaeroides* cells can spin in this way for long periods, I have observed cells spinning for 40 minutes. This argues against tethering by the flagellum as a precursor to biofilm formation, unless the process is very slow or acts only sometimes. The increased motor load does not seem to trigger attachment as it does in *C. crescentus* (Li et al., 2012).

1.13 *R. sphaeroides* biofilms

R. sphaeroides is related to environmental surface colonising species (Dang et al., 2008) and has potential for bioremediation (Bai et al., 2008; Madukasi et al., 2010). How it responds to its environment is of theoretical as well as practical interest because of the complexity of its metabolism and genome. The bacteria commonly used as model species for biofilm studies such as *P. aeruginosa*, *E. coli*, *B. subtilis* and *V. cholerae* do not include a photosynthesiser or a bacterium with more than one chromosome.

There is little published research on *R. sphaeroides* biofilms. *R. sphaeroides* is known to form biofilms on glass surfaces and to form long chains of cells attached to a surface (Hale, 2009). I have observed *R. sphaeroides* cells to aggregate in clumps in some conditions, and to form large thin mats of attached cells in fluid away from surfaces or interfaces. Like many bacteria *R. sphaeroides* can be grown as colonies on agar plates, with colony structure varying in different growth conditions. These familiar colonies are considered as a form of biofilm, and contain a polysaccharide matrix (Ray et al., 2012).

Motility and chemotaxis both influence the formation of a mature *R. sphaeroides* biofilm, with non-motile cells less likely to develop biofilm, and with non chemotactic mutants forming aberrant biofilm structures (Hale, 2009).

The uncharacterised extracellular polysaccharide (EPS) produced by *R. sphaeroides* binds calcofluor, so it can be detected by measuring bound calcofluor using fluorescence under ultraviolet light. The two clusters of genes involved were discovered using transposon mutagenesis and encode proteins similar to the succinoglycan biosynthetic enzymes from the gram-negative soil bacterium *Sinorhizobium meliloti* (Hale, 2009).

Quorum sensing (discussed in section 1.6.2) is used in *R. sphaeroides* to regulate EPS production, CerI mutants unable to produce the quorum sensing signal molecule are hyper EPS producing and hyper biofilm forming (Hale, 2009).

1.14 Aims of this study

The Introduction briefly summarised some of the many signals, behaviours and structures that are known to affect surface attachment in some species of bacteria. For *R. sphaeroides* WS8N, the details of surface attachment are unknown.

R. sphaeroides WS8N can form biofilms on glass and other surfaces, and motility and chemotaxis are involved in the process (Hale, 2009). The sequence of signals and events that leads to a planktonic *R. sphaeroides* WS8N cell reaching a surface, attaching to the surface, and converting to a surface attached phenotype are not understood. The point in biofilm development where chemotaxis and motility have their effects is unknown. The mechanism of surface sensing is unknown.

This study aims to find out more about the role of motility and chemotaxis in *R. sphaeroides* WS8N initial attachment by studying swimming changes near surfaces (Chapters 4 and 6), by comparing behaviour of wild-type cells and cells with altered motility or chemotaxis (Chapters 3 and 9), by altering motility by physical means (Chapter 7), and by comparing predicted to measured attachment using a simple mathematical model (Chapter 5). Specific aims are:

- To test the hypothesis that initial surface attachment in wild-type cells differs from initial surface attachment in non-motile flagellate and aflagellate mutants (Chapter 3).
- To test the hypothesis that initial surface attachment in wild-type cells differs from initial surface attachment in non-chemotactic mutants in the absence of a chemical gradient (Chapter 3).
- To establish whether the movement of wild-type *R. sphaeroides* changes when swimming near a surface and measure the changes (Chapter 4).
- To test the hypothesis that motility differences between strains is sufficient to explain attachment differences (Chapter 5).
- To test the hypothesis that flagellar tethering is needed for *R. sphaeroides* WS8N surface attachment (Chapter 6).
- To test the hypothesis that the flagellum is needed for *R. sphaeroides* WS8N to sense a surface (Chapter 9).
- To test the hypothesis that altering motility will alter surface attachment (Chapter 7)
- To test the hypothesis that non-motile and aflagellate mutants will develop differently from wild-type *R. sphaeroides* WS8N once attached to a surface (Chapter 9).

Chapter 2

Materials and Methods

2.1 Plasmids and strains

The bacterial strains and plasmids used in experiments are listed in Table 2.1.

Table 2.1: The *E. coli* and *R. sphaeroides* strains used in this study.

Strain	Description	Reference/source
E. coli		
XL1-Blue	General *E. coli* cloning strain	Stratagene UK
S17-1λ*pir*	*E. coli* strain able to transfer plasmids to *R. sphaeroides* by conjugation	Penfold and Pemberton (1992)
R. sphaeroides		
WS8N	Spontaneous Nal^R mutant of wild-type *R. sphaeroides* WS8	Sockett and Armitage (1991)
JPA117	WS8N Δ*cheOp1* - first chemotaxis operon deleted	Hamblin et al. (1997)
JPA403	WS8N Δ*cheOp2* - no polar chemotaxis cluster	Shah et al. (2000)

Continued on next page

Table 2.1 – *Continued from previous page*

Strain	Description	Reference/source
JPA452	WS8N Δ*orfE* - non-motile, flagellate	Gift from A. Martin
JPA467	WS8N Δ*fliA* - non-motile, aflagellate	Martin et al. (2006)
JPA517	WS8N Δ*cheB1*	Martin et al. (2001)
JPA565	WS8N Δ*cheR2*	Martin et al. (2001)
JPA620	WS8N Δ*cerI*, overproduces EPS.	Gift from H. Packer, (Hale, 2009)
JPA622	JPA500 Δ*exoY*, underproduces EPS.	Gift from H. Packer, (Hale, 2009)
JPA630	WS8N expresses green fluorescent protein from the chromosome.	This study
JPA631	WS8N expresses mCherry fluorescent protein from the chromosome.	This study
JPA635	WS8N Δ*fliC*	Gift from G. Wadhams
JPA637	WS8N Δ*motA* - missing stator unit.	Gift from G. Wadhams
JPA1213	WS8N with stopped motor - mutation *cheY6* D57N in place of *cheY6* in the chromosome.	Porter et al. (2006)
JPA1215	WS8N with in-frame deletions of *cheY1–3* and the mutation *cheY6* D57N in place of *cheY6* in the chromosome.	Roberts et al. (2012)
JPA1353	WS8N with no chemotaxis genes, non stopping phenotype	Gift from S. L. Porter
JPA1320	WS8N Δ*cheR3*	Porter et al. (2002)
JPA1323	WS8N Δ*cheB2*	Porter et al. (2002)
JPA1336	WS8N Δ*cheY6*	Porter et al. (2002)
JPA1419	WS8N Δ*cheOp3* - no cytoplasmic chemotaxis cluster	Gift from G. Wadhams

Table 2.2: The plasmids used in this study.

Plasmid	Description	Reference/source
plasmids		
pUC19	High copy number cloning vector, Amp^R	Pharmacia
pIND4	*R. sphaeroides* inducible expression plasmid, Kn^R, $P_{A1/04/03}$	Ind et al. (2009)
pIND4-CFP	pIND4 with the gene for cyan fluorescent protein inserted in the cloning site	Gift from Dr M. Roberts
pIND4-YFP	pIND4 with the gene for yellow fluorescent protein inserted in the cloning site	Gift from Dr M. Roberts
pK18*mobsacB*	Allelic exchange suicide vector, $sucrose^S$, Kn^R	Schafer et al. (1994)
pUC19:left	pUC19 containing the left flanking region from the WS8N genome	This study
pUC19:right	pUC19 containing the right flanking region from the WS8N genome	This study
pUC19:mCherry	pUC19 derivative containing mCherry with the pLac promoter	This study
pUC19:GFP	pUC19 derivative containing GFP with the pLac promoter	This study
pK18*mobsacB*: mCherry	pK18*mobsacB* derivative containing mCherry with the pLac promoter for insertion into the *R. sphaeroides* chromosome.	This study
pK18*mobsacB*: GFP	pK18*mobsacB* derivative containing GFP with the pLac promoter for insertion into the *R. sphaeroides* chromosome.	This study

2.2 Standard methods

2.2.1 Media and growth conditions

Media used were succinate media (Appendix 11.0.3), LB (Appendix 11.0.1), HEPES (Appendix 11.0.8) and M22 (Appendix 11.0.2).

2.2.2 *R. sphaeroides* liquid cultures

R. sphaeroides strains were grown in succinate medium (Appendix 11.0.3).

Stationary phase starter cultures were grown at 30^{o}C photoheterotrophically in a light cabinet under white non fluorescent light at 10 Wm^{-2}. They were used to inoculate cultures which were then grown in the dark with shaking at 225rpm at 30^{o}C in a rotary shaking incubator (Innova) for aerobic cultures, or photoheterotrophically without shaking in a light cabinet under white non fluorescent light at 10 Wm^{-2}, in 30 ml vials or 1.8 ml centrifuge tubes, both of which allow light to reach the cultures. While oxygen is present at the surface of these cultures it is quickly used up and the bulk of the culture is anaerobic, shown by the presence of pigments.

2.2.3 *R. sphaeroides* agar plates

R. sphaeroides were grown on LB plates (Appendix 11.0.1) containing LB with 1.5% (w/v) agar at 30^{o}C and incubated for at least 48 hours.

Where antibiotics were used, ampicillin was used at 100μg/ml, carbenicillin at 50μg/ml, kanamycin at 25μg/ml and nalidixic acid at 25μg/ml.

2.2.4 *E. coli* liquid cultures

E. coli strains were grown in LB medium (Appendix 11.0.1) in the dark with shaking at 225rpm at 37^{o}C in a rotary shaking incubator (Innova).

2.2.5 *E. coli* agar plates

E. coli were grown on LB plates (Appendix 11.0.1) containing LB with 1.5% (w/v) agar at 37^{o}C and incubated overnight.

2.2.6 Preparation of *R. sphaeroides* chromosomal DNA from colonies

Part of a colony was added to 100μl of water and vortexed to mix. 1μl of the mixture was used as a template for PCR. If there was not a 10 mins 98^{o}C initial denaturing step in the PCR protocol, the preparation was boiled for 10 minutes before use. The DNA was resuspended in sterile water and stored at -20^{o}C.

2.2.7 Preparation of *R. sphaeroides* chromosomal DNA from cultures

R. sphaeroides genomic DNA was extracted using the protocol in Giuliano et al. (1988). 1.5 ml of aerobic stationary phase culture was centrifuged at 13000g for 1 minute. The pellets were frozen in liquid nitrogen and then resuspended in 0.5 ml lysis buffer (10 mM Tris pH8, 1mM EDTA, 1%SDS, pH 8) at 65^{o}C. 100 μg proteinase K was added and the tube was incubated at 45^{o}C for 2 hours. The suspension was extracted twice with phenol:chloroform:isoamyl alcohol (25:24:1 v/v). DNA was precipitated by adding 1ml of 100% ethanol, washed with 70% ethanol, and dried. The DNA was resuspended in 50 μl of sterile water and stored at -20^{o}C.

2.2.8 Preparation of *E. coli* plasmid DNA

The QIAprep Spin Miniprep Kit (Qiagen) was used, following the manufacturer's instructions.

2.2.9 Restriction Digest

Enzymes were from New England Biolabs and used according to the manufacturer's instructions.

2.2.10 Ligation

Ligations were done using Invitrogen T4 ligase, following the manufacturer's instructions.

2.2.11 Agarose Gel Electrophoresis

Agarose gel elecrophoresis was used to separate DNA fragments by size. Roche multi-purpose agarose was made up with 0.5x TBE buffer (90 mM Tris-borate, 2mM EDTA, pH 8.0) to between 0.8% (w/v) and 2% (w/v) depending on the sizes of DNA to be separated. Electrophoresis was at 120 V, gels were run until the bromophenol blue marker dye has run to 3/4 the length of the gel , stained with 1ng/ml ethidium bromide in water for 20 minutes and visualised with an ultra violet transilluminator, λ_{max}=360nm (Syngene GBOX).

2.2.12 Gel Extraction

DNA bands were cut from agarose gels with a razor blade. The QIAquick Gel Extraction Kit (QIAGEN) was used according to the manufacturer's instructions to obtain purified DNA, which was eluted in 20-50 μl of sterile water.

2.2.13 Polymerase Chain Reaction (PCR)

Pfu DNA polymerase (Promega) was used according to the manufacturer's instructions, and thermocycling was performed in a Thermal Cycler (Techne).

Unless otherwise stated the following protocol was used for all PCRs. A 98^{o}C denaturing step for 10 minutes, then 30 cycles of 90^{o}C for 2 minutes, 55^{o}C for 1 minute 30 seconds, 72^{o}C for 2 minutes, then 10 minutes at 72^{o}C and then left at 4.0^{o}C until used.

Because *R. sphaeroides* DNA has a high GC content (69.1%, Porter et al. (2011)), up to 10% DMSO can help reduce hydrogen bonding and hence secondary structure. Each reaction was done with three levels of DMSO, 1μl (2% v/v), 2.5μl (5% v/v), and 5μl (10% v/v); and the volume of sterile water was adjusted to keep the total volume of each reaction to 50μl.

2.2.14 Overlap extension PCR

Overlap extension PCR was used to produce DNA fragments combining promoters and fluorescent protein genes (Higuchi et al., 1988; Horton et al., 1990).

Each of the two DNA fragments A and B to be joined was amplified by PCR using primers which added approximately 15 extra bases at both ends.

At the outer ends the extra bases contained recognition sites for restriction enzymes needed in later steps, at the inner ends where the fragments must join, the extra bases matched the other fragment, so A ended with a section complementary to B and B started with a section complementary to A.

For this work, first the genes for the fluorescent proteins GFP and mCherry were amplified by PCR from lab stocks, and the required promoter region was amplified separately from the pInd plasmid (Ind et al., 2009). The primers (Table 12) added the extra bases needed for overlap.

Then the two DNA templates, the fluorescent protein (A) and the promoter

region (B), were incubated with the forward primer for the promoter region and the reverse primer for the fluorescent protein

After the melting and annealing step of PCR, some of the A strands anneal to some of the B strands and are completed by the DNA polymerase to form full length strands with A joined to B.

The PCR products were checked by agarose gel electrophoresis (Section 2.2.11) and bands of the expected size were extracted and purified (Section 2.2.12) .

The process is shown in Fig. 2.1.

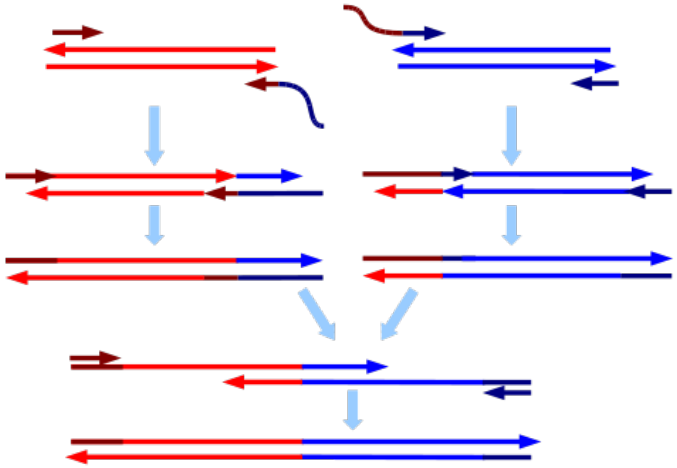


Figure 2.1: Splicing DNA fragments A (red) and B (blue) by overlap extension PCR. The arrows show the 3' ends of the strands. The small arrows are the primers. During the first melting and annealing step the primers add to each strand sections of DNA complementary to the other strand. At each subsequent melting and annealing step some of the DNA strands will anneal to the complementary strand and will be extended, and finally joined strands of DNA are produced and will be amplified. Image adapted from Wikipedia Commons

2.2.15 DNA purification

DNA fragments were purified from solution (restriction enzyme digests or PCRs) or from agarose gel bands using the QIAquick Gel Extraction Kit (Qiagen) according to the manufacturer's instructions.

2.2.16 Preparing *E. coli* competent cells (Rubidium Chloride protocol)

The RbCl method was used to prepare competent *E. coli* cells (Hanahan, 1983).

1 ml of *E. coli* stationary phase culture was inoculated into 50 ml of LB. The culture was incubated at 37^{o}C until OD_{600} = 0.4, transferred to falcon tube and incubated for 30 minutes on ice. Cells were centrifuged at 1000 x g for 10 minutes at 4^{o}C, resuspended in 16ml ice cold TFB I (Appendix A) and incubated on ice for 1 hour. The cells were then centrifuged at 750 x g for 10 minutes at 4^{o}C, resuspended in 2ml ice cold TFB II (Appendix A) divided into in 200 μl aliquots, and immediately stored at -80^{o}C.

2.2.17 Transforming plasmids into *E. coli* competent cells

200 μl of competent *E. coli* cells were mixed with 0.5μg of plasmid DNA and left for 1 hour on ice, followed by 1.5 minutes at 42^{o}C and then 2 minutes on ice. 800μl LB was added and the mixture incubated at 37^{o}C for 1 hour. The mixture was spread on LB agar plates containing appropriate antibiotics.

2.2.18 Transferring plasmids to *R. sphaeroides* from *E. coli* donor strain by conjugation

350μl of donor *E. coli* S17-1λ*pir* cells were incubated in 5ml of LB (Appendix A) at 37^{o}C until at OD_{600} = 0.4 and mixed with early stationary phase aerobiically grown *R. sphaeroides* cells in the ratio 1:10 v/v. The mixture was pipetted onto a sterile filter (Millipore 0.22μm white surfactant free) on a dry LB agar plate.

The filter was incubated at 30^{o}C for 6 hours then transferred to a 1.8ml centrifuge tube containing 800μl LB and vortexed vigorously to wash off the cells. 200μl of the mixture was plated onto LB agar plates containing antibiotics to select for cells containing the plasmid. For the plasmid pInd, these would be kanamycin and nalidixic acid, the kanamycin kills cells without the plasmid, the nalidixic acid kills remaining *E. coli* cells, *R. sphaeroides* WS8N is resistant to nalidixic acid. The remaining mixture was centrifuged at 1000 x g for 2 minutes and resuspended in 200μl LB and plated in the same way.

The LB plates were left for 48 hours and examined for colonies. When colonies were found they were transferred to succinate medium with appropriate antibiotics, grown at 30^{o}C aerobically until at OD_{700} = 0.4 and used to prepare frozen stocks.

2.2.19 DNA insertion into the *R. sphaeroides* chromosome

The 'suicide plasmid' pK18*mobsacB* is used to replace or insert DNA in the *R. sphaeroides* chromosome. It is unable to replicate and encodes kanamycin resistance. When pK18*mobsacB* is introduced into *R. sphaeroides* cells, their daughter cells will only have kanamycin resistance if the plasmid DNA has been incorporated into the genome by recombination. Recombination takes place between homologous DNA sequences so the plasmid DNA can be introduced into the *R. sphaeroides* genome in a specific place if sections of

genomic *R. sphaeroides* DNA are included in the pK18*mobsacB* plasmid. Cells containing the plasmid DNA can be selected by growth in the presence of kanamycin.

The cells selected as incorporating pK18*mobsacB* are then grown in antibiotic free succinate media to allow a second recombination event to occur leading to removal of the integrated construct.

Cultures are then serially diluted and plated on M22 media with 1.5% agar, containing 10 % (w/v) sucrose to select for the loss of the *sacB* gene. *sacB* encodes levansucrase which converts sucrose into a toxin. Therefore, cells that grow in the presence of sucrose have lost the pK18*mobsacB* vector backbone. Depending on how this happened, they may have reverted to wild-type or they may have the new DNA in the chromosome.

These colonies are replica plated onto LB agar plates containing nalidixic acid and kanamycin and LB agar plates containing only nalidixic acid. Sucrose resistant, kanamycin sensitive colonies are wild-type or mutant and can be distinguished by chromosomal DNA extraction and southern blotting.

The process is illustrated in Fig. 2.2

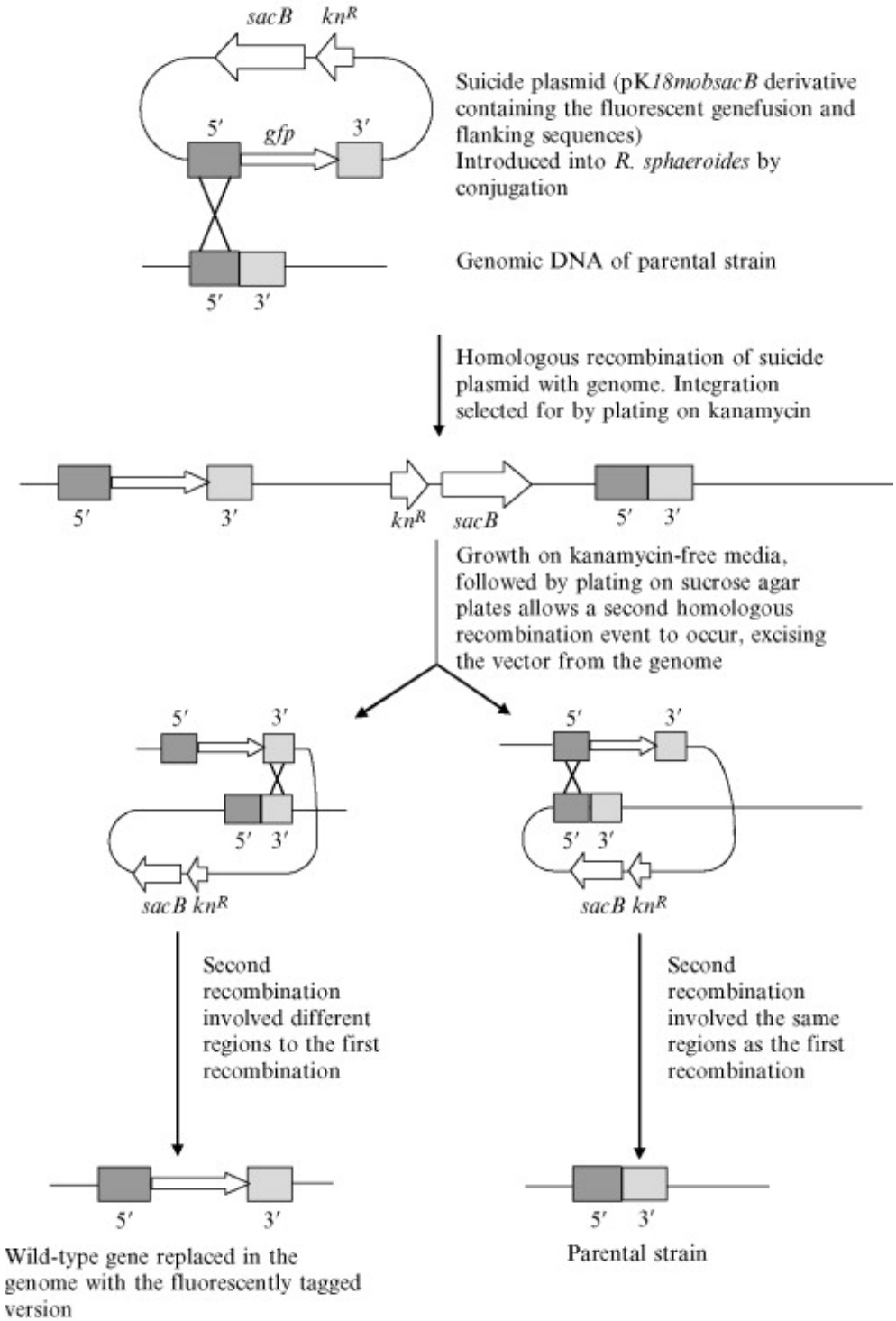


Figure 2.2: How a new gene or fusion can be inserted into the genome by two homologous recombination events. Image taken from Porter et al. (2007).

2.2.20 DNA sequencing

DNA was sequenced at the in-house Source BioScience LifeSciences DNA sequencing facility.

2.2.21 Frozen stocks

Strains of *R. sphaeroides* and *E. coli* were grown to mid log phase in the appropriate media (succinate media or LB). 40 μl 50% v/v glycerol was mixed with 60 μl of cell culture, flash frozen in liquid nitrogen and stored at -80^{o}C.

2.2.22 Soft agar swim plates

Strains of *R. sphaeroides* were analysed for motility and chemotaxis using an adaption of the protocol in Wolfe and Berg (1989). Chemotactic strains swim up the chemoattractant gradient that they generate as they use up nutrients. Non chemotactic strains make smaller rings because without being able to reorient they are unable to negotiate round obstructions or bias their path to swim up the gradient. Non motile strains hardly move beyond the site of inoculation.

0.25% w/v BiTek agar (BD Biosciences UK) swim plates were made using M22 minimal media (Appendix 11.0.2) with the attractant sodium propionate at 100μM. The plates were inoculated with 5μl drops of stationary phase culture, grown photoheterotrophically at 30^{o}C. Swim diameters were measured after 48 hours of growth at 30^{o}C. All strains to be compared were inoculated on the same plate (up to 9 strains can be tested this way), and each swim plate assay was done in triplicate.

2.2.23 Growth Curves

The growth rates of *R. sphaeroides* wild-type and mutant strains were measured by diluting stationary phase cultures 1:1000 v/v into succinate medium (Appendix A) in 96 well plates (Corning Costar, from Sigma Aldrich UK) and recording the OD_{700} at regular intervals of 20 minutes in a platereader (Tecan Magellan, Tecan UK Ltd.) in the dark with shaking at 30^{o}C. The doubling times for each sample were calculated for the exponential phase, by finding the gradient of the straight line corresponding to exponential growth when the log of the OD is plotted. If this gradient is m, and the number of cells (proportional to the OD) is n, during exponential growth ln(n) = mt so $n = e^{mt}$ and when n doubles, $2 = e^{mt_1}/e^{mt_0} = e^{mt_1 - mt_0}$, so $m(t_1 - t_0) = \ln(2)$ and doubling time is ln(2)/m.

2.3 Staining Techniques

2.3.1 Crystal violet staining to measure attachment

The method in Merritt et al. (2005) was used with 10% v/v acetic acid as the solvent (100% DMSO was also effective with *R. sphaeroides*).

100 μl of bacteria cultures was added to the wells of non tissue cultures treated 96 well plates (BD Falcon, BD Biosciences UK) which were left for 30 minutes in a light cabinet, under white light at 10 Wm^{-2} at 30^{o}C. The wells were washed by emptying out the cultures and submerging each plate once in a container of water, then emptying out again to remove unattached cells.

125 μl 0.1M Crystal Violet stain in water was added to each well and left for 10 minutes. The wells were washed by emptying out the cultures and stain and submerging each plate twice in containers of water, then emptying out to remove extra stain.

The wells were air dried for 10 minutes and then destained using 10% v/v

acetic acid. 200μl was added to each well and the plate left for 10 minutes. This solvent extracts the crystal violet from the cells. (This step can be delayed, once the wells are stained and dried the stain is stable)

125 μl of the acetic acid was transferred from each well to a well in a clear bottomed 96 well plate (Corning Costar, from Sigma Aldrich UK) that could be used in a plate reader.

A plate reader (Tecan Magellan, Tecan UK Ltd.) was used to measure the absorbance at 595nm of the acetic acid. The OD gives a measure of the amount of crystal violet dissolved, and thus the amount of attached cells in the original well.

2.3.2 Ryu staining to visualise flagella using bright-field, phase contrast or DIC microscopy

Ryu stain (Ryu, 1937) was prepared as in Heimbrook et al. (1989). To stain bacteria for observation of flagella, a 10μl drop of culture was placed on a glass microscope slide and covered by a coverslip.

A 20μl drop of stain was placed at one edge of the coverslip and flowed under by capillary action. A tissue was used at the opposite side to draw the stain through, and then a drop of fresh media was placed at the edge and drawn partially through in the same way. This leaves different areas of the slide stained to different extents, and it is then possible to find fields of view where the conditions were correct and flagella can be seen. The slide was examined by microscopy immediately.

2.3.3 Cy3 staining for *E. coli* and *R. sphaeroides* to visualise flagella using fluorescence

The protocol used was given to me by Dr. Mostyn Brown.

5ml of mid exponential *E. coli* culture were washed into 80μl MB buffer (10

mM potassium phosphate, 67mM NaCl, 0.1mM EDTA, ph7.5) by centrifuging for 2 minutes at 5000 x g and resuspending twice, gently, using cut off pipette tips. 4μl 1M $NaHCO_3$ was added to shift the pH to 8.0. Cy3 dye (GE Healthcare) was diluted into MB buffer using 10μl per sample, and 10μl of the diluted Cy3 dye was added to each *E. coli* sample. The samples were covered with foil to exclude light and stirred by gyration for 90 minutes. Excess dye was removed by centrifuging at 5000 x g and resuspending in MB+ buffer (10 mM potassium phosphate, 67mM NaCl, 0.1mM EDTA, 0.5% glucose v/v, 0.002% v/v Tween20 (Sigma Aldrich) pH 7.0) three times, then each sample was diluted to 500 μl with MB+ buffer.

40 μl cells were introduced into a tunnel slide (Section 2.4.4) by capillary action and imaged using the x60 objective on a Nikon A1 microscope with Andor EMCCD camera, using a YFP filter set.

This Cy3 staining protocol stains *R. sphaeroides* successfully but motility is lost because *R. sphaeroides* does not swim in phosphate buffers (Poole et al., 1991).

2.3.4 Calcofluor plates to assess cellulose-like exopolysaccharide (EPS) production

The method used was based on Hale (2009). A *R. sphaeroides* colony from an LB (Appendix A) agar plate was grown in succinate media (Appendix A) aerobically (Section 2.2.2) for 48 hours, diluted 1:1000 v/v in fresh succinate medium and grown to stationary phase. 1.5% LB agar plates containing 10 μgml^{-1} Calcofluor White (Sigma Aldrich) were point inoculated with 5μl of the stationary phase culture and incubated for 4 days at 30^{o}C. The colonies were photographed under ultraviolet light using a transilluminator/imaging system (Syngene GBOX). Calcoflour fluoresces under uv light and is incorporated by cellulose. Colonies producing more cellulose-like material are brighter than those producing less.

Table 2.3: Fluorophore characteristics and Nikon A1 confocal microscope settings. All these fluorophores can be excited and detected using a range of wavelengths, the 'Excitation max' in the table is the optimum wavelength to excite that fluorophore.

Fluorophore	Excitation max	Emission range	Laser	Band Pass Filter
Fluorescent proteins				
CFP	436nm	464-499nm	457nm	482/35
GFP	488nm	500-550nm	488nm	525/50
YFP	514nm	525-555nm	514nm	540/30
mCherry	587nm	570-620nm	561nm	595/50
Fluorescent stains				
Cy3	555nm	570nm	514nm	540/30
Calcofluor White	350nm	450-500nm	405nm	

2.4 Microscopy techniques

2.4.1 Microscopes and filters

A phase contrast microscope (Nikon Optiphot, with x20 or x40 objective) was used for free swimming videos and to check motility by eye.

A confocal microscope (Nikon A1) was used for fluorescence microscopy. Lasers, filters and dichroic mirrors were selected to correspond with the fluorophore in use, shown in table 2.3, and Differental Interference Contrast Microscopy was used to show the outlines of cells independently of fluorescence levels.

2.4.2 Cleaning slides and coverslips

Coverslips used for attachment assays were cleaned with potassium hydroxide.

5 or 6 potassium hydroxide tablets were added to 100 ml 70% v/v ethanol in a pyrex beaker large enough to take the coverslips and stirred until dissolved. The coverslips were put in the beaker and left for 20 minutes. They were

rinsed in sterile water water and washed in ethanol. They were stored in a sterile Duran bottle in ethanol and washed in sterile water and air dried before use.

2.4.3 Agarose pad preparation

Agarose pads were used to immobilise cells for microscopy. 1% w/v agarose in sterile water was heated for 1 minute in a microwave and used while molten. Two coverslips were placed on a glass slide, around 1 cm apart. 200 μl molten agarose was pipetted on the slide between the coverslips and another coverslip immediately placed on top, supported at either end by the first two coverslips. The top coverslip was gently tapped at each side to press it down and the agarose was left to set. Then all three coverslips were carefully removed and the agarose pad cut to a rectangle with the edge of a coverslip, leaving an even flat surface.

2.4.4 Tunnel slide preparation

Tunnel slides were made using double sided adhesive tape (Scotch tape), a glass slide and a glass coverslip. Two pieces of double sided tape were stuck to a slide, leaving a narrow channel (0.2 - 0.5 cm) between. A coverslip was carefully pressed down on top of the tape and the edges of the tape trimmed flush with the coverslip (Fig. 2.3). Bacterial cultures flow into the channel by capillary action when a drop of culture is placed at one end. Depending on the experiment, the ends were left open or sealed with clear nail varnish (Boots Natural Collection).

2.4.5 Single channel flowcell preparation

Home made flowcells were made using double sided adhesive tape (Scotch tape), a glass slide (Fisher Scientific), 1 mm internal diameter silicone tubing (VWR International) and a long (50 mm) glass coverslip (Roth).

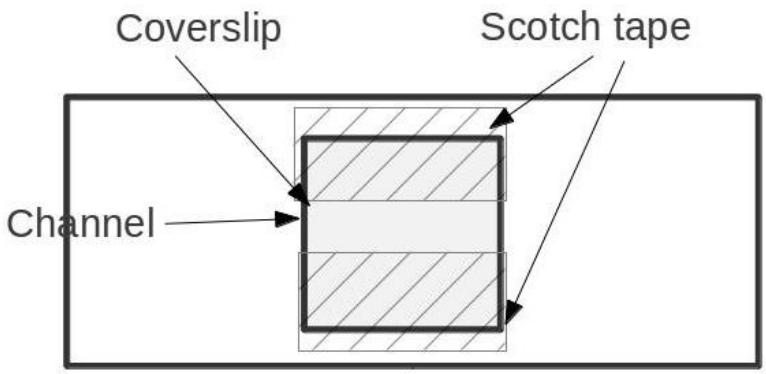


Figure 2.3: A tunnel slide.

Two holes were drilled in the glass slide, 2mm closer together than the coverslip length. Around 5 cm of tubing was pushed through both holes a very short way. The tubing was taped down at either end. Araldite glue (Araldite UK) was mixed and spread around the tubing in the holes, on the side with most of the tubing (Fig. 2.4) and left to set. The short ends of tubing were sliced flush with the surface.

To finish the flowcell, a pieces of double sided tape (Scotch tape) was stuck to the slide, covering both holes. A channel was cut with a razor blade, between the holes (Fig. 2.5) and the coverslip carefully placed on top. A matchstick was used to gently rub the coverslip where it touched the scotch tape to seal it. The flowcells were left for a day before use.

These flowcells are watertight and the drilled slide base can be reused. Fluid flows in through one piece of tubing, along through the channel cut in the tape, and out through the other piece of tubing.

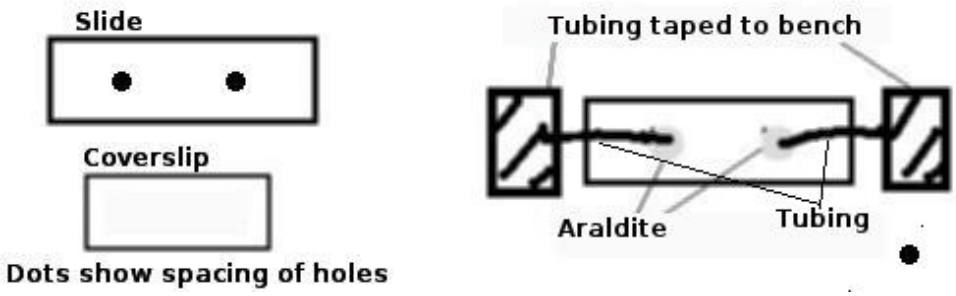


Figure 2.4: Preparing the flowcell base. The tubing is fixed in place with the araldite and is taped down while the araldite dries to bend the pieces of tubing away from the flowcell, and make them fairly flat.

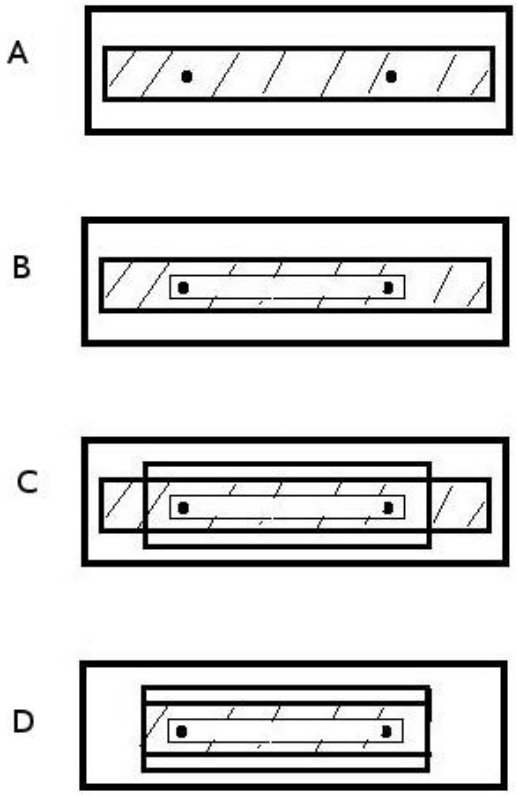


Figure 2.5: Finishing the flowcell. A) Double sided tape stuck over both holes, the other side from the protuding tubing. B) A channel cut round the holes. C) The coverslip pressed down over the tape. D) The tape trimmed flush with the coverslip. (The tubes are on the other side.)

2.5 Methods adapted for this study

2.5.1 Competitive assays in static conditions

A simple experiment to compare attachment in different strains is to grow them together in a culture containing a glass coverslip and to count attached cells after a set time. This is similar to early methods of detecting environmental biofilms by suspending a microscope slide in water or earth and seeing what attaches.

The advantages of this method are its simplicity and the ability to compare many conditions or strains.

Using a static culture limits the experimental duration since eventually the culture will reach stationary phase and *R. sphaeroides* biofilm coverage will reduce. Also the conditions change continuously as wastes build up and nutrients are used up and as the bacteria become more crowded. The glass coverslip has to be removed for observation, which disturbs the attached cells and may detach delicate structures. Observing each coverslip can only be done once.

The method is shown in Fig. 2.6. The bacterial strains to be compared were engineered to express fluorescent proteins, either genomically or using inducible plasmids. In case of differences in expressing or detecting the fluorescent proteins, all four possible combinations of colour and strain were used.

The same volume of a culture of each strain at the same OD was introduced into 20 ml of the required medium in a 50 ml Falcon tube with a clean glass coverslip and left for the required time. The coverslip was removed and gently rinsed by dipping it in a beaker of fresh media to remove unattached cells. The coverslip was carefully supported on a microscope slide with strips of double sided sellotape to either side. The upper surface was cleaned by wiping gently with 70% ethanol, and fresh media allowed to flow through to keep the lower coverslip surface hydrated and to allow space for surface

structures.

The quantity and arrangement of the cells attached to the coverslip was examined by confocal microscopy. Four cultures were used, with three replicates of each.

1. Strain A expressing colour 1 with Strain A expressing colour 2
2. Strain A expressing colour 1 with Strain B expressing colour 2
3. Strain A expressing colour 2 with Strain B expressing colour 1
4. Strain B expressing colour 2 with Strain B expressing colour 2

The main data for each comparison comes from mixtures 2 and 3, directly comparing attachment of the two strains in identical circumstances. Mixtures 1 and 4 allow any effect due to the expression or detection of the different fluorescent proteins to be noticed, since attachment should be the same for both strains. Confounding issues due to the mixture of the strains, such as complementation, can be identified by looking at each strain both alone and with the other strain.

This method was used to look at colony development over 24 and 48 hours. *R. sphaeroides* tends to detach when the culture becomes overcrowded so very small amounts of the initial cultures were used, 2 μl of each strain at stationary phase in 20 ml of medium, giving a starting density of $5.5x10^4$ cells/ml (Fif. 3.9).

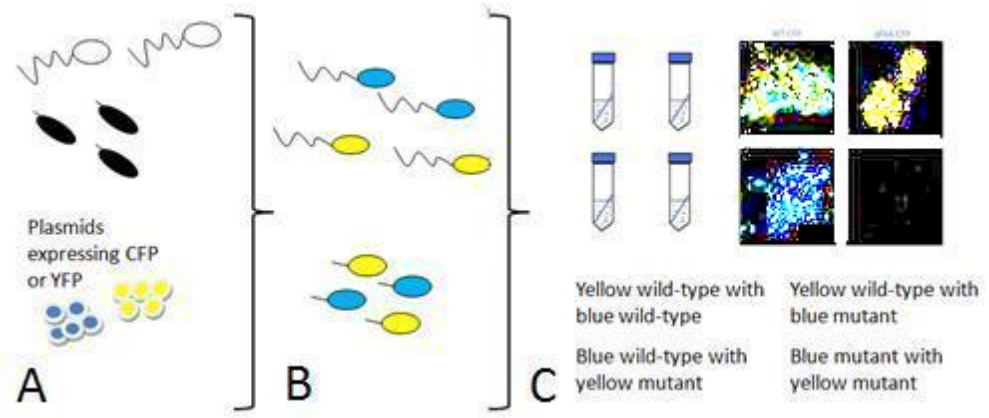


Figure 2.6: Static competition assay. Two strains are made to express different fluorescent proteins and left over time to attach to glass. The cells attached can be examined by microscopy and the numbers of cells of each type determined. A) Plasmids expressing a fluorescent protein are introduced into *R. sphaeroides* bacteria by conjugation. B) Both *R. sphaeroides* strains to be compared are made to express both fluorescent proteins, giving four strains. C) Cultures containing all four combinations of a strain expressing one protein with a strain expressing the other are left in a falcon tube containing a clean coverslip for a set time. D) The coverslips are viewed by microscopy and fluorescence measurements are used to identify the two strains. If the proportion of the two strains on the coverslip is different from the proportion in the culture, then they attach to different extents.

2.5.2 Three channel flowcells and bubbletraps (DTU)

Biofilms were grown at room temperature in flow chambers with individual channel dimensions of 1 by 4 by 40 mm.

The flowcells (bought from Denmark Technical University) were made up by attaching a 60 mm length clean glass coverslip (Fisher Scientific) to the flowcell base with silicon glue (RS Components Ltd).

The flowcell and bubbletrap (Denmark Technical University) was set up as described previously (Moller et al., 1998; Thormann et al., 2004). The assembled system is shown in Fig. 2.7.

A programmable syringe pump (Harvard Apparatus) was used with Terumo 50 ml syringes. The whole apparatus apart from the syringes and pump was connected up and autoclaved at 105^{o}C for 20 minutes before use, and 70% ethanol pumped through and left overnight to sterilise the connected system. 50 ml of sterile water was pumped through to remove the ethanol and check for leaks. Then the system was filled with succinate media, with the appropriate antibiotics and 0.1 mM IPTG if necessary.

The flow chambers were inoculated by injecting 500 μl of overnight culture diluted to an OD_{700} of 0.4 into each flow channel with a small syringe (Becton Dickinson 1 mm, needle gauge). After inoculation, flow channels were left without flow for 1 h, after which flow was started at 3 ml/h.

The flowcell was left on the microscope stage throughout an experiment and images taken at regular intervals.

2.5.3 Free swimming assay for *R. sphaeroides*

Under the conditions used, *R. sphaeroides* are most reliably motile from $OD_{700} = 0.4$ to 0.6. At stationary phase ($OD_{700} > 1.0$) most *R. sphaeroides* cells stop swimming (Personal communication, Dr D. Wilkinson.).

Nine cultures of *R. sphaeroides* WS8N were grown photoheterotrophically in

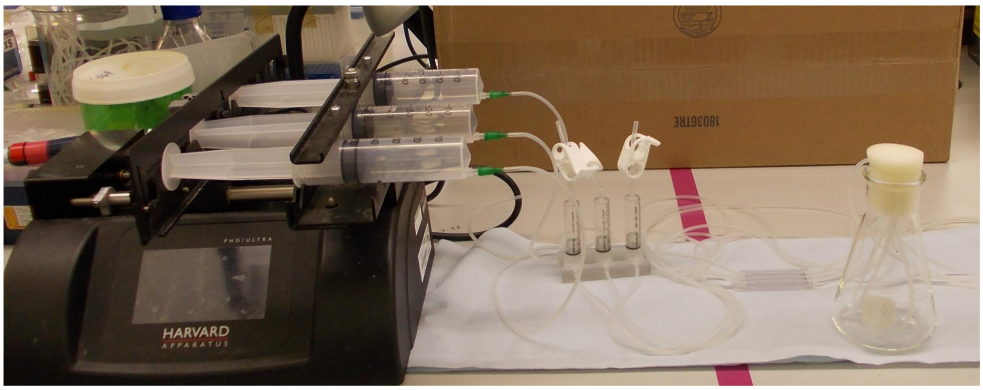


Figure 2.7: The DTU flowcell and bubbletrap connected to the pump and waste

succinate medium (Appendix 11.0.3) to OD_{700} 0.6 (Section 2.2.2). 100μl of cells from each culture were centrifuged at 1,000g for 1 minute in a benchtop centrifuge. The supernatant was removed and the cell pellet was gently resuspended in 1 ml of 10mM HEPES motility buffer (Appendix 11.0.8).

A 0.2 x 2 x 100 mm rectangular glass capillary tube (CM Scientific) was put into 50 μl of the prepared culture in an 1.8ml centrifuge tube, where it filled by capillary action. When completely full the ends were sealed with silicon grease and the tube was placed on a microscope slide.

2 minute videos were recorded at 50 frames per second using the x20 phase contrast objective on a Nikon Optiphot microscope with a DALSA Genie-HM640 video camera.

For swimming at a surface, videos were taken at the upper glass surface of the capillary tube, for swimming in bulk media the stage was moved to roughly half way between the upper and lower surfaces.

Observation and video recording were done immediately after slide preparation.

The analysis of these videos is explained in section 2.6

2.6 Characterising swimming patterns by analysing video data

Video recordings of swimming bacteria were analysed to identify changes in swimming when bacteria were near or far from a surface, and changes in swimming behaviour of motility mutants. The software used to analyse videos was developed by several people. The core module for identifying bacterial tracks in videos was written by Trevor Wood and Gabriel Rosser and is described in Wood et al. (2012). The module for allocating sections of tracks to runs and stops was written by Gabriel Rosser and is described in Rosser et al. (2013). Functions to clean, visualise and analyse the data were written in the Armitage Laboratory by David Wilkinson, Jennifer de Beyer and Sarah Chacko. The software is written in MATLAB (The MathWorks, 2009) and runs on Linux and Windows. The overall process is shown in Fig. 4.1.

2.7 Free swimming analysis

2.7.1 Identifying swimming cells

A video of swimming bacteria consists of a sequence of image frames, each of which is a matrix of numbers representing the light intensity at each element of the field of view. The smallest elements making up the image are called pixels. The pixel size depends on the magnification and also on the camera used. Larger pixels give a grainy image.

The software has to analyse these matrices of numbers to decide which numbers correspond to bacteria.

This is done by 'segmenting' - dividing each image into objects and background. With phase contrast microscopy the bacteria appear either as dark outlines against a grey background, or as light objects against a grey back-

ground, depending on their distance from the focal plane. To retrieve the maximum track lengths we need both.

The custom written software we use, written by Gabriel Rosser and Bogoslaw Obara, is the first part of the 'Tracker' software stored on

`\\HPSWA\Armitage\Useful␣Stuff\Tracking␣GUI`

It offers a choice of segmentation methods, the simplest being 'global threshold' where every pixel brighter than a threshold is selected, together with every pixel below another threshold. Values between the two thresholds correspond to background. Using a global threshold is not ideal when there are variations in light intensity across the image, and we find that the most reliable segmentation methods for our video data use 'local thresholding', and compare each pixel to its local area instead of the whole image. For the work here I used 'local mean', comparing each pixel to the mean of the values surrounding it. The parameters are the upper and lower thresholds and the size of the local area to use. The software allows you to set a minimum size so that objects much smaller than a bacterium (eg. random bright pixels due to noise and some dust) are not identified as objects. The threshold values depend on the data and are set interactively, checking that results for every video in a batch are acceptable. The tracking software is tolerant of false positives, it is possible to remove spurious tracks in processing, while objects that are never identified can never be tracked, so we err towards identifying more rather than fewer objects.

The segmentation process is illustrated in Fig. 2.8. Image A is part of an original frame, B is image A segmented into objects and background, image C shows only the centroids of each object. The files saved for each frame after segmentation contain only the list of co-ordinates of the centroids of the objects.

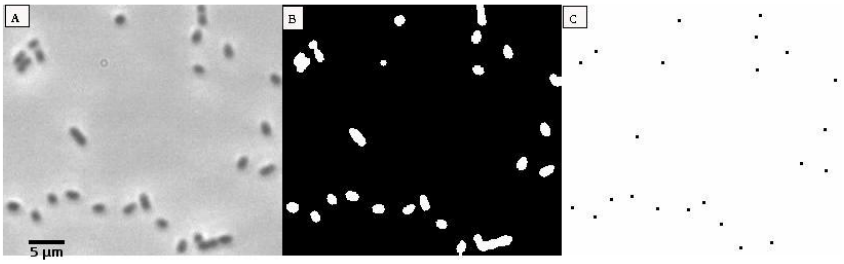


Figure 2.8: A field of view (A), the same field segmented into objects and backgrounds (B), and the centroids of the detected objects (C).

2.7.2 Tracking paths of swimming cells

The next step is tracking, using the list of centroids in each video frame to decide on the path of each swimming bacterium. Tracking software has to determine where bacteria have moved between frames, allowing for bacteria appearing for the first time or disappearing, possible temporarily, from view. This is complicated when there are many almost identical bacteria and when tracks cross.

The simplest tracking method is 'nearest neighbour' where the next position of a cell is the nearest cell in the next frame, but this can be inaccurate when cells approach closely.

The software used here was written by Trevor Wood and is described in detail in Wood et al. (2012). It is stored on

`\\HPSWA\Armitage\Useful␣Stuff\Tracking␣GUI␣`

It uses an adapted version of the Probability Hypothesis Density Filter to work out the most likely tracks based on the lists of centroids and some prior knowledge of bacterial motion.

The input is the list of centroids of objects detected in each frame of a video, and the output is a list of the same centroids sorted into tracks. The output file for a video contains a list of tracks, where each track is a list of centroids, and also the frame where the track starts, the frame where it ends, and the

length of the track.

The tracks can later be filtered to remove noisy or incorrect tracks using criteria such as length of track, mean speed or distance moved, this can remove non-motile cells and dirt in the field of view, but care must be taken not to bias results.

Some examples of bacterial tracks are shown in Fig. 2.9. We can visually confirm the accuracy of a track by superimposing it on the original video, and this is done for a small percentage of the tracks as a spot check of accuracy. The most common tracking errors are dead cells or dust in the microscope - which give tracks that last a long time but go a very short (or no) distance, and false connections when one track is joined to a near but different track, which often gives a long jump in one place in the track. These can be detected and removed as described later. Another problem is very wiggly 'tortuous' tracks (Fig. 2.9 D) in which the regular movement of the centroid as the cell body rotates adds a regular wobble to the forward motion. These can bias later analysis and may also be removed. The problem in censoring unwanted tracks is to be consistent and not to introduce bias. Which tracks are considered unwanted may also vary depending on what the data are to be used for.

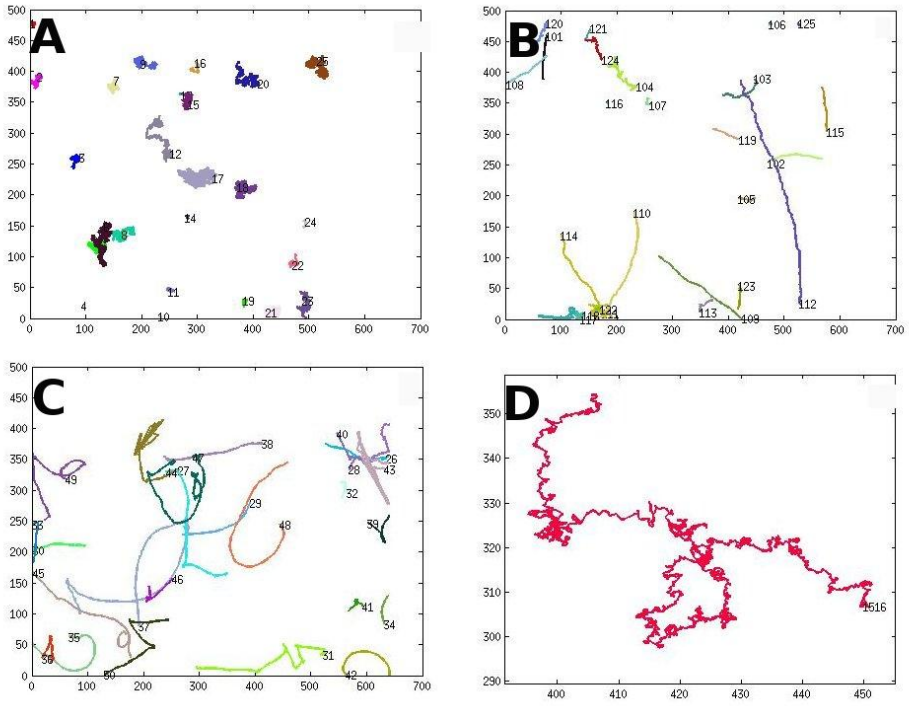


Figure 2.9: Some bacterial tracks produced by the tracking software from phase contrast videos of swimming *R. sphaeroides*. The axes show xy position in pixels, and each video is 2 minutes long. The tracks are shown without time information, only the positions in each track are shown. A shows tracks from a non-motile mutant, B shows tracks from a 'smooth swimming' mutant which rarely stops, C shows wild type *R. sphaeroides* tracks near a surface where paths become curved, and D shows a 'tortuous' track which may be produced by longer or almost divided cells, where the rotation of the cell body gives a regular wobble to the centroid position. The axes are marked in pixels, so the position on the image matches the positions of the cell in the video frame.

2.7.3 Censoring tracks - detecting and removing spurious tracks

The tracking software, 'Tracker', returns tracks from every detected object. Some are very short, only one or two frames - meaning the object was in focus for only 0.04s, some are very long, running through the whole video with very little actual movement. These very long tracks may be due to dirt in the microscope. The software can allow for temporary loss of an object and will interpolate intermediate positions but this can sometimes lead to inappropriate joins between what should be separate tracks.

The tracks described above can be automatically removed by setting a maximum and a minimum track length, and a minimum overall movement by setting a minimum bounding radius round a track and discarding tracks that stay within too small a circle. Inappropriate joins can often be removed by limiting the distance that a bacterium can move in one frame, though this has the danger of introducing bias based on our assumptions about behaviour.

Some tracks can be wanted in one situation and unwanted in another. When analysing the movement due to drift and Brownian motion of a non-motile strain non-motile cells are necessary, but when analysing swimming speed we want to consider only tracks from actively swimming cells and remove any dead or non-motile cells. Very wiggly ('tortuous') tracks present another problem and while they are real tracks of swimming cells they can bias some analysis, particularly stop and run calculations.

Applying several ad hoc rules to remove problem tracks can introduce bias, as we remove tracks that do not fit our theories, but leaving all tracks tends to swamp information with noise. Track censoring can be done within the angle/speed and run/stop analysis software described later. For this work a specially written routine, CensorTracksFull.m, stored at

`\\HPSWA\Armitage\Useful␣Stuff\Tracking␣GUI\Extras`

written by Jennifer De Beyer was used to preprocess the file of tracks removing tracks in four categories and recording the numbers removed in each

category. The categories are: low bounding radius, long jumps between consecutive points, tortuosity and track length. The actual values used are chosen based on prior knowledge of *R. sphaeroides* behaviour. Track files before and after removal are viewed to check the process.

Values set to remove non-motile cells: Minimum Bounding Radius 9 μm, Top Speed Cutoff 90 μms^{-1} and discard the 5% most tortuous tracks, where tortuosity is defined as the median curvature, where curvature is the absolute value of the change of angle divided by the distance moved, taken for each frame to frame transition (Rosser 2013).

Values set to leave non-motile cells but remove badly connected tracks or tracks from dust in the system: Minimum Bounding Radius 0 μm, Top Speed Cutoff 90 μms^{-1}, do not discard tortuous tracks.

2.7.4 Analysing tracks - velocity, angles, runs and stops

Velocity and turns

The tracks files output by the tracking software can be analysed further.

Each track is a list of co-ordinates of object centroids in each frame in pixels, so speeds and angle changes can be calculated using the pixel size and frame rate. Between two frames of the video a bacterium moves from one place to another in a known time. This gives a speed for the frame to frame transition. After the first frame in which a particular bacterium appears, it has a direction of motion which will change from frame to frame. This gives an angle change for each frame to frame transition apart from the first transition (where we have no previous direction).

The fact that bacteria are swimming in three dimensions while this system measures tracks in two dimensions introduces some inaccuracy. Cells will move out of focus and a cell swimming at a steep angle to the field of view will appear to be moving more slowly since the measured distance is the projection onto the horizontal plane. Tracks moving roughly parallel to the

field of view will be measured more accurately, and will also stay in focus for longer and contribute more transitions to the data.

An example is shown in Fig. 2.10 which illustrates three consecutive positions for two different bacteria. The black cell moves from A to B to C in three consecutive frames, and the grey cell from a to b to c. The black cell has moved further in a frame, so is moving faster, and the grey cell has changed direction more, shown by the angle between the line segments ab and bc compared to that between AB and BC. With our videos we can not see the actual orientation of the bacteria, we just have the centroid positions, but this is enough to calculate speed and angle change at each point along a track.

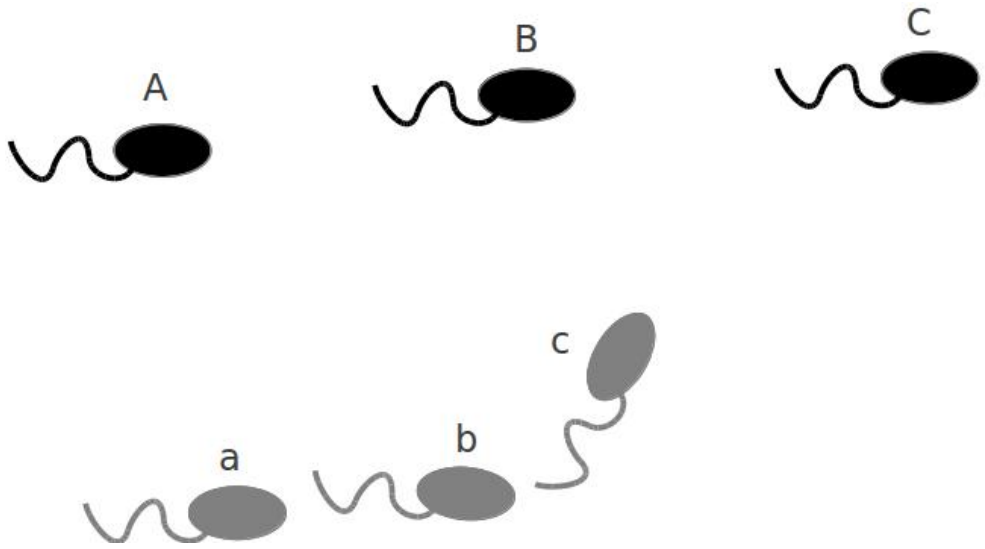


Figure 2.10: A drawing showing three consecutive positions of two bacteria moving at different speeds and angles.

If we take all speeds and angle changes in this way for all positions in all tracks of all cells, we can plot a two dimensional histogram of angle against speed for every frame to frame transition for all bacteria in the video, which gives a picture of the overall range of speeds and angles, and how the angle change between frames relates to the speed. A typical histogram of this sort for *R. sphaeroides* WS8N motile cells is shown in Figure 2.11. The software to calculate the speeds and angles which was used to produce this image was

written by David Wilkinson and is stored on

\\HPSWA\Armitage\Useful␣Stuff\Tracking␣GUI␣

.

2.7.5 MAC/NEMS plot

The two dimensional histogram of all transitions (Fig. 2.11) shows individual transition information not whole track information. To summarise the swimming behaviour of whole tracks a useful plot is MAC/NEMS, described by Mino et al. (2011) and used for checking censoring in Rosser et al. (2013).

Each track is summarised using two measures: the Mean Absolute Framewise Angle Change (MAC) and the Normalised Effective Mean Speed (NEMS).

The MAC is the mean of all the absolute values of angle changes for every transition in the track. For a straight line track it would be near zero, and for a tortuous track with many changes in direction it would be large.

The NEMS is a number between 0 and 1 and is also a measure of the straightness of the track, in terms of the distance actually travelled. It is calculated by finding the diameter of the smallest circle containing the track, the 'Minimum Bounding Diameter MBD' and diving it by the track duration to give the 'Effective Mean Speed' or EMS. The EMS is divided by the mean framewise speed to give the 'Normalised Effective Mean Speed' NEMS. If the whole track is a straight line, the NEMS will be 1. It measures directional persistance rather than actual speed of movement.

Plotting a 2D histogram of MAC against NEMS for a mixed population of swimmers and non swimmers gives two peaks, one with large angle changes and small actual movement, for the non swimmers, and one with smaller angle changes and larger movements for the swimmers. An example is Figure 2.12. This is very similar to the angle against speed histogram (Fig. 2.11) but for whole tracks. It can be used to check that non-motile cells have been removed correctly by the censoring process.

2.7.6 Noise and smoothing

The tracks can be noisy, swimming cells rotate and regular deviations in the centroid position can be due to wobble rather than forward motion. Smoothing, for example with a median filter, can be performed using MATLAB routines (The MathWorks, 2009) and will improve noisy tracks at the cost of losing detailed information.

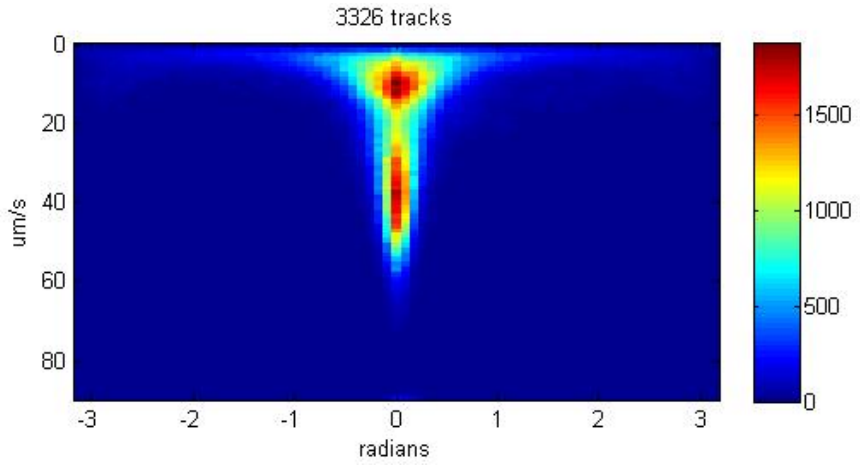


Figure 2.11: A two dimensional histogram showing speed and angle counts for all transitions of all tracks from a set of 9 videos of motile *R. sphaeroides* bacteria. There were 3326 tracks recorded, some long and some short. The data points plotted are from transitions between frames, so that a long track will contribute more data points than a short track. The scale shows the colour coding for the histogram, so that an orange cell indicates that 1500 data points had that value of angle and speed, blue cells show low counts. The measurements cluster around two peaks, one with high speed and the other with lower speed. The larger angles seem to correspond generally to lower speeds. The appearance of this histogram is consistent with the idea that some transitions belong to parts of track where the bacterium is swimming (runs) and other transitions correspond to parts of tracks where the bacteria is stopped and reorienting (stops).

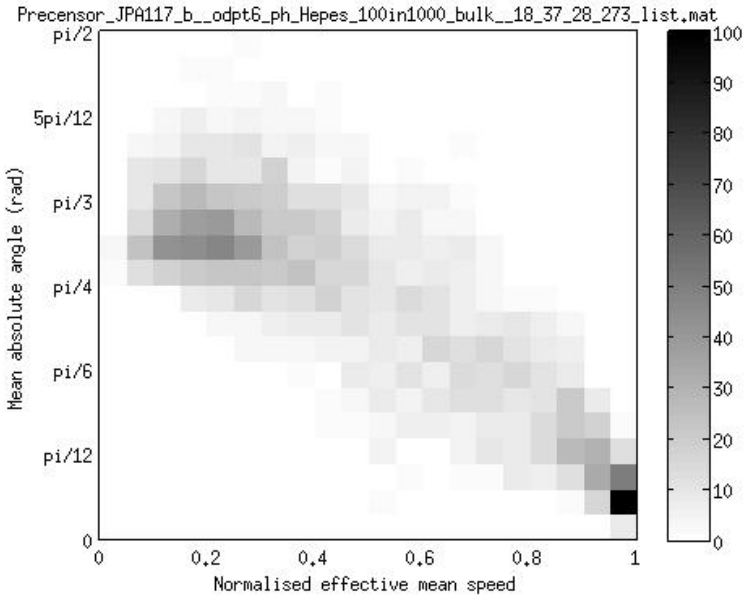


Figure 2.12: A MAC/NEMS plot, a 2 dimensional histogram of Mean Absolute Framewise Angle Change (MAC) against Normalised Effective Mean Speed (NEMS). Each track contributes one point to the histogram, however long it is. The squares in the bottom right corner are fairly straight tracks, those in the top left have high angle changes and did not travel far, so non-motile cells will appear there. A tortuous, wobbly track would travel reasonably far and have high angle changes.

Runs and stops

R. sphaeroides swims in a series of runs and stops, the single flagellum rotates during runs and is still during stops. During stops the cell body is reoriented by Brownian motion, so that the next run is in a different direction. During runs the direction of motion stays more constant, except at surfaces where the paths curve.

The duration of runs and stops is biassed by the presence of chemical or light gradients to allow the bacterium to swim towards favourable conditions. In the absence of such gradients the bacterium is believed to run and stop at random, with characteristic distributions of run and stop lengths (Berg, 1993). Stops are produced by the action of phosphorylated CheY response

regulators binding to the switch complex of the flagellar motor (Introduction section 1.12). The exact sequence of events for producing stops is not known, since in *R. sphaeroides* one flagellum is controlled by two separate sets of chemotaxis proteins and their interaction is only partially understood (Porter et al., 2011).

It is not usually possible to see whether a swimming bacterium has a rotating flagellum or not, and Brownian motion means that a 'stopped' bacterium may be moving with some speed, so it is not trivial to break tracks up into swimming and stopped sections. Information from both angle changes and speeds can be used. The distribution of angle changes differs in swimming and stopped bacteria, so does the distribution of speeds. This is an ideal situation for a Hidden Markov Model (HMM), with two states, running and stopped, which maps the observed speeds and angle changes back to the most likely sequence of underlying states.

The run/stop analysis software was written by Gabriel Rosser and is described in detail in Rosser et al., 2013.It is stored on

`\\HPSWA\Useful␣Stuff\RunStopAnalysisGabriel\gabriel_5_7_12\analysis_gui_WIN`

The program is trained for each new experiment using three reference distributions, as follows:

- Tracks from a non-motile strain are taken under the same conditions as the experimental strain.
- Tracks from a non stopping (smooth swimming) strain are taken under the same conditions as the experimental strain.
- Tracks from the experimental strain are taken.

The first two sets of tracks are used to generate distributions of angle changes and speeds during stops and during runs. The third is used to work out transition probabilities from a stop to a run and from a run to a stop for the experimental strain. Then the transition probabilities and the reference distributions are used together to allocate tracks of the experimental strain to

the most likely sequence of runs and stops. These data can highlight changes in run and stop behaviour in different strains or in different conditions.

A set of reference data is shown in Fig. 2.13 and a track divided into runs and stops is Fig. 2.14.

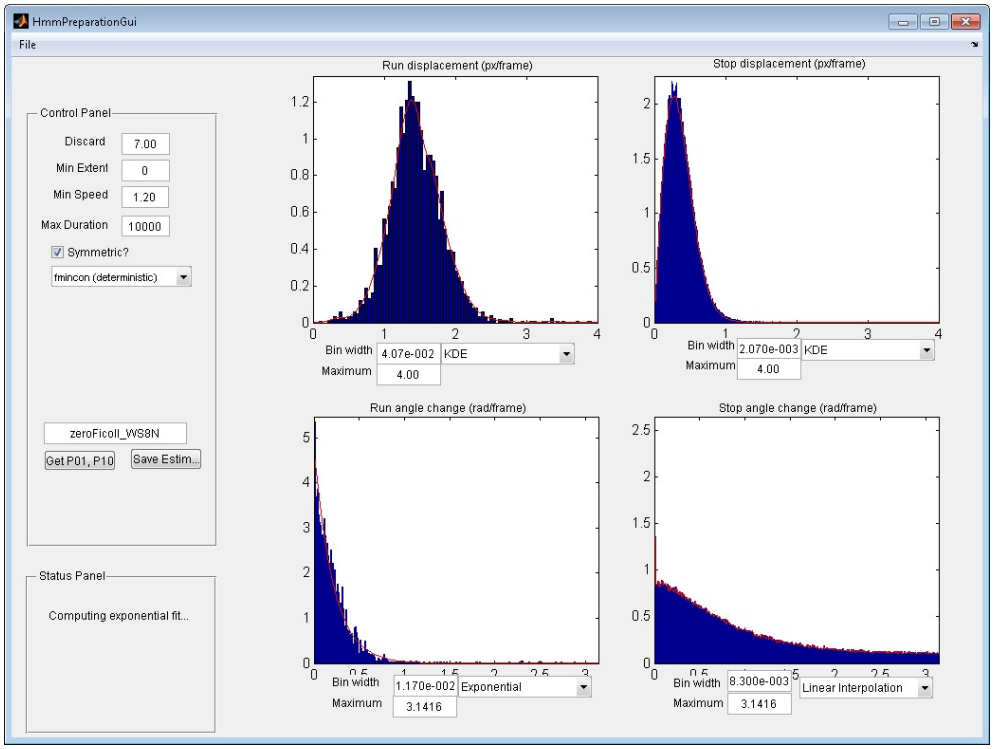


Figure 2.13: Speed and angle data for a non-motile strain and a smooth swimming strain calculated from video data and used to characterise behaviour during stops and runs. The motile strain is to the left, non-motile to the right. Speeds are at the top and angles at the bottom. The speed data show the higher speeds for the smooth swimmer, compared to the non-swimmer, and variability for both. The angle data from non-swimmers is more variable than that from swimmers, with larger angles. The control panel at the side allows you to choose parameters to filter the data set, for example to remove non-motile cells from the smooth swimming population. Under each graph you can choose the method for modelling that distribution. These models are used to break the tracks from the experimental strain into runs and stops.

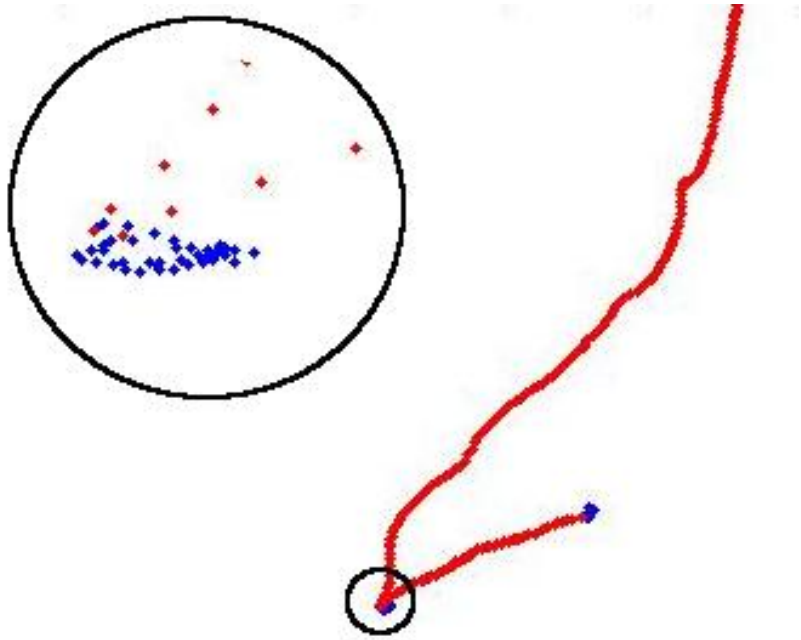


Figure 2.14: A single bacterial track divided into stops and runs using the HMM Run/Stop analysis software. Runs are red and stops are blue. Stops look short here because there is not much movement during a stop. The time between consecutive dots is .02s and the expanded section in the larger circle shows the stop in the small circle magnified to show the separatcompe positions recorded during the stop.

2.8 Analysing Confocal Images

2.8.1 Image Formats

Data from competitive assays between fluorescently labelled strains, time series flowcell data and three dimenstional z-stack data on microcolonies were acquired using the Nikon A1 confocal laser scanning microscope. The software running the microscope is NIS-Elements and the data files are .nd2 files, a proprietary format which is not made public. The NIS software can save or export files to other image formats, and has routines for image analysis.

The A1 microscope with the NIS software allows complex experiments to be

specified, for example a time series of three dimensional image stacks, and all image data and metadata for all captured images is stored in one .nd2 file.

Loci Bio-Formats open source java image file conversion software version 4.4.7 (Linkert et al., 2010) was used to read Nikon .nd2 files into the image analysis software MATLAB version 2009b (The MathWorks, 2009) and ImageJ version 1.46a (Schneider et al., 2012). Bio-Formats software is decribed here:

`loci.wisc.edu/software/bio-formats`

The .nd2 format occasionally changes without warning so external conversion programs can become out of date, this usually affects the metadata but has in the past changed the order of channels in the image files, so care is needed to make sure analysis programs stay correct.

The ImageJ plugin from Bio-Formats, loci_tools.jar, allows Nikon proprietary files to be directly understood and displayed in ImageJ, the MATLAB conversion produces a complex cell array that needs to be decoded programatically.

2.8.2 Image Channels

The A1 confocal allows several lasers and filter sets to be used at one time, as well as a DIC light channel. This gives several images of the specimen at different wavelengths. These can be analysed separately or combined to give a composite image.

The lasers and filters recommended by Nikon for CFP and YFP, or for GFP and mCherry were used, and 'bleed through' where one fluorophore is detected in the channel used for another, was minimised by using the 'line' scan setting as recommended by Nikon and by the choice of laser and gain settings.

The fluorophores were used to identify cells as being one type or another, the single image from one channel was used to count attached cells of one type, the combined image of both channels was used to see the positions of

all cells, for example to decide whether chains and microcolonies had both cell types, or whether the two strains being compared had different patterns of attachment. The DIC light channel was used to give a background image of cells and to check for contamination or non fluorescent cells.

2.8.3 Image Analysis

Software exists for analysing biofilm structure and coverage - COMSTAT (Heydorn et al., 2000) - but it is not suitable for the earliest stages of attachment nor for biofilms expressing more than one fluorophore.

To count cells and areas covered by cells a MATLAB script 'countCells' (Appendix 13) was written. The input is a series of Nikon format .nd2 files and the output is a set of files containing the centroid position and area of all detected objects in each channel. For each .nd2 file the two fluorescent images are displayed and there are options to display the centroids and objects detected. A global threshold is used, which is initialised using the MATLAB graythresh function, which is a global image threshold calculated using Otsu's method (Otsu, 1979). This can be changed by the user, independently for each channel, until the detected objects for each image in the set adequately match what is visible by eye.

Since fluorescence is used for identification and not for quantifying fluorescent protein, accurate matching by software of what is visible on an image is good enough for analysis, though for high throughput analysis an automatic threshold would be better. A global threshold can be used here when a local threshold was needed for phase contrast videos, because the fluorescent images are more uniform.

Noise is reduced and very small objects removed using MATLAB routines for morphologically opening and closing images. It is possible to subtract background for a set of images from measurements of image background and cell autofluorescence, and once settings for thresholding have been chosen there is an option to process all files with the same settings. There is an

option to superimpose detected objects on the original image and to magnify regions to check the accuracy of object detection.

Attachment begins with single bacterial cells and continues to groups of cells. When the cells are very close on the image it becomes difficult and unreliable to separate them into individual bacteria, even using a local threshold. To measure overall coverage a group of cells is detected as one object, and the area of the object shows that it consists of many cells.

Balancing CFP and YFP levels is important. The area around a cell or a group of cells has higher fluorescence than background, and the measured area is therefore sensitive to the threshold used. If this effect is different in the two channels, there may be bias in the measured areas, such that the same area of cells would appear larger in one channel than in the other. To avoid this, first the images should be taken carefully, without saturation. Then the different channels can be calibrated by measuring the area for individual cells or similar groups of cells in both channels. The experiments here compared cells expressing both fluorophores (Section 2.5.1), and so differences in detection levels will be noticed, and in fact there did seem to be a slight consistent bias overestimating the YFP channel.

The countCells interface is shown in Fig. 2.15. It will run on any operating system that can run MATLAB (The MathWorks, 2009).

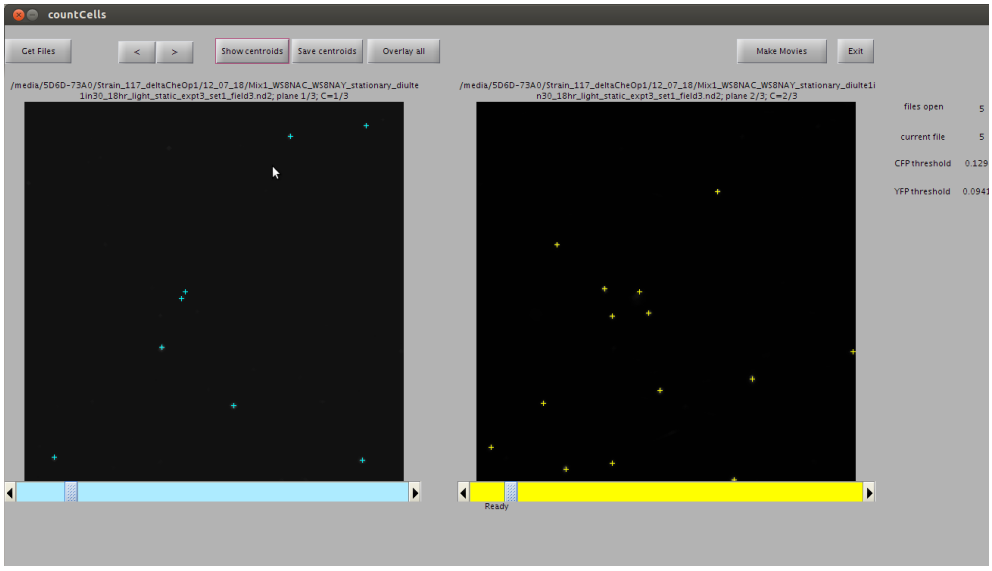


Figure 2.15: The 'countCells' interface showing centroids of objects in two channels of a confocal image. The two image panes show the two channels of one image. The sliders allow the threshold to be independently varied for each channel. The buttons at the top allow image files to be loaded, stepped through and viewed, show or hide the centroids of the detected areas, show the channels overlaid as a single image, and save the current set of detected centroids and areas to a file. The panel on the right shows the current settings, which are the number of open files, the current file being viewed, and the threshold values for each channel. The output is a file of centroids and areas of objects after thresholding.

2.9 Statistical Analysis

Statistical analysis of data was performed using scripts written in the R statistical software package (R Core Team, 2013).

2.9.1 Comparing two datasets

Where two datasets were compared, the Student's t-test was used for normally distributed data, and the Wilcoxon Signed Rank Test, (or Mann Whitney U Test) (Howell, 1995), a non-parametric alternative to the Students t-test which does not assume normally distributed data. was used for data that

was not normally distributed. For paired data the matched-pairs Wilcoxon test was used.

2.9.2 Comparing several datasets

Where several datasets were compared, Analysis of Variance (ANOVA) was used to test significant differences between groups when the variances were equal, and ANOVA with Welch's correction was used when the variances were not equal.

One way ANOVA (Fisher, 1928) can be used to show the existence of significant differences between groups of data, provided the data in each group is normally distributed, the group variances are equal and the data samples are independent. Independence of the data samples is part of the design of the experiment. Normality was tested using a Q-Q plot, and Bartlett's test was used to test the assumption of equal variances.

Where the variances of the groups were not equal, ANOVA was used with Welch's correction, using the R function oneway.test, and if significant differences were found between the means pairwise t tests with p values adjusted using Holm's method were used to determine which groups differed (Dalgaard, 2008; Holm, 1979; Welch, 1951).

2.10 Modelling

Modelling bacterial movement and attachment using partial differential equations was carried out using the MATLAB Partial Differential Equation Toolbox (The MathWorks, 2009).

Chapter 3

Attachment of motility and chemotaxis mutants of *Rhodobacter sphaeroides*

3.1 Introduction

Many bacteria, like *R. sphaeroides*, swim using one or more flagella, rigid helical structures which are turned by the flagellar motor to propel the cell through liquid medium.

Motility affects surface attachment in many species, some of which are listed in Section 1.8.

Chemotaxis, the sensitive and tuneable sensory system that stops or reverses the flagellar motor and leads to movement in a favourable direction, is sensitive to signal change across several orders of magnitude, adapts to recent conditions (Kojadinovic et al., 2013), and integrates many different signals so is ideal for controlling complex decision making in other areas than swimming (Section 1.8).

The *R. sphaeroides* chemotaxis system is discussed in Section 1.12. Previous

work in *R. sphaeroides* WS8N has found that mature biofilm structure is affected by deletions in both motility and chemotaxis genes, and that loss of any of the chemotaxis operons including the relatively uncharacterised chemotaxis operon 1 affects mature biofilm structure (Hale, 2009). It is not known at what point in *R. sphaeroides* WS8N biofilm development these differences first appear.

3.2 Aims

Initial surface attachment in various *R. sphaeroides* motility and chemotaxis mutants was compared to wild-type attachment, to find out whether and how motility and chemotaxis affect initial attachment in *R. sphaeroides*.

3.3 Strains used for motility experiments

The strains used are listed in Table 3.1. They include two without flagella, four with a flagellum but non motile, and two motile strains. The reason for using more than one mutant of each type was to decrease the chance that any measured changes are due to other changes associated with the mutation. In particular, for the four non-motile strains with flagella, *R. sphaeroides* JPA1213 and *R. sphaeroides* JPA1215 have a mutation in CheY6 that permanently stops the motor, *R. sphaeroides* JPA637 has one of the stator units deleted, so the motor is incomplete and does not turn, and *R. sphaeroides* JPA452 is non-motile for unknown reasons.

Table 3.1: The strains of *R. sphaeroides* used for motility experiments.

Strain	Description	Flagellum	Motile	Reference/source
WS8N	Wild type strain of *R. sphaeroides*	yes	yes	Sockett and Armitage (1991)
JPA452	Δ*orfE*	yes - possibly reduced number	no	Gift from A. Martin
JPA467	Δ*fliA*	no	no	Martin et al. (2006)
JPA635	Δ*fliC*	no	no	Gift from G. Wadhams
JPA637	Δ*motA* (missing stator unit)	yes, but may be detached	no	Gift from G. Wadhams
JPA1213	stopped motor - mutation *cheY6* D57N in place of *cheY6* in the chromosome	yes	no	Porter et al. (2006)
JPA1215	in-frame deletions of *cheY1–3,6* and the mutation *cheY6* D57N in place of *cheY6* in the chromosome	yes	no	Roberts et al. (2012)
JPA1353	no chemotaxis genes, non stopping phenotype	yes	yes - smooth swimmer	Porter et al. (2006)

These strains were constructed and characterised previously for chemotaxis experiments. In case of mutation or contamination they were checked in this work for motility and flagellation. Motility was checked using microscopy and swim plates (Materials and Methods 2.2.22). As expected, only *R. sphaeroides* WS8N and *R. sphaeroides* JPA1353 show any motility in swim plates (Fig. 3.1, 3.2).

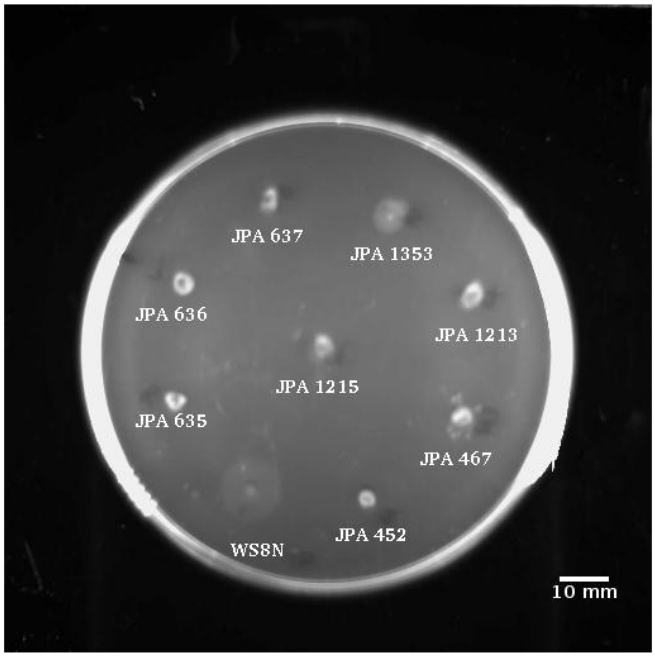


Figure 3.1: A swim plate, the larger thinner rings made by *R. sphaeroides* WS8N and *R. sphaeroides* JPA1353 can be seen, all other strains have hardly moved from the point of inoculation.

The presence of flagella were checked by Ryu staining (Heimbrook et al., 1989)(Figs. 3.3 - 3.8). This unexpectedly showed that *R. sphaeroides* JPA637 the MotA deletion strain seems to discard flagella as every image of this strain showed detached flagella on the slide.

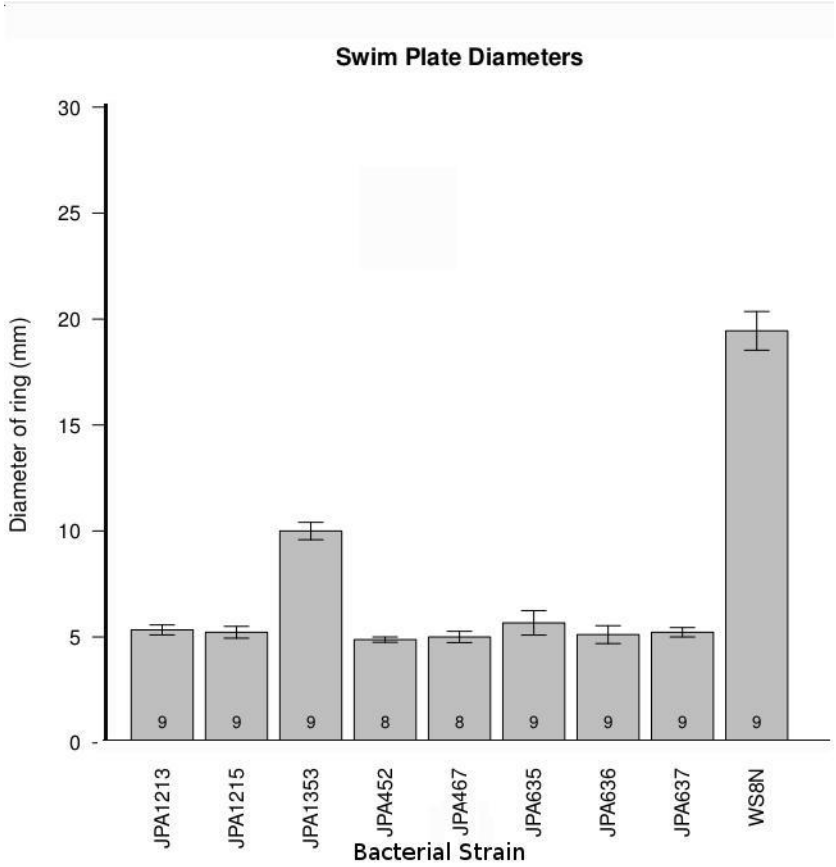


Figure 3.2: Diameters (mm) of rings formed in swim plates by strains used in motility experiments. Non motile strains do not move from the point of inoculation, motile and chemotactic strains make a large ring and motile but non-chemotactic strains make a smaller ring. Error bars are standard error, number of samples shown on bars. A one-way between subjects ANOVA was conducted to compare the effect of strain on swim ring diameter. Swim ring diameter differed significantly as a function of strain, $F(8,72) = 118.4$, $p<0.001$. Tukey's post hoc tests showed that the *R. sphaeroides* WS8N swim ring diameter differed from all others ($p<0.001$) and *R. sphaeroides* JPA1353 swim ring diameter differed from all others ($p<0.001$) but no other differences were significant.

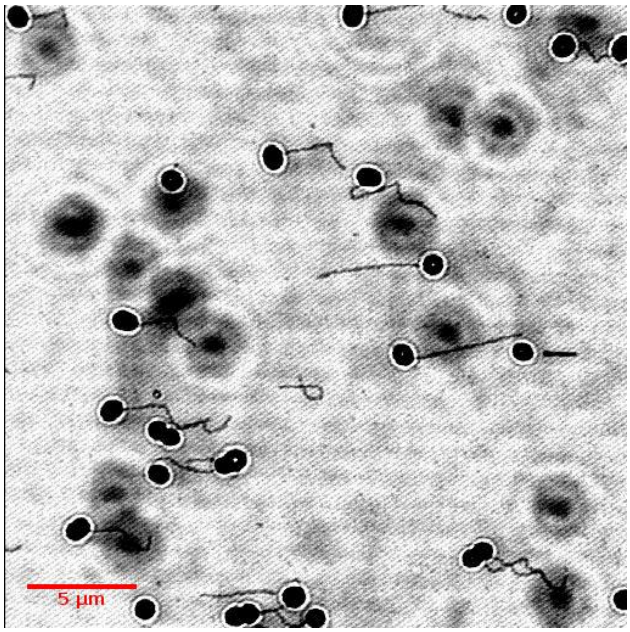


Figure 3.3: Ryu (Section 2.3.2) staining of log phase *R. sphaeroides* WS8N showing flagella.

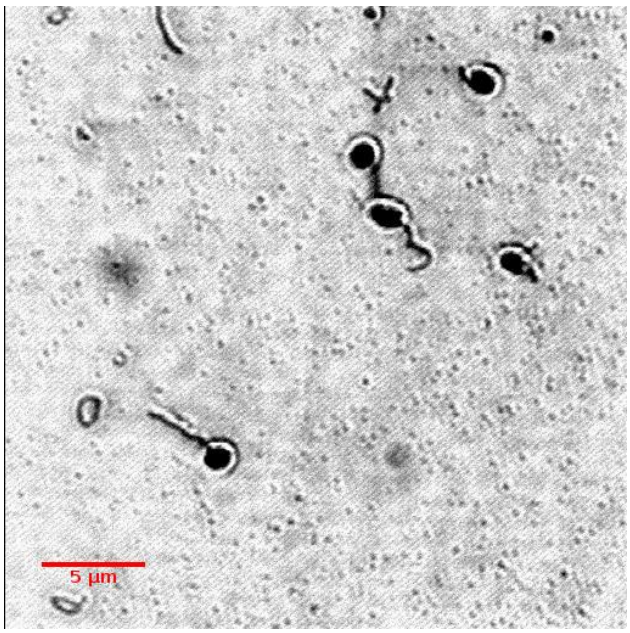


Figure 3.4: Ryu (Section 2.3.2) staining of log phase *R. sphaeroides* JPA1353 showing flagella.

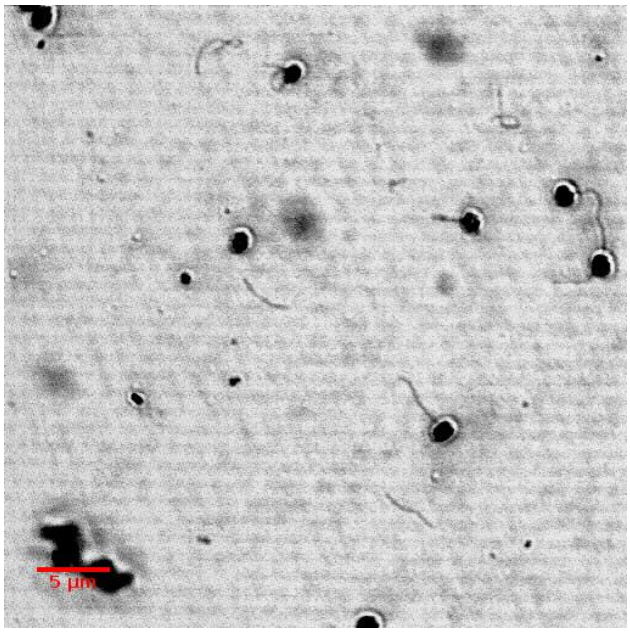


Figure 3.5: Ryu (Section 2.3.2) staining of log phase *R. sphaeroides* JPA1213 showing flagella.

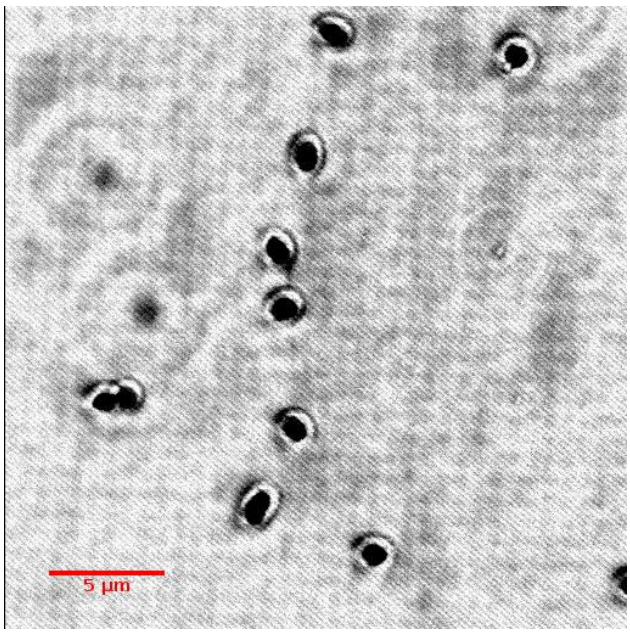


Figure 3.6: Ryu (Section 2.3.2) staining of log phase *R. sphaeroides* JPA467 showing no flagella.

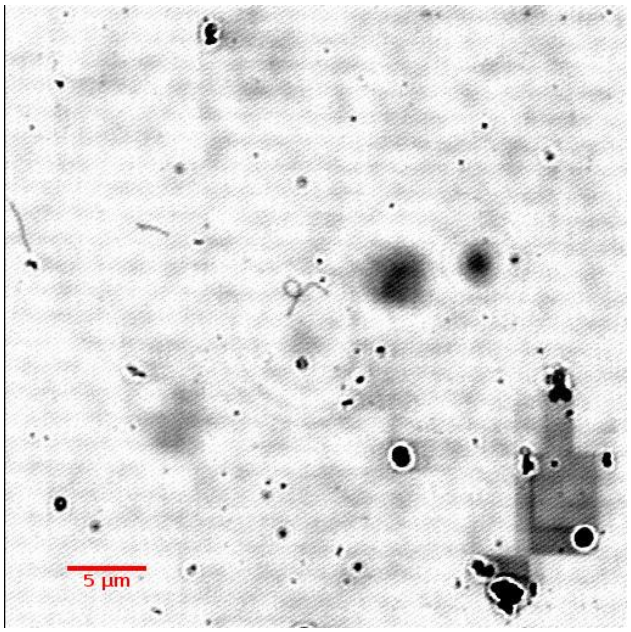


Figure 3.7: Ryu (Section 2.3.2) staining of log phase *R. sphaeroides* JPA452 showing some flagella.

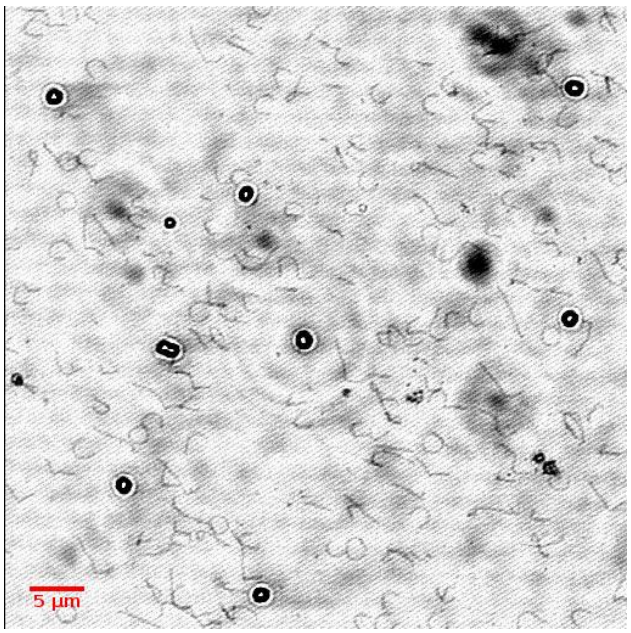


Figure 3.8: Ryu (Section 2.3.2) staining of log phase *R. sphaeroides* JPA637 showing many detached flagella.

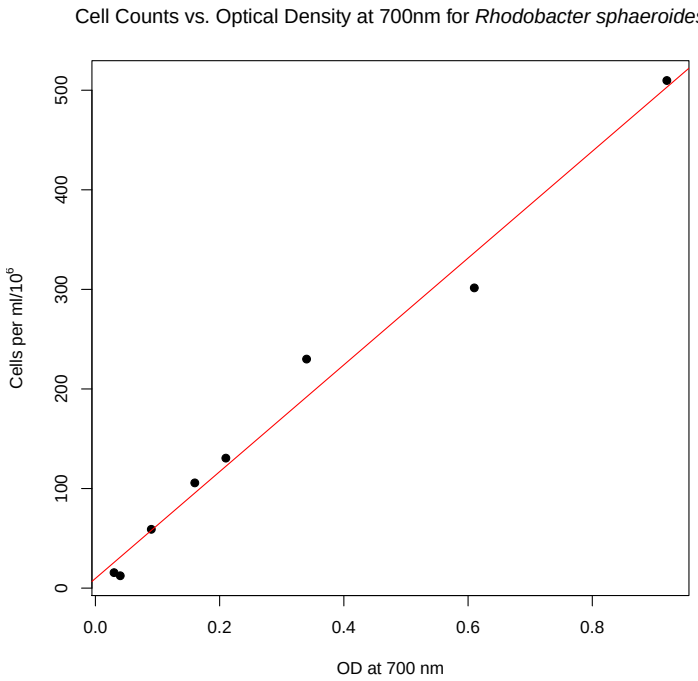


Figure 3.9: Cell numbers related to OD_{700} for aerobically grown *R. sphaeroides*. Graph adapted from Gauden (1996).

3.4 Attachment in motility mutants

Non-motile mutants of *R. sphaeroides* are known to form reduced amounts of biofilm over 5 days (Hale, 2009) compared to motile strains.

The experiments in this section were designed to find out whether motility affected attachment at earlier stages, from 30 minutes to 6 hours after first access to a sterile surface.

It was assumed that the levels of growth, nutrients and wastes will not change very much in 30 minutes, since *R. sphaeroides* is slow growing. *R. sphaeroides* doubling time in when grown photoherotrophically as described in Section 2.2.2 is roughly 2 hours (data not shown). Over 6 hours there will be changes in the composition of cultures which may affect attachment.

3.4.1 In static assays do *R. sphaeroides* motile strains attach more in 30 minutes than non-motile strains?

This experiment was designed to test the hypothesis that non-motile strains attach to an abiotic surface less frequently than motile strains over 30 minutes. Photoheterotrophically grown cells in log phase were used, so that the motile cells were actively swimming during the experiment.

Three separate cultures of each strain in Table 3.1 were grown photoheterotrophically to OD_{700} approximately 0.4 (Section 2.2.2). The cultures were then diluted with succinate medium (Appendix 11.0.3) in proportion to their measured OD_{700}, so that all were at OD_{700} 0.3 and the number of cells in each well was roughly the same, around $1.8x10^8$ cells per ml (Fig. 3.9). 100 μl of each culture was incubated in the light in 96 well plates as described in Section 2.3.1. Each plate contained eight samples of each strain and eight control wells containing only succinate medium (Appendix 11.0.3) and was assayed for biofilm formation by crystal violet staining (Section 2.3.1). The mean of the control wells was subtracted from the measured absorbances shown on Figure 3.10.

A one-way between subjects ANOVA was conducted to compare the effect of strain on attachment. Attachment differed significantly as a function of strain for log phase photoherotrophically grown cultures (Fig. 3.10).

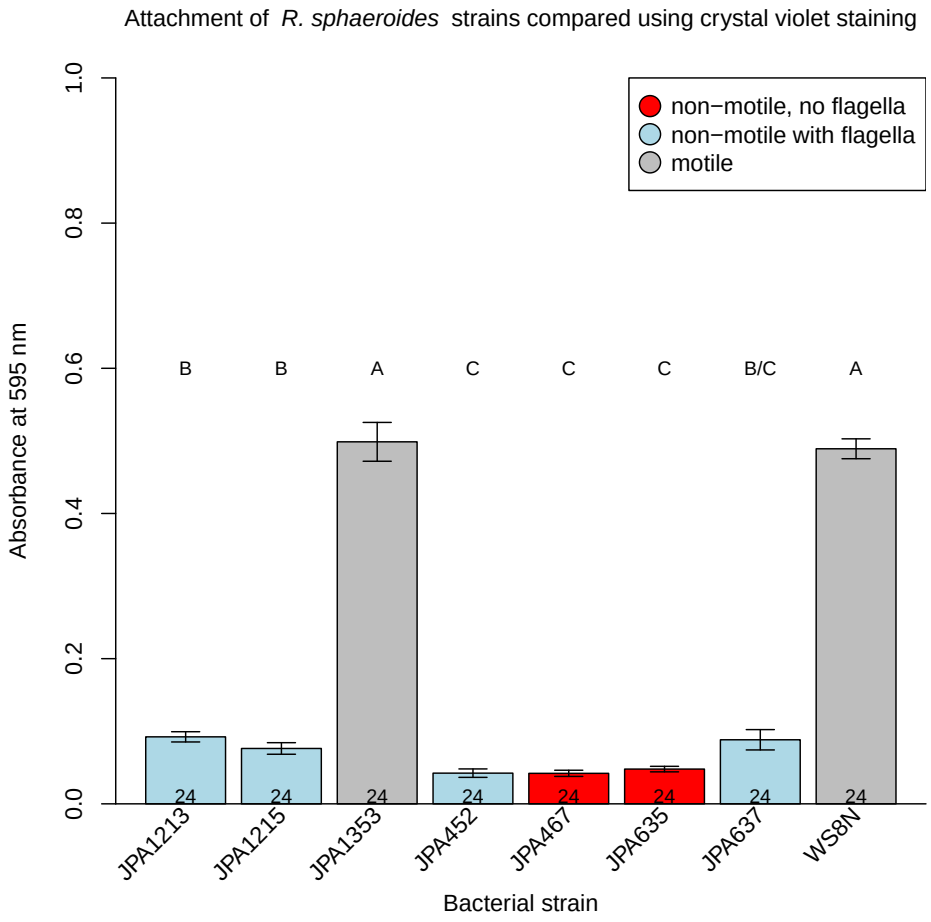


Figure 3.10: Absorbance measured at 595nm of Crystal violet released from attached log phase photoheterotrophically grown cells after 30 minutes incubation in light. Error bars are standard error. Numbers of wells tested are shown at the base of each bar. A one-way between subjects ANOVA with Welch's correction (Section 2.9.2) was conducted to compare the effect of strain on absorbance. Absorbance differed significantly as a function of strain for log phase photoheterotrophic cultures, $F(7,77.5) = 177.1$, $p<2.2e-16$. Post-hoc pairwise t-tests with Holm's correction (Section 2.9.2) showed that the two motile strains had significantly higher absorbance, and hence attachment, than the other groups ($p<0.001$). The letters above the bars show three groups of strains, A, B and C clustered by significant differences at $p<0.05$. This suggests that the flagellated but non-motile strains attach more than the aflagellate strains, though *R. sphaeroides* JPA452 groups with the aflagellate strains. *R. sphaeroides* JPA637 could be assigned to either group B or C.

3.4.2 Non motile strains - does having a flagellum help or hinder attachment in static conditions?

Some bacteria attach to surfaces less when they have a non-functional flagellum than when they have no flagellum (Merritt et al., 2007). This does not seem to be the case for *R. sphaeroides*. Focussing only on the non motile strains using the same data as in the previous section shows the differences more clearly (Fig. 3.11).

R. sphaeroides flagella are known to stick to surfaces, spontaneously tethering the cells, so possessing a flagellum, even if non-functional, could increase stickiness. However, *R. sphaeroides* flagella curl up near the cell when unpowered (Fig. 3.12) and the shape may hinder access of the cell body to the surface after initial flagellar attachment. A possible reason for a slight advantage of having a flagellum is the presence of discarded flagella seen on the stained slides of some flagellated but non-motile mutants, particularly *R. sphaeroides* JPA637, which may make the surface stickier (Fig. 3.8). This possible preconditioning should be tested in further work. *R. sphaeroides* JPA452, the *orfE* deletion strain, seems more like the two aflagellate strains, and when the presence of flagella were checked using Ryu staining, though flagella were seen they were very sparse (Fig. 3.7) suggesting that not all cells of that strain produce flagella.

3.4.3 In stationary phase cultures, motile strains no longer swim. Does this affect attachment?

This experiment was designed to test the hypothesis that motile strains attach to an abiotic surface less frequently in stationary phase, when the motile strains are not actively swimming, and that the difference between motile and non-motile attachment will be reduced in stationary phase cells.

Cultures of each strain in Table 3.1 were grown photoheterotrophically to OD_{700} approximately 1.2 (Section 2.2.2). and were incubated for 30 min-

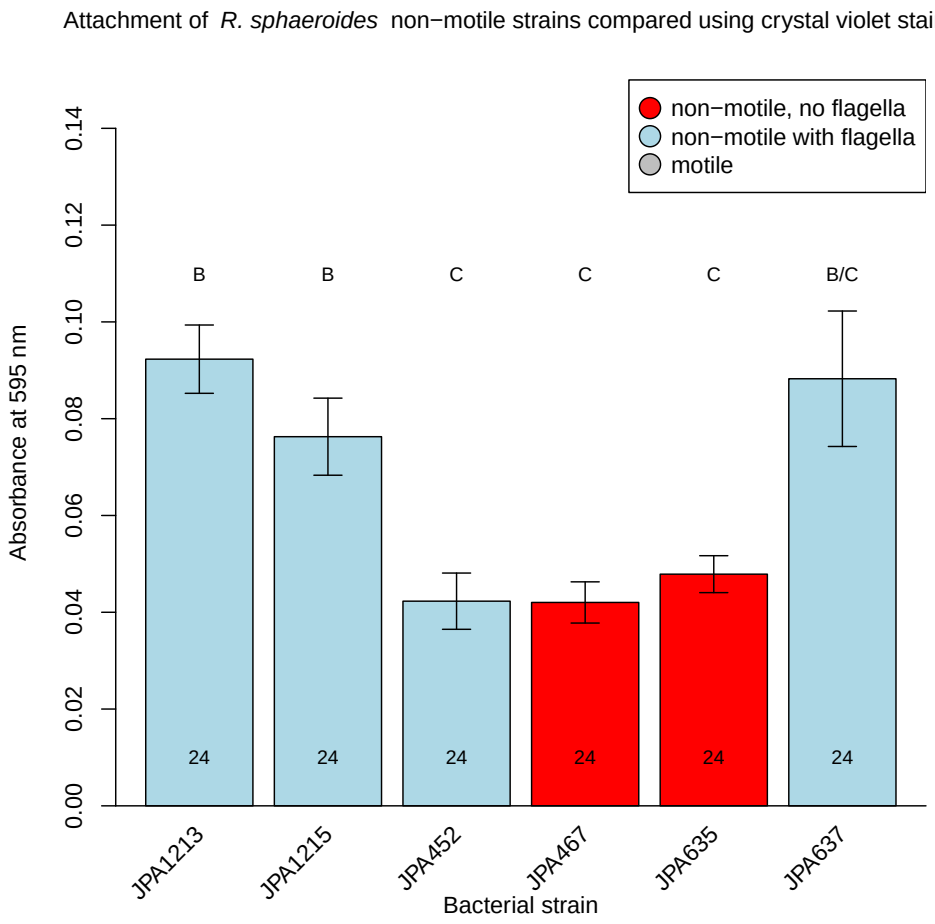


Figure 3.11: The non-motile strain data extracted from Fig. 3.10. The letters B and C show clustering by significant differences at $p<0.05$ using ANOVA with Welch's correction and post-hoc pairwise t-tests with Holm's correction (Section 2.9.2)

.

utes in light in 96 well plates as described in Section 2.3.1. This implies around 7.2×10^8 cells per ml (Fig. 3.9). The actual numbers could differ since the straight line relationship between OD_{700} and cell count breaks down as cells reach stationary phase (personal communication, Dr.David Wilkinson). However, the numbers of cells should be similar in each culture and greater than in the log phase cultures shown in Figure 3.10.

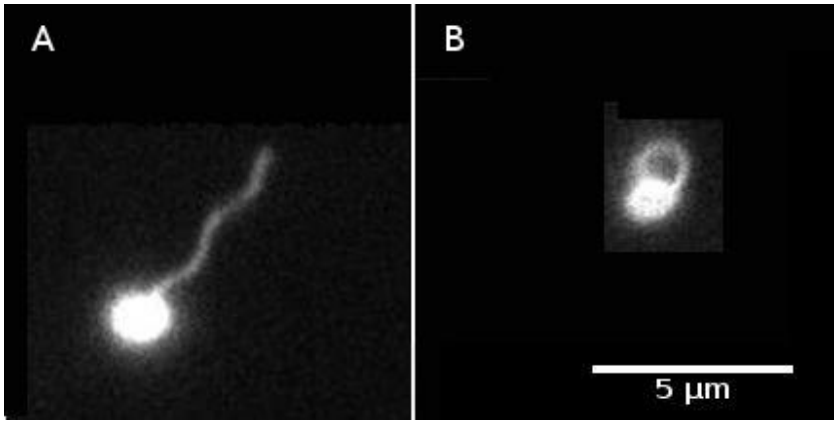


Figure 3.12: Swimming *R. sphaeroides* stained with Cy3 fluorescent dye, A) swimming and B) stopped. The image was taken using the staining protocol in Section 2.3.3. The separate images were selected from video frames, and whether a bacterium was swimming or stopped was judged by eye.

Attachment was reduced for the motile strains compared to log phase cultures of the same strains, and the difference between motile and non motile strains was reduced (Figs 3.13,3.14). This suggests that it may be the loss of motility in stationary phase cultures that reduces attachment. Other possibilities are that adhesins necessary for attachment are not produced at stationary phase or that the more crowded conditions inhibit attachment through quorum sensing. In figure 3.14, some of the non motile strains seems to have increased attachment at stationary phase, but in fact there were far more bacteria per well. There are many changes at stationary phase that could also influence attachment, but they are unlikely to act differently in the motile strains specifically and it is likely that at least part of the reduction in attachment is due to the reduction in motility of cells in stationary phase.

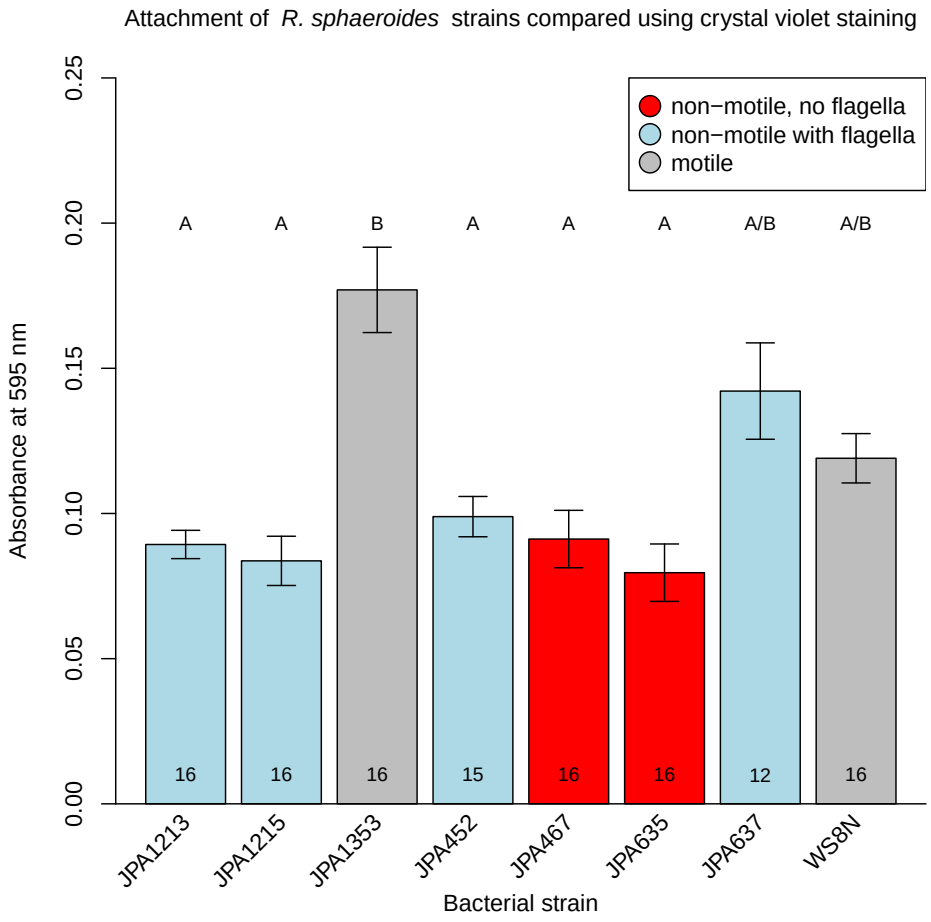


Figure 3.13: Absorbance measured at 595nm of Crystal violet released from attached stationary phase photoheterotrophically grown cells after 30 minutes incubation in light. Error bars are standard error. Numbers of wells tested are shown at the base of each bar. A one-way between subjects ANOVA with Welch's correction (Section 2.9.2) was conducted to compare the effect of strain on absorbance. Absorbance differed significantly as a function of strain for stationary phase photoheterotrophic cultures, $F(7,47.6) = 6.86$, $p = 1.184e\text{-}05$. Post-hoc pairwise t-tests with Holm's correction (Section 2.9.2) showed that only the smooth swimming strain *R. sphaeroides* JPA1353 had significantly higher absorbance, and hence attachment, other groups ($p<0.05$). The letters above the bars show two groups of strains, A and B clustered by significant differences at $p<0.05$. *R. sphaeroides* JPA637 and WS8N could be assigned to either group A or B. This suggests that the greater attachment of the motile strains disappears or is reduced in stationary phase cultures.

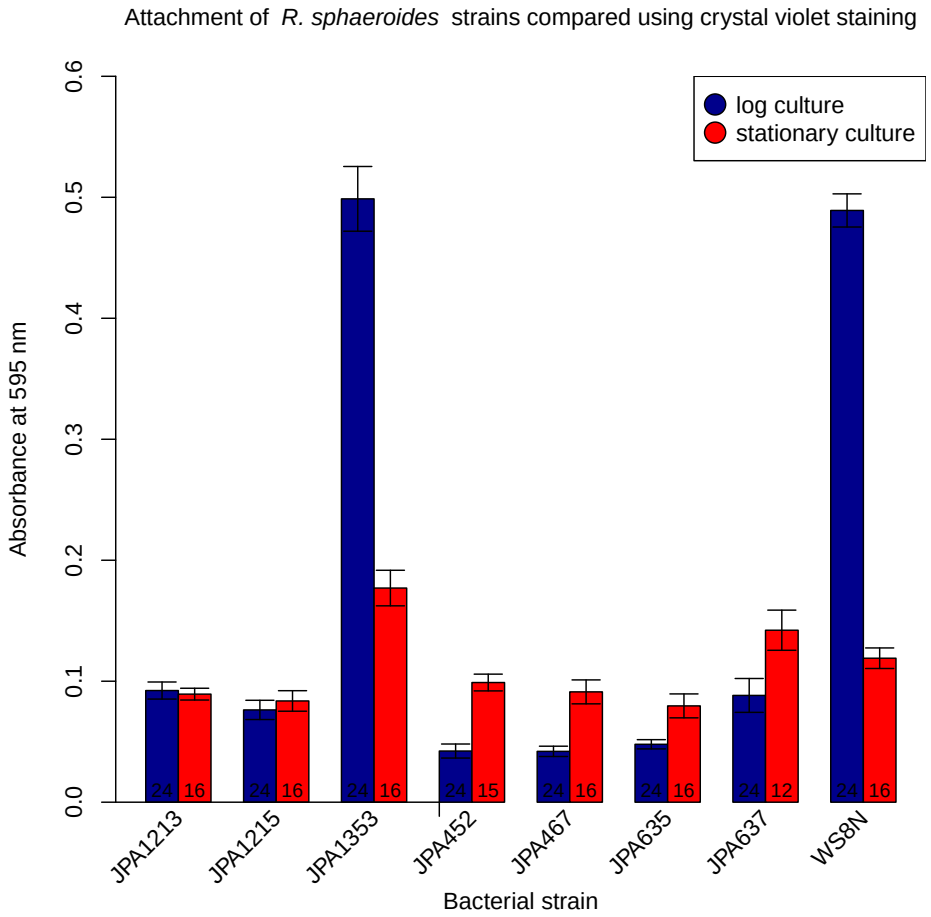


Figure 3.14: Absorbance measured at 595nm of Crystal violet released from attached stationary and log phase photoheterotrophically grown cells after 30 minutes incubation in light. Error bars are standard error. Numbers of wells tested are shown at the base of each bar. This graph shows the data from Fig. 3.10 and Fig. 3.13 together to show that the effect of being in a stationary phase culture is different for the motile and the non motile cells. The two datasets were not compared to each other statistically because of the different concentrations of cells, which means that nearly equal attachment, as for JPA1213, is hard to interpret. However the large drop in attachment for the motile cells is not seen in the non-motile cells.

3.4.4 In many species non-motile cells attach more in moving than in static conditions, does shaking the culture change the relationship between motility and attachment?

This experiment was designed to discover whether non-motile strains attach to an abiotic surface less frequently than motile strains over 30 minutes when the culture is moved by shaking. Photoheterotrophically grown cells in log phase were used, so that the motile cells were actively swimming during the experiment.

Separate cultures of each strain in Table 3.1 were grown photoheterotrophically to OD_{700} approximately 0.4 (Section 2.2.2). The cultures were then diluted with succinate medium (Appendix 11.0.3) in proportion to their measured OD_{700}, so that all were at OD_{700} 0.3 and the number of cells in each well was roughly $1.8x10^8$ cells per ml. 200μl samples of each culture were added to 96 well plates as described in Section 2.3.1. The 96 well plates were then incubated for 30 mins at 30^{o}C in a rotary shaking incubator (Innova) at 225 rpm. The aim was to see whether movement in the fluid altered the attachment advantage of motile cells. Each plate contained eight samples of each strain and eight control wells containing only succinate medium (Appendix 11.0.3). The wells were assayed for biofilm formation by crystal violet staining (Section 2.3.1). The mean of the control wells was subtracted from the measured absorbances shown on Figure 3.15.

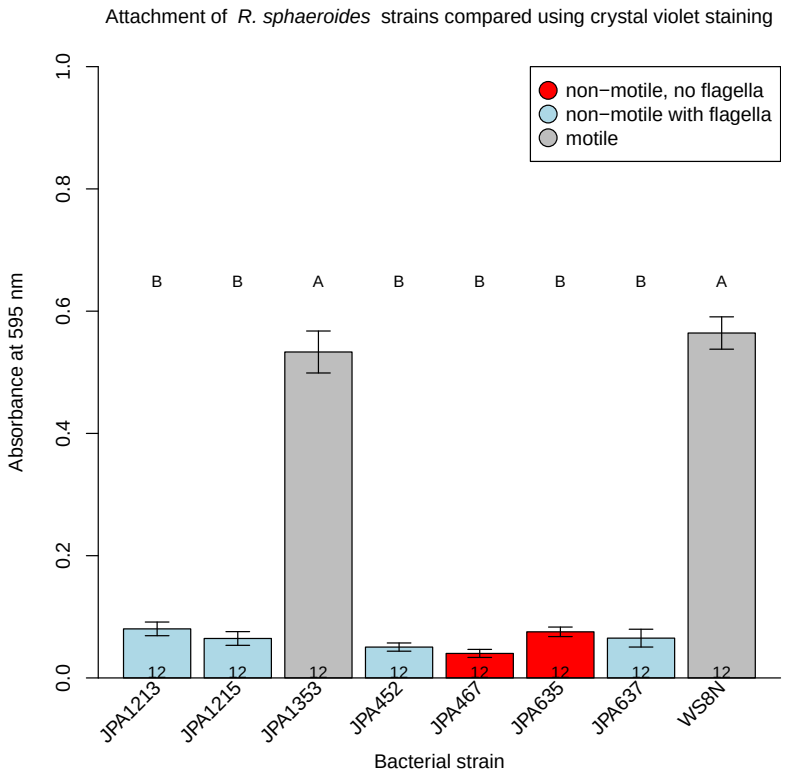


Figure 3.15: Absorbance measured at 595nm of Crystal violet released from attached log phase photoheterotrophically grown cells after 30 minutes incubation with shaking at 225 rpm. Error bars are standard error. Numbers of wells tested are shown at the base of each bar. A one-way between subjects ANOVA with Welch's correction (Section 2.9.2) was conducted to compare the effect of strain on absorbance. Absorbance differed significantly as a function of strain for log phase photoheterotrophic cultures incubated with shaking, $F(7,37.2) = 72.5$, $p < 2.2e\text{-}16$. Post-hoc pairwise t-tests with Holm's correction (Section 2.9.2) were performed to identify different strains. The letters above the bars show two groups of strains, A and B, clustered by significant differences at $p < 0.05$. This suggests that the actively swimming strains attach more than non-motile strains in moving fluid. The differences in attachment between aflagellate strains and non-motile strains with flagella were not significant.

Comparing the results from Figure 3.10 and Figure 3.15 shows that there is little difference between attachment in still and moving conditions, for log phase photoheterotrophically grown *R. sphaeroides* strains. The results are compared in Figure 3.16. Where any difference was found between still and shaking conditions, attachment was greater in still conditions. This could be because bacteria are more likely to be dislodged before they can firmly attach when the fluid around them is moving. However, for most of the strains no difference was found.

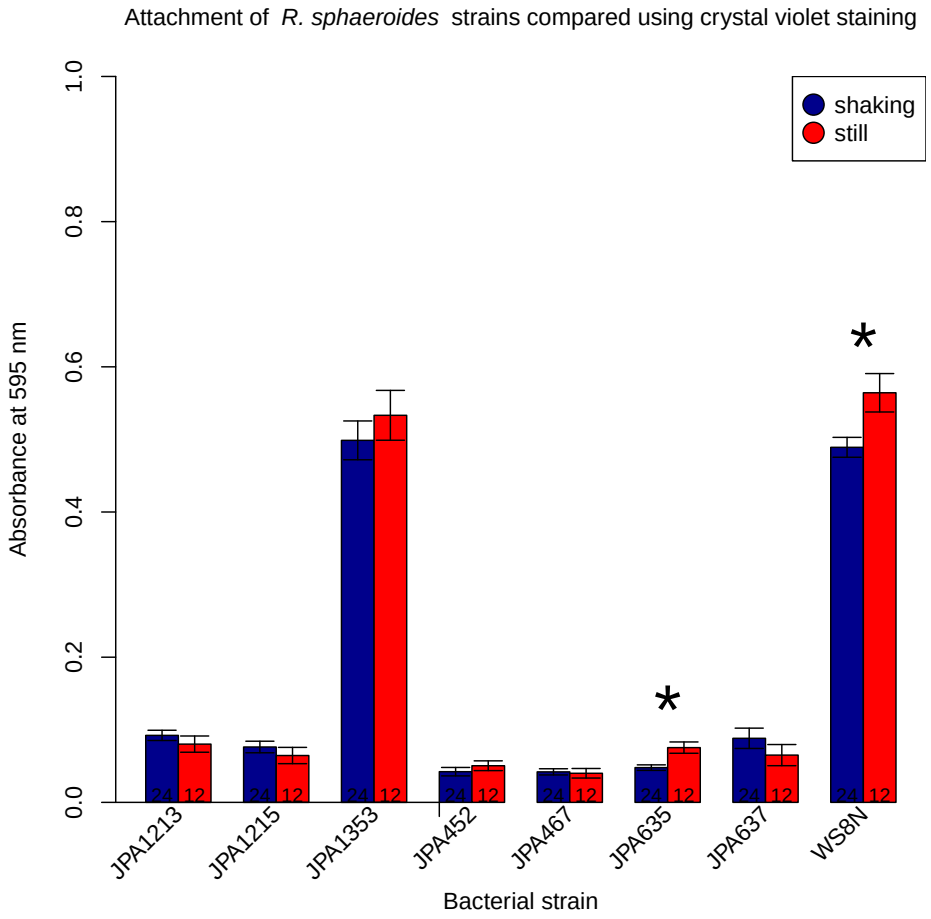


Figure 3.16: Absorbance measured at 595nm of Crystal violet released from attached log phase photoheterotrophically grown cells after 30 minutes incubation, still (red) or with shaking (blue) at 225 rpm. Error bars are standard error. Numbers of wells tested are shown at the base of each bar. Student's t-tests were performed (Section 2.9) to compare the means for each strain in the two conditions. Where differences were significant at the $p<0.05$ level, the bars are marked by a star. There was a significant difference in attachment for WS8N and *R. sphaeroides* JPA635, a motile and a non-motile strain, and in both cases attachment was higher in still conditions.

3.5 Attachment of chemotaxis mutants

It is known that the loss of any of the three *R. sphaeroides* chemotaxis operons (Figure 3.17) affects biofilm formation after 5 days (Hale, 2009) but it is not known how early a difference can be detected, or whether the difference is simply due to chemotaxis as nutrient, waste and oxygen gradients build up in a developing biofilm. The chemotaxis system is involved in sensing light and oxygen as well as chemoattractants (Section 1.12) and could potentially be involved in surface sensing.

The presence of a largely uncharacterised chemotaxis operon (*cheOp1*) and the involvement of chemotaxis-like operons in biofilm formation in other species is another reason for testing chemotaxis mutants for attachment (Section 1.8). Chemotaxis in *R. sphaeroides* is described in more detail in Section 1.12.

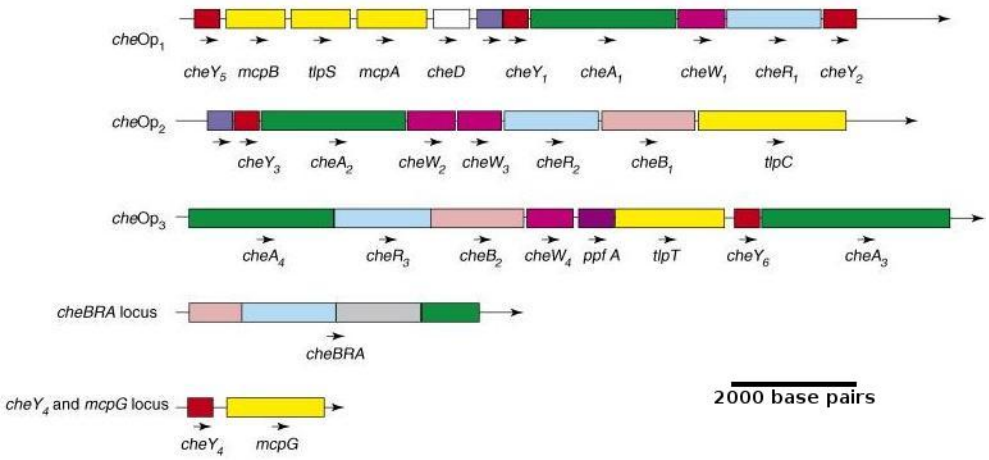


Figure 3.17: The chemotaxis operons and gene clusters in *R. sphaeroides*. The arrows show the direction of transcription, the cheBRA locus is a single fusion protein. The colours highlight homologous genes, for example *cheA*-like genes and parts of genes are coloured green. There are several homologues of each of the chemotaxis genes found in *E. coli*, organised in three main operons. As well as the six chemoreceptor genes shown here (*mcp* and *tlp* genes, yellow) there are seven more chemoreceptors in unlinked loci. It is not yet known what each chemoreceptor is sensing. Image adapted from Porter et al. (2008)

Table 3.2: The strains of *R. sphaeroides* used for chemotaxis attachment experiments.

Strain	Description	Chemo tactic	Motile	Reference/source
WS8N	Wild type strain of *R. sphaeroides*	yes	yes	Sockett and Armitage (1991)
JPA635	Δ*fliC*	no	no	Gift from G. Wadhams
JPA117	Δ*cheOp1* - no known phenotype change	yes	yes (wild-type)	Hamblin et al. (1997)
JPA403	Δ*cheOp2* - no polar chemotaxis cluster	no	yes ('stoppy')	Shah et al. (2000)
JPA1419	Δ*cheOp3* - no cytoplasmic chemotaxis cluster	no	yes (smooth)	Gift from G. Wadhams
JPA1353	No chemotaxis genes	no	yes (smooth)	Gift from S. L. Porter
JPA1336	Δ*cheY6*	no	yes (smooth)	Porter et al. (2002)

3.5.1 Strains used for chemotaxis experiments

Strains are shown in Table 3.2. The classification of swimming as 'stoppy' (frequent stops) or smooth (few stops) compared to wild-type is based on visual impression of log phase cultures using phase contrast microscopy, but is explored in more detail using tracking and free swimming analysis in Chapter 4. The chemotactic behaviour of the strains was established previously (Hamblin et al., 1997; Porter et al., 2002; Shah et al., 2000).

R. sphaeroides WS8N and *R. sphaeroides* JPA635 were used as controls, showing wild-type and non-motile levels of attachment respectively.

3.5.2 Comparison between attachment of photoheterotrophically grown chemotaxis mutants over 30 minutes

Starting with log phase cultures

This experiment was done to test the hypothesis that there would be no difference in attachment between chemotactic and non-chemotactic motile cells in the first 30 minutes of attachment.

Separate cultures of each strain in Table 3.2 were grown photoheterotrophically to OD_{700} approximately 0.4 (Section 2.2.2). The cultures were then diluted with succinate medium (Appendix 11.0.3) in proportion to their measured OD_{700}, so that all were at OD_{700}=0.3 and the number of cells in each well was roughly the same, around $1.8x10^8$ cells per ml. 200μl samples of each culture were incubated in light in 96 well plates as described in Section 2.3.1. Each plate contained eight samples of each strain, and eight wells containing only succinate medium (Appendix 11.0.3). The wells were assayed for biofilm formation using crystal violet (Section 2.3.1). The mean of the control wells was subtracted from the measured absorbances shown on Figure 3.18.

The results show statistically significant differences between the strains ($p<0.05$), with all strains attaching more than the non-motile control (Fig 3.18).

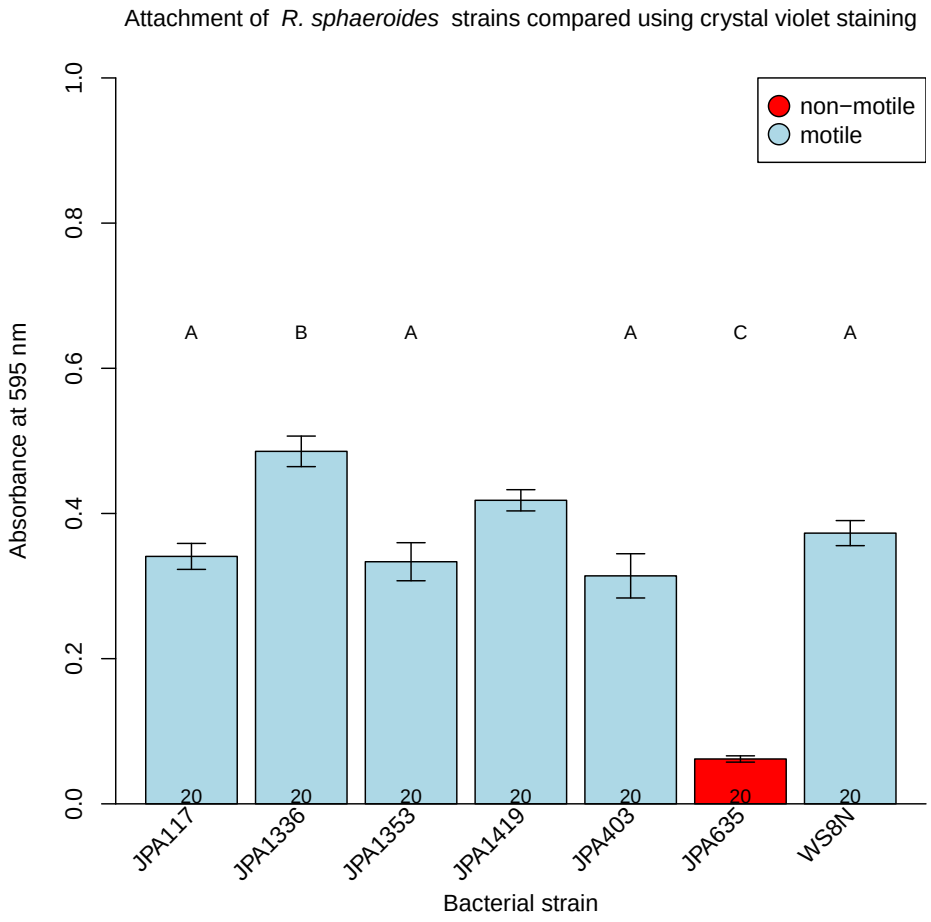


Figure 3.18: Absorbance measured at 595nm of Crystal violet released from attached log phase photoheterotrophically grown cells after 30 minutes incubation in light. Error bars are standard error. Numbers of wells tested are shown at the base of each bar. A one-way between subjects ANOVA with Welch's correction (Section 2.9.2) was conducted to compare the effect of strain on absorbance. Absorbance differed significantly as a function of strain for log phase photoheterotrophic cultures incubated with shaking, $F(6,54.3) = 211.945$, $p<2.2e\text{-}16$. Post-hoc pairwise t-tests with Holm's correction (Section 2.9.2) were performed to identify different strains. The letters above the bars show three groups of strains, A, B and C, clustered by significant differences at $p<0.05$. Strain JPA1419 was significantly different from Strain JPA403 ($p = 0.047$) in group A but not different from *R. sphaeroides* WS8N or JPA1336, and did not fit into either group.

The only strain attaching significantly more than wild type *R. sphaeroides* WS8N was the smooth swimming *cheY6* deletion strain *R. sphaeroides* JPA1336 ($p = 0.003$), and the only strain attaching significantly less than WS8N was the non-motile mutant control *R. sphaeroides* JPA635. Of the chemotaxis operon deletions, *R. sphaeroides* JPA403, the *cheOp*2 deletion, which stops more frequently than WS8N, attached significantly less than *R. sphaeroides* JPA1419 ($p = 0.047$), the smooth swimming *cheOp*3 deletion. These data suggest that smooth swimming strains may attach better to surfaces than strains with frequent stops.

However, in this experiment the smooth swimming *R. sphaeroides* JPA1353 strain with all chemotaxis genes deleted attached at levels indistinguishable from wild-type WS8N. If it is true that, other things being equal, smoother swimmers will attach more than swimmers which stop frequently , there could be another reason for the wild-type initial attachment behavour of smooth swimming *R. sphaeroides* JPA1353. For example, it could swim more slowly, or have a higher proportion of non swimmers in a population. Frequency of stops in different *R. sphaeroides* mutants has been classified by eye (Brown, 2009) but has been difficult to quantify in free swimming cells.

Starting with stationary phase cultures

This experiment was done to test the hyothesis that motile cells, whether chemotactic or not, have reduced attachment in stationary phase, and differ less from non-motile cells.

Separate cultures of each strain in Table 3.2 were grown photoheterotrophically to OD_{700} approximately 1.2 (Section 2.2.2). The cultures were then diluted with succinate medium (Appendix 11.0.3) in proportion to their measured OD_{700} , so that all were at OD_{700} 0.3 and the number of cells in each well was roughly the same, around 7.2×10^8 cells per ml. 200μl samples of each culture were incubated in light in 96 well plates as described in Section 2.3.1. Each plate contained eight samples of each strain, and eight wells containing only succinate medium (Appendix 11.0.3). The wells were assayed

for biofilm formation using crystal violet (Section 2.3.1). The mean of the control wells was subtracted from the measured absorbances shown on Figure 3.19.

As seen previously (Fig. 3.14), growth to stationary phase significantly reduced the level of attachment of the potentially motile strains compared to starting with mid log phase cultures. (Fig 3.19).

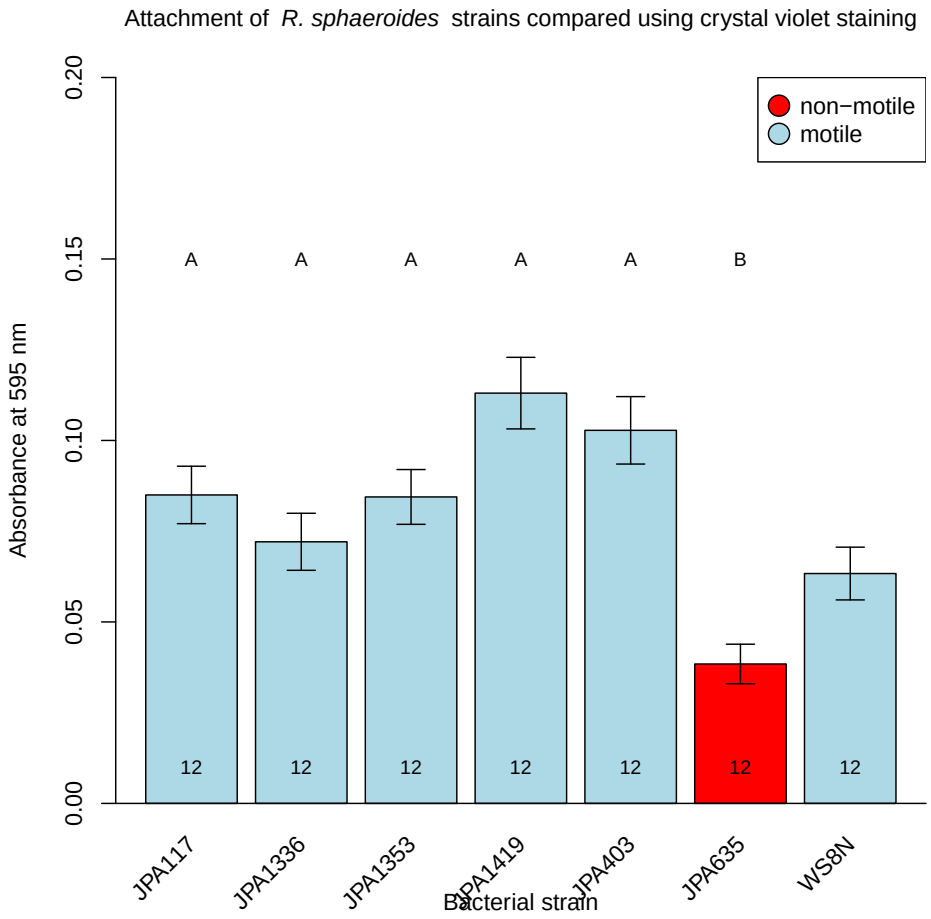


Figure 3.19: Absorbance measured at 595nm of Crystal violet released from attached stationary phase photoheterotrophically grown cells after 30 minutes incubation in light. Error bars are standard error. Numbers of wells tested are shown at the base of each bar. A one-way between subjects ANOVA with Welch's correction (Section 2.9.2) was conducted to compare the effect of strain on absorbance. Absorbance differed significantly as a function of strain for log phase photoheterotrophic cultures incubated with shaking, $F(6,34.1) = 11.08$, $p = 7.788e\text{-}07$. Post-hoc pairwise t-tests with Holm's correction (Section 2.9.2) were performed to identify different strains. The letters above the bars show two groups of strains, A, and B, clustered by significant differences at $p<0.05$. WS8N fitted into neither groups, attaching significantly less than *R. sphaeroides* JPA1419 and *R. sphaeroides* JPA403 (p, 0.05) but the same as all other strains.

3.5.3 Comparison between attachment of photoheterotrophically grown chemotaxis mutants over 6 hours

To see whether the initial differences in attachment between strains are maintained over time, the cultures were left to attach for 6 hours. This experiment is to test the hypothesis that cells which have attached by 30 minutes are still attached at 6 hours.

Separate cultures of each strain in Table 3.2 were grown photoheterotrophically to OD_{700} approximately 0.4 (Section 2.2.2). The cultures were then diluted with succinate medium (Appendix 11.0.3) in proportion to their measured OD_{700}, so that all were at OD_{700}=0.3 and the number of cells in each well was roughly the same, around $1.8x10^8$ cells per ml. 200μl samples of each culture were incubated in light in 96 well plates as described in Section 2.3.1. Each plate contained eight samples of each strain, and eight wells containing only succinate medium (Appendix 11.0.3). The wells were assayed for biofilm formation using crystal violet (Section 2.3.1). The mean of the control wells was subtracted from the measured absorbances shown on Fig. 3.20.

Identical starter plates were incubated for 30 minutes and 6 hours. The results for 6 hours show that overall the attachment of the motile strains is reduced compared to 30 minutes, whereas the non-motile control had attached significantly more in 6 hours ($p<0.05$) (Fig. 3.20).

These data show that between 30 minutes and 6 hours no significant biofilm growth has taken place, and that some detachment of the motile cells has probably occurred. *R. sphaeroides* doubling time is approximately 2 hours in succinate medium in light (data not shown) and a culture starting at OD_{700} 0.3 will be approaching stationary phase after 6 hours, with the cells changing behaviour. As well as this, the greater crowding may itself encourage detachment.

Longer term experiments to follow surface attachment up to 48 hours are described in Chapter 9.

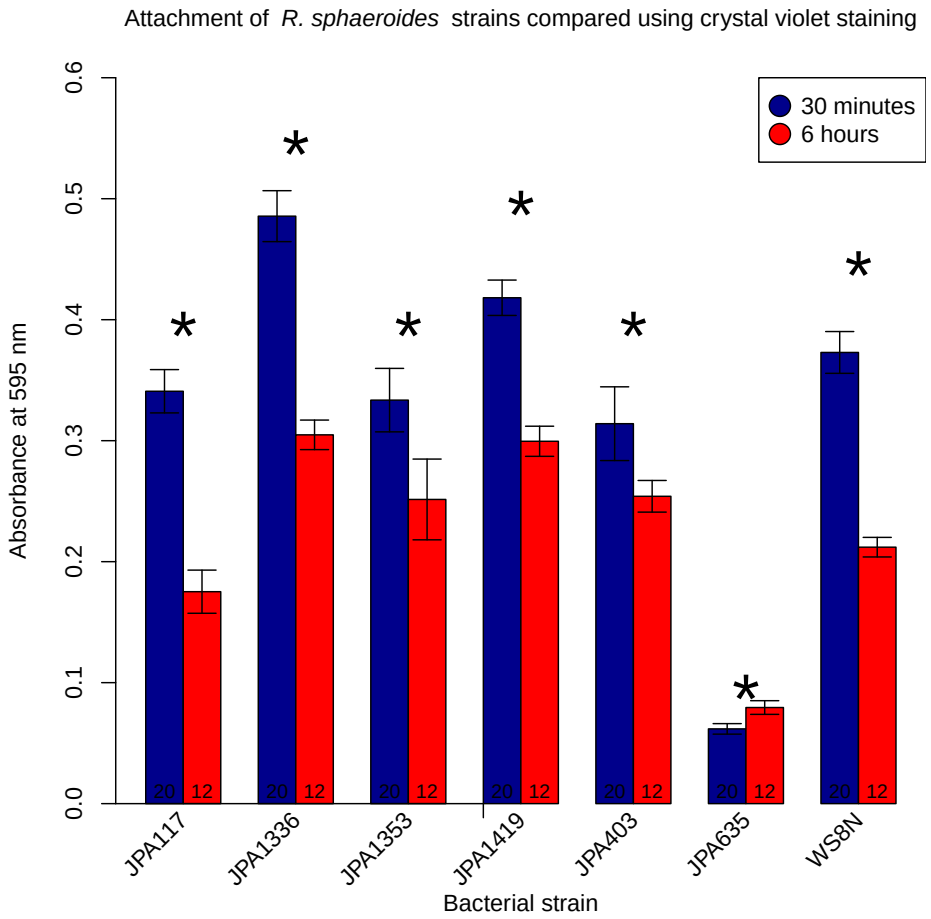


Figure 3.20: Absorbance measured at 595nm of Crystal violet released from attached photoheterotrophically grown cells after 30 minutes or 6 hours incubation in light. Error bars are standard error. Numbers of wells tested are shown at the base of each bar. Student's t-tests were performed (Section 2.9) to compare the means for each strain in the two conditions. Where differences were significant at the $p<0.05$ level, the bars are marked by a star. The only strain to attach more in 6 hours than in 30 minutes was the non-motile control *R. sphaeroides* JPA635.

3.6 Does changing swimming patterns by deleting single chemotaxis genes affect attachment?

Deleting the polar chemotaxis operon 2 led to lower attachment at log phase, and 'stoppy' swimming. Deleting the cytoplasmic chemotaxis operon 3 led to smooth swimming and higher attachment. To investigate whether the attachment changes are linked to the swimming changes, or are due to other effects from deleting the operons, the attachment was measured for *cheB* and *cheR* deletion mutants. The methyltransferase, CheR is constitutively active and transfers methyl groups to specific glutamate residues of the MCPs. CheB removes the methyl groups and its activity is increased by phosphorylation. CheB and CheR work together to modulate the sensitivity of chemotaxis receptors, methylated MCPs are more active than unmethylated MCPs. For more details see Section 1.7.

R. sphaeroides has several CheR and CheB proteins encoded in the different chemotaxis operons. The CheR1 protein from chemotaxis operon 1 has no apparent effect on chemotaxis or swimming. Those in chemotaxis operons 2 and 3 do affect swimming. The absence of *cheB* and *cheR* from the same operon have opposite effects on swimming and the effects are reversed for the two operons (Personal communication, J. de Beyer) (Table 3.3). This means that if attachment follows the same pattern it is likely that it is the motility change that causes the attachment difference, rather than sensing surfaces through the chemotaxis pathway.

The strains whose swimming is smoother than wild-type show increased attachment. The strains whose swimming is stoppier than wild-type show similar attachment to wild type, possibly reduced, but not, from this data, significantly. These data support the hypothesis that smooth swimming increases the initial attachment of *R. sphaeroides* to surfaces.

Table 3.3: The strains of *R. sphaeroides* with deletions of *cheB* and *cheR* genes. Swimming changes personal communication, J. de Beyer.

Strain	Description	Operon	Effect on swimming	Reference/source
JPA517	Δ*cheB1*	2	Smooth - swims with fewer stops than wild-type	Martin et al. (2001)
JPA565	Δ*cheR2*	2	Stoppy - swims with more stops than wild-type	Martin et al. (2001)
JPA1320	Δ*cheR3*	3	Smooth - swims with fewer stops than wild-type	Porter et al. (2002)
JPA1323	Δ*cheB2*	3	Stoppy - swims with stops than wild-type	Porter et al. (2002)

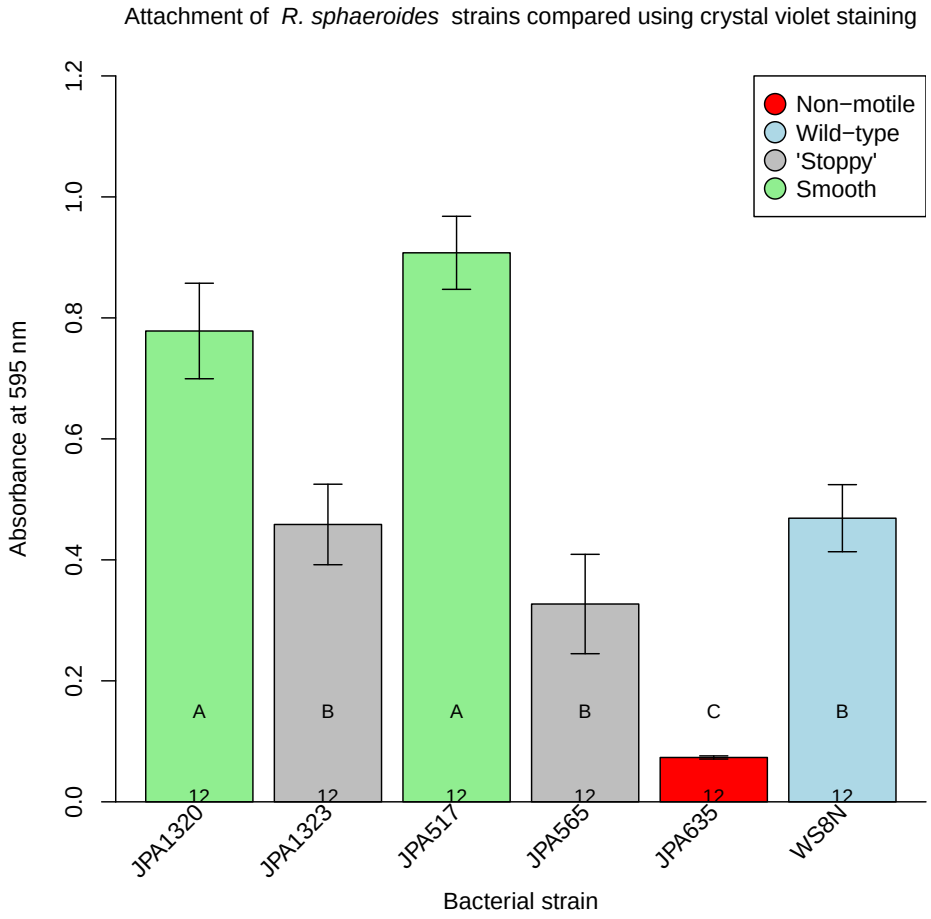


Figure 3.21: Absorbance measured at 595nm of Crystal violet released from attached log phase photoheterotrophically grown cells after 30 minutes incubation in light. Error bars are standard error. Numbers of wells tested are shown at the base of each bar. A one-way between subjects ANOVA with Welch's correction (Section 2.9.2) was conducted to compare the effect of strain on absorbance. Absorbance differed significantly as a function of strain for log phase photoheterotrophic cultures incubated in light, $F(5,25.7) = 65.6$, p=8.03e-14. Post-hoc pairwise t-tests with Holm's correction (Section 2.9.2) were performed to identify different strains. The letters in the bars show three groups of strains, A, B and C, clustered by significant differences at $p<0.05$.

3.7 *R. sphaeroides* produces cellulose-like extracellular polysaccharide that binds calcofluor. Does the over or under-production of this EPS affect initial attachment?

Strains overproducing and underproducing (Hale, 2009), the calcofluor binding EPS produced by the *exoLAMP* gene cluster in *R. sphaeroides* (Table 3.4) were checked for motility and initial attachment to plastic, using 96 well plates inoculated with log phase and stationary phase cultures. The test for EPS production (Section 2.3.4) is done over several days (Hale, 2009) so it is not known how early the overproduction starts in strain *R. sphaeroides* JPA620.

Separate cultures of each strain in Table 3.4 were grown photoheterotrophically to OD_{700} approximately 0.4 (Section 2.2.2). The cultures were then diluted with succinate medium (Appendix 11.0.3) in proportion to their measured OD_{700}, so that all were at OD_{700}=0.3 and the number of cells in each well was roughly the same, around $1.8x10^8$ cells per ml. 200μl samples of each culture were incubated in light in 96 well plates as described in Section 2.3.1. Each plate contained eight samples of each strain, and eight wells containing only succinate medium (Appendix 11.0.3). The wells were assayed for biofilm formation using crystal violet (Section 2.3.1). The mean of the control wells was subtracted from the measured absorbances shown on Fig. 3.22.

The Δ*cerI* EPS overproducer, JPA620, attached at wild-type levels while the Δ*exoY* strain JPA622 attached significantly more than wild-type. This implies that the calcofluor binding EPS is not needed for initial attachment, and may be in some way a hindrance to surface attachment (Fig 3.22).

To compare the effect of starting with inoculations of stationary phase cultures, separate cultures of each strain in Table 3.4 were grown photoheterotrophically to OD_{700} approximately 1.2 (Section 2.2.2). 200μl samples of each cul-

Table 3.4: The strains of *R. sphaeroides* used for EPS attachment experiments.

Strain	Description	Motile	Reference/source
WS8N	Wild type strain of *R. sphaeroides*	yes	Sockett and Armitage (1991)
JPA620	Δ*cerI*, lacks quorum sensing signal, overproduces EPS	yes (this study)	Gift from H. Packer, (Hale, 2009)
JPA622	JPA500 Δ*exoY*, mutation affecting *exoLAMP* gene cluster, underproduces EPS	yes (this study)	Gift from H. Packer, (Hale, 2009)
JPA635	Δ*fliC*	no	Gift from G. Wadhams

ture were incubated in light in 96 well plates as described in Section 2.3.1. Each plate contained eight samples of each strain, and eight wells containing only succinate medium (Appendix 11.0.3). The wells were assayed for biofilm formation using crystal violet (Section 2.3.1). The mean of the control wells was subtracted from the measured absorbances shown on Fig. 3.23.

At stationary phase the position is reversed (Fig. 3.23). The EPS overproducer JPA620 attached significantly more than wild-type while wild-type WS8N attached at similar levels to the EPS deletion mutant JPA622. This could imply that overproducing EPS helps attachment at stationary phase when cells are less likely to be motile. However, it is not known whether EPS production is maintained at stationary phase.

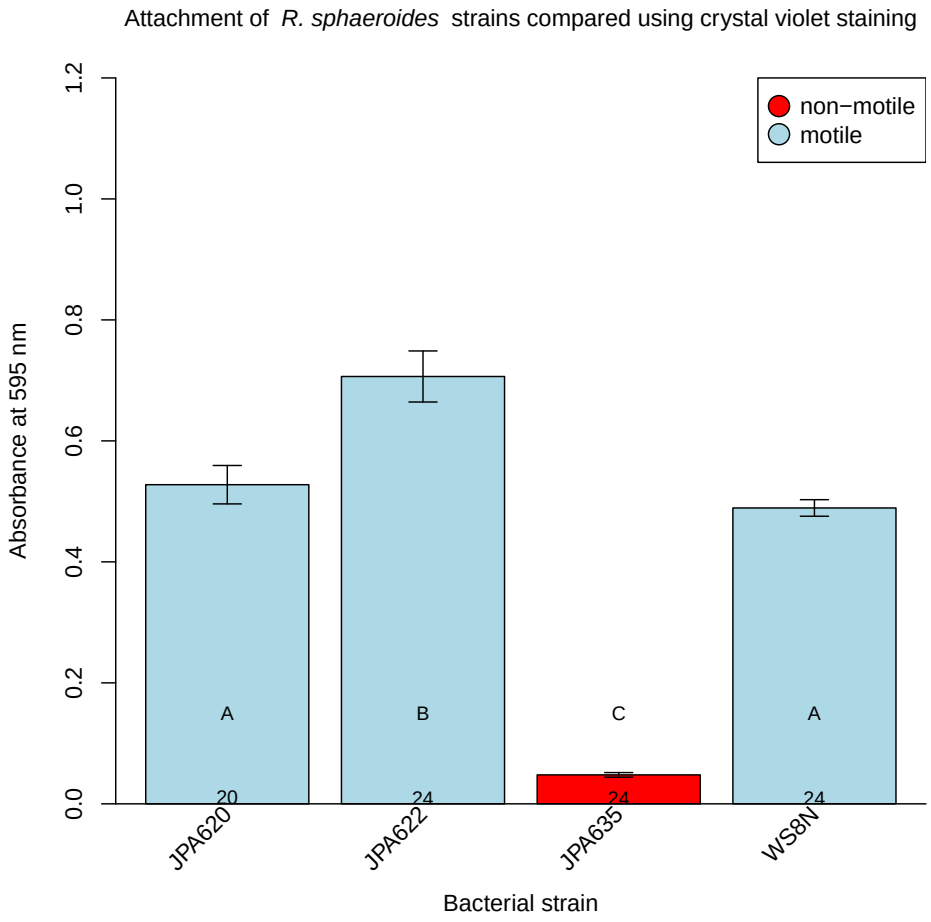


Figure 3.22: Absorbance measured at 595nm of Crystal violet released from attached log phase photoheterotrophically grown cells after 30 minutes incubation in light. Error bars are standard error. Numbers of wells tested are shown at the base of each bar. A one-way between subjects ANOVA with Welch's correction (Section 2.9.2) was conducted to compare the effect of strain on absorbance. Absorbance differed significantly as a function of strain for log phase photoheterotrophic cultures incubated in light, $F(3,37.9) = 442.4$, $p<2.2e\text{-}16$. Post-hoc pairwise t-tests with Holm's correction (Section 2.9.2) were performed to identify different strains, which are shown by letters above the bars. The wild-type *R. sphaeroides* WS8N grouped with the EPS overproducing strain JPA620, JPA622 attached significantly more ($p<0.05$) and the non-motile control JPA653 attached significantly less ($p<0.05$)

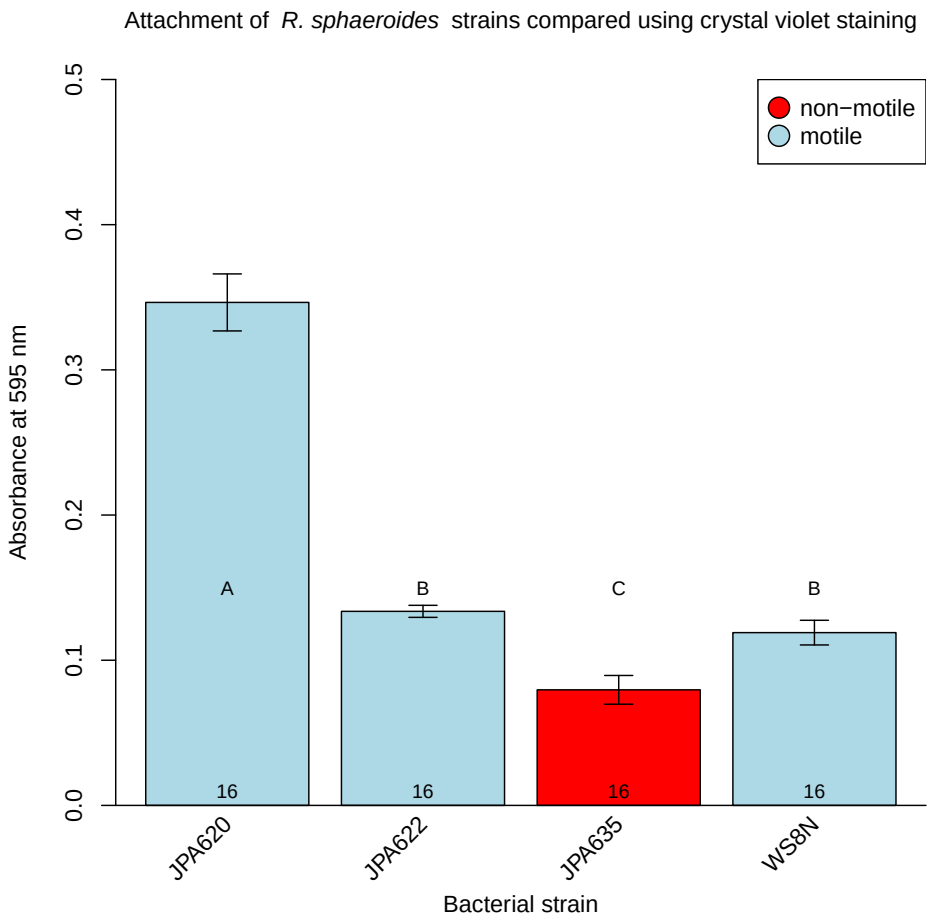


Figure 3.23: Absorbance measured at 595nm of Crystal violet released from attached stationary phase photoheterotrophically grown cells after 30 minutes incubation in light. Error bars are standard error. Numbers of wells tested are shown at the base of each bar. A one-way between subjects ANOVA with Welch's correction (Section 2.9.2) was conducted to compare the effect of strain on absorbance. Absorbance differed significantly as a function of strain for log phase photoheterotrophic cultures incubated in light, $F(3,29.9) = 47.8$, p=1.641e-11. Post-hoc pairwise t-tests with Holm's correction (Section 2.9.2) were performed to identify different strains, which are shown by letters above the bars. The wild-type *R. sphaeroides* WS8N grouped with the EPS underproducing strain JPA622, JPA620 attached significantly more ($p<0.05$) and the non-motile control JPA653 attached significantly less ($p<0.05$)

Comparing the attachment of EPS mutants with 30 minutes incubation of cultures at log and stationary phase, Student's t-tests between the same strain in the two conditions (Fig. 3.24) show significant differences for every strain, and as before (Fig. 3.14) only the non motile control JPA635 attached more at stationary phase. (The numbers of cells per well is four times greater at stationary phase).

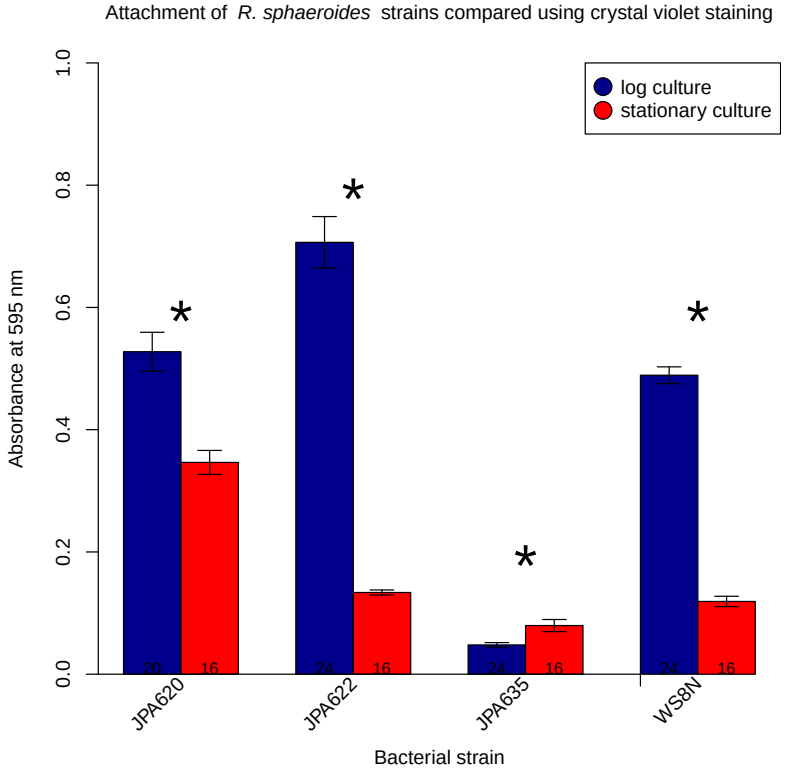


Figure 3.24: Absorbance measured at 595nm of Crystal violet released from attached stationary and log phase photoheterotrophically grown cells after 30 minutes incubation in light. Error bars are standard error. Numbers of wells tested are shown at the base of each bar. Student's t-tests were performed (Section 2.9) to compare the means for each strain in the two conditions. Where differences were significant at the $p<0.05$ level, the bars are marked by a star.

3.8 Discussion of initial attachment data

The aim of this chapter was to determine whether and how motility and chemotaxis affect the initial attachment of *R. sphaeroides* WS8N to glass surfaces.

In all conditions tested, motility has an influence on attachment rates in the first 30 minutes. For non motile strains there may be a slight increase in attachment if they posess a flagellum, compared to aflagellate strains.

Interestingly, the effect on attachment of deleting each of the two essential chemotaxis operons is different, loss of the cytoplasmic cluster leads to significantly higher attachment than loss of the polar cluster. Deleting the first chemotaxis operon does not seem to affect initial attachment. The chemotaxis system co-ordinates the response to chemical gradients and, in *R. sphaeroides*, to light levels (Porter et al., 2002), but it does so by modulating motor stops and thus swimming behaviour, so chemotaxis mutants have altered swimming behaviour which may affect attachment for mechanical rather than sensing reasons.

The loss of the cellulose-like EPS of *R. sphaeroides* seems to encourage high levels of initial attachment in log phase cultures, but its overproduction leads to higher attachment in stationary phase cultures. This could mean that in the absence of motility at stationary phase, the extra production of sticky polysaccharide increases the ability of a cell to stick to a surface when random movement brings it near.

After 6 hours the differences, while still clear and significant, are reduced. Non motile strains have built up a larger number of attached cells, while motile strains seem to have slightly reduced attachment. A possible reason for this is that non motile cells, once attached, have no way to actively detach, while motile cells can attach briefly and swim away. Quorum sensing has been shown to affect EPS production in *R. sphaeroides* WS8N (Hale, 2009) and in static cultures the increased crowding as cells divide may encourage detachment of motile cells over 6 hours.

These data for early attachment shows that motility affects surface attachment in *R. sphaeroides*, and that more subtle changes in motility than motile/non-motile seem to be reflected in changes in attachment.

They also imply that some detachment from the surface takes place, so a general model of reversible attachment followed by a transition to irreversible attachment is likely to apply to *R. sphaeroides*.

Differences in *R. sphaeroides* biofilm development and structure previously seen at late stages for chemotaxis and motility mutants appear as early as initial attachment in some cases, but there does not seem to be any involvement of the first chemotaxis operon under the conditions used here. Smooth swimming strains seem to attach in greater numbers than 'stoppy' strains, whilst non-motile strains consistently attach at low levels.

Motility is not the only factor affecting attachment. Mutants and bacteria in different growth stages may have altered surface properties, such as changes in relative hydrophobicity, and surface conditioning may change for different strains, an example is the apparent tendency of *R. sphaeroides* JPA637 to leave detached flagella on the surface (Fig. 3.8), or as byproducts build up in a culture over time. Further work could investigate these possibilities, using surface coatings on wells, preconditioning wells with culture supernatants, and resuspending log phase cells in the supernatant from stationary phase culture to see whether molecules in the supernatant discourage attachment.

However, the effect of motility seems to be important, and this is investigated further in the next chapters.

Chapter 4

Rhodobacter sphaeroides swimming at and away from surfaces

4.1 Introduction

In Chapter 3 it was established that in *R. sphaeroides* WS8N attachment to surfaces is affected by changes in motility. However, reliable measurements of bacterial motility have been difficult to obtain and some features, for example stop frequencies of free swimming bacteria, have been estimated by visual impression (eg. Brown (2009)). Changes in bacterial swimming near a solid surface have been observed for several species of bacteria and have been explained mathematically (Frymier and Ford, 1997; Shum et al., 2010).

If changes in motility affect attachment to surfaces, then changes in motility as cells approach surfaces before attachment may be important, and if mutant strains attach to different extents, quantifying changes in their swimming behaviour is important.

Bacteria swimming in the absence of a chemoeffector or other gradient can be modelled as diffusing (Berg, 1993), and previous work has led to equations

relating the effective diffusion coefficient to the swimming speed, mean run length, mean stop length and mean turn angle between runs (Lovely and Dahlquist, 1975). Diffusion is a good measure of the amount of overall movement and thus numbers of cells reaching the surface, so these data would lead to a useful preliminary model, helping decide whether the contribution of motility to suface attachment is simply a matter of the number of cells reaching the surface.

Li et al. (2011) report that swimming *Caulobacter crescentus* accumulate within a micrometer from the surface, and that the extent of accumulation is affected by swimming speed and cell size. They suggest collisions with the surface and reorientation of the cells as a reason. *E. coli* has been observed to swim in circular paths near plane surfaces (Lauga et al., 2006), and this has been attributed to hydrodynamic forces which depend on cell and flagellum shape (Shum et al., 2010). However, Li et al. (2011) report that circular trajectories are rarely seen in *Vibrio alginolyticus* and *C. crescentus*, and suggest that hydrodynamic forces are not the main influence on surface accumulation. Kudo et al. (2005) saw curved trajectories near surfaces in *V. alginolyticus* only when reversing. There is thus evidence that swimming changes at surfaces, that swimming cells may accumulate, and that the details vary for different bacteria.

We have been working with a suite of programs to track swimming bacteria and detect when they are stopped or swimming, which is not a trivial question because of Brownian motion. The tracking and run/stop analysis programs are described in Materials and Methods Section 2.7 and in Wood et al. (2012) and Rosser et al. (2013).

To analyse bacterial swimming speeds and behaviour the swimming bacteria were recorded using video microscopy (Materials and Methods Section 2.5.3), and the images analysed as described in Materials and Methods Section 2.7. The overall process is illustrated in Figure 4.1.

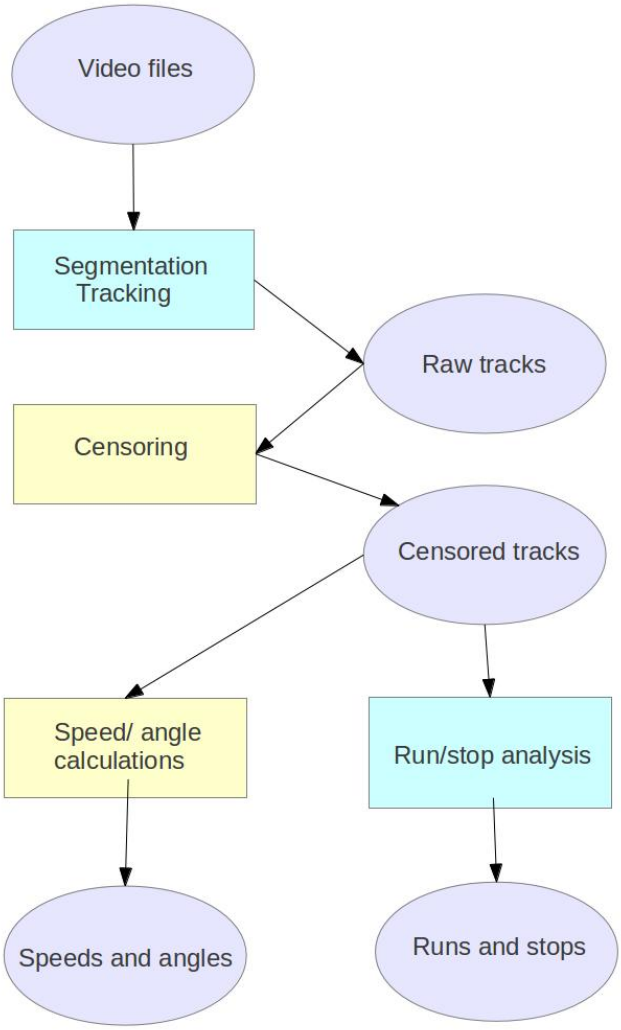


Figure 4.1: Extracting data from video files. Data files are ellipses, programs are rectangles. Arrows show data flow. The green rectangles show programs described in papers Wood et al. (2012) - Tracker - and Rosser et al. (2013) - Run/Stop Analysis. The yellow rectangles show programs written by J. de Beyer, D. Wilkinson and S. Chacko to censor data and remove invalid tracks - Censoring - and to calculate speeds and angles from tracks. We have also written visualisation programs to check tracks against videos and to plot censored and uncensored tracks. These programs are described in more detail in Materials and Methods Section 2.7.

4.2 Aims

The aim of this chapter is to measure swimming speeds, angle changes and lengths of stops and runs in motile *R. sphaeroides* at and away from a solid surface, and then to show that the visual impression that one strain stops more or less than another can be quantified. The ability to measure details of swimming behaviour will make it possible to assess more accurately the effect of motility changes on attachment to a surface.

4.2.1 Tracking swimming bacteria

Nine cultures of *R. sphaeroides* WS8N were grown photoheterotrophically in succinate medium (Appendix 11.0.3) to OD_{700} 0.6 (Section 2.2.2). For each culture 2 minute videos were taken at the capillary surface and in the bulk medium, as described in Materials and Methods 2.5.3.

The videos were processed using the Tracker software to identify bacterial tracks, and the tracks were analysed to give a speed and an angle change for each transition, (Materials and Methods 2.7.4). In Figure 4.1 this corresponds to going directly from 'Raw tracks' to 'Speed/angle calculations' without censoring.

Plotting the angle against the speed for each frame to frame transition as a two dimensional histogram gives Figure 4.2. There are a large number of transitions with speeds between 0 and 10 μms^{-1}, higher speeds tend to correspond to angles near zero, and at low speeds there is a wider range of angle changes. Measured speeds for a single transition vary between 0 and around 60 μms^{-1}.

The large peak at low speeds corresponds partly to non-motile cells, and partly to the 'stopped' portions of the tracks of swimming cells. The higher speeds correspond to 'running' portions of tracks. Every culture of a motile strain has a proportion of non-motile cells, it may be that some cells stop swimming temporarily, perhaps because of damage to the flagellum. These

cells tend to stay in focus and produce longer tracks and so stopped transitions swamp the data for actively swimming cells.

Therefore non-motile cells should be removed from the analysis to give a clearer picture of swimming behaviour.

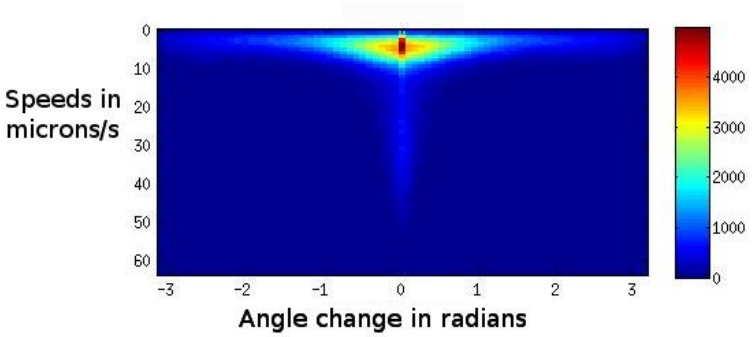


Figure 4.2: Two dimensional histogram showing angle change and speed for every frame transition in every track for a video of log phase *R. sphaeroides* WS8N swimming in 10 mM HEPES motility buffer (Appendix 11.0.8) half way between the surfaces of a glass capillary tube. The scale bar shows the colours corresponding to numbers in the histogram, so a green square in the histogram represents just under 3000 counts of transitions with that speed and angle change. There is a peak at 0 radians and 5 μms^{-1} and above zero counts can be detected up to 60 μms^{-1}, and for all angle changes. These data can not be used to calculate the mean or median swimming velocity because there is too much noise from non-swimming cells, and the modal speed is that of the non swimmers, which is not zero because of Brownian motion.

4.3 Optimal speed cutoff to remove non-motile cells

The cutoff speed should remove non swimmers without removing slower swimmers. The movement expected from non-motile cells can be found in two ways, by calculation and by experiment.

4.3.1 The expected movement in one frame transition due to Brownian motion

Brownian motion is the motion of very small objects due to continual bombardment by moving atoms and molecules around them. It was observed by Robert Brown in 1827 in pollen grains, and is also seen in dust particles in a light beam. Brownian motion is responsible for diffusion. The speed of a moving object due to Brownian motion can be very high, but the number of collisions means that the direction constantly changes and the actual displacement is not great. The expected displacement of a particle in a liquid or gaseous medium in a given time can be calculated and for three dimensions the root mean square displacement is given by 6Dt where t is time and D is the diffusion coefficient of the particle in the medium (Berg, 1993).

In these videos the time between frames is 0.02s, and the diffusion coefficient of *R. sphaeroides* in HEPES motility buffer (Appendix 11.0.8) can be estimated by that of a sphere of radius 1μm in water, which is 2.2 x 10^{-13}m^2 s^{-1} (Berg, 1993).

Experimentally determined values of the diffusion coefficients of various non-motile bacteria in water given in Rijnaarts et al. (1993) agree with this value, coming between 1 and 6 x 10^{-13}m^2 s^{-1}.

The mean squared displacement between frames in three dimensions is then given by

$$
\begin{aligned}
< x^2 > &= 6Dt \\
&= 0.02 \times 6 \times 2.2 \times 10^{-13} m^2 \\
&= 2.64 \times 10^{-14} m^2
\end{aligned}
$$

giving expected displacement d of 0.16μm

This is at a random angle θ to the XY plane and the measured projection would be d$\cos\theta$.
The mean of $\cos\theta$ is 0.637 so the expected displacement measured is 0.16 x 0.637 $\approx$ 0.1μm in 0.02 s, giving 5μm s^{-1} as the expected mean velocity measured from frame to frame.

4.3.2 Determining the movement due to Brownian motion by experiment

The cutoff that will be best to remove dead and non swimming cells can be found experimentally using a reference strain that does not swim. Several non swimming mutants of *R. sphaeroides* WS8N exist, here we have used JPA1215 which has a flagellum but which has CheY1 - 5 deleted and a mutation in CheY6 (D57N) that alters binding to the switch complex and keeps the motor stopped.

Nine cultures of JPA1215 *R. sphaeroides* were grown photoheterotrophically in succinate medium (Appendix 11.0.3) to OD_{700} 0.6 (Section 2.2.2). 100μl of cells from each culture were centrifuged at 1,000xg for 1 minute in a benchtop centrifuge. The supernatant was removed and the cell pellet was gently resuspended in 1 ml of 10mM HEPES motility buffer (Appendix 11.0.8).

A 0.2 x 2 x 100 mm rectangular glass capillary tube (CM Scientific) was put into 50 μl of the prepared culture in an 1.8ml centrifuge tube, where it filled by capillary action. When completely full the ends were sealed with silicon grease and the tube was placed on a microscope slide.

Videos were recorded at 50 frames per second using the x20 phase contrast objective on a Nikon Optiphot microscope (Materials and Methods 2.5.3).

The videos were processed using the Tracker software to identify bacterial tracks, and the tracks were analysed to give a speed and an angle change for each transition, using basic geometry (Materials and Methods 2.7.4). In Figure 4.1 this corresponds to going directly from 'Raw tracks' to 'Speed/angle calculations' without censoring.

Plotting the angle against the speed for each frame to frame transition as a two dimensional histogram gives Figure 4.3A.

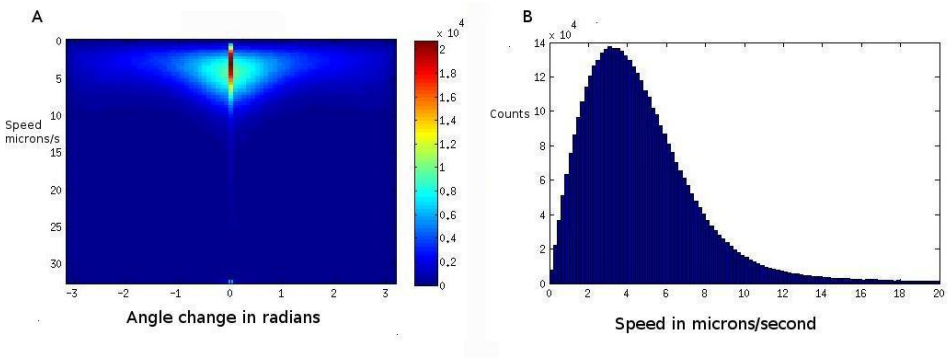


Figure 4.3: Speeds and angles for non-motile cells. A) Two dimensional histogram showing angle change and speed for every frame transition in every track for a video of log phase non-motile JPA1215 *R. sphaeroides* in 10 mM HEPES motility buffer (Appendix 11.0.8) half way between the surfaces of a glass capillary tube. There were 4193954 transitions from 15018 tracks from nine 2 minute videos of non-motile *R. sphaeroides* JPA1215. The scale bar shows the colours corresponding to numbers in the histogram, so a green square in the histogram represents just over 10000 counts of transitions with that speed and angle change. There is a peak at 0 radians and near $5\mu ms^{-1}$ and counts can not be seen for speeds higher than $15\mu ms^{-1}$. B) Speed data only. The data is asymmetric so the median is a good measure of the average speed, the median speed is 4.2 μms^{-1}. The variation in measured speeds includes genuine variation as well as measurement errors. The 99th percentile is $15.3\mu ms^{-1}$ so to remove 99% of non-motile cells a speed cutoff of $15\mu ms^{-1}$ would be effective.

We can see Fig. 4.3 that log phase photoheterotrophically grown non-motile *R. sphaeroides* cells in HEPES motility buffer have speeds with a median

value of 4.2μm s^{-1}, which agrees with the theoretically predicted value. With the JPA1215 swimming data, a swimming cutoff requiring 1/3 of the track to be above 15μm s^{-1} reduces the 15018 tracks recorded to 112 tracks. Thus a speed cutoff of 15μm s^{-1} would remove 99% of non-motile cells. It is better to require a proportion of the track to be above the selected minimum speed, rather than the overall average speed, because the overall average speed is affected by any changes in the proportion of swimming time spent in stops.

4.4 Angle speed data after removing non-motile cells

Nine cultures of *R. sphaeroides* WS8N were grown photoheterotrophically in succinate medium (Appendix 11.0.3) to OD_{700} 0.6 (Section 2.2.2). For each culture 2 minute videos were taken at the capillary surface and in the bulk medium, as described in Materials and Methods 2.5.3.

The videos were processed using the Tracker software to identify bacterial tracks, and the tracks were analysed to give a speed and an angle change for each transition, (Materials and Methods 2.7.4). Tracks were then removed if they were classified as non-swimming, with less than 1/3 of the track having speeds above 15μm s^{-1}. In Figure 4.1 this corresponds to removing tracks corresponding to non-swimming cells in the censoring stage.

After applying the speed cutoff, the angle-speed histograms show a clearer peak for swimming cells.

Fig. 4.4 and Fig. 4.5 show that there is a range of swimming speeds with a clear maximum between 30 and 40 μm s^{-1} and there are fewer of the low speed transitions, which spread out over a much wider range of angles. Since the remaining transitions come from tracks of swimming cells, the lower speeds should mainly correspond to stopped parts of the tracks. A slight asymmetry in the surface data can be seen (Fig. 4.5). This difference can be established statistically but the whole set of transitions are not independent samples - transitions from the same track may be related, so a statistical test cannot be applied to the whole dataset. Therefore a randomly selected turn angle was selected from each track.

A Wilcoxon signed-rank test (Section 2.9) showed a statistically significant change in turn angle in bacteria swimming at a surface compared to bacteria swimming away from a surface (Z = 4.95, p = 7.4e-07).

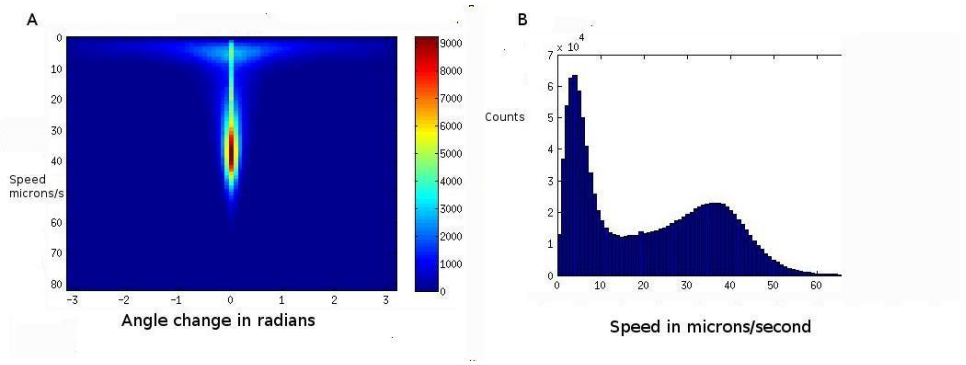


Figure 4.4: Speeds and angles for motile cells. A) Two dimensional histogram showing angle change and speed for every frame transition in every track for a video of log phase *R. sphaeroides* WS8N in 10 mM HEPES motility buffer (Appendix 11.0.8) half way between the surfaces of a glass capillary tube. Tracks were from nine 2 minute videos of actively swimming *R. sphaeroides* WS8N. The scale bar shows the colours corresponding to numbers in the histogram, so a green square in the histogram represents just over 5000 counts of transitions with that speed and angle change. B) Speed data only. The data is bimodal, so that neither the mean nor the median is a good measure of average speed.

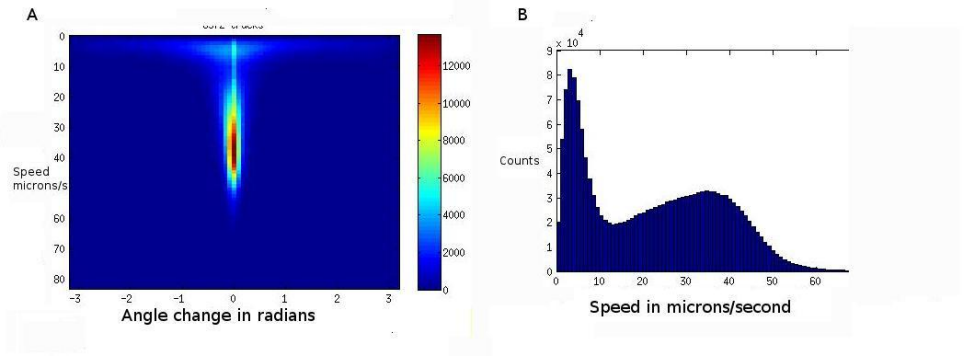


Figure 4.5: Speeds and angles for motile cells. A) Two dimensional histogram showing angle change and speed for every frame transition in every track for a video of log phase *R. sphaeroides* WS8N in 10 mM HEPES motility buffer (Appendix 11.0.8) swimming close to the upper surface of a glass capillary tube. Tracks were from nine 2 minute videos of actively swimming *R. sphaeroides* WS8N. The scale bar shows the colours corresponding to numbers in the histogram, so a green square in the histogram represents just over 8000 counts of transitions with that speed and angle change. B) Speed data only. The data is bimodal, so that neither the mean nor the median is a good measure of average speed.

4.5 Calculating *R. sphaeroides* swimming speed

4.5.1 Published data on *R. sphaeroides* swimming speed

Swimming speeds for *R. sphaeroides* WS8 (the ancestral strain of WS8N) were measured for motile cells resuspended in 10mM HEPES motility buffer (Appendix 11.0.8) in Armitage et al. (1999), tracking 32 cells. They found average speeds of 27 μm s^{-1} with a maximum of 62 μm s^{-1}.

4.5.2 Estimating velocity during runs and stops using data on all transitions

When swimming data was collected as described in Section 4.4, each video had a subpopulation of non swimming cells and these were removed from analysis using the swimming cutoff of 15μm s^{-1} for at least 1/3 of the track, which under these conditions removed 99% of the non-motile cells. Speed/angle 2D histograms of each frame to frame transition of these swimming cells show two regions, a low speed region with angle changes that can be large, and a higher speed region with angle changes near to zero (Figs. 4.4, 4.5).

A histogram of measured speeds for swimming *R. sphaeroides* WS8N bacteria in 10 mM HEPES motility buffer is bimodal (Fig. 4.6). It is likely that the higher speed peak corresponds to frame to frame transitions during runs while the lower speed peak corresponds to transitions when the bacterium is stopped and reorienting. There is a region of overlap between the distributions for stopped and running cells. There is likely to be some overlap between faster Brownian motion transitions and slower swimming transitions. It is difficult to estimate this and the most reliable speed estimate is therefore the modal value, which is based on the position of the peaks and does not depend on exactly where the speed cutoff is taken.

Under the conditions used, for wild-type WS8N bacteria this gives modal

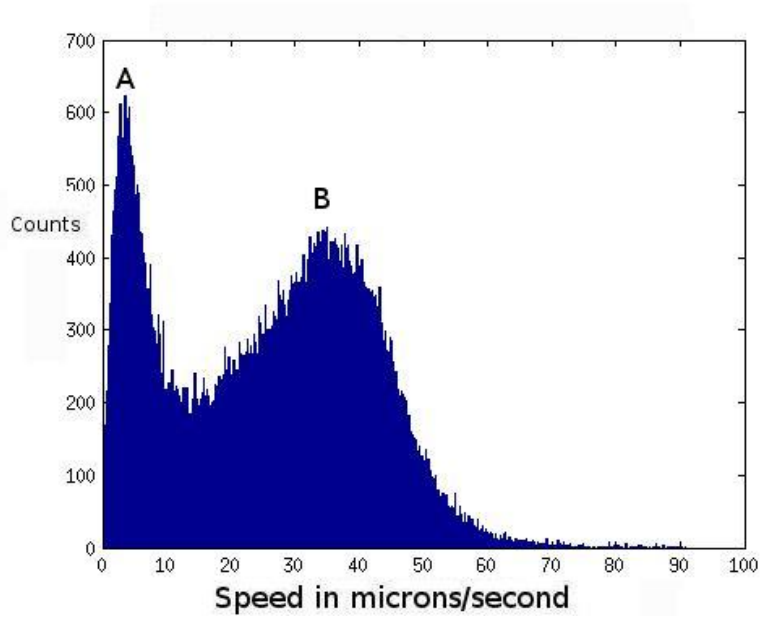


Figure 4.6: Histogram showing the relative frequencies of different speeds measured for single transitions. The data is from nine 2 minute videos of swimming *R. sphaeroides* WS8N bacteria in 10 mM HEPES motility buffer. Peak A is likely to correspond to stops in tracks and peak B to runs. Peak B is wider, and this variation in measured speed has several causes including measurement error, different sizes of cell and lengths of flagella, and tracks at different angles to the capillary surface.

speeds of 35.4 μms^{-1} away from the surface, and 33.7 μms^{-1} at the surface. The difference is not significant (Welch Two Sample t-test, t = -1.3797, df = 9.117, p = 0.2006)

The measured speeds during stops are 4.2 μms^{-1} away from the surface, and 3.6 μms^{-1} at the surface. The difference is significant (Welch Two Sample t-test, t = -4.9227, df = 11.577, p = 0.0003914).

These results suggest that being near a surface reduces the movement of bacteria which are not actively swimming, but does not greatly influence the speed of swimming bacteria, but the significance of the difference disappears with a different method of calculation (Section 4.5.3). They confirm that these methods of tracking and data analysis produce results consistent with

theoretical analysis and previously published experimental data. They also provide a baseline for comparison with the behaviour of mutant strains, or in different conditions.

4.5.3 Estimating velocity during runs using run/stop analysis

When the tracking data is considered as a set of speed/angle transitions, the transitions are considered separately from the tracks. A clearer picture of the behaviour of the individual cells can be seen by analysing the tracks using the run/stop HMM custom written software, described in Materials and Methods Section 2.7.6.

Two minute phase contrast videos were taken in glass capillaries as decribed in Materials and Methods Section 2.5.3, the cultures were log phase photoheterotrophic *R. sphaeroides*, OD at 700nm 0.6, grown in succinate medium and resuspended in 10 mM HEPES motility buffer (Appendix 11.0.8).

Each of three independent biological cultures was sampled three times giving 9 capillaries and two videos of each, one at a surface and one in bulk media. As well as wild-type *R. sphaeroides* WS8N, smooth swimming mutants JPA1353 and non-motile JPA1215 mutants were used for comparison.

Each capillary was made up and immediately filmed, the time between introducing the culture to the capillary and taking the first video was less than 30s. Since two videos were taken in each capillary, one was taken two minutes after the other. The location (bulk media or surface) of the first video was varied so that neither condition was regularly taken first.

The videos were segmented and tracked as described inMaterials and Methods 2.7. The segmentation was done using local mean thresholding with a disk radius of 15 and minimum cluster size of 5, and the upper and lower bounds were both .04.

The run/stop reference distributions and probabilities were calculated as

described in Materials and Methods 2.7.6. The reference files were used to allocate sections of each track in the experimental strain as run or stop.

Once tracks are divided into runs and stops, behaviour was further analysed to find the speed during runs. The difference from the previous calculations is that the information about which transition corresponds to which track is used. It is then possible to look at the variation of speed or stop lengths over tracks from individual cells as well as over the whole population. The allocation to runs and stops uses both speed and angle data as opposed to the simple speed cutoff used earlier. It gives similar results, though the swimming speeds are slightly lower and the stopped speeds slightly higher (Fig. 4.7). The use of angle data as well as speed data means that transitions are allocated to runs and stop differently, mainly in the overlapping region between the two distributions. The mean speed was used, and this will also tend to lower the swimming speed and increase the stopped speed compared to using the modal value, this can be seen from the shape of the histograms in Fig. 4.6.

These data show that photoheterotrophically grown wild-type *R. sphaeroides* WS8N swims at similar speeds near surfaces and in bulk medium. There is still a slightly lower speed at the surface, but with this method of calculation it is not statistically significant (Fig. 4.7).

It also shows that either method of analysis - using individual transitions or using whole runs - gives swimming speeds consistent with published data. Either method can be used so long as the same method is used whenever speeds are to be compared.

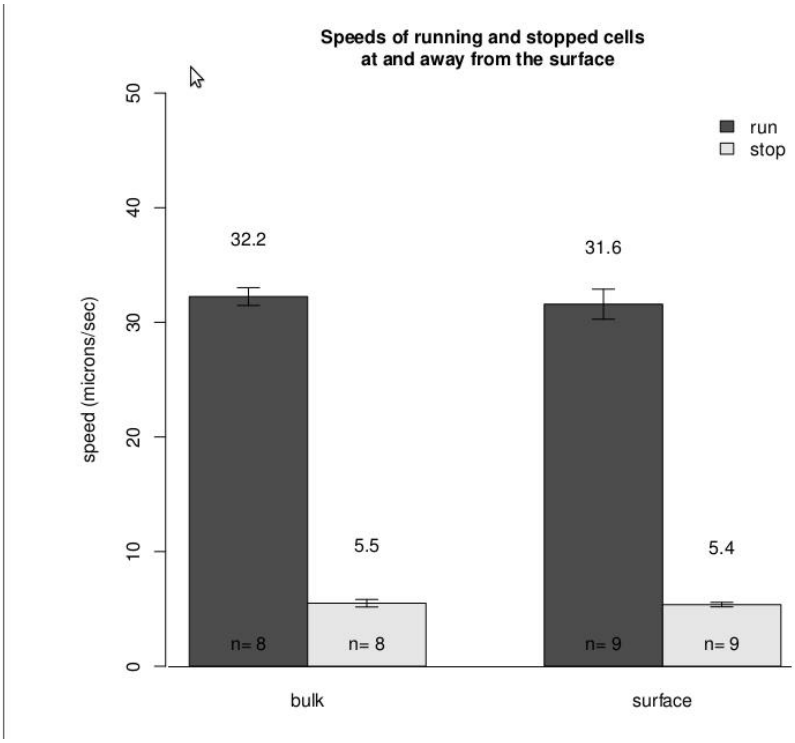


Figure 4.7: Average speeds during runs and stops, of log phase photoheterotrophically grown (Materials and Methods 2.2.2) swimming *R. sphaeroides* WS8N in HEPES motility buffer at and away from surfaces, calculated using both speed and angle data. Error bars are standard error. The average speed is slightly less near the surface ($31.6\mu ms^{-1}$ vs. $32.2\mu ms^{-1}$), which is predicted theoretically because of increased drag, but the difference is small and not significant (Welch Two Sample t-test, t = -1.2832, df = 13.246, p = 0.2214). The measured speeds during stops are $5.5\mu ms^{-1}$ away from the surface, and $5.4\mu ms^{-1}$ at the surface. The difference is not significant (Welch Two Sample t-test, t = -0.9045, df = 11.12, p =0.3849).

4.6 Changes of direction

As well as speeds, changes in swimming direction can be compared at and away from surfaces. The deviations from straightness of a track during a run is one measurement, using angle changes for each transition. The other angle of interest is the angle between successive runs, which is the change in direction after a stop. Direction changes are of interest because a nearby surface may affect swimming direction, either because of physical forces or because of a bacterial response to detection of a signal. Changes of direction due to surfaces may affect access to the surface and hence attachment. It was shown in Section 4.4 that taking one randomly selected transition from each track in a set of videos gives a significant difference ($p<0.05$) between turn angles in bacteria swimming near the glass surface and away from it.

4.6.1 Angle changes between transitions, at and away from a surface

Plotting a histogram of angle changes of cells between frames of videos taken at a surface or in bulk media shows a bias in swimming direction for cells swimming close to a surface (Fig. 4.8).

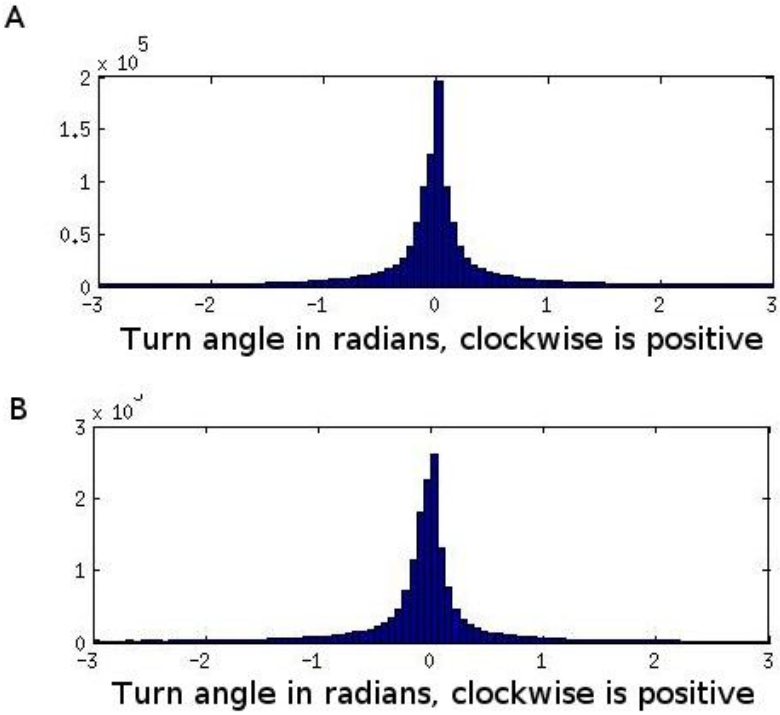


Figure 4.8: Histograms of every angle change at every transition in swimming photoheterotrophically grown log phase *R. sphaeroides* WS8N in HEPES motility buffer (Appendix 11.0.8) away from the surface and B) at a surface. The directional bias in movement at the surface is apparent as a shoulder on the left hand side of the lower histogram. Angles are positive if the turn was clockwise. The mean turn for surface swimmers is -0.05 radians, for the swimmers away from the surface it was 0.001 radians. A Student's t-test (Materials and Methods 2.9) shows the difference of the surface mean from zero to be significant, with a confidence interval for the mean of -0.0468 to -0.0446 and t: -79.1612, df: 1727846, sd: 0.7589, p=0, while the mean angle change in the bulk medium is not significantly different from zero, with a confidence interval for the mean of -0.0002 to 0.0028, t = 1.6910, df: 1189614, sd: 0.8332. It could be argued as in Section 4.4 that the data is not independent, as angle changes in one track are linked, but even taking one sample angle from each track gives a significant difference between bulk and surface turn angles (Section 4.4).

4.6.2 The angle change between two runs is related to stop length for short stops, but becomes random for longer stops

Eighteen two minute phase contrast videos were taken in glass capillaries as decribed in Materials and Methods Section 2.5.3, nine at the glass surface and 9 midway between the glass surfaces. The cultures were log phase photoheterotrophic *R. sphaeroides*, OD at 700nm 0.6, grown in succinate medium and resuspended in 10 mM HEPES motility buffer (Appendix 11.0.8) as described in Materials and Methods Section 2.5.3.

The change in swimming direction between the end of one run and the start of the next provides a measure of the degree of reorientation (or persistence) that the cell has undergone during the stopped period. Plotting the angle change between the last transition of a run and the first transition of the next run, after a stop, against the stop length shows a relationship for stops up to around 18 frames, or 0.36 secs, for longer stops the new direction is random (Fig. 4.9).

If the angle change was uniformly distributed, the expected root mean square angle change would be 1.8 radians ($\sqrt{(\frac{\pi^2}{3})}$), and the mean angle change settles down to this value for stops longer than 0.36 secs in the bulk fluid, or 0.48 secs at the surface. This is consistent with the predictions of rotational Brownian motion analysis for an object of around a micron in size. In Dusenbery (2009), the rotational time constant, which is the time for complete loss of orientation due to rotational Brownian motion for a microorganism moving in three dimensions varies with the cube of the radius, and is relevant to the organism's ability to control its direction of swimming. For *R. sphaeroides*, whose radius is around 1 μm the predicted value is given by the equation

$$\tau = \frac{1}{2D_R}$$
$$= \frac{4\pi\eta a^3}{k_B T}$$
$$3s$$

where η is viscosity, k_B is Boltzmann's constant, T is absolute temperature, D_R is the rotational diffusion coefficient, and τ is the rotational time constant (Dusenbery, 2009). The data shown in Fig. 4.9 shows that under the experimental conditions used, the initial direction of a run after a stop is unrelated to the final direction of the previous run when the stop is longer than 0.4 seconds (the video rate was 50 frames a second). This is shorter than predicted but of the same order of magnitude, and the shape of a stopped *R. sphaeroides* bacterium is not spherical, the curled up flagellum may influence the change in direction. Since a high proportion of stops are short, this suggests the possibility that *R. sphaeroides* could control the amount of reorientation between successive runs by controlling the stop length. However, there is no experimental evidence for stop length control.

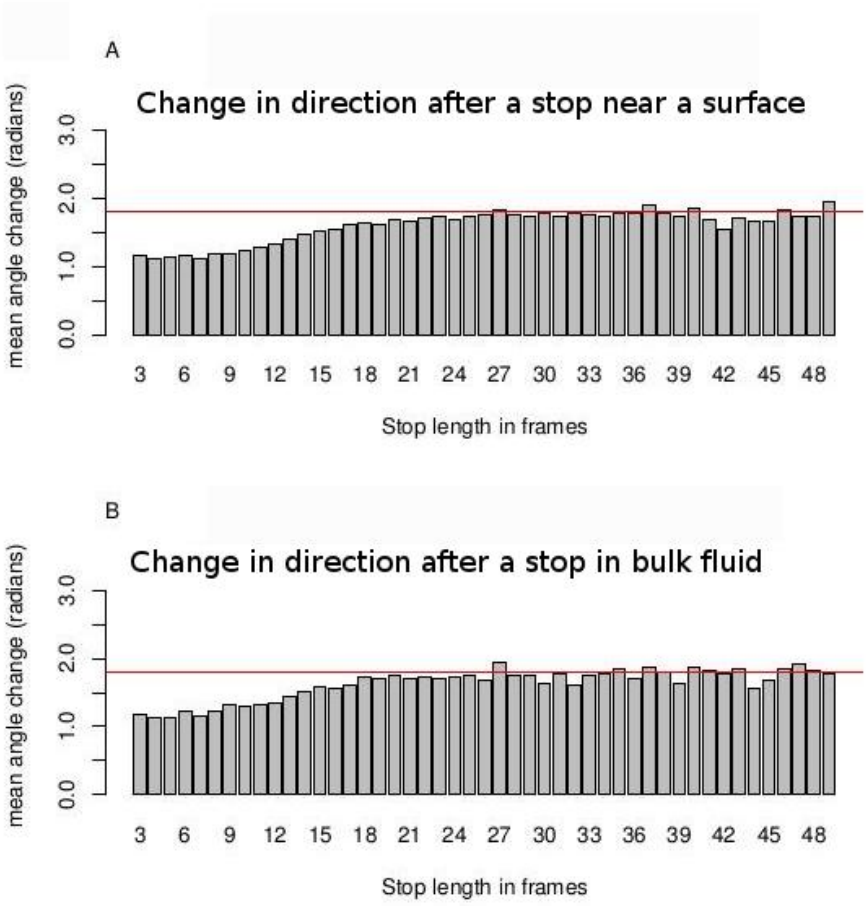


Figure 4.9: The root mean square change in angle of the track during a stop. During a stop, the cell reorients due to rotational Brownian motion, and the next run starts off in a different direction. The mean angle change is zero as it may be turned in either direction, so to look at the size of the angle change the root mean square angle change is used. The red line is the expected value if the angle change was random. This shows that for short stop less than 20 frames (0.4s) the angle change is not random, and the new direction is related to the old direction.

Both swimming and stopped cells turn through low angles more than high, though stopped cells have more high angle change transitions (eg. Fig. 4.2).

Dividing data for actively swimming cells between runs and stops, at and away from surfaces, shows that the ratio of anticlockwise turns to clockwise turns during a run is very near one for bacteria away from surfaces, and is consistently biassed in one direction for bacteria at surfaces (Fig. 4.10).

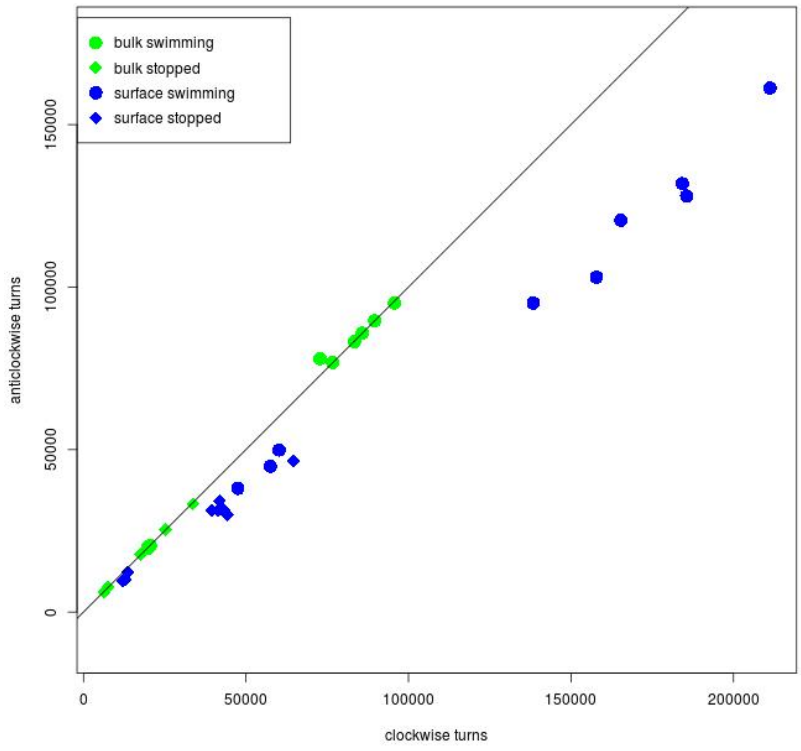


Figure 4.10: Counts of clockwise vs. anticlockwise angle changes at frame transitions for *R. sphaeroides* at and away from a glass surface. Angle changes of zero were omitted. Bacteria away from a surface are equally likely to turn either way, but near a surface turns are biassed in one direction. Each data point is from one video. The diagonal line shows equal turns in both directions.

In bulk medium the cell paths are roughly straight during runs, though they can be diverted by Brownian motion and by forces from fluid flow and other

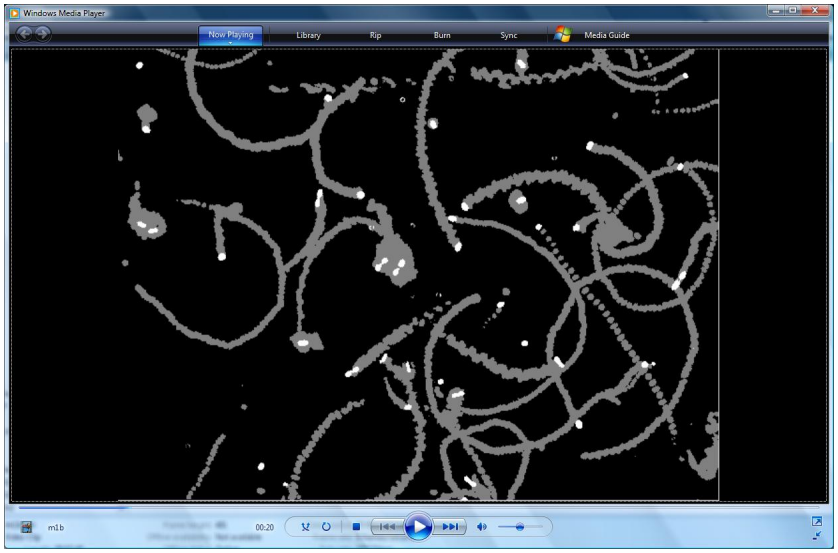


Figure 4.11: Curved tracks seen by superimposing fields of view of *R. sphaeroides* swimming near a glass surface. The white regions show the current position of cells, the grey their paths. The image was created by superimposing frames from a video of log phase photoheterotrophically grown *R. sphaeroides* WS8N swimming in HEPES motility buffer, using a MATLAB script (The MathWorks, 2009).

cells. When near a surface the paths become curved (Fig. 4.11), as reported for several other species of bacteria (Frymier and Ford, 1997; Lauga et al., 2006).

4.6.3 Counts of bacteria at and away from the surface

There is evidence that some motile bacteria gather at surfaces, and theoretical evidence that this could happen passively due to physical forces rather than by accumulating near nutrients adsorbed on a surface or by biassing swimming to reach the surface (Section 1.9). This experiment was designed to test the hypothesis that motile *R. sphaeroides* WS8N tends to gather at surfaces. This is a factor that will affect surface attachment and is different for motile and non-motile cells.

Free swimming videos of log phase wild-type *R. sphaeroides* WS8N were

taken as described previously. Three biological replicates and three samples of each were used, and videos taken at and away from the upper glass surface. For each sample, there were two videos, and which was taken first was varied. The two videos were both taken within 5 minutes of making up the capillary slide.

In the culture there were swimming and non swimming bacteria. The cutoff of at least 1/3 of a track having speed greater than 15μm s^{-1} was used to discard non swimmers and the percentage of recorded cells which were swimming was calculated for each video. Since two videos were taken for each culture the underlying proportion of swimmers to non swimmers should be the same for the video pairs and the cultures were well mixed before the capillaries were made up, so we would expect both types of cell to be evenly distributed at the start.

The percentage of swimming cells was consistently higher at the upper surface than in the middle of the capillary (Figure 4.12). This was true whichever video was taken first.

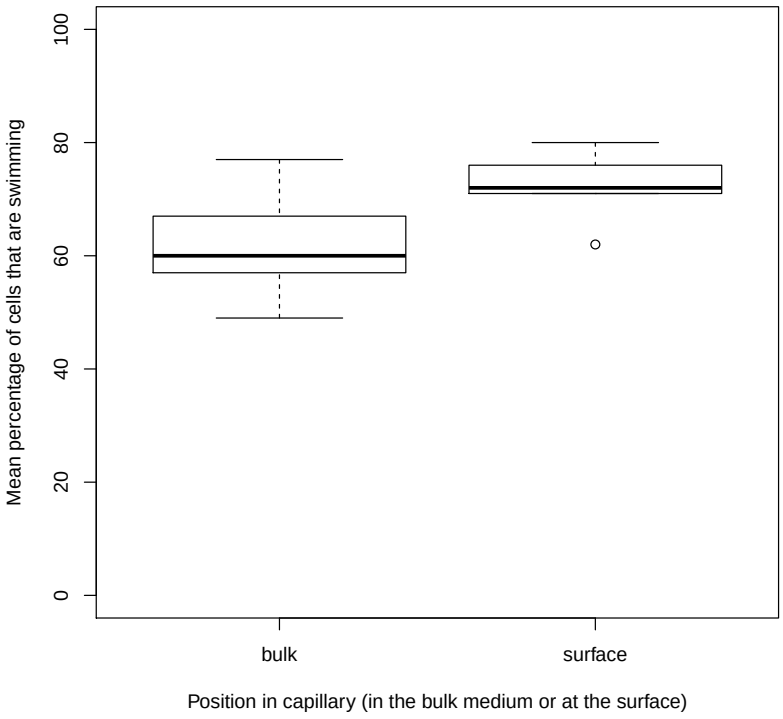


Figure 4.12: Boxplot showing the percentage of swimming cells, at and away from a surface, in 18 videos showing log phase *R. sphaeroides* WS8N grown photoheterotrophically in succinate medium and resuspended in 10mM HEPES motility buffer (Appendix 11.0.8). The Wilcoxon signed rank test shows the difference to be significant at $p<0.01$, $W = 10$, $p = 0.007812$. Since the same cultures with the same proportions of swimmers and non-swimmers are used for videos at and away from a surface, this implies that actively swimming cells are more likely to be found near the upper surface than non swimming cells, and thus that the access to a surface may depend on motility. This should be considered when measuring attachment.

4.6.4 Lengths of stops at and away from a surface

When a cell has stopped swimming it does not move far and it is likely to stay in focus. This means that usually whole stops will be tracked and it is reasonable to assume that the stop lengths are accurate. There will also be stops that started before tracking and continue after tracking. Some of the stops that continue to the end of a video taken at the surface may be cells which have attached.

Eighteen two minute phase contrast videos were taken in glass capillaries as described in Materials and Methods Section 2.5.3, nine at the glass surface and 9 midway between the glass surfaces. The cultures were log phase photoheterotrophically grown *R. sphaeroides*, OD at 700nm 0.6, grown in succinate medium (Section 2.2.2) and resuspended in 10 mM HEPES motility buffer (Appendix 11.0.8) as described in Materials and Methods Section 2.5.3. The distributions of measured stop and run lengths is shown in Fig. 4.13. Stops and runs shorter than the frame rate can not be detected. Stops were slightly longer at the surface (Fig. 4.13). The data is comparable to the stop lengths measured by Brown (2009), which were 0.66 $\pm$ 1.01s, calculated by shearing the flagella and attaching a bead, holding the cell still in an optical trap, and recording the rotation of the bead.

To calculate the mean stop lengths, only complete stops were used. Stops which occurred at the beginning or end of the track were discarded since their full length was unknown. This might have meant that longer stops were more likely to be excluded. Since the mean stop length is less than 1 second in both cases, and the videos were 2 minutes long, this seems unlikely to have biassed the data.

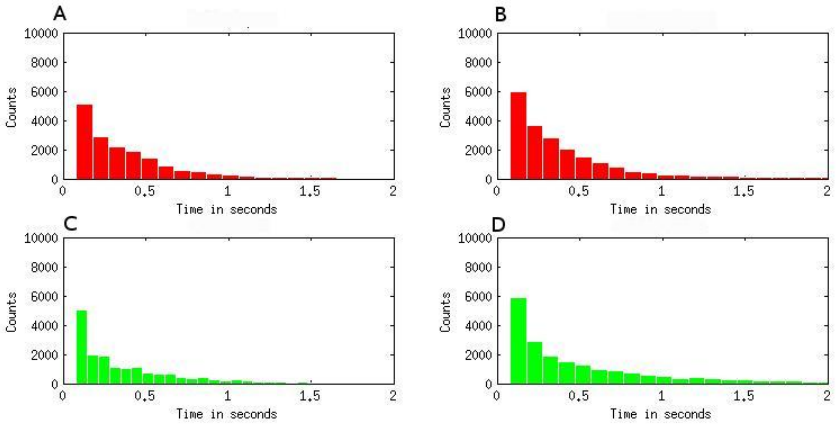


Figure 4.13: Histogram showing counts of run (green) and stop (red) lengths in seconds, for log phase photoheterotrophically grown *R. sphaeroides* WS8N swimming in HEPES motility buffer. A: stop lengths in the bulk medium, B: stop lengths at the surface, C: run lengths in the bulk medium, D: run lengths at the surface. The data can be fitted with exponential curves, giving estimates for the means and 95% confidence intervals for run and stop lengths. The mean stop length at the surface is 0.73 seconds, with 95% confidence interval of 0.72s - 0.74s. The mean stop length away from the surface is 0.64 seconds, with 95% confidence interval of 0.63s - 0.65s. Run lengths also seem to be exponentially distributed, and the mean run lengths from these data are 0.42 seconds away from the surface (confidence interval 0.41 - 0.43 s) and 0.61 seconds at the surface (confidence interval 0.60 - 0.62 s), but the difference between run lengths can not be directly compared since most runs leave the field of view and lengths of complete runs will be biased differently at and away from the surface. Shorter runs are more likely to stay in focus, so the run lengths here are unreliable.

4.7 Swimming behaviour of chemotaxis mutant strains compared to *R. sphaeroides* WS8N

The next sections will track freeswimming bacteria to compare the speeds and stop/run ratios of mutant strains with those of *R. sphaeroides* WS8N. These experiments are to test the hypothesis that swimming speed during runs is unchanged in the motile mutant strains with chemotaxis operons 1, 2 and 3 separately deleted, JPA117, JPA403 and JPA1419 respectively. JPA403 and JPA1419 are non chemotactic from swarm plate analysis and tethering experiments, while JPA117 is chemotactically indistinguishable from wild type (Porter et al., 2002). *R. sphaeroides* JPA1353 has all chemotaxis genes deleted and is motile but non chemotactic (Section 3.5).

4.7.1 Swimming behaviour of strain *R. sphaeroides* JPA117 (Δ*che*Op1)

R. sphaeroides JPA117 has the first chemotaxis operon deleted (Figure 3.17). The loss of this operon has not been found to affect chemotactic behaviour in any conditions studied so far (Porter et al., 2008), but has been reported to affect the structure of biofilms after 5 days (Hale, 2009).

Nine cultures of JPA117 *R. sphaeroides* were grown photoheterotrophically in succinate medium (Appendix 11.0.3) to OD_{700} 0.6 (Section 2.2.2).

For each culture 2 minute videos were taken at the capillary surface and in the bulk medium, as described in Materials and Methods 2.5.3.

The videos were processed using the Tracker software to identify bacterial tracks, and the tracks were analysed to give a speed and an angle change for each transition, (Materials and Methods 2.7.4). Tracks from non-motile cells were removed using a speed sutoff of $15\mu ms^{-1}$ as described in Section 4.4. The speed data is shown in Figs. 4.14 and 4.15.

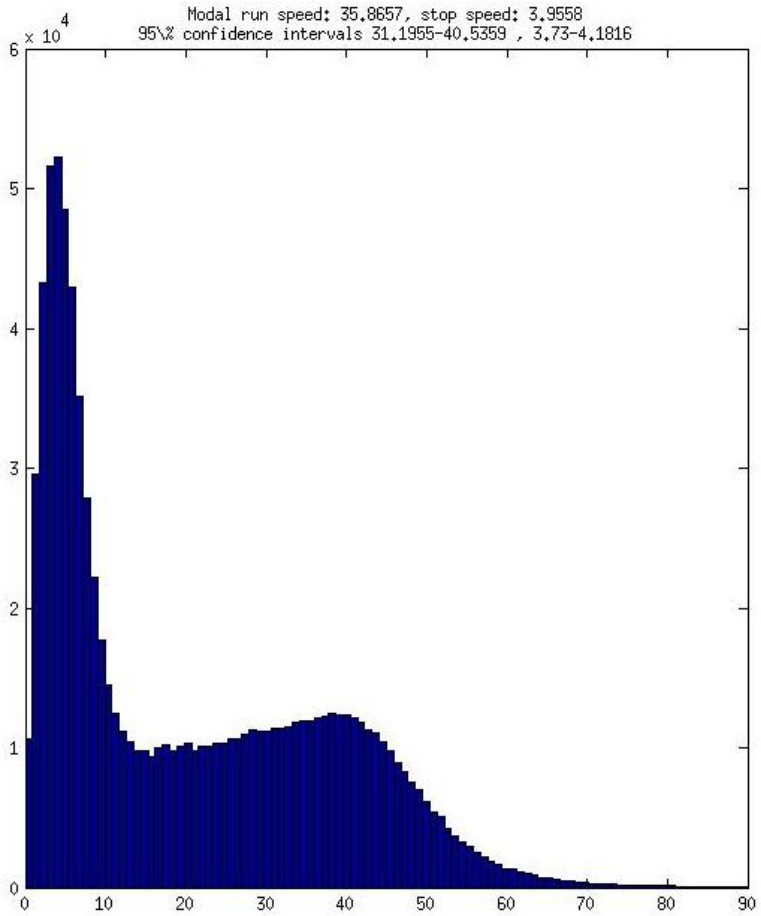


Figure 4.14: Histogram showing the relative frequencies of different speeds (μms^{-1}) measured for single transitions, for log phase photoheterotrophically grown *R. sphaeroides* JPA117 swimming in HEPES motility buffer away from a surface for all tracks from nine 2 minute videos. The peaks corresponding to stops and runs can be seen at near 5 μms^{-1} and near 40 μms^{-1}, run speeds are up to 70 μms^{-1} and the run and stop speed peaks overlap. The variation in run speeds is likely to be real variation in the population as well as measurement error.

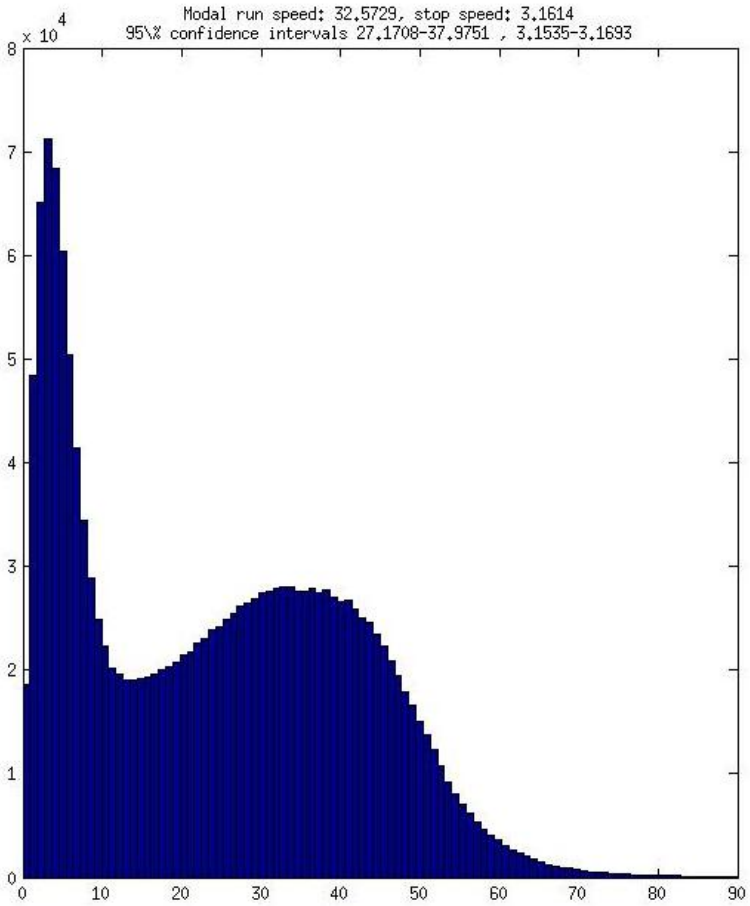


Figure 4.15: Histogram showing counts of different speeds (μms^{-1}) measured for single transitions, for log phase photoheterotrophically grown *R. sphaeroides* JPA117 swimming in HEPES motility buffer at a glass surface for all tracks from nine 2 minute videos. The peaks corresponding to stops and runs can be seen at near 5 μms^{-1} and near 35 μms^{-1}, run speeds are up to 70 μms^{-1} and the run and stop speed peaks overlap. The variation in run speeds is likely to be real variation in the population as well as measurement error.

4.7.2 Swimming behaviour of the smooth swimming strains, *R. sphaeroides* JPA1353 and *R. sphaeroides* JPA1419 (Δ*che*Op3)

R. sphaeroides JPA1353 has all chemotaxis genes deleted, and JPA1419 has chemotaxis operon 3 deleted (Figure 3.17). Neither strain is chemotactic and both are motile, swimming with few or no stops (Porter et al., 2008). Biofilm growth after 5 days is affected by these deletions (Hale, 2009).

Nine cultures of each of *R. sphaeroides* JPA1419 and *R. sphaeroides* JPA1353 were grown photoheterotrophically in succinate medium (Appendix 11.0.3) to OD_{700} 0.6 (Section 2.2.2). For each culture 2 minute videos were taken at the capillary surface and in the bulk medium, as described in Materials and Methods 2.5.3.

The videos were processed using the Tracker software to identify bacterial tracks, and the tracks were analysed to give a speed and an angle change for each transition, (Materials and Methods 2.7.4). Tracks from non-motile cells were removed using a speed sutoff of $15\mu ms^{-1}$ as described in Section 4.4. The speed data is shown in (Figs. 4.16,4.17,4.18,4.19)).

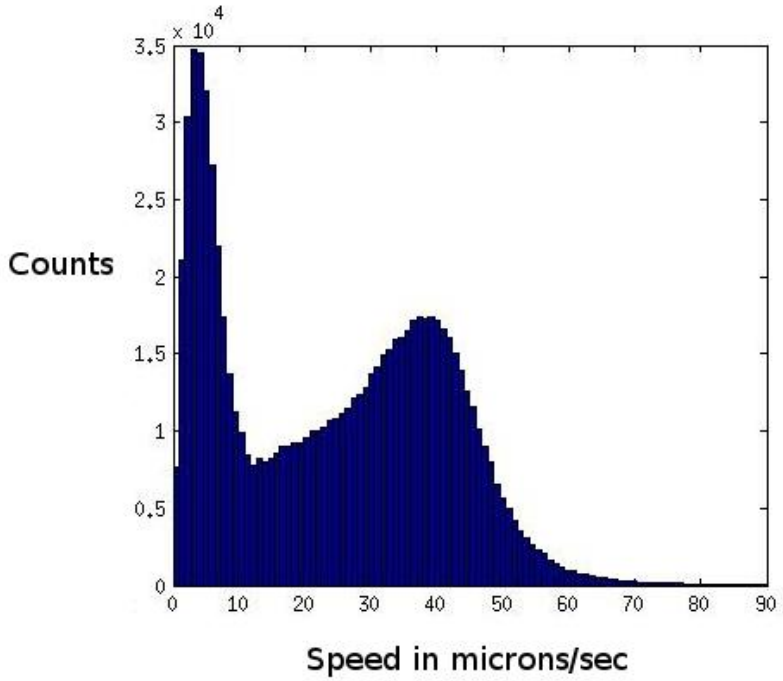


Figure 4.16: Histogram showing counts of different speeds (μms^{-1}) measured for single transitions, for log phase photoheterotrophically grown *R. sphaeroides* JPA1353 swimming in HEPES motility buffer away from a glass surface for all tracks from nine 2 minute videos. The peaks corresponding to stops and runs can be seen at near 5 μms^{-1} and near 40 μms^{-1}, run speeds are up to 70 μms^{-1} and the run and stop speed peaks overlap. Stop transitions are recorded even though *R. sphaeroides* JPA1353 is a smooth swimmer. These could be due to incomplete removal of non swimmers, or to tracks at high angles being measured at lower speeds than they really are, factors that will affect all strains and contibute to experimental error. The variation in run speeds is likely to be real variation in the population as well as measurement error.

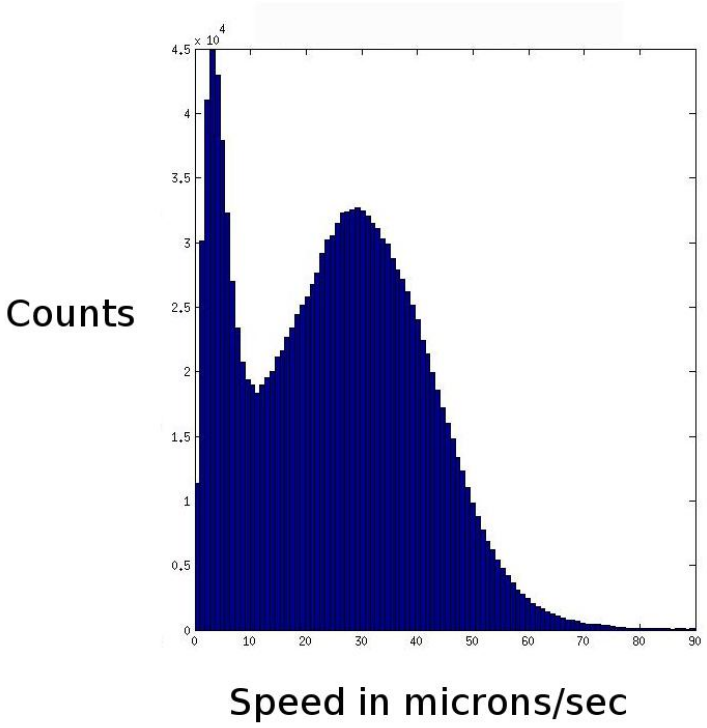


Figure 4.17: Histogram showing counts of different speeds (μms^{-1}) measured for single transitions, for log phase photoheterotrophically grown *R. sphaeroides* JPA1353 swimming in HEPES motility buffer at a glass surface for all tracks from nine 2 minute videos. The peaks corresponding to stops and runs can be seen at near 5 μms^{-1} and near 30 μms^{-1}, run speeds are up to 70 μms^{-1} and the run and stop speed peaks overlap. Stop transitions are recorded even though *R. sphaeroides* JPA1353 is a smooth swimmer. These could be due to incomplete removal of non swimmers, or to tracks at high angles being measured at lower speeds than they really are, or to transient surface attachment, factors that will affect all strains and contibute to experimental error. The variation in run speeds is likely to be real variation in the population as well as measurement error.

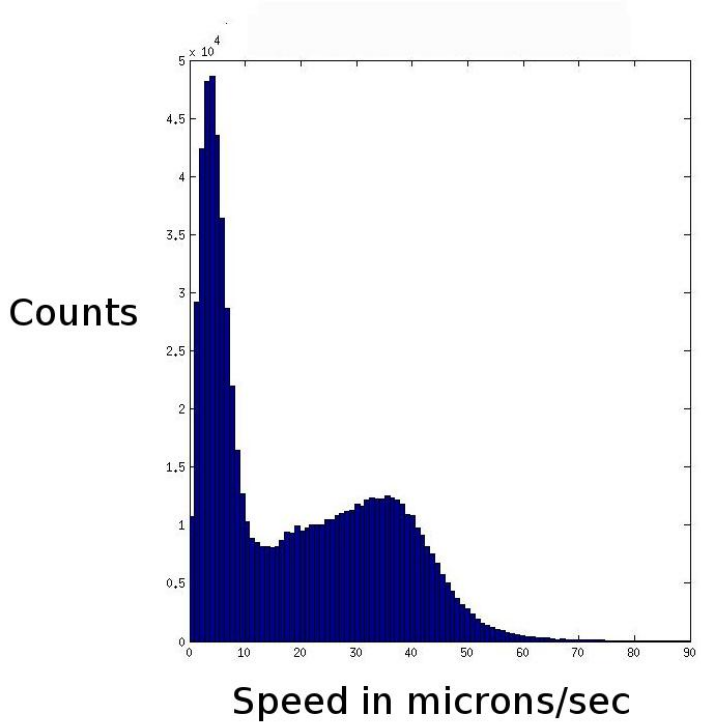


Figure 4.18: Histogram showing counts of different speeds (μms^{-1}) measured for single transitions, for log phase photoheterotrophically grown *R. sphaeroides* JPA1419 swimming in HEPES motility buffer away from a glass surface for all tracks from nine 2 minute videos. The peaks corresponding to stops and runs can be seen at near 5 μms^{-1} and near 40 μms^{-1}, run speeds are up to 70 μms^{-1} and the run and stop speed peaks overlap. Stop transitions are recorded even though *R. sphaeroides* JPA1419 is a smooth swimmer. These could be due to incomplete removal of non swimmers, or to tracks at high angles being measured at lower speeds than they really are, factors that will affect all strains and contibute to experimental error. The variation in run speeds is likely to be real variation in the population as well as measurement error.

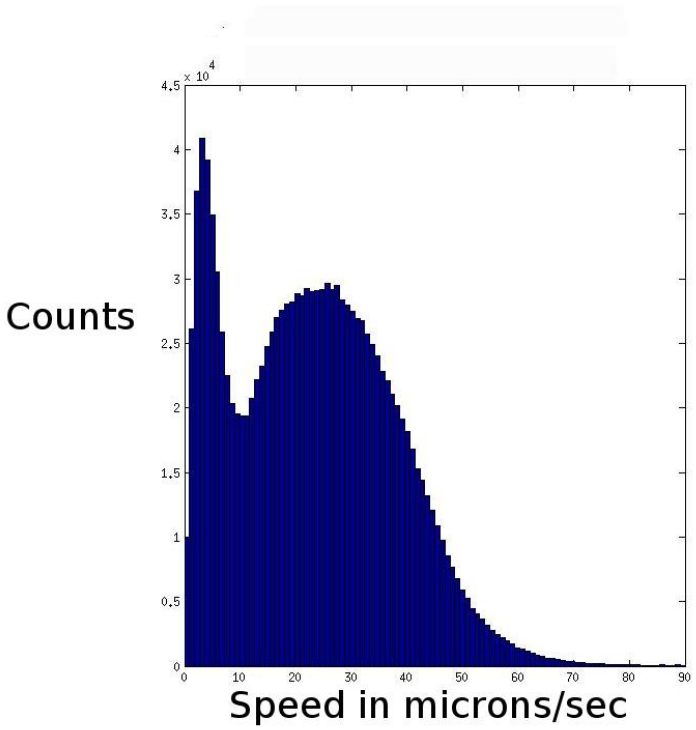


Figure 4.19: Histogram showing counts of different speeds (μms^{-1}) measured for single transitions, for log phase photoheterotrophically grown *R. sphaeroides* JPA1419 swimming in HEPES motility buffer at a glass surface for all tracks from nine 2 minute videos. The peaks corresponding to stops and runs can be seen at near 5 μms^{-1} and near 30 μms^{-1}, run speeds are up to 70 μms^{-1} and the run and stop speed peaks overlap. Stop transitions are recorded even though *R. sphaeroides* JPA1419 is a smooth swimmer. These could be due to incomplete removal of non swimmers, to transient attachment, or to tracks at high angles being measured at lower speeds than they really are, factors that will affect all strains and contibute to experimental error. The variation in run speeds is likely to be real variation in the population as well as measurement error.

4.7.3 Swimming behaviour of the frequently stopping strain *R. sphaeroides* JPA403 (Δ*che*Op2)

R. sphaeroides JPA403 has the second chemotaxis operon deleted (Figure 3.17). It is motile but not chemotactic (Porter et al., 2008) and has altered biofilm structure compared to *R. sphaeroides* WS8N after 5 days (Hale, 2009). It appears to stop more frequently than wild-type *R. sphaeroides* WS8N.

Nine cultures of each of *R. sphaeroides* JPA403 were grown photoheterotrophically in succinate medium (Appendix 11.0.3) to OD_{700} 0.6 (Section 2.2.2). Tracks from non-motile cells were removed using a speed sutoff of $15\mu ms^{-1}$ as described in Section 4.4 (Figs. 4.20,4.21).

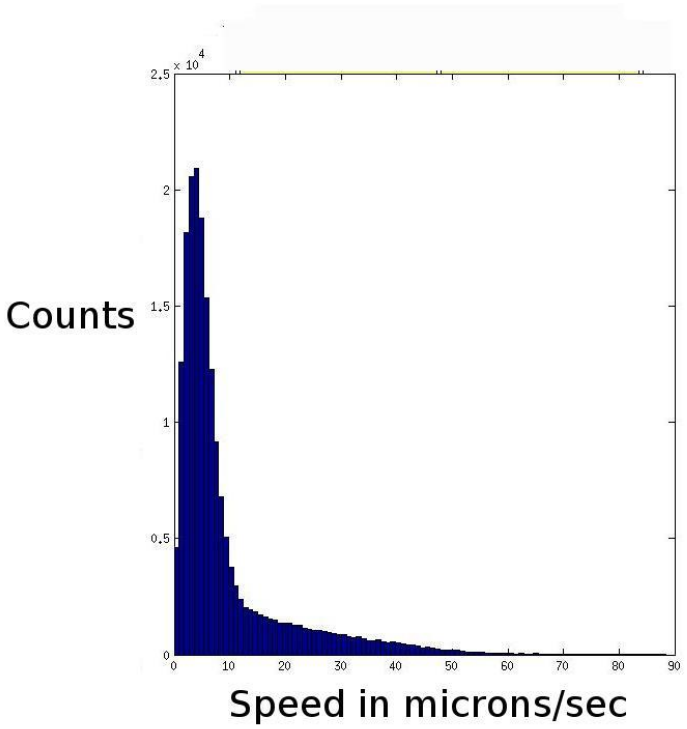


Figure 4.20: Histogram showing counts of different speeds (μms^{-1}) measured for single transitions, for log phase photoheterotrophically grown *R. sphaeroides* JPA403 swimming in HEPES motility buffer away from a glass surface for all tracks from nine 2 minute videos. There are fewer running transitions than in Figs. 4.14 to 4.19. The range of speeds is up to around 70μms^{-1} but a clear peak cannot be distinguished.

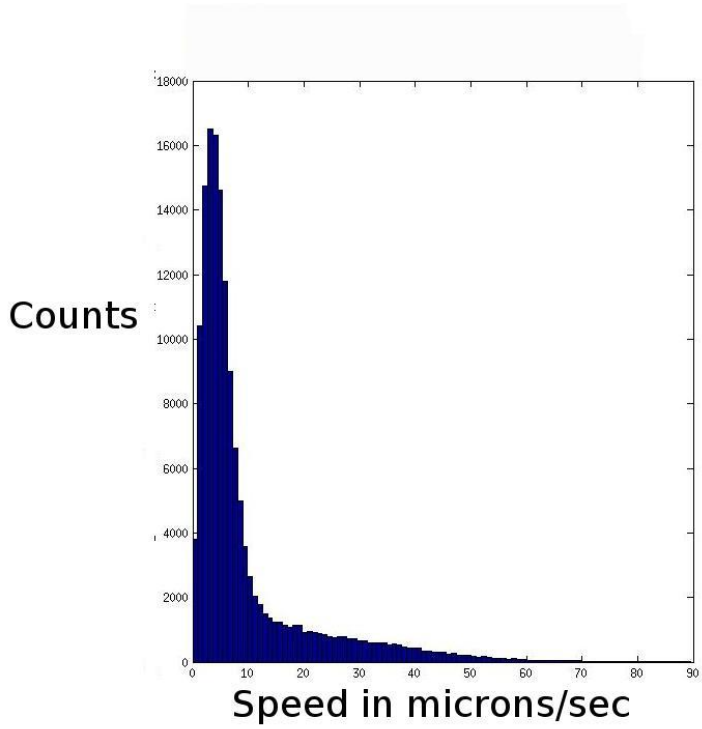


Figure 4.21: Histogram showing counts of different speeds (μms^{-1}) measured for single transitions, for log phase photoheterotrophically grown *R. sphaeroides* JPA403 swimming in HEPES motility buffer at a glass surface for all tracks from nine 2 minute videos. There are fewer running transitions than in Figs. 4.14 to 4.19. The range of speeds is up to around 70μms^{-1} but a clear peak cannot be distinguished.

4.7.4 Speeds of wild-type, smooth and stoppy strains

The range of measured speeds for the strains *R. sphaeroides* JPA117, JPA403, JPA1419 and JPA1353 shown in Figures 4.14 to 4.21 are the same as the range of measured speeds for *R. sphaeroides* WS8N shown in figure 4.6, speeds of up to $70\mu\text{ms}^{-1}$ with the lower swimming speeds overlapping the measured speeds for stopped cells. There is no evidence from these data that the range of swimming speeds has changed in any of these mutant strains, though the amount of time spent swimming may have changed.

Figure 4.22 gives the mean swimming speed per sample for each strain. Although some differences between strains were significant, the mean swimming speeds were close. There may be some bias in the data because the speed cutoff will remove some cells which are actually swimming and leave some which are stopped, and this may vary between strains. However, any effect of motility on attachment in these strains is unlikely to be a result of changed swimming speed.

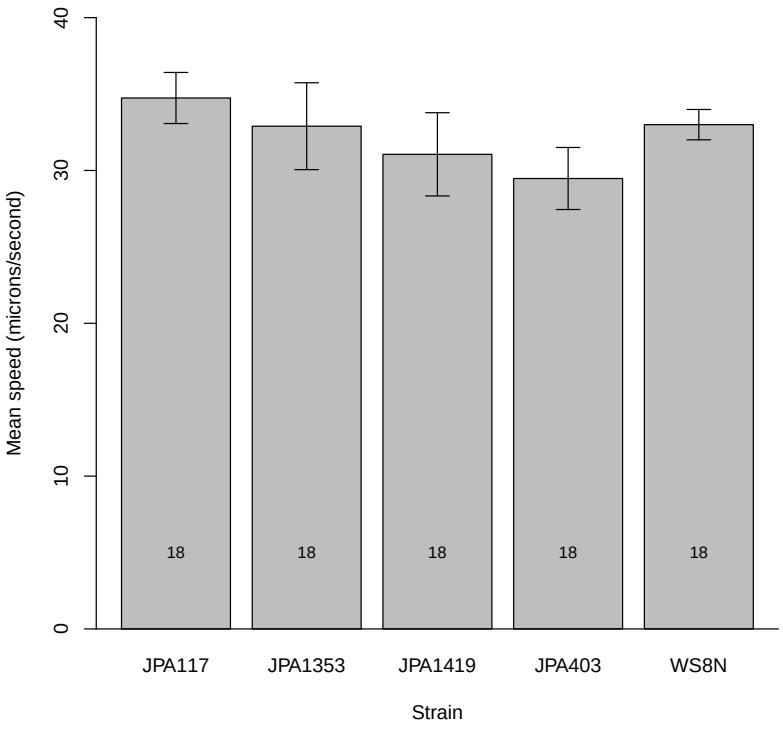


Figure 4.22: Comparing mean speeds for strains with different swimming patterns, at a surface and in the bulk fluid. Numbers of samples are shown on the bars. The error bars are standard deviation. The data were calculated by selecting transitions above the cutoff speed of $15\mu\text{ms}^{-1}$ and calculating the mean speed for each of 18 videos of log phase *R. sphaeroides* cells swimming in HEPES motility buffer. All swimming speeds are between 30 and $40\mu\text{ms}^{-1}$. A one-way between subjects ANOVA with Welch's correction (Section 2.9.2) was conducted to compare the effect of strain on mean swimming speed. Mean speed differed significantly as a function of strain for log phase photoheterotrophic cultures, F(4,40.525) = 19.19, p = 6.334e-09. Post-hoc pairwise t-tests with Holm's correction (Section 2.9.2) were performed to identify different strains. The strains did not cluster into separate groups, but there were significant differences ($p<0.05$) between WS8N and JPA403, and JPA403 and JPA117. However, the size of the difference is small.

4.8 Measuring the proportion of tracks which correspond to stops

In Chapter 3 it was stated that some mutant strains stopped more or less frequently than *R. sphaeroides* WS8N when swimming in the absence of a chemical gradient (Section 3.5.1), and it was suggested that this change in swimming might be linked to measured changes in surface attachment. However the classification of swimming behaviour as having more or fewer stops than normal has been done by visual inspection and has not been easy to extract from video data. The next sections show that the visual impression can be confirmed by analysing tracks.

By dividing tracks into run and stop transitions we can measure the proportion of time each cell spends stopped for each track, and compare the mean value between strains.

Nine cultures of each of *R. sphaeroides* JPA1419, JPA403, JPA117, JPA1353, JPA1215 and WS8N were grown photoheterotrophically in succinate medium (Appendix 11.0.3) to OD_{700} 0.6 (Section 2.2.2). For each culture 2 minute videos were taken at the capillary surface and in the bulk medium, as described in Materials and Methods 2.5.3. The videos were processed using the Tracker software to identify bacterial tracks, and the tracks were analysed to give a speed and an angle change for each transition, (Materials and Methods 2.7.4). Tracks from non-motile cells were removed using a speed cutoff of $15\mu ms^{-1}$ as described in Section 4.4. The remaining data was divided into run transitions and stop transitions using the same speed cutoff of $15\mu m\ s^{-1}$. Each video was treated as an independent sample and the mean stop/run proportion for all tracks in that video was calculated. This gave 18 data points for each strain. The strains were significantly different at the 0.05 level, grouping into four distinct groups (Fig. 4.23).

This agrees with the visual impression that JPA403 (*che*Op3 deletion) has a 'stoppy' phenotype while JPA1419 (*che*Op3 deletion) and JPA1353 (all chemotaxis operons deleted) have a 'smooth' phenotype, with fewer stops

than wild-type, while JPA117 (*che*Op1 deletion) has a similar proportion of stops to WS8N.

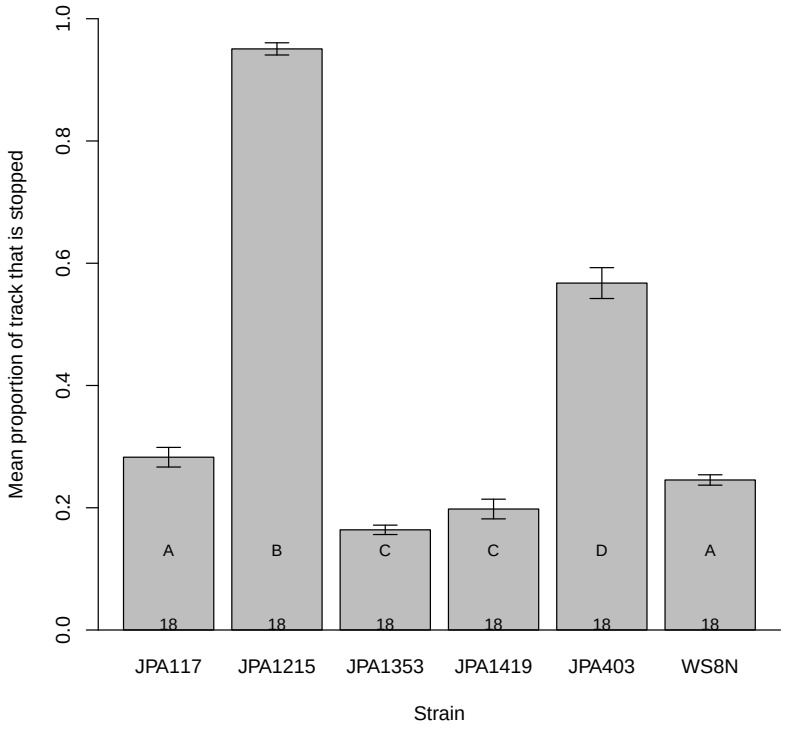


Figure 4.23: Proportion of track that is stopped, for strains JPA117, JPA1419, JPA1335, JPA403 compared to WS8N (wild-type) and JPA1215 (non-motile). The error bars are standard error. A one-way between subjects ANOVA with Welch's correction (Section 2.9.2) was conducted to compare the effect of strain on proportion of transitions that are in stops. This 'stop proportion' differed significantly as a function of strain for log phase photoheterotrophic cultures, $F(5,46.7) = 856.3699$, $p<2.2e\text{-}16$. Post-hoc pairwise t-tests with Holm's correction (Section 2.9.2) were performed to identify different strains. The letters in the bars show four distinct groups of strains, A, B, C and D clustered by significant differences at $p<0.05$. This implies that the visual impression that JPA403 stops more frequently than WS8N is correct, as is the impression that JPA1353 and JPA1419 stop less frequently than WS8N. The non-motile strain JPA1215 has a stop ratio of nearly 1, as expected, but the two strains that seem to stop rarely do show some stops, though at low levels. Experimental error could come from random movements in the non-motile strain being classified as runs, and from small runs at high angles to the slide plane being classified as stops.

4.9 Discussion of free swimming results

This chapter aimed to quantify the swimming behaviour of *R. sphaeroides* strains in order to more accurately assess the effects of motility changes on surface attachment.

The tracking, censoring and analysis methods used here provide data that is consistent with earlier studies for the wild-type strain *R. sphaeroides* WS8N.

The swimming speed is very variable from cell to cell, but the range of speeds and mean swimming speed are very similar for all the strains tracked (Section 4.7.4). Using the proportion of runs and stops in tracks shows clear differences between strains that look 'stoppier' or 'smoother' than wild-type, confirming the visual impression (Section 4.8).

From this tracking data we could estimate the mean stop length of wild-type *R. sphaeroides* WS8N, and the value was similar to that obtained previously (Brown, 2009). There were slightly longer stops near a surface than far from a surface. Mean run length could not be easily calculated from these data because few runs were complete, so that most run lengths were unknown and the complete runs measured were probably shorter ones (Section 4.6.4).

The data from this chapter show that swimming speed is not significantly different for *R. sphaeroides* WS8N swimming parallel to a surface or swimming in bulk medium. They show that the direction of swimming does change, as seen in other bacteria (Frymier and Ford, 1997; Lauga et al., 2006), with curved paths near the surface and straighter paths in bulk medium. Interestingly, prelimiary data from Section 4.6.3 suggest that *R. sphaeroides* WS8N does accumulate at surfaces, and this could be confirmed by further experiments.

Relating motility to the attachment results in Chapter 3, swimming speed is unlikely to be a factor affecting attachment in these strains, but stop frequency might be. Non-motile cells did not accumulate at surfaces as much as motile cells which could affect their attachment. Some bacterial species need the flagellum and motor to sense the surface (Section 1.2.3) but these

data suggests that motility itself may account for much of the attachment difference between strains in *R. sphaeroides* WS8N.

Chapter 5

Modelling attachment

5.1 Introduction

It is clear from the work in Chapter 3 that motility has an effect on *R. sphaeroides* surface attachment. Smooth swimmers attach more than frequently stopping swimmers, motile strains attach more than non motile strains, potentially motile strains in a non swimming condition attach at a similar level to non motile strains. Since changes in swimming behaviour are associated with changes in attachment behaviour in *R. sphaeroides*, perhaps the swimming behaviour alone is enough to predict the attachment behaviour. Watching swimming cells through a microscope, it is clear that non-motile cells will take a very long time to move away from their position, while motile cells move fast in all directions. Diffusion is a simple way to quantify this random movement.

The motion of a bacterium swimming in the absence of a chemical gradient can be modelled as diffusion, with the diffusion coefficient calculated from the characteristic swimming speed and angle change of the bacteria (Lovely and Dahlquist, 1975; Berg, 1993). Values of the diffusion coefficient are worked out from formulae linking the diffusion coefficient to swimming behaviour. 'In all cases of self-propulsion, ... the diffusion coefficient is proportional to

the square of the swimming speed and at least approximately proportional to the interval between changes of direction' (Dusenbery, 2009).

For *E. coli* Berg (1993) calculates the effective diffusion coefficients for normal and smooth swimming strains. Non motile *E. coli* , a rod shaped bacterium whose dimensions are 1 μm by 2 μm, should have approximately the diffusion coefficent of a sphere of radius 1 μm in water, which is around 0.2 μm^2 s^{-1} (Berg, 1993). This agrees with experimentally determined values for diffusion in several non-motile bacterial species. Rijnaarts et al. (1993). Using formulae derived in Lovely and Dahlquist (1975), Berg (1993) shows that swimming wild type *E. coli* K12 should have a diffusion coefficient D of around 400 $\mu m^2 s^{-1}$ (similar to a small molecule, for sucrose D = 520 $\mu m^2 s^{-1}$), and smooth swimming strains should have D = 2000 $\mu m^2 s^{-1}$, similar to that for oxygen in water. Berg and Turner (1990) estabished these values by experiments in capillary tubes. They also found that smooth swimming *E. coli* K12 diffused more slowly than expected, and suggested that this was because they spent time trapped at surfaces.

The time taken for diffusing objects to cover a distance is inversely proportional to the diffusion coefficient and directly proportional to the square of the distance. As bacteria attach to a surface, the local concentration of free cells drops and cells from further away move to the area. If they are moving at random, by diffusion, the time this takes depends on the diffusion coefficient and the distance travelled. Over the same distance, swimmers arrive 2000 times faster than non swimmers, and smooth swimming strains 10,000 faster.

The effect on attachment in the time scales of the experiments depends on how fast this happens. Immediately after the start, assuming initially constant concentration, the number of cells near enough to attach is the same for all strains, and after a very long time, all cells in the culture can reach the surface and attach. So the difference made by the diffusion coefficient is less at very early and very late times.

5.2 Aims

The aim of this chapter is to use a simple model based on diffusion to see whether it is plausible that the changed swimming characteristics of mutant strains of *R. sphaeroides* measured in Chapter 4 could explain the changed attachment measured in Chapter 3.

If movement alone could explain the greater attachment seen in smooth swimming mutants and the lower attachment seen in non-motile mutants there is no evidence for the need for a flagellum for surface sensing or adhesion in *R. sphaeroides*, although these mechanisms have both been found in other bacteria (Section 1.2.3).

5.3 Effect of motility on attachment

A simplified extreme situation is as follows (Fig. 5.2): We assume

1. Motile and non motile bacteria have the same probability of attaching if they are within d m of the surface.
2. The reservoir of culture is large enough that in the time considered the overall concentration is not affected by bacteria attaching.
3. Non motile bacteria do not move enough to replace attached bacteria in the time considered.
4. Motile bacteria move fast enough to completely replace attached bacteria immediately.

In that case, if the concentration of bacteria in the solution is C, an area A has $N_0 = CAd$ bacteria near enough to attach initially in both cases. In the motile case the concentration of bacteria at the surface stays the same throughout so that if the proportion of these cells attaching in a minute is α then after n seconds $n\alpha N_0$ have attached.

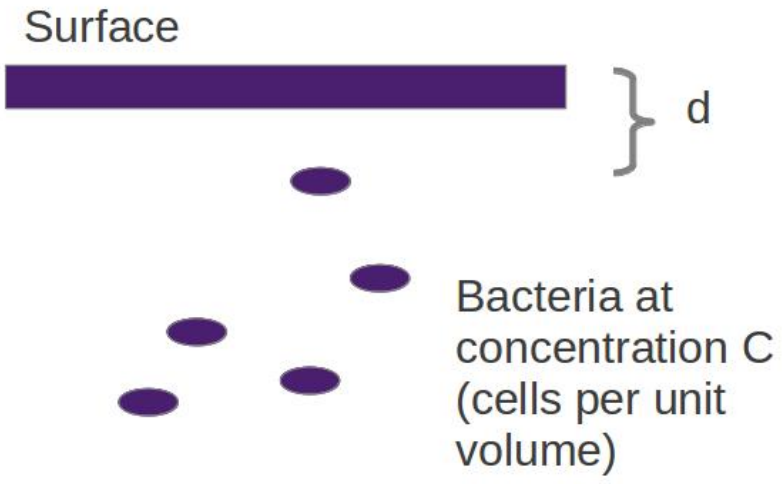


Figure 5.1: Cells can attach to the surface if they are within distance d. The concentration of bacteria in the fluid is C cells per unit volume and is initially constant. A cell which is within d of the surface has a probability α of attaching to the surface. Once a cell has attached the local concentration of cells is reduced until cells from the bulk fluid replaces it. For an area A on the surface, the volume of fluid near enough for cells to attach is Ad. The number of cells in this volume is CAd.

In the non motile case attached bacteria are not replaced and the concentration of bacteria close to the surface will decrease.

In the first minute αN_0 attach and the number near enough to attach decreases to $N_0(1-\alpha)$. So by the nth minute $N_0(1-\alpha)^n$ are left and $N_0 - N_0(1-\alpha)^n$ have attached.

This gives attachment of attached motile and non motile cells over time as shown in Fig. 5.2. The attachment of motile cells would in reality be less, since movement to replace them close to the surface is not instantaneous, and the attachment of non motile more, since there is some movement, so this model gives upper and lower bounds for times short enough that the overall concentration of bacteria in the media is not affected. The rate at which

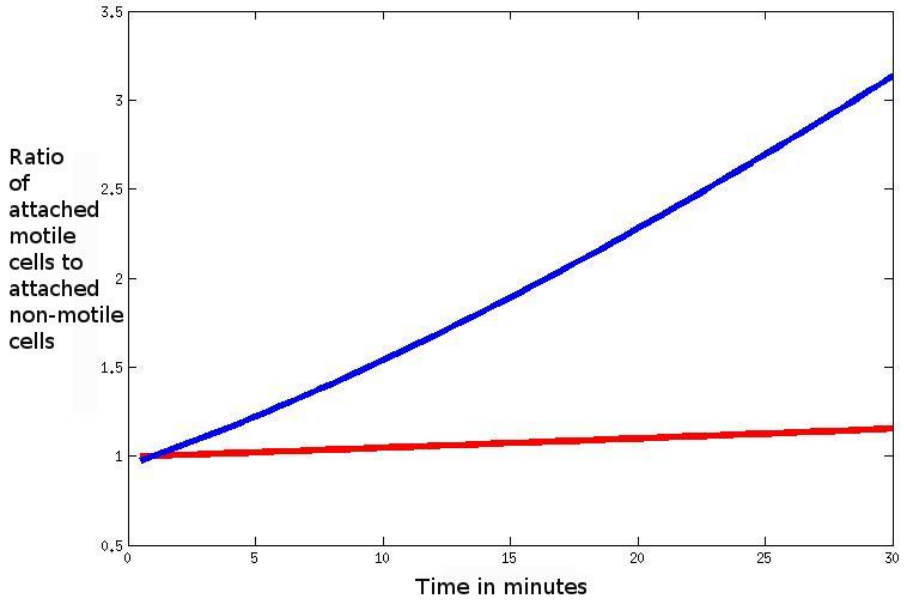


Figure 5.2: The red line shows the predicted ratio of motile to non-motile attached cells over the first 30 minutes when $\alpha = 0.01$ and the blue line shows the same ratio when $\alpha = 0.1$. The reason for the difference is that if cells rarely attach, even if near the surface, the numbers of nearby cells of both types stays the same for longer. If cells close to the surface frequently attach the speed of the motile cells replacing those lost to attachment has more effect.

attachment diverges between motile and non motile cells depends on the value of α, for low values the concentration drops slowly and the attachment rates stay similar for longer. For high values, the concentration of non motile cells near the surface drops fast and without replacement attachment levels off. This suggests that differences in attachment can be produced without the actual cells having a different probability of attaching.

If a cell with no flagellum could not detect and respond to the surface as well as not being able to swim, the value of α would be different from that for a cell with a working flagellum. This difference between cells may not be necessary to produce the observed differences in early attachment.

After 30 minutes incubation in light, the ratio of motile to non motile attachment for log phase photoheterotrophically grown cells is approximately 5 (Fig. 3.10). Using this figure,

$$\frac{30\alpha N_0}{N_0 - N_0(1-\alpha)^{30}} = 5 \tag{5.1}$$

$$\Rightarrow 30\alpha N_0 = 5(N_0 - N_0(1-\alpha)^{30}) \tag{5.2}$$

$$\Rightarrow 30\alpha = 5(1-(1-\alpha)^{30}) \tag{5.3}$$

$$\Rightarrow 30\alpha \approx 5(1-(1-30\alpha + \frac{30\times 29}{2}\alpha^2) \tag{5.4}$$

$$\Rightarrow 30\alpha = 5(30\alpha - \frac{30\times 29}{2}\alpha^2) \tag{5.5}$$

$$\Rightarrow 120\alpha = 5\times \frac{30\times 29}{2}\alpha^2 \tag{5.6}$$

$$\Rightarrow \alpha \approx 0.06 \tag{5.7}$$

This rough calculation implies that attachment results similar to experimental data at 30 minutes could be obtained on the assumption that motility alone leads to the difference between motile and non motile attachment.

5.4 Estimating the diffusion coefficients for the *R. sphaeroides* experimental strains

R. sphaeroides WS8N swims differently from *E. coli* K12, with higher velocity and longer stops. Their size is similar and therefore the same estimate of D=0.2 μm^2 s^{-1} can be used for the non-motile strain.

Lovely and Dahlquist (1975) derive the formula

$$D = \frac{v^2\tau}{3(1-\alpha)} \tag{5.8}$$

where D is the diffusion coefficient, τ is the mean run length, v is the velocity, and α is the mean value of the cosine of the angle between successive runs.

For smooth swimming strains, there is no angle between runs and the run length is unlimited, but then the runs are affected by rotational diffusion - because the bacterium is knocked so as to turn it, the path of a long run is not straight, and the formula for the diffusion coefficient becomes:

$$D = \frac{v^2}{6D_R} \tag{5.9}$$

where D_R is the rotational diffusion coefficient of the cell.

To allow for rotational diffusion, Lovely and Dahlquist (1975) suggest considering a bacterial track as a Poisson process resulting from two independent Poisson processes, one the sequence of runs and large angle changes with mean cosine α_t and the other very short runs with small angle changes with mean cosine α_r.

To allow for stops of non-zero time, Lovely and Dahlquist (1975) suggest the assumption that zero distance is traversed during a stop, in which case 5.8 becomes

$$D = (\frac{\tau}{\tau + \tau_s})(\frac{v^2\tau}{3(1-\alpha)}) \tag{5.10}$$

where τ is the mean duration of a trajectory and τ_s is the mean duration of a stop.

Therefore, values needed from bacterial tracks are mean speed, mean angle change between runs and mean run and stop durations.

For photoheterotrophically grown log phase *R. sphaeroides* WS8N the mean swimming speed was approximately 35 μms^{-1} (Section 4.5.2). The mean stop duration when swimming away from a surface was 0.6 seconds and the mean run duration away from the surface was 0.4 seconds. However there was bias in the data towards shorter runs (Section 4.13). Studies using different methods of measuring baseline run and stop durations of *R. sphaeroides*

without a chemical gradient have usually found runs three or four times longer than stops (Rosser et al., 2013). Because of the bias in my run length measurements I will use the values from Rosser et al. (2013), which are mean run length 1.16 seconds and mean stop length 0.4 seconds.

Using these figures in equation 5.10, and assuming random angle change between runs, so that the mean value of $\cos \alpha = 0$ (Berg, 1993), the estimated diffusion co-efficient for swimming WS8N *R. sphaeroides* is

$$D = (\frac{\tau}{\tau + \tau_s})(\frac{v^2\tau}{3}) \tag{5.11}$$

$$= (\frac{1.16}{1.16 + 0.4})(\frac{35^2 \times 1.16}{3}) \tag{5.12}$$

$$= 352\ \mu m^2 s^{-1} \tag{5.13}$$

This is similar to that worked out for *E. coli* in Berg (1993).

5.5 Partial differential equation model based on motility only

The swimming behaviour can be modelled in one dimension, using the diffusion equation, and ignoring gravity, growth, and surface forces. It is assumed that when bacteria reach the surface a proportion will attach. This proportion is assumed to be the same for all bacteria, whether or not they possess a flagellum or are able to swim.

The bacterial culture is modelled as a continuous concentration along a line, where the initial concentration is constant and attaching bacteria are represented by some loss at both ends, the loss being proportional to the concentration at the ends.

We will base the calculations on the well established *E. coli* statistics used

by Berg (1993), and then consider the effect of the differences in the *R. sphaeroides* data.

The boundary conditions at the ends are therefore flux proportional to concentration. This is Robin boundary conditions.

In one dimension on the region $0 <= x <= L$

$$\frac{\partial c}{\partial t} = D\left(\frac{\partial^2 c}{\partial x^2}\right) \tag{5.14}$$

Where c is the concentration of bacteria at position x, D is the diffusion coefficient, t is time and x is the position in space.

At each boundary some of the bacteria will attach to the surface. This is assumed to be proportional to the concentration. So at x = 0

$$\frac{\partial c}{\partial x} = \alpha c \tag{5.15}$$

and x = L

$$\frac{\partial c}{\partial x} = -\alpha c \tag{5.16}$$

Initially the culture was well mixed in the experiments, so we assume that initially c is constant.

At $t = 0$

$$c = c_0 \tag{5.17}$$

The behaviour is dependent on time and space. As bacteria leave the system (by attaching), diffusion evens out the concentration in the media, and the eventual steady state will be the same whatever the diffusion coefficient. This steady state is irrelevant in reality as attachment is slow and cells divide so longer times invalidate the assumptions. We are interested in the time and length scales used in the experiments, and in whether in this initial transient stage the changed diffusion coefficient is sufficient to explain the changed attachment.

By non dimensionalising the equation we can recover results that are independent of the units used.

Suitable substitutions are:

$$X = \frac{x}{L} \tag{5.18}$$

$$T = \frac{Dt}{L^2} \tag{5.19}$$

The equation then becomes

$$\frac{\partial c}{\partial T} = \frac{\partial^2 c}{\partial X^2} \tag{5.20}$$

and the boundary conditions at X = 0 and X = 1

$$\frac{\partial c}{\partial X} = L\alpha c \tag{5.21}$$

The initial condition is constant concentration of cells in the media.

This equation can be solved numerically with the explicit finite difference method. The method converges for suitable choices of space and time discretisation. The boundary conditions are applied at each timestep and the depleted concentration recorded, as this is proportional to attached cells in this model.

The solution of the nondimensionalised equation shows an initial rise in attached cells which eventually plateaus, and a drop in concentration of unattached cells at the ends of the region, spreading through the region over time (Fig. 5.3). For a given attachment coefficient α, the shape of the solution is the same for any value of the diffusion coefficient, but the time taken to reach a given place will vary and can be calculated for changes in the diffusion coefficient.

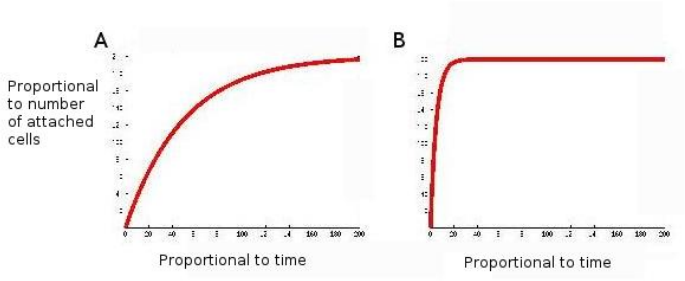


Figure 5.3: Modelling attached cells as cells lost from a one dimensional region due to flux at the boundaries proportional to concentration. A) The probability of attachment, $\alpha = 0.00001$, B) $\alpha = 0.0001$.

The substitution

$$T = \frac{Dt}{L^2}$$

shows that the timescale is inversly proportional to the diffusion coefficient. Thus the position on the curve at a given time will depend on the diffusion coefficient, and if that is divided by 10 the time taken will be multiplied by 10.

This means that this simplified model predicts that at early timepoints there will be more attached cells the higher the diffusion coefficient, and that swimmers will thus initially attach more for that reason alone.

To substitue actual numbers, the length scale for the staining experiments is the radius of a well, mm, and the timescale is seconds. The diffusion coefficients are 2.2 x 10^{-13}m^2 s^{-1}

An unknown number that has a large effect is the proportion of cells at the surface which attach at each timepoint. We can see from observation of surfaces with a microscope that cells can swim near the surface without attaching and attachment is not universal if cells approach. Small values of the attachment coefficient α in the boundary condition increase the time

taken for the early increasing part of the graph.

The conclusion from this model is that it is likely that the different motility properties of non swimmers, normal swimmers and smooth swimmers will give different amounts of attachment at timescales short enough to ignore cell division. If we had a value for the proportion of cells that do attach at a distance of δx from a surface we could predict the actual differences in the three cases, assuming no other forces or properties were involved.

We could use the values from the experiments in Chapter 3 to estimate the attachment coefficient α given the lengths and times used and assuming it is constant and the same for all strains.

This is very rough and to improve the model it would be useful to have an independent measurement of the attachment coefficient α and to see whether the assumption that *E. coli* swimming is sufficiently similar to *R. sphaeroides* swimming is reasonable.

5.6 Diffusion and attachment in three dimensions

The experiments in Chapter 3 are done using 96 well plates. In the simplified case where the time is short enough to neglect growth and gravity (any sedimentation of cells is very slow and takes days rather than minutes (personal observation)), and any bulk movements in the fluid are ignored, the situation can be modelled exactly. It is reasonable to assume that the attachment coefficient α is the same for all solid surfaces of the well. The boundary conditions are different at the top of the well, instead of attachment there is no flux, since bacteria do not leave the culture. Using cylindrical co-ordinates for one well, if the z axis is central the bevaviour is symmetrical for ϕ and a 2 dimensional model in ρ and z can be used (Fig. 5.4.

If the z axis is central in a well, boundary conditions are flux at the well surface proportional to concentration (modelling attachment as loss through

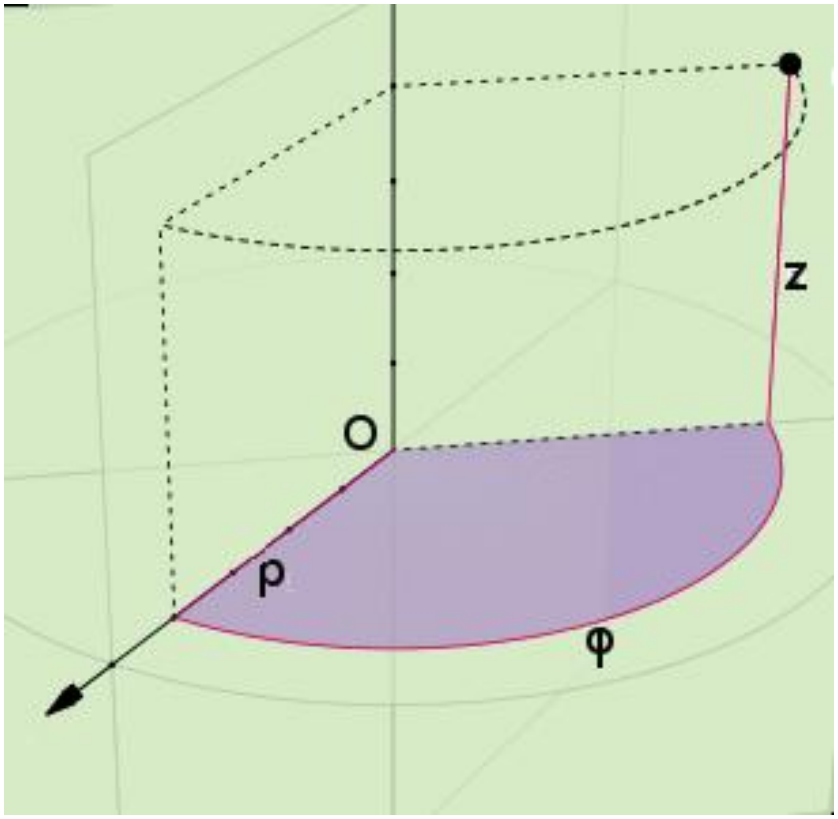


Figure 5.4: Cylindrical co-ordinates (Image adapted from Wikipedia Commons)

the wall), no flux at the top of the well (bacteria do not leave the culture into the air) and no flux at the artificial boundary at $\rho = 0$ up the centre of the well, since by symmetry there is no overall movement there.

The diffusion equation with constant diffusion coefficient in cylindrical co-ordinates is:

$$\frac{\partial C}{\partial t} = D\left(\frac{\partial^2 C}{\partial \rho^2} + \frac{1}{\rho}\frac{\partial C}{\partial \rho} + \frac{1}{\rho^2}\frac{\partial^2 C}{\partial \phi^2} + \frac{\partial^2 C}{\partial z^2}\right) \tag{5.22}$$

where C is concentration, t is time, D is the diffusion coefficient and the co-ordinates are as above.

Since diffusion in the wells does not depend on the angle ϕ, $\frac{\partial C}{\partial \phi}$ is zero and

the term $\frac{1}{\rho^2}\frac{\partial^2 C}{\partial \phi^2}$ disappears, leaving

$$\frac{\partial C}{\partial t} = D\left(\frac{\partial^2 C}{\partial \rho^2} + \frac{1}{\rho}\frac{\partial C}{\partial \rho} + \frac{\partial^2 C}{\partial z^2}\right) \tag{5.23}$$

The boundary conditions are no flux at the top and at one side, and flux proportional to concentration at the bottom and the other side. The initial condition is constant concentration.

At each boundary some of the bacteria will stick. This is assumed to be proportional to the concentration. So at $\rho = r_0$ and at $z = h$

$$\frac{\partial c}{\partial x} = \alpha c \tag{5.24}$$

Initially the culture was well mixed in the experiments, so we assume that initially c is constant.

At $t = 0$

$$c = c_0 \tag{5.25}$$

The steady state solution is zero concentration and all cells attached, but the time taken to reach this will be very long and the assumption of no growth would be violated. The interesting solutions are the time dependent solutions at early time points.

The wells are 6.4 mm diameter and the volume of culture used is 100 μl. The initial concentration at OD 0.3 is roughly 200 x 10^6 cells/ml (Fig. 3.9). The diffusion coefficient of a non motile cells is approximately 2.2 x $10^{-9} cm^2 s^{-1}$ (Berg, 1993). The proportion of cells attaching is unknown. Experimental data in the previous chapter shows the ratios of attached cells after 30 minutes incubation in wells.

Using the diffusion coefficients calculated for wild type and smooth swimming *E. coli* in Berg (1993) we can estimate the difference in attachment at early time points for motile, wild-type and smooth swimming cells on the assumption that the proportion of cells attaching is the same. We know that

the size and shape of the cells is the same, and so is the growth rate.

The equation can be non-dimensionalised as before, setting

$T = Dt/{r_0}^2$

$R = \rho/r_0$

$Z = z/r_0$

where r_0 is the radius of the well.

Then

$$\frac{\partial T}{\partial t} = \frac{D}{r_0}^2$$
$$\frac{\partial R}{\partial \rho} = \frac{1}{r_0}$$
$$\frac{\partial Z}{\partial z} = \frac{1}{r_0}$$

and equation 5.23 becomes

$$\frac{\partial C}{\partial T} = \left(\frac{\partial^2 C}{\partial R^2} + \frac{1}{R}\frac{\partial C}{\partial R} + \frac{\partial^2 C}{\partial Z^2}\right) \tag{5.26}$$

with boundary conditions

At $R = 1$

$$\frac{\partial c}{\partial R} = \frac{1}{r_0} \times \alpha c \tag{5.27}$$

At $R = 0$

$$\frac{\partial c}{\partial R} = 0 \tag{5.28}$$

At $Z = 0$

$$\frac{\partial c}{\partial Z} = \frac{1}{r_0} \times \alpha c \tag{5.29}$$

At $Z = h/r_0$

$$\frac{\partial c}{\partial Z} = 0 \tag{5.30}$$

and initial condition constant concentration as before.

Using the MATLAB PDE toolbox and solving equation 5.23 using the Finite Element Method, the results for the three cases non-motile, motile and smooth swimming are shown in Fig. 5.5, with the proportion of cells attaching as 0.01*concentration per second.

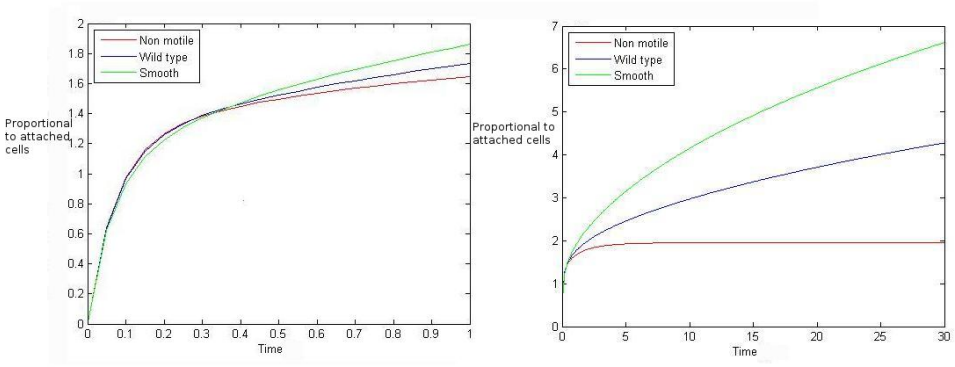


Figure 5.5: Predicted attached cells for non motile, motile and smooth swimming cells after A) 1 s and B) 30 s, assuming that the proportion of near surface cells attaching is 0.01*concentration per second.

Since the time of the experiments is known (30 minutes) and the results of the attachment assays give ratios of attached cells for non-motile, motile and smooth swimming strains, this model could be adjusted to estimate the rate of *R. sphaeroides* attachment under these assumptions. The diffusion coefficients of wild-type and smooth swimming *R. sphaeroides* cells, estimated using the data from Chapter 4 and from Rosser et al. (2013), and calculated using the formulae in Section 5.4 and Berg (1993), are shown in Table 5.1. These are rough estimates, since different studies have found different values for speeds and run and stop lengths in both *E. coli* and *R. sphaeroides* . Reasons for the differences are discussed in Rosser et al. (2013) and include different experimental techniques and different media. *R. sphaeroides* swims faster than *E. coli* and has longer runs and stops, according to the results

Table 5.1: The predicted diffusion coefficients in $\mu m^2 s^{-1}$ of *R. sphaeroides* strains compated to those given for *E. coli* in Berg (1993).

Strain	*R. sphaeroides*	*E. coli*
wild-type	474	400
wild-type including stops	352	-
smooth swimming	3293	2000
non-motile	0.2	0.2

in Rosser et al. (2013). However, the proportional differences between non-motile, wild-type and smooth swimming are similar and could lead to large differences in access to a surface over a period of 30 minutes.

5.7 Discussion of 'motility only' model and assumptions

This chapter aimed to develop a very simple mathematical model to see if altered swimming alone could be sufficient to explain the different attachment seen in chapter 4.

Interestingly, motility alone predicts differences in attachment which match observations to some extent. Non motile cells attach less than wild-type cells, and smooth swimming cells attach more. Using the crystal violet assay, attachment for the different non motile strains was similar, but the different smooth swimming strains attached to noticeably different extents, with JPA1353 being very similar to wild-type WS8N, and JPA1336 being significantly more likely to attach.

The assumption that any cell that is near a surface has an equal chance of attaching may be false. Cells with a flagellum might attach more often than cells without, either because the effective size of the cell and thus the likelihood of it touching the surface changes, or because attachment by the flagellum is a common precursor to permanent attachment, or because the

flagella of attached cells and discarded flagella on the surface increase stickiness for swimming cells.

Modelling swimming in the absence of a chemical gradient as diffusion may break down near the surface. The equations used to derive the diffusion coefficents are based on the following assumptions about tracks (Lovely and Dahlquist, 1975).

- The path of a bacterium is a sequence of straight line trajectories joined by instantaneous turns.
- Speed is constant.
- When a bacterium turns its new direction comes from a probability distribution symmetric about the initial direction.
- The angle between trajectories does not depend on information such as the original direction or trajectory duration.
- For any direction the probability density function for the length of a trajectory is a decaying exponential.

These assumptions can be modified to include rotational diffusion and longer stops, but may be invalidated if, for example, rotational diffusion is not random (Lovely and Dahlquist, 1975). While diffusion may model swimming in bulk fluid adequately, and thus predict differences in approaching surfaces, several studies suggest that the presence of a nearby surface affects swimming in many bacteria (Frymier and Ford, 1997; Lauga et al., 2006; Shum et al., 2010), and this is also true for *R. sphaeroides* (Chapter 4).

Nevertheless, this simple model does suggest that the effects on swimming behaviour seen with the mutant strains could be sufficient to explain their different abilities to colonise surfaces, without the need to involve the flagellum either as an attachment organelle or as a surface sensor.

Chapter 6

Rhodobacter sphaeroides attachment of single cells to a surface.

6.1 Introduction

In Chapter 3 initial attachment for motility mutants was compared using crystal violet staining, which gives an estimate for the quantity of attached cells. In Chapter 4 the swimming differences between strains and at surfaces was compared. It seems possible from the data so far that swimming differences alone could explain the large attachment differences between motile and non motile strains. Aflagellate cells can attach to surfaces and non motile cells with flagella attach only slightly more than aflagellate cells. This means that the flagellum is not essential for initial attachment and if it helps, it doesn't help much.

There are several roles for the flagellum in surface attachment in other bacterial species, described in Section 1.2.3.

R. sphaeroides flagella spontaneuosly stick to glass surfaces such as microscope slides (personal observation). Looking through a microscope at a motile

strain of *R. sphaeroides* near a surface, there are usually several tethered cells spinning in place, with the flagellum stuck to the surface and the cell body free to rotate. However, *R. sphaeroides* can continue to rotate in this way for at least an hour without stopping and attaching more firmly. It is not clear whether flagellar attachment precedes attachment of the cell body and permanent surface attachment, or whether spontaneously tethered cells tend to detach and swim away, and surface attachment leading to biofilm formation is a separate process.

6.2 Aims

The aim of this chapter is to examine the behaviour of single *R. sphaeroides* cells as they approach a surface and attach, and to test the hypothesis that *R. sphaeroides* cells always attach to a surface initially by flagellar tethering.

6.3 Initial attachment to a glass surface

6.3.1 The attachment process in *R. sphaeroides* WS8N

When a glass slide is immersed in a culture of motile *R. sphaeroides* cells in succinate medium (Appendix 11.0.3), cells begin to attach to the surface of the slide within seconds. Unattatched cells swim or show Brownian motion whereas attached cells may be rotating, tethered by the flagella, completely still, or wobbling about a fixed point. The different motion of attached cells can be seen by superimposing video frames as in Fig. 6.1

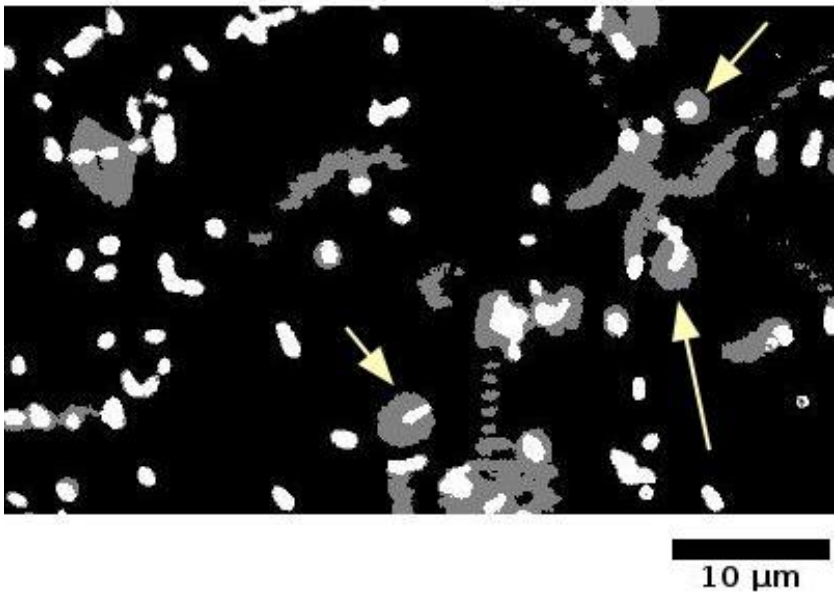


Figure 6.1: Superimposed frames from a 2 second video of *R. sphaeroides* WS8N cells at a surface. White shows the position of the cells in the final frame, grey shows the cell positions in previous frames. Circular regions show tethered cells (arrows). There are also some bacteria which have moved very slightly and some which have not moved in the time (2s). The triangular grey region in the top left of the image is a short chain of cells anchored at one end and waving from side to side.

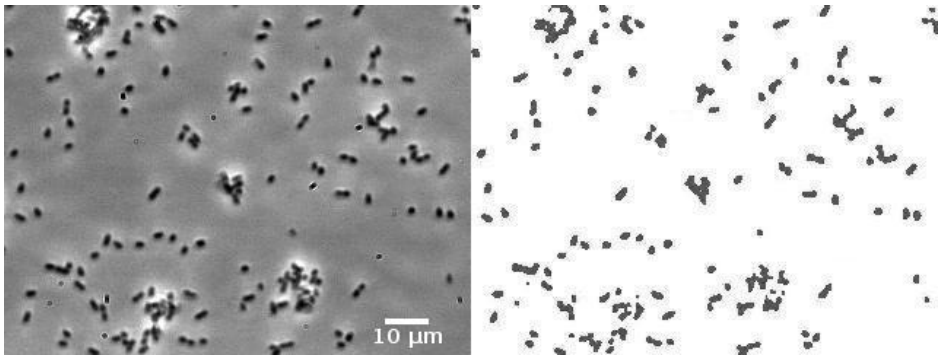


Figure 6.2: Field of view 20 minutes after immersion in *R. sphaeroides* WS8N log phase culture in succinate medium (Appendix 11.0.3). The second image has been segmented by thresholding, the first is the original image. There are attached cells a few minutes after immersion in bacterial culture.

6.3.2 Recording the first exposure of cells to a surface

When a slide is immersed in culture and removed for microscopy, or when a capillary is made up and moved to a microscope, there are usually already a set of attached cells in the first images (Fig. 6.2). Cells that attach to the surface immediately may differ from cells that do not attach. Possibly a proportion of cells are ready to attach, or possibly all the cells have an equal chance of attaching.

To capture this initial approach the first five minutes of attachment were recorded using a tunnel slide (Materials and Methods 2.4.4). Nine cultures of *R. sphaeroides* WS8N were grown photoheterotrophically to OD_{700} 0.6 (Section 2.2.2) in succinate medium (Appendix 11.0.3). A mark was made on a coverslip to enable focusing, then the tunnel slide was constructed with the mark on the lower (inside) surface of the coverslip (Materials and Methods 2.4.4). Recording was started at 50 frames s^{-1} as described in Section 2.5.3, and then the culture was allowed to flow in using capillary action.

The recordings show the initial flow as cells fill the tunnel, the flow stops when the tunnel is full and attaching cells were counted and classified. This was done manually, first all cells in focus at the final timepoint were identified and then the video file was processed to show the tracks made by those cells, making a library of 565 individual tracks. Attached cells were then classified into tethered (rotating) and still (Table 6.1). To be recorded as still a cell had to be motionless for 10 frames, to be classified as tethered it had to be rotating in place for at least 10 frames.

For each cell attached at 5 minutes, the time it attached was recorded. This was done by tracking back through the videos of attached cells to find the point where they attached. There was a peak in attachment in the first minute, followed by a fairly stable rate of attachment for the next four minutes (Fig. 6.3). This could support the idea that some cells are in a state which facilitates attachment, but the conditions throughout the experiment change since there is flow for a few seconds as the culture fills the tunnel slide, which is an alternative explanation.

Table 6.1: 5 minute Tunnel Slide Results. 565 cells from 9 tunnel slides were checked by eye to classify their mode of attachment.

Property	Value
Number of cells in focus after 5 minutes in 12 samples	565
Percentage attached	63
Percentage of attached that are tethered (rotating)	53

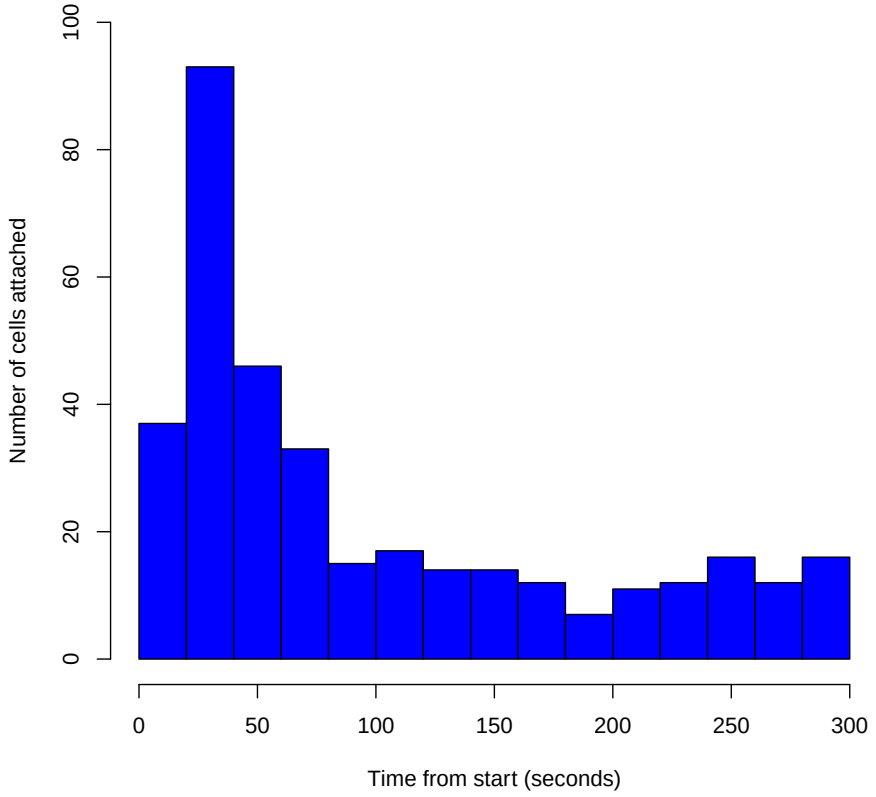


Figure 6.3: The counts of cells attached at different times after the start, for all cells attached at 5 minutes. There is a peak early on, showing that many of the cells attached to the surface at 5 minutes had attached in the first minute. After the first minute the rate of attachment of new cells looks stable. This supports the suggestion that some cells are ready to attach, but could also be due to the different flow conditions at the early stages of this experiment.

6.3.3 Time the first cell attached

After flow started the first attached cell appeared within seconds in all cases. These earliest attached cells appeared as the flow slowed and the cells appeared to be still, not rotating. The first cell to attach remained attached and unmoving for the entire 5 minute video in all videos. The average time from start of flow to first attachment was 7 seconds and the standard deviation was 3 seconds. This implies that at least some planktonic cells are immediately ready to attach firmly to a surface.

6.3.4 Type of initial attachment

Fig. 6.4 shows that cells attached to a glass surface 5 minutes after first access to the surface are divided into still and rotating roughly 50:50, and that few of the cells changed their attachment type within the 5 minutes of observation.

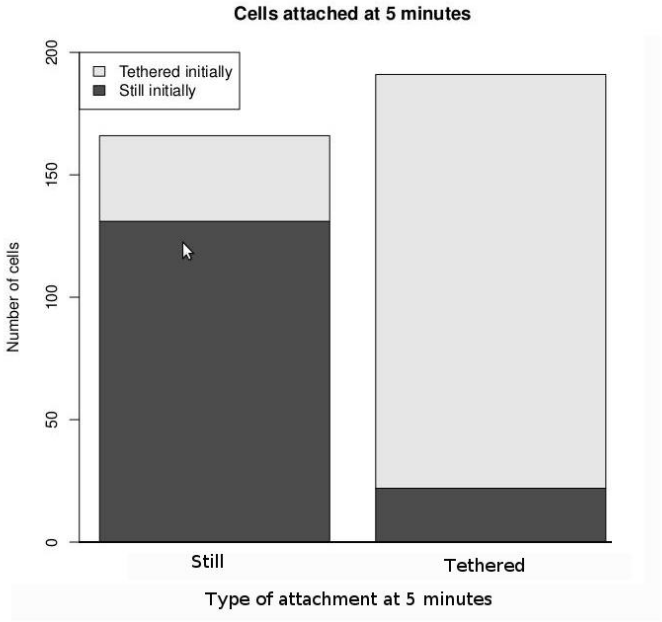


Figure 6.4: Cells attached after 5 minutes in 9 tunnel slides. Cells are finally still or rotating (tethered). Cells can attach by tethering or by sticking and stopping still. Some cells attach as tethered and become still, some attach still and later rotate, but most cells do not change their attachment type in the 5 minute period.

Table 6.2: Log phase photoheterotrophically grown *R. sphaeroides* WS8N cells which were tracked in a tunnel slide for 5 minutes and had attached to the coverslip by one minute from the start. Counts were taken of cells which were still attached or detached at 5 minutes, and whether they were still or rotating initially. Pearson's chi-squared test gives X-squared = 1.2221, df = 1, p = 0.269, so the type of initial attachment has no effect on the likelihood of detaching over 5 minutes at the 0.05 significance level.

	Detached at 5 mins	Attached at 5 mins
Initially still	8	70
Initially tethered (rotating)	18	87

To measure detachment in the first 5 minutes the same process was followed with an intermediate timepoint, cells were identified as stuck, tethered or unattached, and their initial attachment (tethered or still) and final fate (attached or detached) were recorded. The aim was to see whether there was any connection between the initial method of attachment and the permanence of attachment. It could be that tethering by the flagellum is the main mechanism, or it could be that tethered cells tend to detach and attachment by another method is more permanent. However, from these data there is no evidence that cells which first attach by tethering are more or less likely to detach over the first 5 minutes than cells which are initially still (Table 6.2).

6.4 Build up of attached cells over 6 hours in a static microcosm

Static microcosms were set up as explained in Materials and Methods Section 2.5.1. Coverslips cleaned with KOH were placed in 50 ml Falcon tubes, each of which contained 15 ml of *R. sphaeroides* WS8N culture at OD 0.2 at 700 nm (early log phase). Three independent cultures were used and 12 identical Falcon tubes made up for each. The Falcon tubes were incubated in microaerobic conditions in white light at 10 Wm^{-2}. Every hour one coverslip from each culture was removed, prepared as described in Material and Methods, and three short videos taken at set points on the coverslip. The OD of the culture was also recorded. The images were segmented to identify cells and clusters of cells.

Videos were used so as to identify moving cells in focus near the coverslip but not attached. 9 10-frame videos were taken at a frame rate of 5Hz at each timepoint. The background was calculated by averaging all the first frames of the 9 different videos - any constant features that showed in each video will be artefacts in the microscope and were removed. Then still cells were identified by averaging the 10 frames of each video and selecting the darkest objects. Moving objects were lighter gray. The number of attached objects at each timepoint was then calculated (Fig. 6.5). The number of cells attached in a single field of view can clearly be seen to increase over the time.

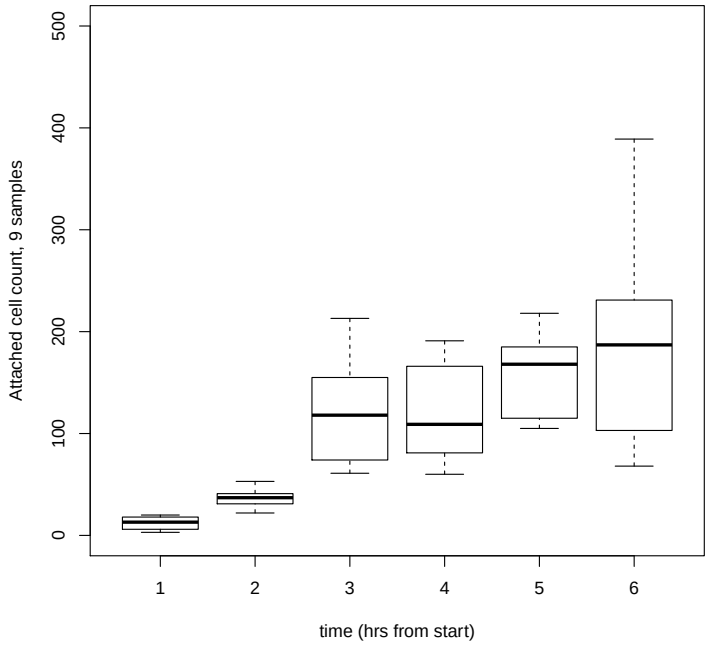


Figure 6.5: A box plot showing counts of *R. sphaeroides* WS8N cells attached to a coverslip at hourly intervals for 6 hours in succinate medium, starting with log phase cells (OD 0.4 diluted to OD 0.2). In these data, the number of attached cells increases over time, and the range of the data also increases, ie the coverage becomes more variable at later timepoints. Measured OD at 700 nm: 1 hr 0.28; 2hrs 0.35; 3 hrs 0.49; 4hrs 0.67; 5 hrs 0.86; 6 hrs 1.34. The cultures reached stationary phase by 6 hours.

Reasonable conclusions are that cells can both attach and detach, that coverage does increase over time in these circumstances, but with considerable variation, and that cell positions are more clustered at later timepoints. A possible explanation is that cells attach, some detach but those that remain nucleate clusters, which may develop by cell division or by new cells frequently attaching near already attached cells.

6.4.1 Discussion of single cell attachment experiments

The aim of this chapter was to determine how cells initially attach to a glass surface.

The data suggest that while initial attachment by the flagellum is common, it is not the only mechanism. Attachment by the flagellum does not quickly lead to more stable attachment. Flagellar tethering and cell body attachment may be separate mechanisms in *R. sphaeroides* WS8N, and it is possible to move from one form of attachment to the other during the first minutes after attachment. For comparison, the majority of *C. crescentus* cells which tethered to a glass surface stopped spinning in seconds, and those that continued to spin went on to detach (Li et al., 2011).

One question is whether we can always detect tethered cells. It is likely that for *R. sphaeroides* we can since the flagellum is subpolar and the cells are elongated (non-spherical). A cell attached at the pole could spin undetected but flagellar attachment at the pole is not likely. However, it is possible that the occasional spinning cell is wrongly classified. Spinning cells appear to set up a small vortex which affects nearby cells, and inability to detect this is also a sign that a cell is not tethered.

As cells grow a new flagellum is produced for the daughter cell. Cells that are at the point of division or about to separate may have two flagella and if both attached this would hold the cell still. This may explain some of the still cells.

It is possible that all attached cells start as tethered but unmoving cells

have attached during a natural stop of the flagellar motor. Since the *R. sphaeroides* motor is stopped by a 'brake' mechanism that does not allow the cell to move relative to the flagellum (Brown, 2009), this would lead to stillness. There are published accounts of the frequency and duration of stops in *R. sphaeroides*, as well as the analysis presented in chapter 4. In the absence of chemoattractants the motor was found to stop 'typically several times a minute for up to several seconds each' (Armitage and Macnab, 1987) in free swimming and tethered cells. A more recent approach using beads attached to flagellar stubs gave the mean stop duration at steady state as 0.66 $\pm$ 1.01 s and the mean number of stops as 0.31 $\pm$ 0.19 s^{-1} (Brown (2009)). It is unlikely that a cell which approaches the glass surface during a run, attaches and remains motionless for several minutes is simply experiencing a normal motor stop.

The data shown in Fig. 6.5 seem to contradict the lower attachment at 6 hours measured by crystal violet staining in Fig. 3.20. This may be because the cultures in Fig. 6.5 had only just reached stationary phase by the end of the experiment, and the cultures in Fig. 3.20 started at OD_{700}=0.3 not OD_{700}=0.2 and are likely to have reached stationary phase earlier.

The results from this chapter seem to confirm the modelling results and support the conclusion that *R. sphaeroides* cells do not require the flagellum as an attachment organelle to stick to solid surfaces, even if in about 50% of cases initial attachment is via the flagellum if it is present on the cells.

Chapter 7

Viscosity

7.1 Introduction

Motility mutations affected attachment, with a general trend for strains that swam more to attach more. Motility can also be changed environmentally by increasing the viscosity of the culture. This chapter analyses swimming changes at different viscosities and looks at whether attachment is affected.

Some of the videos in this chapter were taken by Wilson Kong Tang.

The viscosity of a fluid is a measure of its resistance to flow and is caused by internal friction. It is defined using the force F required to maintain a velocity gradient between parallel plates of area A, $F = \eta A \frac{dv}{dx}$ where η is viscosity (Berg and Turner, 1979).

More viscous fluids are harder to move through, because more energy is expended moving the fluid aside. Viscosity is measured in poise (P), the SI unit is the pascal second, Pa·s. Water at 20^{o}C has viscosity 1.0020 cP (centipoise) which is 0.001002 Pa.s.

Coping with viscous environments has been suggested as one reason for the different shapes and swimming styles of bacteria, with spirochaetes particularly well adapted to moving through viscous fluids (Berg and Turner, 1979).

The effect of viscosity on bacterial swimming has been studied since the 1960s. Shoesmith (1960) measured the average swimming speed of *Pseudomonas viscosa*, *Bacillus brevis* and *Escherichia coli* by counting the number of cells crossing a small aperture in a given time. He found that speed increased with a small increase in viscosity, but then decreased with higher viscosity. The substances used to increase viscosity were gelatin, methylcellulose, carragheenin and dextran.

Schneider and Doetsch (1974) measured swimming speed at different viscosities for 7 species of bacteria, *Bacillus megaterium*, *E. coli* , *P. aeruginosa*, *Sarcina ureae*, *Serratia marcecens*, *Spirillum serpens* and *Thiospirillum jenense*. These bacteria vary in shape, size and flagellation. They found that swimming velocity increased in more viscous solutions for all the bacteria, but after a certain level of viscosity, different for each species, velocity decreased. The bacteria with polar flagella had their maximum velocity at lower viscosities than those with peritirchous flagella. The substances used to increase viscosity were polyvinylpyrollidone (PVP) and methylcellulose, the speed increase was seen with both. Swimming speed was measured by recording bacteria on video, tracing individual tracks by hand and using the mean of the 10 fastest tracks, a few measurements were made using long exposures to photograph the tracks.

Greenberg and Canale-Parola (1977) found that the lowest viscosity that immobilised *P. aeruginosa*, *Spirillum serpens* and *E. coli* was 60 cP, while some flagellated bacteria selected for ability to move through agar gels could move in viscosities up to 1000cP. They suggested that bacteria living in viscous habitats had 'specialised motility apparatus'. They had previously shown that many spirochetes were not immobilised until viscosities of 300 - 1000 cP. They measured velocity by timing bacteria swimming over a set distance, and taking only runs, excluding any tracks with stops or changes of direction. They increased viscosity using polyvinylpyrrolidone (PVP).

Petrino and Doetsch (1978) found that *Leptospira interrogans* (biflexa) strain b16 moved towards higher viscosity, which they called viscotaxis. They increased viscosity using PVP.

Berg and Turner (1979) looked at the properties of the viscous solutions for an explanation of the unexpected result of faster swimming. They found that solutions of viscous agents were often gel like rather than simply viscous, especially where the agent used had long chains which tended to form a loose network, so that the viscosity measured for large objects could be high, while the viscosity for microscopic objects was hardly different from that of the solvent without the viscous agent. Comparing a long chain polymer, methylcellulose, with a highly branched polymer, Ficoll, they found that even at low concentrations there were differences between *E. coli* swimming in solutions of the two polymers at the same apparent viscosity. They conclude that highly branched polymers are best for increasing viscosity at the microscopic level, and that for bacteria high osmolarity and high ionic strength rule out some possibilities, leaving Ficoll as probably the best available substance for slowing the motion of a microorganism without changing the hydrodynamics.

More recently, viscosity has been found to be involved in surface detection in *Proteus mirabilis* (Belas and Suvanasuthi, 2005; Lee et al., 2013). In a viscous environment, *P. mirabilis* differentiates from short rods with few flagella to long cells with many flagella. Lee et al. (2013) report that *P. mirabilis* detect surfaces by monitoring motor rotation, and that the protein FliL is involved in this sensing. The viscous agent used by Belas and Suvanasuthi (2005) was PVP.

Li et al. (2012) found that *Caulobacter crescentus* detected surfaces and produced the adhesive holdfast by monitoring load on the flagellar motor, and that this process could be triggered away from a surface by high viscosity produced by Ficoll, which they describe as a 'polymer crowding agent'. They report similar processes of surface detection followed by adhesion production in *Asticcacaulis biprosthecum* and *Agrobacterium tumefaciens*.

7.2 Aims

The aim of the work in this chapter was to test the hypothesis that *R. sphaeroides* WS8N attachment to a glass slide would be reduced by using viscosity to reduce movement.

7.3 Ficoll_{400}

Ficoll is a very soluble high molecular weight synthetic branched co-polymer of sucrose and epichlorhydrin which increases viscosity but not viscoelasticity, Ficoll radii range from 2-7 nm, Ficoll_{400} has Stokes radius of 10nm (Bohrer et al., 1979). It contains no ionised groups, is very stable in physiological conditions and can be used at concentrations of up to 50% with 'normal physiological osmolality'. It does not tend to cross cell membranes (Ficoll Data File, Amersham Biosciences).

The viscosity of Ficoll_{400} solutions at the concentrations used here are given by Fig. 7.1.

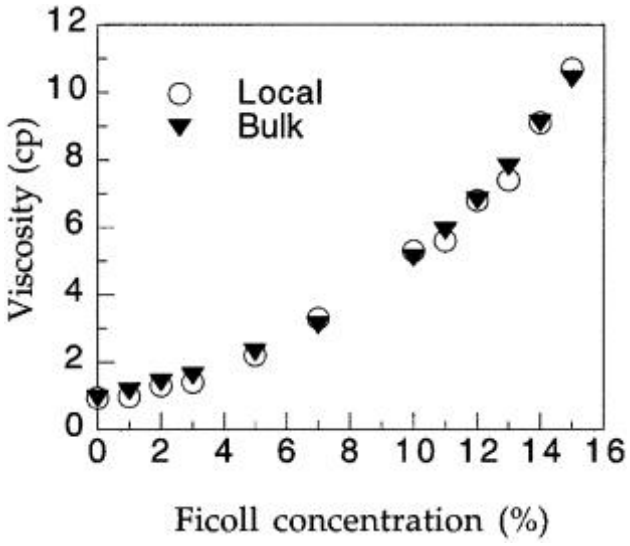


Figure 7.1: Local (measured using sedimentation) and bulk (measured in a capillary viscometer) viscosities of Ficoll_{400} at 22.7^oC, image from Chen and Berg (2000).

7.4 How does *R. sphaeroides* react to Ficoll?

The aim of adding Ficoll to the medium is to increase viscosity and change swimming behaviour. It may also affect *R. sphaeroides* in other ways. The density of the medium will change as well as the viscosity, and since Ficoll is made of branched sugars it is possible that *R. sphaeroides* could break it down and release nutrients. It will also change osmolarity.

The effect of Ficoll on *R. sphaeroides* was assessed using growth curves. The results show that *R. sphaeroides* do not grow successfully in Ficoll and that the more Ficoll, the lower the growth rate, and the smaller the final population (Fig. 7.2). This suppliers notes were checked to make sure this was not due to a toxic additive.

This means that longer timecourse experiments with *R. sphaeroides* using Ficoll_{400} are not possible. Also, it is possible that Ficoll_{400} leads to a stress response which might affect attachment, as well as the swimming changes.

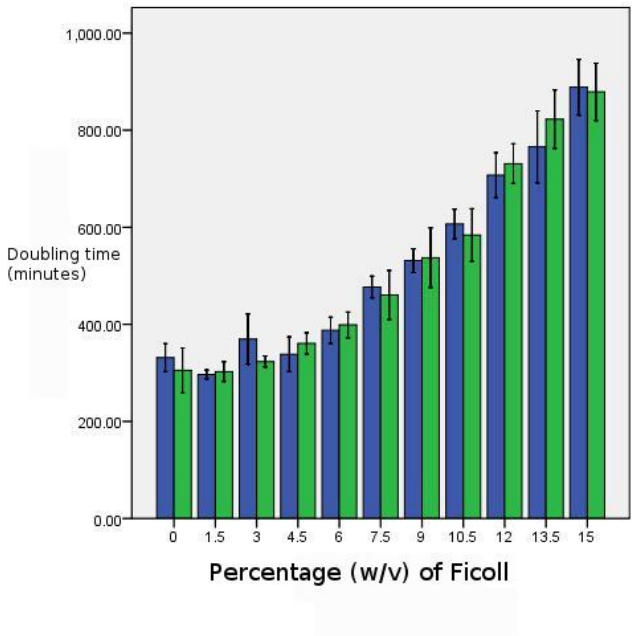


Figure 7.2: The mean doubling time of *R. sphaeroides* WS8N (green) and JPA635 (blue) grown in a 96 well plate in different concentrations of Ficoll_{400} dissolved in succinate medium (Appendix 11.0.3). Optical density at 700nm was measured every 20 minutes for 24 hours in a platereader (Tecan Magellan), in the dark with shaking. Wells containing succinate medium alone were used as negative controls, and the mean of the control absorbance was subtracted from the measured absorbances. The doubling times were calculated as described in Materials and Methods 2.2.23. Error bars are 95% confidence intervals, there were 3 samples of each strain. The growth of both strains was affected by the Ficoll_{400}.

7.5 How does swimming change with increased viscosity for *R. sphaeroides* ?

Free swimming assays were done as described in Materials and Methods, at and away from surfaces in flat glass capillaries, with wild type *R. sphaeroides* WS8N in mid log phase, in media with 11 concentrations of Ficoll_{400}, 0% w/v, 1.5% w/v, 3% w/v, 4.5% w/v, 6% w/v, 7.5% w/v, 9% w/v, 10.5% w/v 12% w/v, 13.5% w/v and 15% w/v to increase viscosity. Using the graph in Fig.

7.1 these correspond to viscosities of 1.0cp, 1.3cp, 2.2cp, 2.8cp. 3.5cp, 4.3cp, 5.3cp, 6.6cp. 8.3cp and 10.0cp.

To identify runs and stops reference videos were taken at each Ficoll_{400} concentration of a strain that is unable to swim (JPA 1215, which has a mutation in CheY6 leading to a stopped motor) , and a strain that is smooth swimming (JPA1353, which has no chemotaxis genes).

The tracks were censored using the principles explained in Materials and Methods 2.7.3, to remove spurious and extremely tortuous tracks from all data and tracks from dead or non-motile cells from data on motile strains, with the aim of reducing noise and preventing features of swimming behaviour being obscured. The remaining transitions, plotted on an angle/speed histogram, are shown in Figs. 7.3 to 7.6.

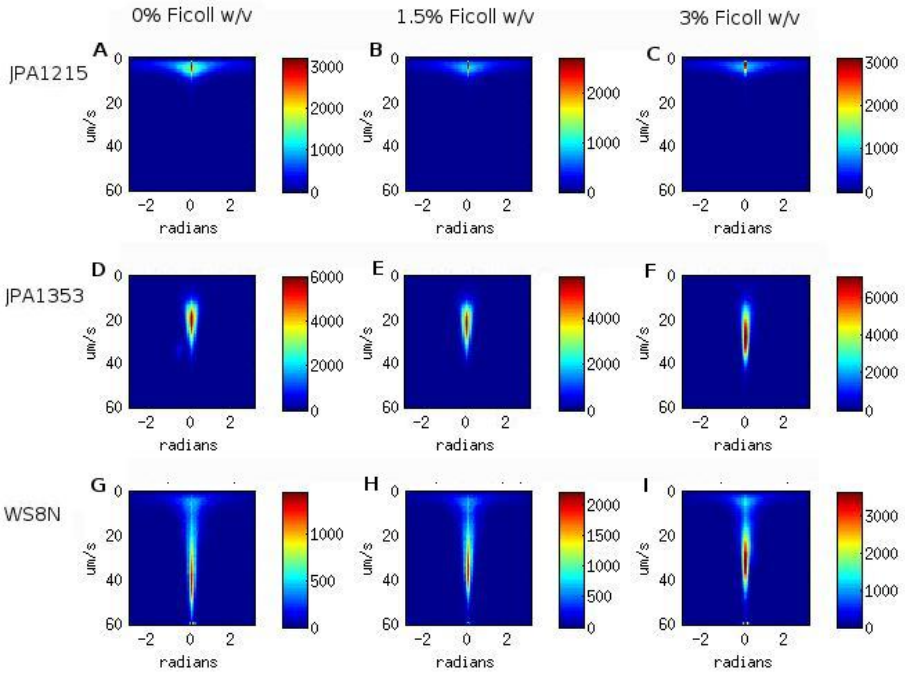


Figure 7.3: Speed/angle histograms of censored tracks at different concentrations of Ficoll dissolved in HEPES near the glass surface. The top row is the stopped strain *R. sphaeroides* JPA1215, the middle row is the smooth swimming strain *R. sphaeroides* JPA1353 and the bottom row is *R. sphaeroides* WS8N. Ficoll percentages are in columns, 0% w/v, 1.5% w/v and 3% w/v. Each histogram has speed in μms^{-1} from 0 to 60 on the vertical axis and angle change in radians on the horizontal axis. The colour bar shows numbers of counts of transitions. The top row shows the low speeds measured for *R. sphaeroides* JPA1215, the middle row shows the single peak from smooth swimming cells with few stops in their tracks, and the bottom row shows both a high narrow peak from runs and a low wide peak from stops from swimming wild-type *R. sphaeroides* WS8N. The mean running speeds measured for these samples are shown on Fig. 7.7, Fig. 7.8 and Fig. 7.9.

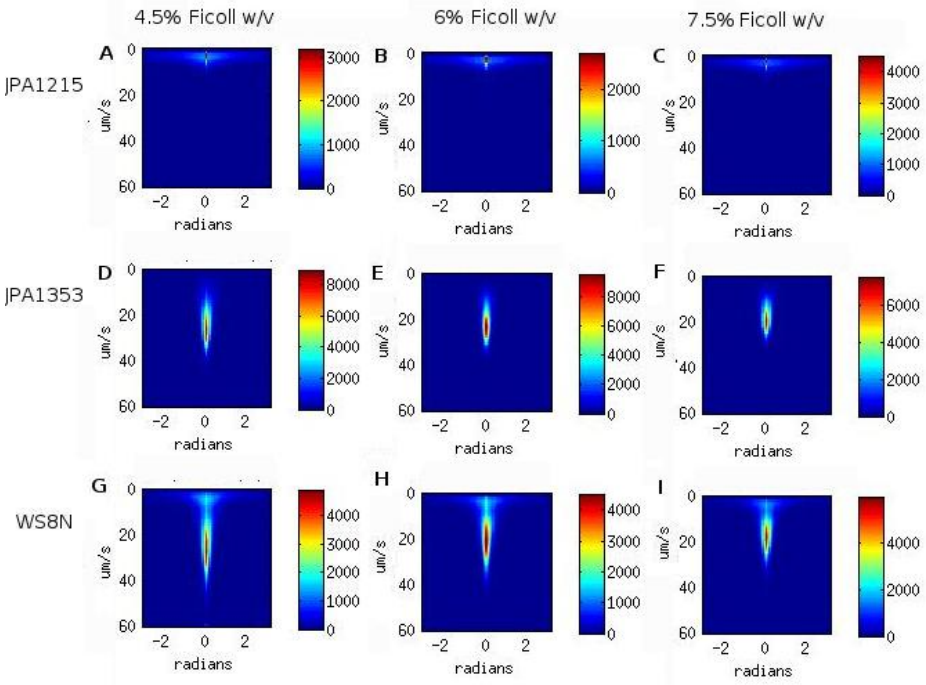


Figure 7.4: Speed/angle histograms of censored tracks at different Ficoll concentrations near the glass surface. The top row is the stopped strain *R. sphaeroides* JPA1215, the middle row is the smooth swimming strain *R. sphaeroides* JPA1353 and the bottom row is *R. sphaeroides* WS8N. Ficoll percentages are in columns, 4.5% w/v, 6% w/v and 7.5% w/v. Each histogram has speed in μms^{-1} from 0 to 60 on the vertical axis and angle change in radians on the horizontal axis. The colour bar shows numbers of counts of transitions. The top row shows the low speeds measured for *R. sphaeroides* JPA1215, the middle row shows the single peak from smooth swimming cells with few stops in their tracks, and the bottom row shows both a high narrow peak from runs and a low wide peak from stops from swimming wild-type *R. sphaeroides* WS8N. The mean running speeds measured for these samples are shown on Fig. 7.7, Fig. 7.8 and Fig. 7.9.

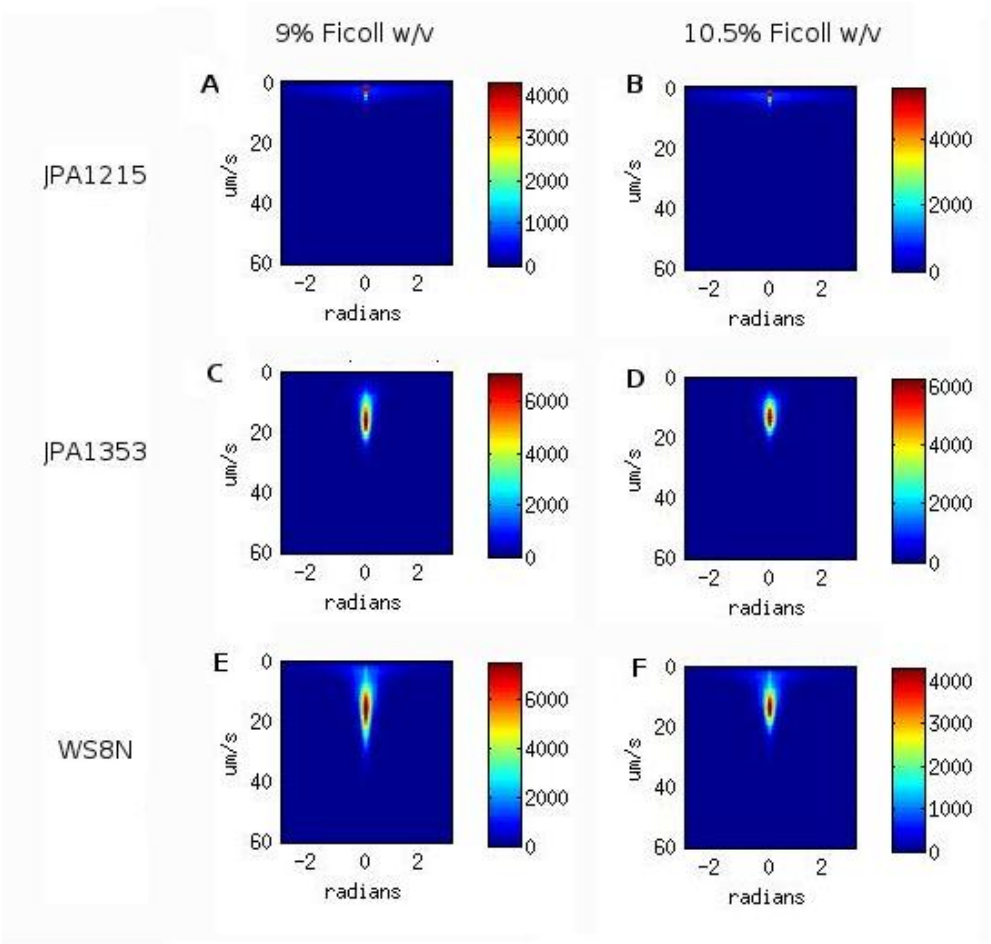


Figure 7.5: Speed/angle histograms of censored tracks at different Ficoll concentrations near the glass surface. The top row is the stopped strain *R. sphaeroides* JPA1215, the middle row is the smooth swimming strain *R. sphaeroides* JPA1353 and the bottom row is *R. sphaeroides* WS8N. Ficoll percentages are in columns, 9% w/v and 10.5% w/v. Each histogram has speed in μms^{-1} from 0 to 60 on the vertical axis and angle change in radians on the horizontal axis. The colour bar shows numbers of counts of transitions. The top row shows the low speeds measured for *R. sphaeroides* JPA1215, the middle row shows the single peak from smooth swimming cells with few stops in their tracks, and the bottom row shows both a high narrow peak from runs and a low wide peak from stops from swimming wild-type *R. sphaeroides* WS8N. The mean running speeds measured for these samples are shown on Fig. 7.7, Fig. 7.8 and Fig. 7.9.

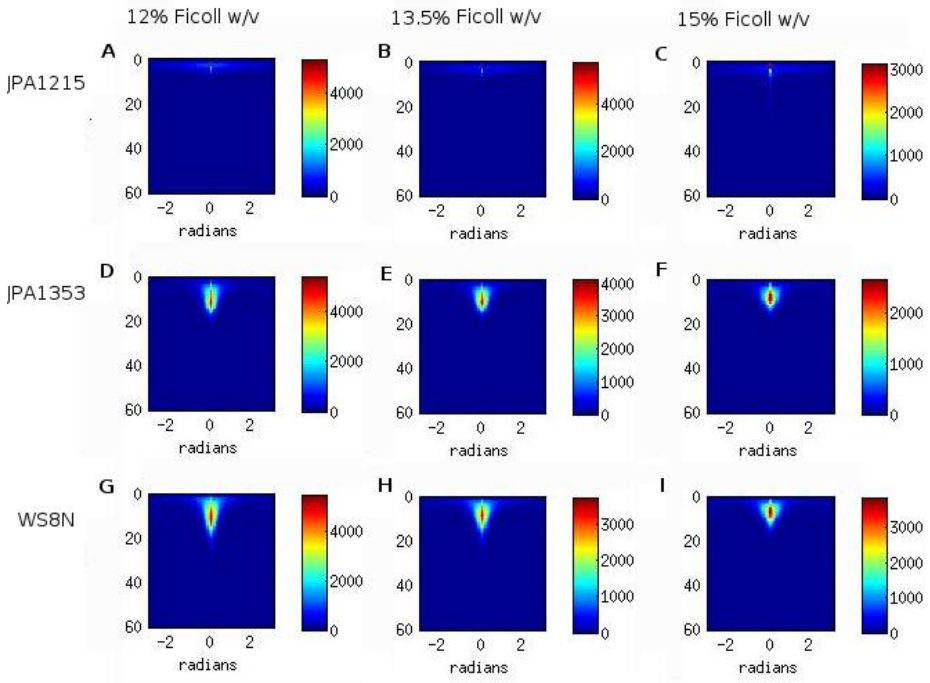


Figure 7.6: Speed/angle histograms of censored tracks at different Ficoll concentrations near the glass surface. The top row is the stopped strain *R. sphaeroides* JPA1215, the middle row is the smooth swimming strain *R. sphaeroides* JPA1353 and the bottom row is *R. sphaeroides* WS8N. Ficoll percentages are in columns, 12% w/v, 13.5% w/v and 15% w/v. Each histogram has speed in μms^{-1} from 0 to 60 on the vertical axis and angle change in radians on the horizontal axis. The colour bar shows numbers of counts of transitions. The top row shows the low speeds measured for *R. sphaeroides* JPA1215, the middle row shows the single peak from smooth swimming cells with few stops in their tracks, and the bottom row shows both a high narrow peak from runs and a low wide peak from stops from swimming wild-type *R. sphaeroides* WS8N. The mean running speeds measured for these samples are shown on Fig. 7.7, Fig. 7.8 and Fig. 7.9.

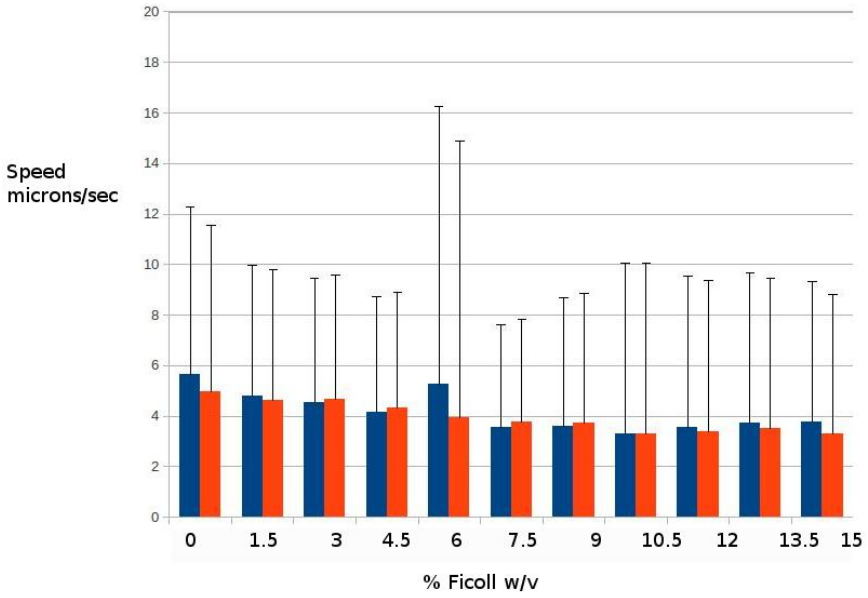


Figure 7.7: The mean speeds of log phase photoheterotrophically grown non-motile *R. sphaeroides* JPA1215 cells in different concentrations of Ficoll dissolved in HEPES motility buffer (Appendix 11.0.8). Red is at the capillary surface and blue is in the bulk medium. The error bars are standard deviation. The speeds at and away from the surface are almost the same at all concentrations. The data is the same as for Figs. 7.3 to 7.6'.

The results suggest that swimming speed decreased with increased viscosity, both in the bulk fluid and at the surface (Fig. 7.4). It also looks as though swimming speed increases before decreasing, in the two motile strains.

As viscosity increases, it becomes harder to distinguish runs from stops. Both movement during stops and speed during runs decrease. To be as accurate as we can about swimming behaviour, we can use the smooth swimming and non motile strains to produce reference distributions at each viscosity which can be used with the HMM software described in Materials and Methods

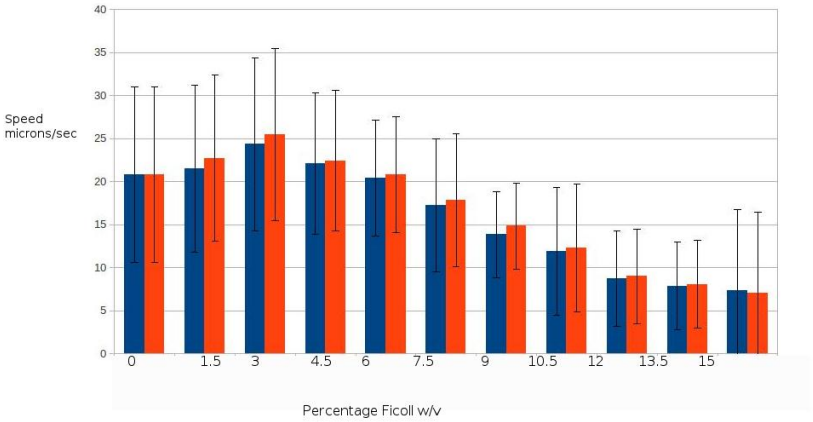


Figure 7.8: The mean swimming speeds of log phase photoheterotrophically grown *R. sphaeroides* JPA1353 cells in different concentrations of Ficoll dissolved in HEPES motility buffer (Appendix 11.0.8). Red is at the capillary surface and blue is in the bulk medium. The error bars are standard deviation. At the highest concentration of 15% Ficoll, the swimming speed is close to that of non-motile cells (around 5 microns/sec). The speeds at and away from the surface are almost the same at all concentrations. The data is the same as for Figs. 7.3 to 7.6.

2.7.6 to make the most likely allocation of transitions into runs and stops.

The results for the experiments with least and most Ficoll are shown in Fig. 7.10. As Ficoll concentration increases, the speeds reduce, for both motile and non-motile strains. The mean swimming speed of motile cells at each concentration is shown in figure 7.9.

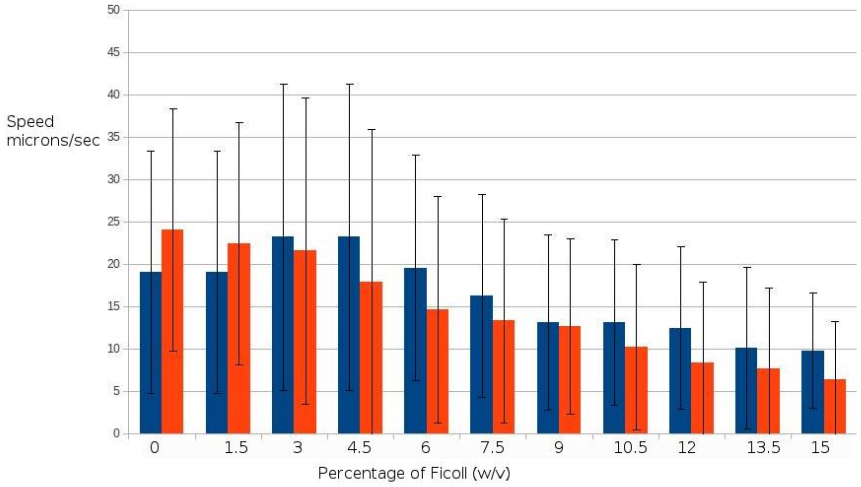


Figure 7.9: The mean swimming speeds of log phase photoheterotrophically grown *R. sphaeroides* WS8N cells in different concentrations of Ficoll dissolved in HEPES motility buffer (Appendix 11.0.8). Red is at the capillary surface and blue is in the bulk medium. The error bars are standard deviation. At the highest concentration of 15% Ficoll, the swimming speed is close to that of non-motile cells (around 5 microns/sec). The speeds at and away from the surface are almost the same at all concentrations. The data is the same as for Figs. 7.3 to 7.6. A one-way between subjects ANOVA with Welch's correction (Section 2.9.2) was conducted to compare the effect of concentration on mean swimming speed for a sample of motile cells. Mean swimming speed differed significantly as a function of Ficoll concentration for log phase photoheterotrophic cultures swimming in HEPES (Appendix 11.0.8), F (10,12.9) = 101.432, p = 1.239e-10. Post-hoc pairwise t-tests with Holm's correction (Section 2.9.2) were performed to identify which concentrations led to swimming speed differences that were significant at the 0.05 level. Swimming speeds were significantly different from those at 0% Ficoll (w/v) for concentrations of over 7.5% Ficoll.

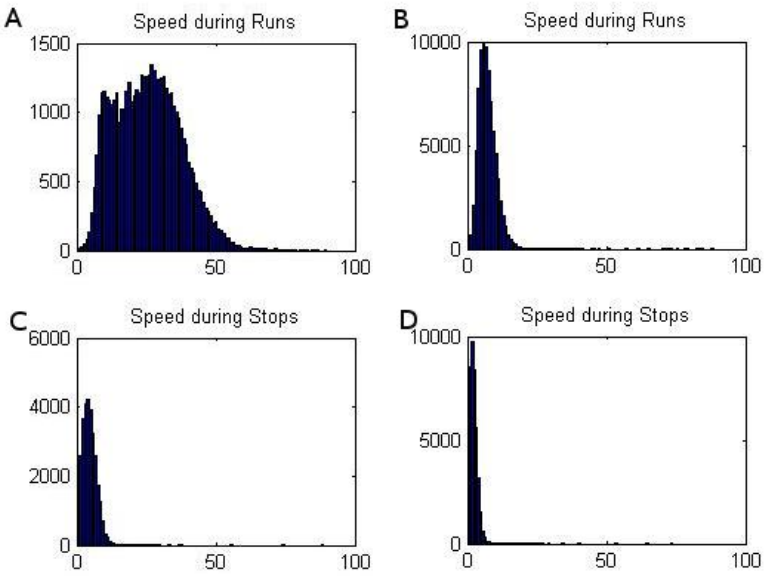


Figure 7.10: The speeds in μms^{-1} of motile *R. sphaeroides* WS8N during runs and stops in HEPES motility buffer with 0% (A and C) and 15% (B and D) w/v dissolved Ficoll$_{400}$. The speeds during runs form a narrower peak in 15% w/v Ficoll with a maximum near 10 μms^{-1}, not well separated from the speeds during stops, which form a narrow peak with maximum near 4 μms^{-1}. The difference between these histograms and those shown in Chapter 4 is that all information available has been used to allocate transitions to runs or stops, using reference distributions of smooth swimmers and non-motile cells and calculating the most likely sequence of runs and stops for each track as described in Materials and Methods 2.7.6. This is particularly useful as the speeds slow down and runs and stops become harder to distinguish.

7.6 Does increased viscosity have an effect on attachment?

Cultures were grown to OD_{700}=0.6 (mid log phase). 500μl was spun down at 1000rpm for 4 minutes and resuspended in 1ml of a solution of Ficoll in succinate medium at the required concentration, incubated in wells for 30 minutes, then treated with crystal violet as described in section 2.3.

Ficoll concentrations used were made up in concentrations of 0 - 15% w/v Ficoll as before.

The results shown in Fig. 7.11 were unexpected and show that attachment in wells is dramatically reduced even at the lowest Ficoll concentration, though swimming is hardly affected (Fig. 7.9).

The reason for the lack of attachment may be connected with the reduced growth in Ficoll (Fig. 7.2), and due to metabolic changes, or it may be that Ficoll preconditions the surface of the well, or surrounds the bacterial cell and hinders attachment.

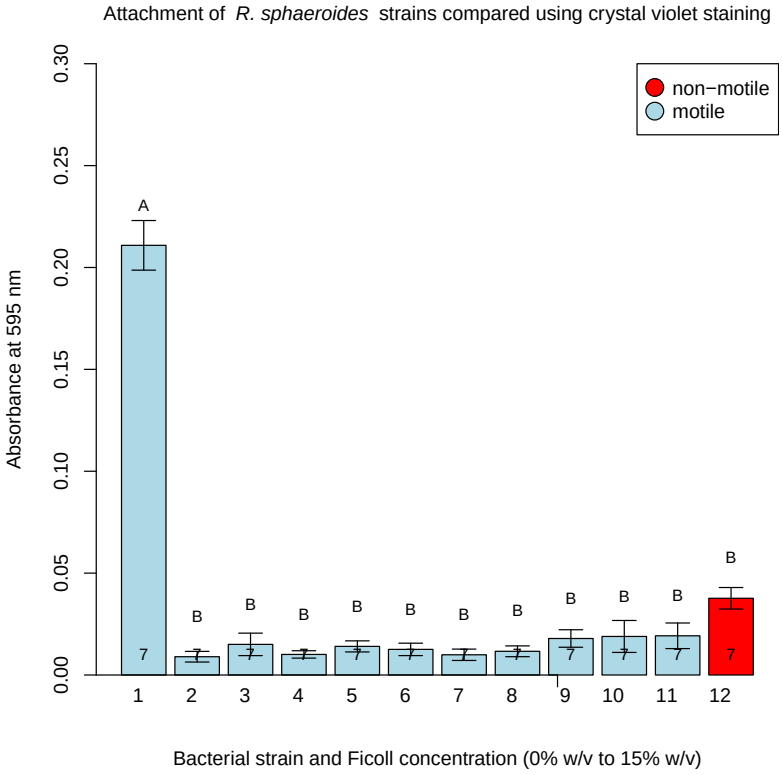


Figure 7.11: Absorbance measured at 595nm of crystal violet staining of attached log phase photoheterotrophically grown *R. sphaeroides* WS8N cells after 30 minutes incubation in light (Materials and Methods 2.3.1, in varying concentrations of Ficoll_{400}. The blue bars are *R. sphaeroides* WS8N swimming in increasing concentrations of Ficoll_{400} dissolved in succinate medium from 0% w/v to 15% w/v in steps of 1.5% w/v. The red bar on the right is the non motile control in 0% Ficoll. A one-way between subjects ANOVA with Welch's correction (Section 2.9.2) was conducted to compare the effect of strain on absorbance. Absorbance differed significantly as a function of Ficoll percentage for log phase photoheterotrophic cultures,$F(11,28.2) = 21.66$, $p = 6.935\text{e-}11$. Post-hoc pairwise t-tests with Holm's correction (Section 2.9.2) were performed to identify different strains. The letters above the bars show two groups, A and B, clustered by significant differences at $p<0.05$. There is a sharp drop in attachment as soon as any Ficoll_{400} is present, such that measured attachment drops to that of than the non-motile control. Error bars are standard error. 7 wells were tested for each Ficoll concentration.

7.7 Discussion

The aim of this chapter was to determine whether a reduction in motility by increasing viscosity would affect *R. sphaeroides* attachment to surfaces.

In *C. crescentus* increased viscosity has been shown to trigger holdfast production, which could be detected by a specific lectin bound to a fluorescent dye (Li et al., 2012). For *R. sphaeroides* we do not have a specific signal to detect, and it is not yet known whether a similar substance is produced. However, if cells at high viscosity change to an attached, non swimming phenotype, the proportion of non swimming cells in a culture should increase. This may not lead to more actual attachment, if cells stop swimming they have the non-motile cell's difficulty in reaching a surface, and also in the case of *C. crescentus* , the early production of a holdfast, away from a surface, led to less efficient attachment (Li et al., 2012).

Interestingly, surface attachment for *R. sphaeroides* WS8N was significantly reduced at all concentrations of Ficoll, even those that did not affect swimming behaviour. It is possible that there is some effect of the Ficoll unrelated to motility or viscosity, for example it might coat the surface of the wells or the bacteria, altering surface properties and discouraging attachment, or there may be metabolic changes, related to the effect of Ficoll on *R. sphaeroides* WS8N growth, which affect attachment.

It is unlikely that the *R. sphaeroides* cells are responding to the increased viscosity and trying to attach in the bulk medium, as happened in Li et al. (2012) with *C. crescentus* because in that case they would be likely to stop swimming.

To investigate the reasons for these results experiments could be done using Ficoll pre-treatment of surfaces.

Chapter 8

Fluorescence and Flowcells

8.1 Introduction

In previous chapters attachment has been studied using monocultures. Different strains can be grown in the same culture and distinguished from one another if they are labelled with fluorescent protein.

Previous experiments have also been limited by the use of static microcosms in which over time nutrients are used up, wastes build up and cells become crowded. To track cells for longer, wastes must be removed and nutrients replenished. This can be done using flowcells (Sections 2.4.5, 2.5.2).

8.2 Aims

The aims of the work in this chapter are:

- To produce strains of *R. sphaeroides* WS8N with genes for fluorescent proteins on the chromosome.
- To establish suitable flowcells and rates of flow for tracking *R. sphaeroides* WS8N cells for up to 24 hours.

8.3 Fluorescence using plasmids

The pInd plasmid allows inducible expression of proteins in *R. sphaeroides* (Ind et al., 2009). pInd contains genes for kanamycin resistance, and expression of introduced genes can be induced with IPTG. pInd expressing CFP (pIndCFP) and pInd expressing YFP (pIndYFP) were used to label cells. The plasmid was introduced into the desired strain of *R. sphaeroides* by conjugation (Section 2.2.18) and cells were then grown in succinate medium (Appendix 11.0.3) with 100 μM IPTG and 25 μg/ml kanamycin.

8.4 Expressing fluorescent protein from the chromosome

A strain which expresses a fluorescent reporter constitutively from its chromosome would be useful since the plasmids pIndCFP and pIndYFP require IPTG induction and antibiotics. The copy number of pInd can vary (Ind et al., 2009) leading to variable fluorescence which makes image analysis complicated.

To produce a genomic reporter strain it is necessary to decide on a promoter that is active in all relevant situations and to choose a region of the genomic DNA that can be used to insert the new gene without producing side effects. Then the promoter DNA must be joined correctly to the gene for the fluorescent protein, in frame and with the ribosome binding sites present. Flanking regions from the genome must be extracted and joined to the insert so that the new construct can be incorporated into the genomic DNA by recombination (Section 2.2.19). For two colour competition experiments fluorescent proteins with little overlap in their excitation and emission spectra are needed, such as GFP/mCherry.

8.4.1 Selection of promoter

Many of the known *R. sphaeroides* WS8N promoters react to conditions such as light, oxygen or nitrogen levels. It was decided to use an exogenous promoter that is known to work well in *R. sphaeroides*, an adaption of the lac promoter from *E. coli* , $P_{A1/04/03}$ (Ind et al., 2009), which is constitutively active in *R. sphaeroides* because the lac repressor is not produced.

The sequence is 5'-TTTATCAAAAAGAGTGTTGACTTGTGAGCGGATAA CAATGATACTTAGATTCAATTGTGAGCGGATAAC AATTTCACACAT-3'(-10 red, -35 blue)

It was amplified from the pInd4 plasmid using primers 'promoter forward' and 'promoter reverse' in Appendix 12.

8.4.2 Selection of genomic region

Earlier work by Scott Godfrey identified several possible sites in the *R. sphaeroides* 2.4.1 genome which do not seem to contain coding regions, and which could be used as sites to incorporate new genes (personal communication, Helen Packer). The most promising was an 800 bp region on chromosome 1 between the converging reading frames RSP_2534 and *rhlE* Fig. 8.1.

500bp left and right flanking regions were amplified from genomic DNA using the flanking regions primers in Appendix 12. They were inserted into pUC19 using double digest and ligation to give pUC19:left and pUC19:right, and the results were checked by sequencing.

The promoter DNA was joined to the fluorescent protein DNA by overlap extension PCR (Section 2.2.14), using the fluorescent protein and promoter primers (Appendix 12).

The promoter/fluorescent protein fusions were then inserted into pUC19 between the flanking regions by restriction digest using *Xba*I and *Kpn*I,followed by ligation, producing pUC19:GFP and pUC19:mCherry.

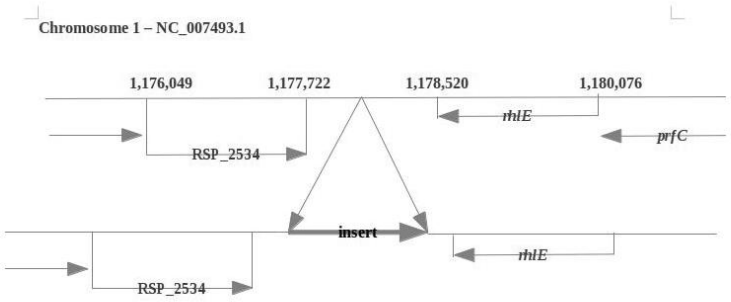


Figure 8.1: The region of chromosome 1 in *R. sphaeroides* 2.4.1 with a non coding region between converging reading frames in which the fluorescent protein constructs can be placed.

Both constructs were then cut out of pUC19 and inserted into pK18*mobsacB* to produce pK18*mobsacB*:GFP and pK18*mobsacB*:mCherry. pK18*mobsacB*:GFP and pK18*mobsacB*:mCherry were transformed into competent *E. coli* S17-1λ*pir* and inserted into *R. sphaeroides* by conjugation.

The promoter/GFP fusion and the promoter/mCherry fusion were introduced into the *R. sphaeroides* WS8N genome through homologous recombination with one of the flanking sequences (Section 2.2.19).

To make sure that the GFP and mCherry were inserted into the correct region, PCR using checking primers that amplify a region starting outside a flanking region and extending through the fluorescent protein gene were used (Appendix 12, Checking). This avoids amplifying any remaining pK18*mobsacB* and means that if the fluorescent protein gene is found, it is in the correct position in the chromosome.

8.4.3 Phenotypic analysis of genomic reporter strains of *R. sphaeroides* WS8N

The addition of the fluorescent reporter proteins does not seem to have changed the behaviour of the strain in any way except for producing flu-

orescence as shown below. These strains were used to track *R. sphaeroides* WS8N biofilm formation over time. They also allow the use of the inducible pInd plasmid to express other proteins.

Fluorescence

The strains were grown in succinate medium (Appendix A) and checked for fluorescence by microscopy, using the Nikon A1 confocal microscope with lasers and filters appropriate for GFP and mCherry (Section 2.4). Typical fields of view are shown in Figure 8.2.

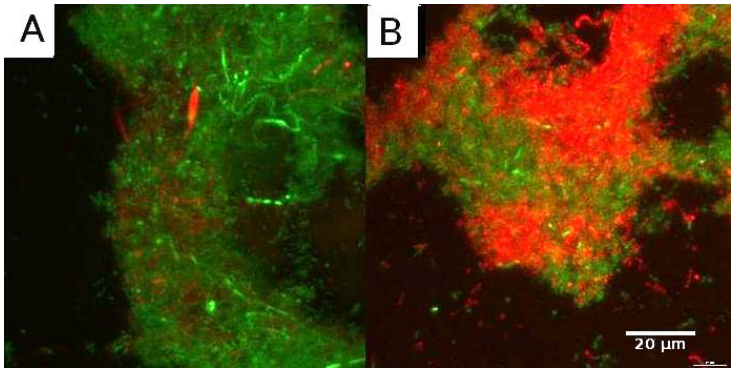


Figure 8.2: Fields of view of cultures on agarose pads, showing microcolonies formed in flowcells by mixed cultures of JPA630 and JPA631.

Growth curves

Growth curves were obtained for three samples of three biological replicates for each strain, WS8N, WS8N with GFP inserted and WS8N with mCherry inseted. Optical densities at 700nm was measured every 20 minutes for 24 hours in a platereader (Tecan Magellan), in the dark with shaking. Wells containing succinate medium alone were used as negative controls, and the mean of the control absorbance was subtracted from the measured absorbances. The doubling times for each sample were calculated as described in 2.2.23 and are shown in Fig. 8.3. There was no significant difference in growth rates.

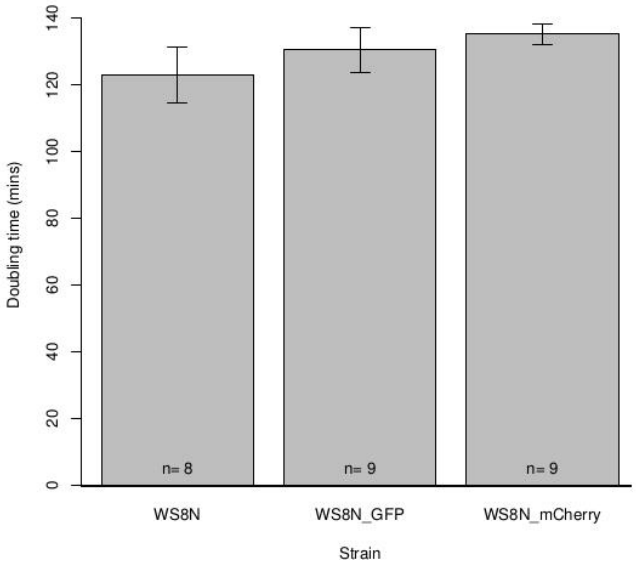


Figure 8.3: Doubling time calculated from the growth curves. Error bars are standard error, of 9 samples. A one-way between subjects ANOVA with Welch's correction (Section 2.9.2) was conducted to compare the effect of strain on doubling time. Doubling time did not differ significantly between strains at the 0.05 level, $F(2,13.58) = 0.8686$, $p=0.44$.

8.5 Flowcells

8.5.1 Flowcell Experiments

Preliminary work

Several types of flowcell were tested (Table 8.1) and the reusable three channel flowcells and bubbletraps purchased from the Technical University of Denmark were selected. They were robust and reusable, and the channels were of standard size and shape. For experiments lasting less than 6 hours home made flowcells were used as described in section 2.4.5.

Small custom made polydimethylsiloxane (PDMS) flowcells were also tried, they allow more complex shapes but this was not necessary for these exper-

Table 8.1: Flow Cells Comparison

Type of flowcell	Comments
'Homemade' drilled slides	Very cheap, channel size and shape variable, edges rough, not robust for long timecourses
PDMS custom made	Difficult to use, inexpensive, not reusable, any design possible
DTU three channel flowcell	Easy to use, robust, inexpensive, reusable

iments, and they were a little more fragile than the other two. Some very expensive flowcell systems can be bought, they were not considered.

After selecting suitable flowcells, it was necessary to determine a suitable rate of flow, this should ideally remove most swimming cells and replenish nutrients without being so fast as to remove stuck cells and colonies. To decide this, flow was gradually increased in a flowcell and the effects recorded. It was found that no speed existed that would remove all swimming cells without also detaching colonies so a compromise was reached, at 2 to 3 ml/hr there was little sliding or detachment of attached cells, but some swimmers could swim against the flow (See table 8.2). This flow rate, with this size of channel, is consistent with that used in the literature for other bacterial species (Pamp et al., 2009). It removes non-motile cells which are not attached but not all swimmers, and this must be remembered in motile/non-motile comparisons.

Table 8.2: Flow Rates and Effects for Three Channel flowcells from DTU

Flow(ml/hr)	Swimmers against flow	Effect on attached cells
1	Yes	No movement
2	Yes	No movement
3	Yes	No movement
4	Yes	A little sliding
6	Yes	Some sliding, some stuck firmly
8	Yes	Some sliding, some stuck firmly
10	Yes	Many dislodged
12	Yes	Many dislodged
14	Not many	Many dislodged
16	No	Most dislodged
18	No	Most dislodged
20	No	Most dislodged
22	No	Most dislodged
24	No	Most dislodged
26	No	Almost all gone
28	No	-
30	No	-

8.6 Discussion

The aim of this chapter was to generate strains of *R. sphaeroides* constitutively expressing GFP and mCherry from their genomes. This was achieved and phenotypic analysis suggests that these strains are not adversely affected by this. Various types of flowcells were evaluated and one selected for further experiments, with this flowcell various flow rates were assessed and an optimal flow rate selected.

Chapter 9

Rhodobacter sphaeroides surface attachment.

9.1 Introduction

The process of biofilm initiation has been studied in many species, and is discussed in Section 1.3.

Swimming behaviour affects initial attachment in *R. sphaeroides*, with fewer non motile cells attaching (Chapter 3). However, there are more influences on eventual biofilm growth than the first attachment to a surface. Once attached, a cell can either detach or convert to a sessile lifestyle, produce EPS and change the pattern of gene expression (Section 1.3). To do this they need to detect that they are at the surface in some way.

Although the form taken by growing biofilms has been shown to change with different nutrients and surfaces for other species, there is a predictable sequence of events in any particular circumstances. The rest of this chapter looks at *R. sphaeroides* development after initial attachment but before the development of mature biofilms, on a glass surface in succinate media.

9.2 Aims

The aims of this chapter are to test the hypothesis that the ratio of non-motile attached cells to motile attached cells will change over 48 hours from first access to a surface, and to observe and describe features of developing microcolonies.

If non-motile cells develop in the same way as motile cells on a surface, then the motility apparatus and flagellum are not needed for surface sensing or to support attachment.

9.3 Do the initial differences in attachment for motile and non-motile strains persist in 48 hour microcolonies?

These experiments were designed to test the hypothesis that non-motile cells would be unable to adapt to a sessile lifestyle and would become less numerous in microcolonies over time.

Cultures of *R. sphaeroides* WS8N, a smooth swimming strain (*R. sphaeroides* JPA1353), an aflagellate strain (*R. sphaeroides* JPA467) and a non motile strain with a flagellum (*R. sphaeroides* JPA452), expressing CFP from the plasmid pIND4-CFP or YFP from pIND4-YFP (Table 2.2) were grown photoheterotrophically to stationary phase in succinate medium with 25μg/ml kanamycin and 0.1 mM IPTG.

They were used in a static competitive assay as described in Materials and Methods Section 2.5.1. Three biological replicates were used for each strain, 2μl of each culture was used in the four mixed cultures. The mixed cultures were left to attach for 48 hours and the coverslips removed and examined on the Nikon A1 confocal microscope. The images were analysed using the countCell software (Materials and Methods Section 2.8)

Imbalance in attached colonies could reflect imbalance in cell growth in the media, rather than different attachment behaviour. This could be a) because one strain grows more slowly or b) because of initial differences in the number of cells added. b) will not give systematic bias in favour of one strain, but a) would. Growth curves for all strains taken as described in Section 2.2.23 showed doubling times that were not significantly different at $p = 0.05$, using ANOVA with Welch's correction, $F(4,19.7) = 1.6446$, $p = 0.2029$ (Section 2.9.2). Images were also taken of a drop from the culture after the coverslip was removed to check for imbalance of the two colours in the medium. The slides were discarded if the medium showed a large discrepancy in numbers of each strain (>3:1).

Each coverslip was searched for microcolonies (Fig. 9.1) and the five largest selected for detailed imaging. The images were analysed using custom written countCell software as described in Materials and Methods Section 2.8. The aim was to find out whether microcolonies contain both cell types, and whether the initial attachment imbalance persists over 48 hours.

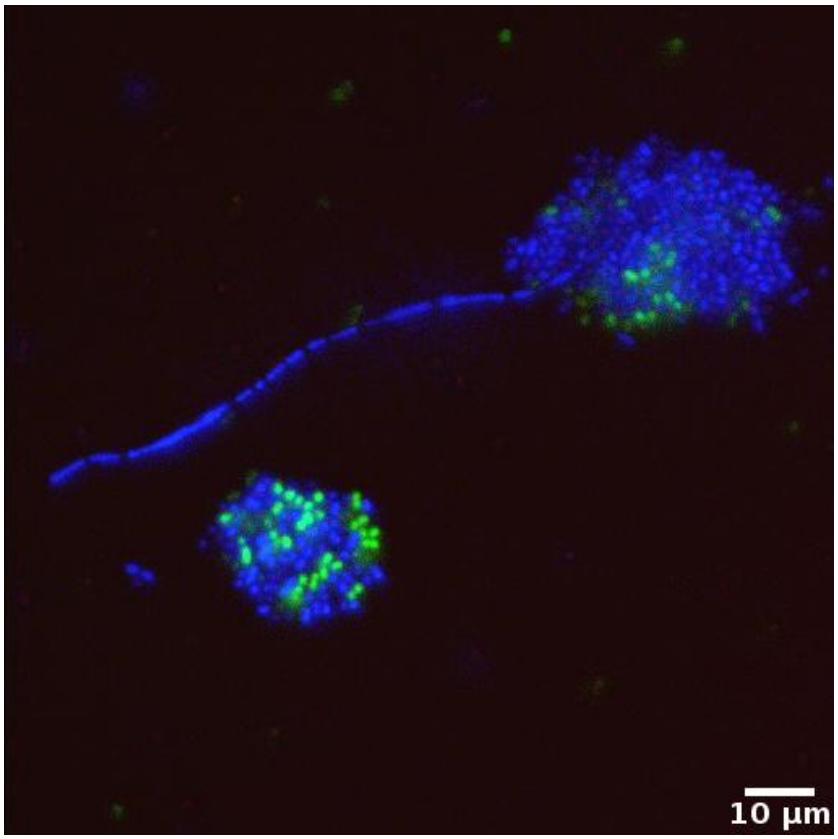


Figure 9.1: An example of microcolonies on a slide immersed in culture grown in succinate media (Appendix 11.0.3) for 48 hours, the blue cells are *R. sphaeroides* WS8N labelled with CFP and the green are *R. sphaeroides* JPA467 (non motile) labelled with YFP. A chain of cells reaches out from one of the colonies. The slide was treated as explained in Section 2.5.1 and imaged on a Nikon A1 confocal microscope using CFP and YFP laser and filter settings as described in Section 2.3.

9.3.1 The non-motile, aflagellate strain *R. sphaeroides* JPA467 contributed fewer cells to 48 hour microcolonies than *R. sphaeroides* WS8N.

Four competitive assays were set up as described in Materials and Methods 2.5.1, using strains expressing fluorescent protiens from the pInd inducible plasmid .
Mix 1 contained WS8N expressing CFP and WS8N expressing YFP
Mix 2 contained WS8N expressing CFP and JPA467 expressing YFP
Mix 3 contained JPA467 expressing CFP and WS8N expressing YFP
Mix 4 contained JPA467 expressing CFP and JPA467 expressing YFP

The area of a slide covered by CFP fluorescent bacteria and YFP fluorescent bacteria was quantified using countCells.

Figure 9.2 shows the breakdown for the different mixtures, Figure 9.3 shows the average coverage for wild-type *R. sphaeroides* WS8N and *R. sphaeroides* JPA467 over all samples, and Figure 9.4 shows the difference between CFP and YFP area on each slide as a scatter plot. The different mixtures are shown by colour and they group separately by mix. The data suggests that there is a significant difference in attachment between wild-type *R. sphaeroides* WS8N and aflagellate *R. sphaeroides* JPA467 after 48 hours whether grown separately or together (Fig. 9.2, Fig. 9.3), and that the proportions of the strains in microcolonies after 48 hours are similar to the proportions in which the cells originally attached (Fig. 9.4, Fig. 3.10).

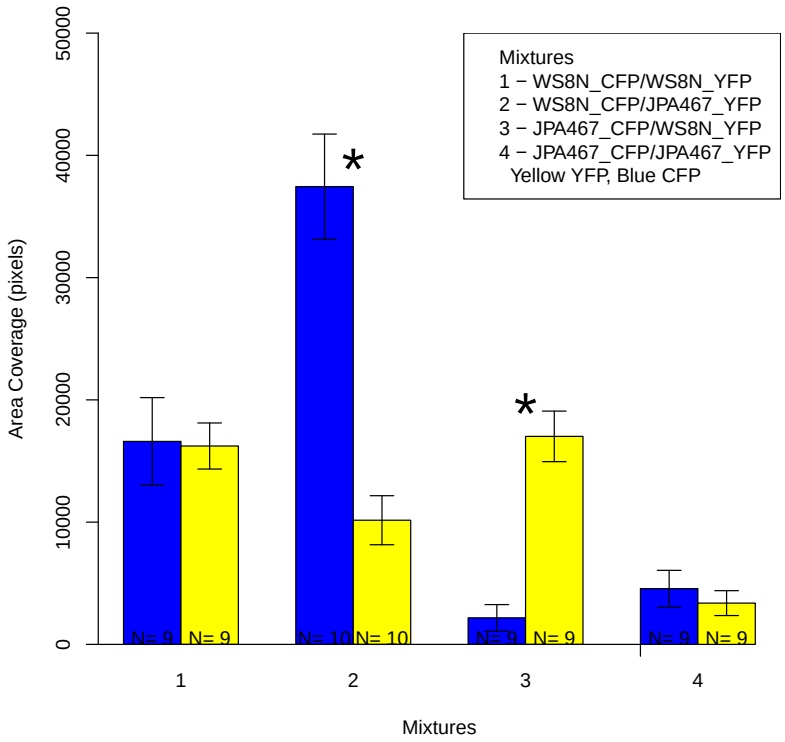


Figure 9.2: For the non-motile, aflagellate strain JPA467, the area covered by CFP labelled and YFP labelled cells in 48 hour microcolonies in four different mixtures of strains. 1) WS8N wild-type cells labelled with CFP and WS8N wild-type cells labelled with YFP, 2) WS8N wild-type cells labelled with CFP and JPA467 cells labelled with YFP, 3) WS8N wild-type cells labelled with YFP and JPA467 cells labelled with CFP, and 4) JPA467 cells labelled with CFP and JPA467 cells labelled with YFP. Error bars are standard error. A Wilcoxon signed rank test was performed for each combination of strains, treating the CFP coverage and the YFP coverage on a single slide as a set of paired values. The results were as follows. Mix 1: $V = 20$, $p = 0.8203$; Mix 2: $V = 0$ $p = 0.001953$; Mix 3: $V = 45$, $p = 0.003906$; Mix 4: $V = 21$, $p = 0.9102$; implying that there is no significant difference between the attachment of CFP and YFP labelled cells in mixtures 1 and 4, but there is a significant difference in the attachment of the different strains in mixtures 2 and 3, at $p<0.05$. Mixtures with significant differences in attachment are indicated by an asterisk above the columns.

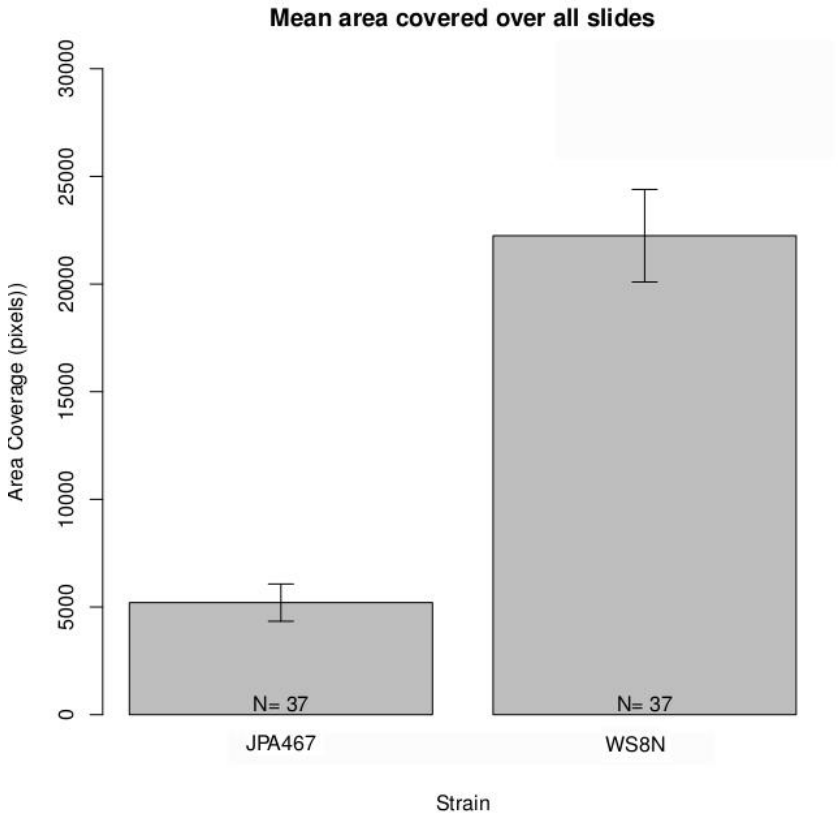


Figure 9.3: For the non-motile, aflagellate strain *R. sphaeroides* JPA467, the area covered by mutant (*R. sphaeroides* JPA467) and wild-type (*R. sphaeroides* WS8N) in all selected 48 hour microcolonies from the four different mixtures of strains. The mutant strain attached less overall. Error bars are standard error. A Student's T test (Section 2.9) was performed to test the hypothesis that the attachment of the mutant strain *R. sphaeroides* JPA467 differed from that of the wild-type strain *R. sphaeroides* WS8N. The results were t = -7.4556, df = 47.382, p = 1.594e-09. This implied that the difference in attachment is significant at the p=0.05 level.

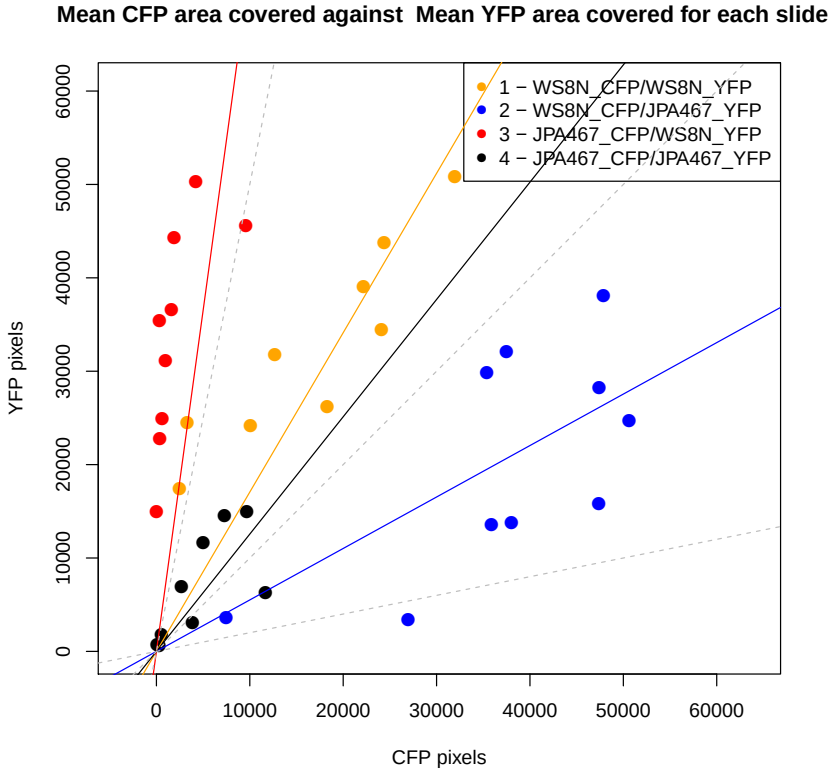


Figure 9.4: For the non-motile, aflagellate strain JPA467, the area covered by CFP labelled and YFP labelled cells in 48 hour microcolonies in four different mixtures of strains.
yellow: WS8N labelled with CFP and WS8N labelled with YFP
blue: WS8N labelled with CFP and JPA467 labelled with YFP
red: WS8N labelled with YFP and JPA467 labelled with CFP,
black: JPA467 labelled with CFP and JPA467 labelled with YFP.
For each sample YFP coverage is plotted against against CFP coverage. Mixture 4 has generally lower levels of coverage than mixture 1. The coloured lines are least squares lines fitted to points in the different mixtures, the R^2 values are: 1 (yellow) 0.93, 2 (blue) 0.87, 3 (red) 0.54 and 4 (black) 0.77. The grey dashed lines show $y = 5x$, $y = 1/5x$ and $y = x$. The proportions of wild-type to non-motile are not greatly changed from the ratio of around 5:1 after 30 minutes attachment.

9.3.2 The non-motile, flagellate strain *R. sphaeroides* JPA452 contributed fewer cells to 48 hour microcolonies than *R. sphaeroides* WS8N.

Four competitive assays were set up as described in Materials and Methods 2.5.1.
Mix 1 contained WS8N expressing CFP and WS8N expressing YFP
Mix 2 contained WS8N expressing CFP and JPA452 expressing YFP
Mix 3 contained JPA452 expressing CFP and WS8N expressing YFP
Mix 4 contained JPA452 expressing CFP and JPA452 expressing YFP

The area of slide covered by CFP fluorescent bacteria and YFP fluorescent bacteria was quantified using countCells.

Figure 9.5 shows the breakdown for the different mixtures, Figure 9.6 shows the average coverage for wild-type *R. sphaeroides* WS8N and *R. sphaeroides* JPA452 over all samples, and Figure 9.7 shows the difference between CFP and YFP area on each slide as a scatter plot. The different mixtures are shown by colour and they group separately by mix.

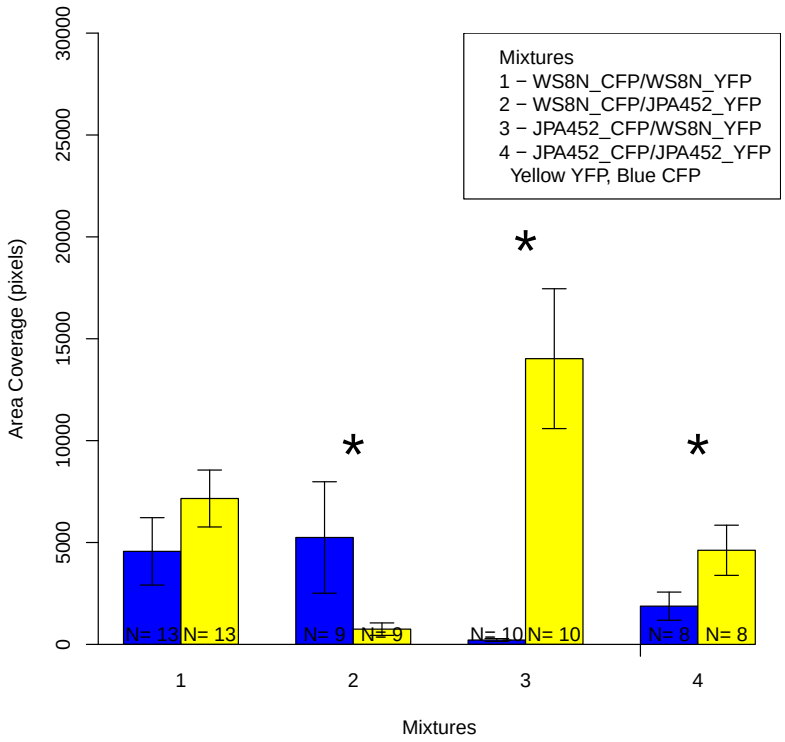


Figure 9.5: For the non-motile, flagellate strain JPA452, the area covered by CFP labelled and YFP labelled cells in 48 hour microcolonies in four different mixtures of strains. 1) WS8N wild-type cells labelled with CFP and WS8N wild-type cells labelled with YFP, 2) WS8N wild-type cells labelled with CFP and JPA452 cells labelled with YFP, WS8N wild-type cells labelled with YFP and JPA452 cells labelled with CFP, and 4) JPA452 cells labelled with CFP and JPA452 cells labelled with YFP. Error bars are standard error. A Wilcoxon signed rank test was performed for each combination of strains, treating the CFP coverage and the YFP coverage on a single slide as a set of paired values. The results were as follows. Mix 1: $V = 71$, $p = 0.08032$; Mix 2: $V = 3$, $p = 0.02402$ Mix 3: $V = 55$, $p = 0.005761$; Mix 4: $V = 36$, $p = 0.007813$; implying that there is no significant difference between the attachment of CFP and YFP labelled cells in mixture 1 but there is a significant difference in the attachment of the different strains in mixtures 2, 3 and 4, at $p<0.05$. Mixtures with significant differences in attachment are indicated by an asterisk above the columns.

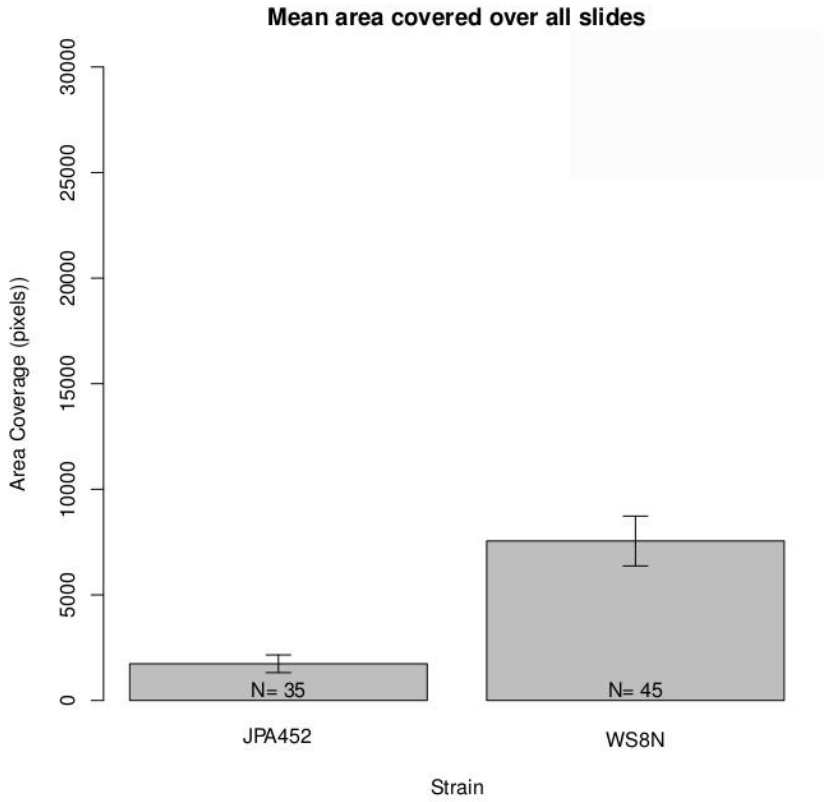


Figure 9.6: For the non-motile, flagellate strain JPA452, the area covered by mutant (JPA452) and wild-type (WS8N) in all selected 48 hour microcolonies from the four different mixtures of strains. Error bars are standard error. A Student's T test (Section 2.9) was performed to test the hypothesis that the attachment of the mutant strain JPA467 differed from that of the wild-type strain WS8N. The results were t = -4.7006, df = 54.603, p = 1.8e-05. This implied that the difference in attachment is significant at the p=0.05 level.

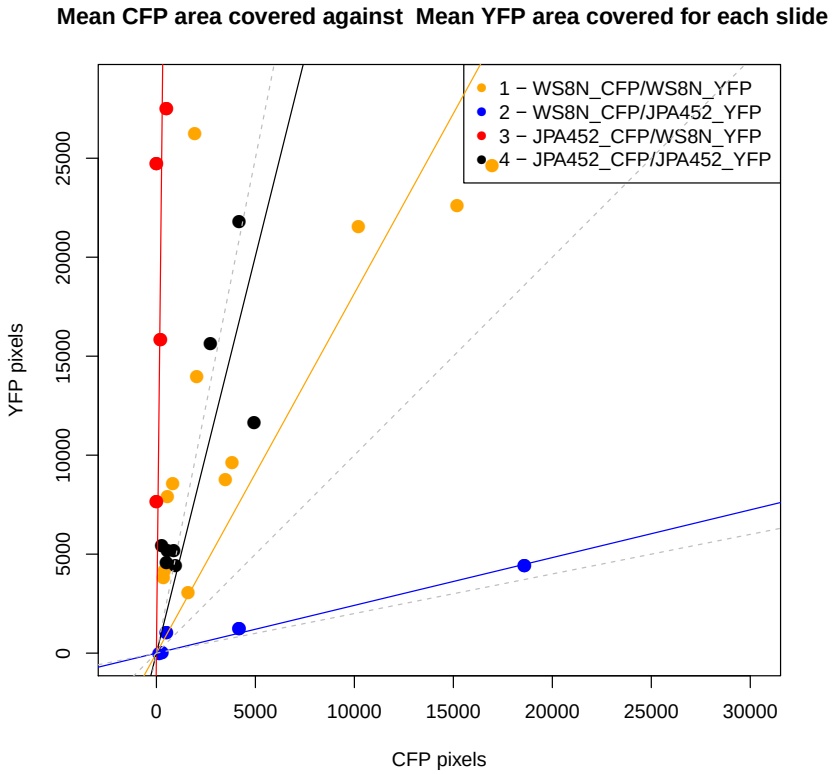


Figure 9.7: For the non-motile, flagellate strain JPA452, the area covered by CFP labelled and YFP labelled cells in 48 hour microcolonies in four different mixtures of strains.
yellow: WS8N labelled with CFP and WS8N labelled with YFP
blue: WS8N labelled with CFP and JPA467 labelled with YFP
red: WS8N labelled with YFP and JPA467 labelled with CFP,
black: JPA467 labelled with CFP and JPA467 labelled with YFP.
Each sample is plotted with YFP coverage against CFP coverage and the colours show which mixture the sample is from. The coloured lines are least squares lines fitted to points in the different mixtures, the R^2 values are: 1 (yellow) 0.58, 2 (blue) 0.96, 3 (red) 0.64 and 4 (black) 0.85. The grey dashed lines show $y = 5x$, $y = 1/5x$ and $y = x$. The proportions of wild-type to non-motile are not greatly changed from the ratio of around 5:1 after 30 minutes attachment. There were five slides in mixture 4 where no colonies could be found, they are plotted at (0,0)

9.3.3 *R. sphaeroides* WS8N and the smooth swimming *R. sphaeroides* JPA1353 show similar levels of attachment in microcolonies after 48 hours.

Four competitive assays were set up as described in Materials and Methods 2.5.1.
Mix 1 contained WS8N expressing CFP and WS8N expressing YFP
Mix 2 contained WS8N expressing CFP and JPA1353 expressing YFP
Mix 3 contained JPA1353 expressing CFP and WS8N expressing YFP
Mix 4 contained JPA1353 expressing CFP and JPA1353 expressing YFP

The area of slide covered by CFP fluorescent bacteria and YFP fluorescent bacteria was quantified using countCells.

Figure 9.8 shows the breakdown for the different mixtures, Figure 9.9 shows the average coverage for wild-type *R. sphaeroides* WS8N and *R. sphaeroides* JPA1353 over all samples, and Figure 9.10 shows the difference between CFP and YFP area on each slide as a scatter plot. The different mixtures are shown by colour.

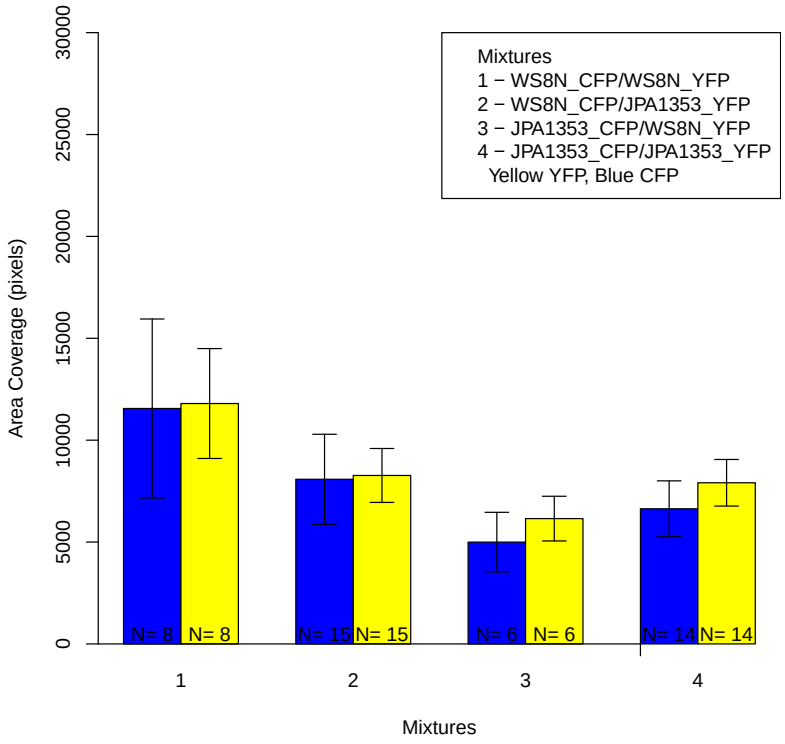


Figure 9.8: For the smooth swimming strain JPA1353, the area covered by CFP labelled and YFP labelled cells in 48 hour microcolonies in four different mixtures of strains. 1) WS8N wild-type cells labelled with CFP and WS8N wild-type cells labelled with YFP, 2) WS8N wild-type cells labelled with CFP and JPA1353 cells labelled with YFP, 3) WS8N wild-type cells labelled with YFP and JPA1353 cells labelled with CFP, and 4) JPA1353 cells labelled with CFP and JPA1353 cells labelled with YFP. Error bars are standard error. A Wilcoxon signed rank test was performed for each combination of strains, treating the CFP coverage and the YFP coverage on a single slide as a set of paired values. The results were as follows. Mix 1: $V = 24$, $p = 0.4609$ Mix 2: $V = 67$, $p = 0.7197$ Mix 3: $V = 18$, $p = 0.1563$; Mix 4: $V = 80$, $p = 0.09058$; implying that there is no significant difference between the attachment of CFP and YFP labelled cells in any of the mixtures at the $p<0.05$ level.

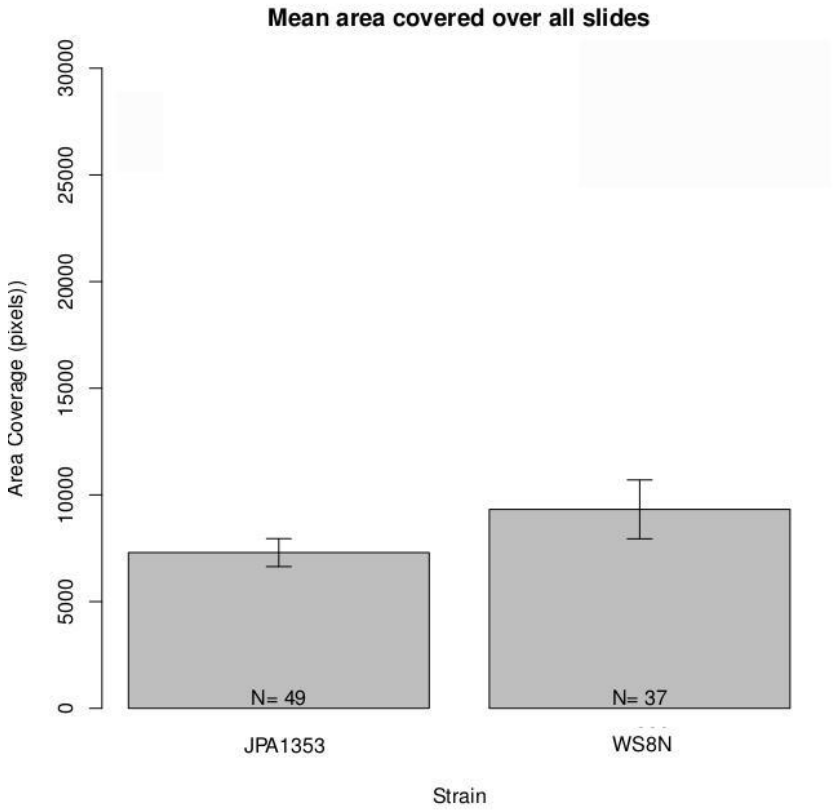


Figure 9.9: For the smooth swimming strain *R. sphaeroides* JPA1353, the area covered by mutant (JPA1353) and wild-type (WS8N) in all examples of 48 hour microcolonies from four different mixtures of strains. Error bars are standard error. A Student's T test (Section 2.9) was performed to test the hypothesis that the attachment of the mutant strain JPA467 differed from that of the wild-type strain WS8N. The results were t = -1.3446, df = 52.284, p = 0.1846. This implied that the difference in attachment is not significant at the p=0.05 level.

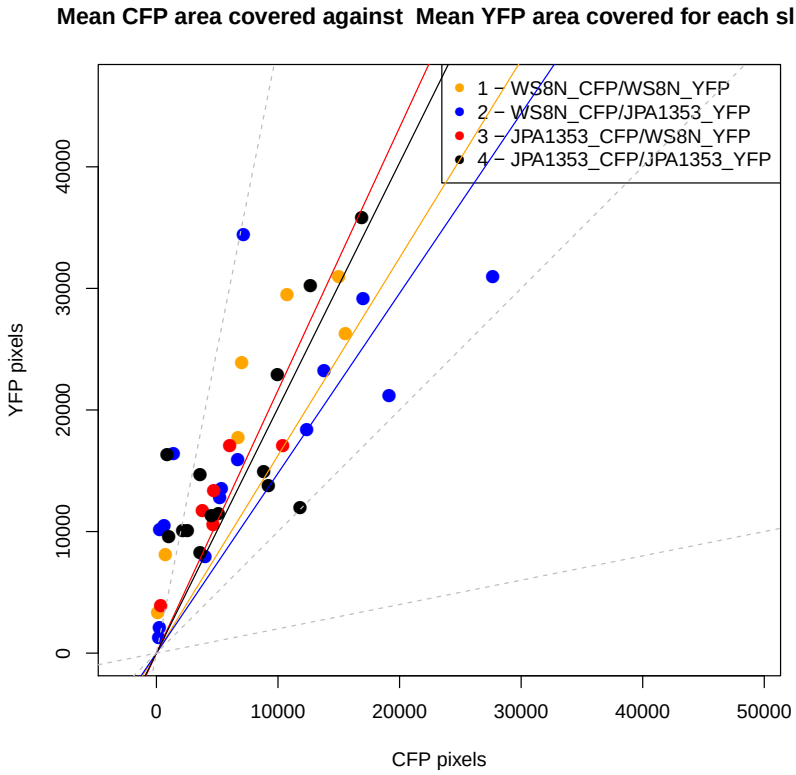


Figure 9.10: For the smooth swimming strain *R. sphaeroides* JPA1353, the area covered by CFP labelled and YFP labelled cells in 48 hour microcolonies in four different mixtures of strains.
yellow: WS8N labelled with CFP and WS8N labelled with YFP
blue: WS8N labelled with CFP and JPA467 labelled with YFP
red: WS8N labelled with YFP and JPA467 labelled with CFP,
black: JPA467 labelled with CFP and JPA467 labelled with YFP.
Unlike the non-motile strains, the data points for the different mixtures do not appear to be grouped separately. The proportions of wild-type to JPA1353 are around 1:1 in 48 hour microcolonies. Each sample is plotted with YFP coverage against CFP coverage and the colours show which mixture the sample is from. The coloured lines are least squares lines fitted to points in the different mixtures, the R^2 values are: 1 (yellow) 0.91, 2 (blue) 0.77, 3 (red) 0.92 and 4 (black) 0.87. The grey dashed lines show $y = 5x$, $y = 1/5x$ and $y = x$.

9.3.4 Discussion of 48 hour colony results

These data support the hypothesis that non motile strains are less likely to be found in colonies at 48 hours than motile strains. Most of the colonies found did contain both strains, shown on the Figures 9.4, 9.7 and 9.10, so that purely clonal colonies are uncommon.

The data was also plotted with the area coverage of CFP and YFP as a percentage of the combined area coverage (not shown). For the data in the previous sections, this led to the same conclusions as shown in Figs. 9.2, 9.5 and 9.8 about the attachment levels of the different strains.

The experiment consists of pairing strains in the same culture and it is possible to analyse the data using a paired test, like the Wilcoxon Signed Rank Test used above. This test found a significant difference in coverage for the JPA452 strain expressing CFP and expressing YFP (Mix 4). CFP and YFP are very similar and they are both expressed from the same plasmid, pInd4, so this result is unlikely to be correct. For the non motile strains it was hard to find any colonies on some of the mutant/mutant slides, and those found were small, so the result could be due to the small size of the dataset.

Another possible reason for the unlikely result in JPA452 Mix 4 is that the detection of CFP and YFP may differ even though every attempt was made to balance laser and gain settings to give similar levels (Section 2.8.3). Measuring areas rather than cell counts is useful when cells are crowded but makes different detection levels of the different fluorophores more problematic. The combinations of each possible pair of strain and fluorophore helps reduce this problem.

Non-motile cells contributed roughly fivefold less overall to the 48 hour microcolonies. This was a similar proportion to that found at 30 minutes. The slight differences from the predicted attachment if the proportions remained the same could be partially explained by higher measurement of YFP labelled strains. For each set of experiments, some initial images were taken to adjust the laser power and gain so that both fluorophores were dectected at

similar levels, laser power was as low as possible to reduce photodamage and photobleaching, and gain was adjusted to reduce background and detection of autofluorescence. The settings chosen were then kept constant for all images in a dataset, so that they could be compared. However, the measured fluorescence varied for different images and over time, and the CFP signal and the YFP signal were not always affected in the same way. The effect on the signal or cells clustering was also slightly different. For these experiments detailed measurements of fluorescence were not required, only counts and areas covered. However, a colony of cells expressing YFP often produced a signal spread over a greater area than a similar sized colony expressing CFP, with the lenses and filter sets used.

9.4 Random fields of view with wild-type and non-motile strains

Cultures of *R. sphaeroides* WS8N, and a non motile strain with a flagellum (*R. sphaeroides* JPA1213), expressing CFP from pIND4 or YFP from pIND4 were grown photoheterotrophically to stationary phase in succinate medium with 25 μg/ml kanamycin and 0.1 mM IPTG.

They were used in a static competitive assay as described in Materials and Methods Section 2.5.1. Three biological replicates were used for each strain, 2μl of each culture was used in the four mixed cultures. The mixed cultures were left to attach for 24 or 48 hours and the coverslips removed and examined on the Nikon A1 confocal microscope.

Fields of view were chosen at random without looking at the slide, to see the coverage without specifically choosing microcolonies. It could be that one of the two strains was able to attach but unable to develop on the surface, or that one strain could only attach in existing microcolonies. The images were analysed using the countCell software (Materials and Methods 2.8.3).

9.4.1 *R. sphaeroides* WS8N/*R. sphaeroides* JPA1213 24 hours random choice of fields

Four competitive assays were set up as described in Materials and Methods 2.5.1.
Mix 1 contained WS8N expressing CFP and WS8N expressing YFP
Mix 2 contained WS8N expressing CFP and JPA1213 expressing YFP
Mix 3 contained JPA1213 expressing CFP and WS8N expressing YFP
Mix 4 contained JPA1213 expressing CFP and JPA1213 expressing YFP

After 24 hours the area of slide covered by CFP fluorescent bacteria and YFP fluorescent bacteria was quantified using countCells (Materials and Methods 2.8.3.

Figure 9.11 shows the breakdown for the different mixtures, Figure 9.12 shows the average coverage for wild-type *R. sphaeroides* WS8N and *R. sphaeroides* JPA1213 over all samples, and Figure 9.13 shows the difference between CFP and YFP area on each slide as a scatter plot. The different mixtures are shown by colour and they group separately by mix.

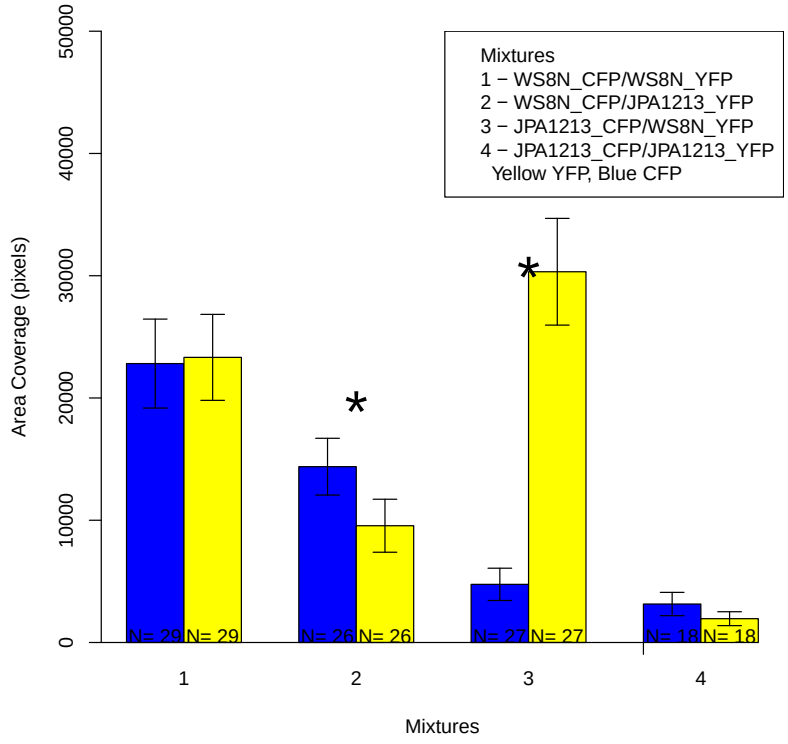


Figure 9.11: For the non-motile *R. sphaeroides* JPA1213, the area covered by CFP labelled and YFP labelled cells in 24 hours was found in four different mixtures of strains. 1) WS8N wild-type cells labelled with CFP and WS8N wild-type cells labelled with YFP, 2) WS8N wild-type cells labelled with CFP and JPA1213 cells labelled with YFP, 3) WS8N wild-type cells labelled with YFP and JPA1213 cells labelled with CFP, and 4) JPA1213 cells labelled with CFP and JPA1213 cells labelled with YFP. Error bars are standard error. A Wilcoxon signed rank test was performed for each combination of strains, treating the CFP coverage and the YFP coverage on a single slide as a set of paired values. The results were as follows. Mix 1: V = 227, p = 0.848; Mix 2: V = 54, p = 0.001298 Mix 3: V = 378, p = 1.49e-08; Mix 4: V = 49, p = 0.1187; implying that when attached bacteria are found by selecting felds of view at random, the non-motile strain still attached significantly less than the motile WS8N after 24 hours of access to a glass surface. Mixtures with significant differences in attachment are indicated by an asterisk above the columns.

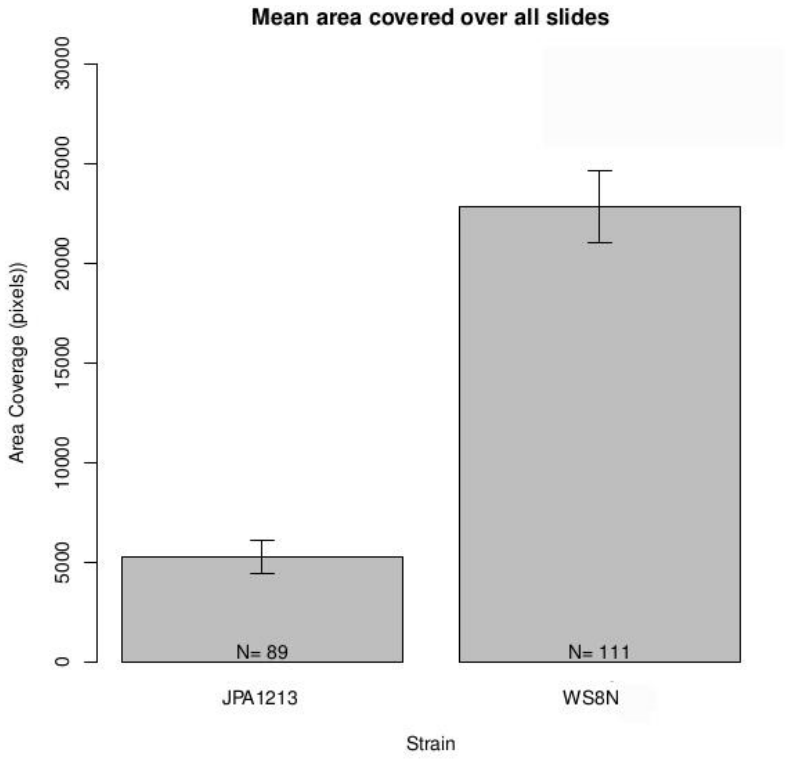


Figure 9.12: For the non-motile strain *R. sphaeroides* JPA1213, the area covered by mutant (JPA1213) and wild-type (WS8N) in all examples of 24 hour random fields of view from four different mixtures of strains. Error bars are standard error. A Student's T test (Section 2.9) was performed to test the hypothesis that the attachment of the mutant strain JPA467 differed from that of the wild-type strain WS8N. The results were t = -8.8578, df = 151.858, p = 2.015e-15. This implied that the difference in attachment is significant at the p=0.05 level.

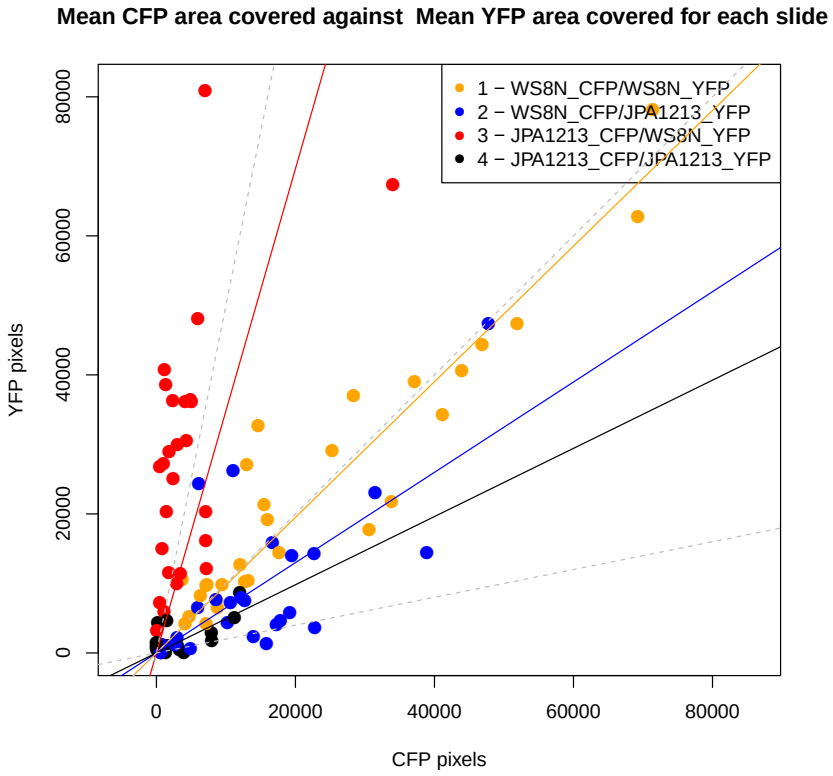


Figure 9.13: For the non-motile strain *R. sphaeroides* JPA1213, the area covered by CFP labelled and YFP labelled cells in 24 hours in four different mixtures of strains.
yellow: WS8N labelled with CFP and WS8N labelled with YFP
blue: WS8N labelled with CFP and JPA467 labelled with YFP
red: WS8N labelled with YFP and JPA467 labelled with CFP,
black: JPA467 labelled with CFP and JPA467 labelled with YFP.
Each sample is plotted with YFP coverage against CFP coverage and the colours show which mixture the sample is from. The coloured lines are least squares lines fitted to points in the different mixtures, the R^2 values are: 1 (yellow) 0.95, 2 (blue) 0.70, 3 (red) 0.58 and 4 (black) 0.65. The grey dashed lines show $y = 5x$, $y = 1/5x$ and $y = x$.

9.4.2 *R. sphaeroides* WS8N/*R. sphaeroides* JPA1213 48 hours random choice of fields

Four competitive assays were set up as described in Materials and Methods 2.5.1.
Mix 1 contained WS8N expressing CFP and WS8N expressing YFP
Mix 2 contained WS8N expressing CFP and JPA1213 expressing YFP
Mix 3 contained JPA1213 expressing CFP and WS8N expressing YFP
Mix 4 contained JPA1213 expressing CFP and JPA1213 expressing YFP

After 48 hours the area of slide covered by CFP fluorescent bacteria and YFP fluorescent bacteria was quantified using countCells (Materials and Methods 2.8.3.

After 48 hours the differences between motile and non motile attachment still exist, in general fields of view as well as in microcolonies. There are some fields of view that are sparsely covered and others are densely populated. Some fields of view had separated attached cells, but several now showed microcolonies.

This is shown in Figures 9.14, 9.15 and 9.16. Figure 9.14 shows the breakdown for the different mixtures, Figure 9.15 shows the average coverage for wild-type *R. sphaeroides* WS8N and *R. sphaeroides* JPA1213 over all samples, and Figure 9.16 shows the difference between CFP and YFP area on each slide as a scatter plot. The different mixtures are shown by colour and they group separately by mix.

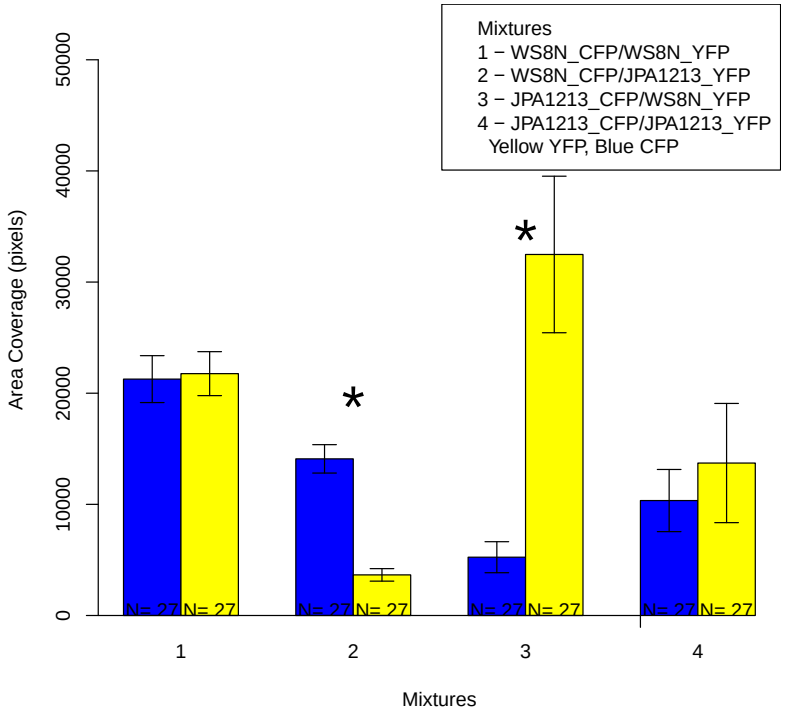


Figure 9.14: For the non-motile *R. sphaeroides* JPA1213, the area covered by CFP labelled and YFP labelled cells in 48 hours was found in four different mixtures of strains. 1) WS8N wild-type cells labelled with CFP and WS8N wild-type cells labelled with YFP, 2) WS8N wild-type cells labelled with CFP and JPA1213 cells labelled with YFP, WS8N wild-type cells labelled with YFP and JPA1213 cells labelled with CFP, and 4) JPA1213 cells labelled with CFP and JPA1213 cells labelled with YFP. Error bars are standard error. A Wilcoxon signed rank test was performed for each combination of strains, treating the CFP coverage and the YFP coverage on a single slide as a set of paired values. The results were as follows. Mix 1: V = 207, p = 0.679; Mix 2: V = 1, p = 2.98e-08; Mix 3: V = 378, p = 1.49e-08; Mix 4: V = 237, p = 0.2584; implying that when attached bacteria are found by selecting felds of view at random, the non-motile strain still attached significantly less than the motile WS8N after 48 hours of access to a glass surface. Mixtures with significant differences in attachment are indicated by an asterisk above the columns.

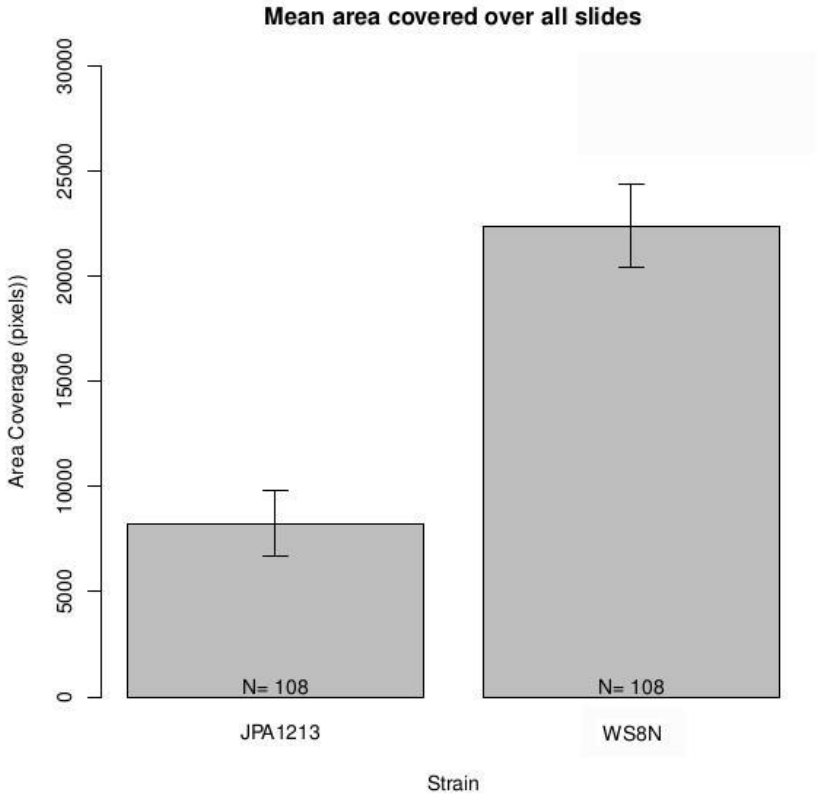


Figure 9.15: For the non-motile strain *R. sphaeroides* JPA1213, the area covered by mutant (JPA1213) and wild-type (WS8N) in all examples of 48 hour random fields of view from four different mixtures of strains. Error bars are standard error. A Student's T test (Section 2.9) was performed to test the hypothesis that the attachment of the mutant strain JPA467 differed from that of the wild-type strain WS8N. The results were t = -5.6371, df = 203.044, p = 5.734e-08 implying that thhe difference is significant at the 0.05 level

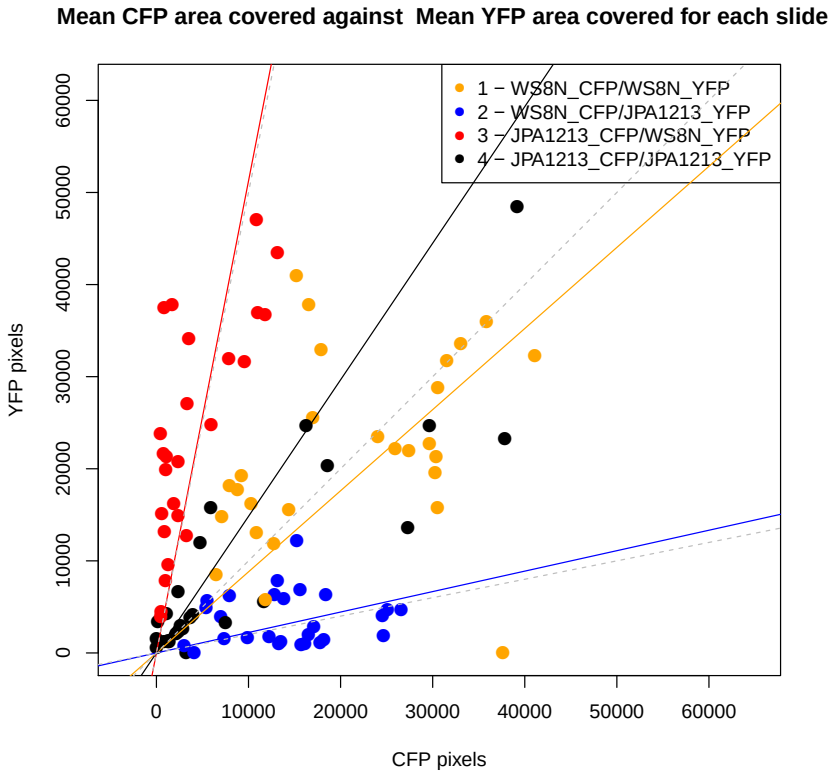


Figure 9.16: For the non-motile strain *R. sphaeroides* JPA1213, the area covered by CFP labelled and YFP labelled cells in 48 hours in four different mixtures of strains.
yellow: WS8N labelled with CFP and WS8N labelled with YFP
blue: WS8N labelled with CFP and JPA467 labelled with YFP
red: WS8N labelled with YFP and JPA467 labelled with CFP,
black: JPA467 labelled with CFP and JPA467 labelled with YFP.
Each sample is plotted with YFP coverage against CFP coverage and the colours show which mixture the sample is from. The coloured lines are least squares lines fitted to points in the different mixtures, the R^2 values are: 1 (yellow) 0.77, 2 (blue) 0.56, 3 (red) 0.87 and 4 (black) 0.73. The grey dashed lines show $y = 5x$, $y = 1/5x$ and $y = x$.

9.5 Discussion of attachment assays for random fields of view.

The attachment data for motile and non-motile cells left to attach to glass for 24 and 48 hours shows the difference between motile and non-motile attachment is present and significant at both timepoints. The experiments were done to see whether attachment of cells to the slide was different from attachment of cells within a microcolony. It is possible that a cell could fail to attach to glass but be capable of attaching to an existing microcolony. It is also possible that some cells might be unable to adapt to growing on a surface and would be present as cells attached to the slide but less common in the microcolonies. However, the data in Sections 9.3 and 9.4 shows similar proportions, and variability is such that more data is needed to uncover any possible subtle differences.

9.6 Flowcell data

Part of this project was to establish reliable methods for observing cell attachment at early stages. To watch cells attach without the disruption of slide preparation and with continuous supply of nutriends and removal of waste, several types of small flowcell were tried. The flowcell setup eventually arrived at is described in Material and Methods 8.5.1.

It was not possible to select a flow rate that removed unattached motile bacteria without dislodging attached colonies (Materials and Methods 8.5.1), though non-motile bacteria were easily swept away by flow. This gives a further advantage to motile cells.

9.6.1 Attachment in Flowcells

Flowcells inoculated with *R. sphaeroides* WS8N bacteria as described in Materials and Methods were placed on the microscope stage and a timeseries was taken, imaging a field of view every 10 minutes for 12 hours.

As a field of view becomes more crowded it becomes difficult to separate individual bacteria by segmentation. To get an overall measure of attachment each image had background subtracted and was thresholded and the proportion of pixels that were black was recorded. Standard ImageJ routines were used, the same for each frame of the timeseries, and the effect was checked by eye.

Background subtraction was done using the 'rolling ball' algorithm (Sternberg) which removes smooth continuous backgrounds from images, in the ImageJ implementation. This removes the effects of variation in lighting, which for these DIC timeseries images cause the worst segmentation problems. Thresholding was done using the default method of ImageJ, a modified IsoData method, with parameters automatically calculated from the image histogram. The results were acceptable when checked by eye.

Results from a data run for three channels seeded with independent biological cultures of *R. sphaeroides R. sphaeroides* WS8N for 10 hours are shown in Fig. 9.17. In the first five hours there is a tendency for greater coverage over time, but it is variable. The upwards trend is more marked after the first 5 hours. This may be due to cells acclimatising to attachment before growing, or to daughter cells detaching more at earlier timepoints. The flowcell data presented here is preliminary and is insufficient for statistical analysis. One noticeable feature of Fig. 9.17 is that in some samples there was a drop at 9 hours, followed by recovery. This seems likely to be experimental error, such as loss and recovery of automatic focus.

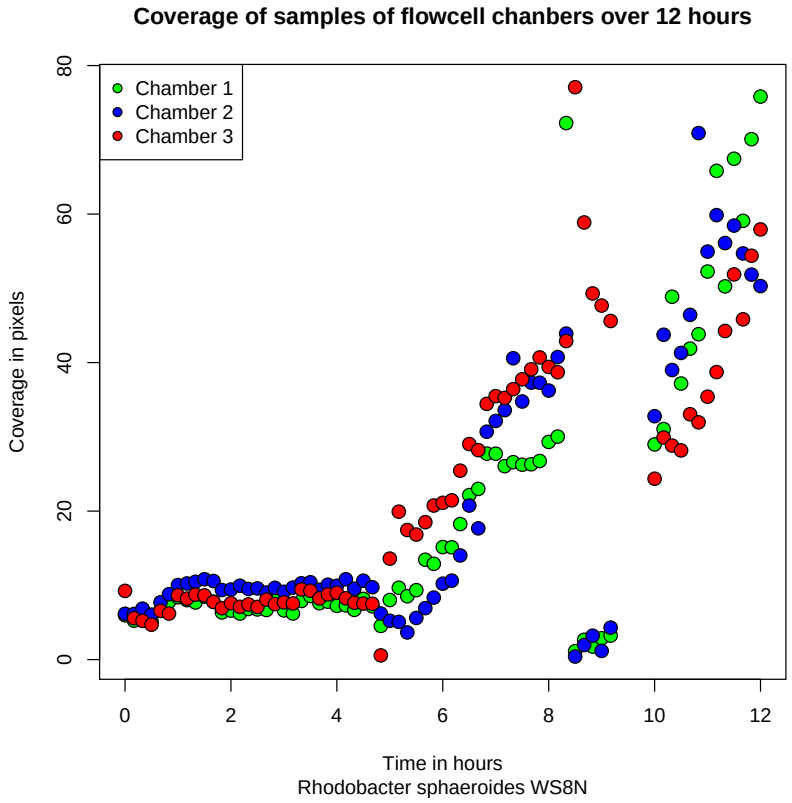


Figure 9.17: Overall coverage of a flowcell surface by *R. sphaeroides* WS8N bacteria over a 12 hour period. The coverage increases slowly for the first five hours, after which the rate of change increases. The increase over time may be caused by both newly attaching cells and division and growth of attached cells.

9.6.2 The development of chained cells

In every condition studied, *R. sphaeroides* starts to form chains of linked cells after several hours of attachment (Fig. 9.18) (Hale, 2009). These chains may be attached at one end and free in the medium over most of their length. Eventually many of them attach to the surface along their entire length, while others join together into tangles of chains (Fig. 9.20). Another common feature is swollen and misshapen cells in chained cells (Fig. 9.22). An early *R. sphaeroides* microcolony can have chains of cells reaching out into the medium along its surfaces, increasing the surface area interacting with the media. Single chains separate from microcolonies are common, as are chains connected to microcolonies (Hale, 2009).

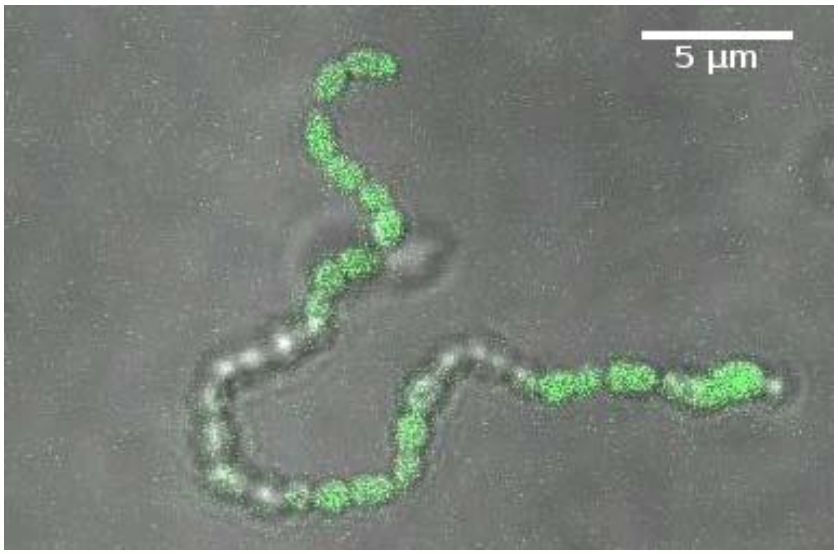


Figure 9.18: A chain of *R. sphaeroides* WS8N cells formed after 2 days attachment in a flowcell. The image is a DIC transmitted light image with false colour highlighting the signal from fluorescence. It was taken with YFP labelled cells using a Nikon A1 confocal microscope.

Are chains of cells found in planktonic cultures?

This experiment was designed to test the hypothesis that chained cells are found in swimming planktonic cells.

Table 9.1: Counts of chains of cells in 9 videos of log phase cultures

one or two cells	three or four cells	five or 6 cells	over 6 cells
1614	26	1	0

R. sphaeroides WS8N were grown photoheterotrophically (Section 2.2.2) to mid log phase, OD_{700}=0.6 in succinate medium (Appendix 11.0.3), three samples from three separate cultures.

Images were taken in tunnel slides, away from the surface. The images were examined and scored by eye, looking for chains of cells under and over 4 cells. The cutoff of 4 cells was chosen because preliminary data suggested that chains of two, three or four cells do occur in planktonic cultures, and in fact they seem to swim actively, but that longer chains are uncommon. This suggests that chains in planktonic cultures may be cells dividing quickly, so that one division is incomplete when another starts, and that at a later time they will divide fully. The results showed no chains longer than 6 cells in any sample (Table 9.1). Therefore it seems likely that forming very long chains of linked cells is a response to surface attachment in *R. sphaeroides* .

A sequence of fields of view from a timeseries taken in a flowcell (Fig 9.19) shows a chain of *R. sphaeroides* WS8N cells developing on a glass surface.

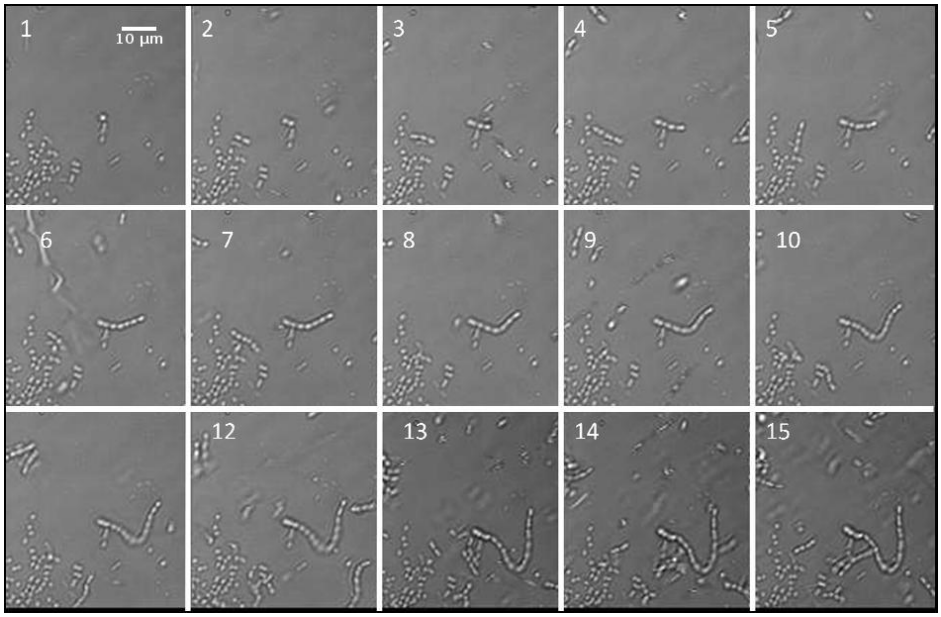


Figure 9.19: Images extracted from a timeseries showing a chain of undivided cells developing from a single attached cell. Just under two hours elapsed between consecutive images. (The original timeseries has images every 10 minutes.) While one cell starts the formation of a chain of cells, many neighbouring cells have not changed during the time.

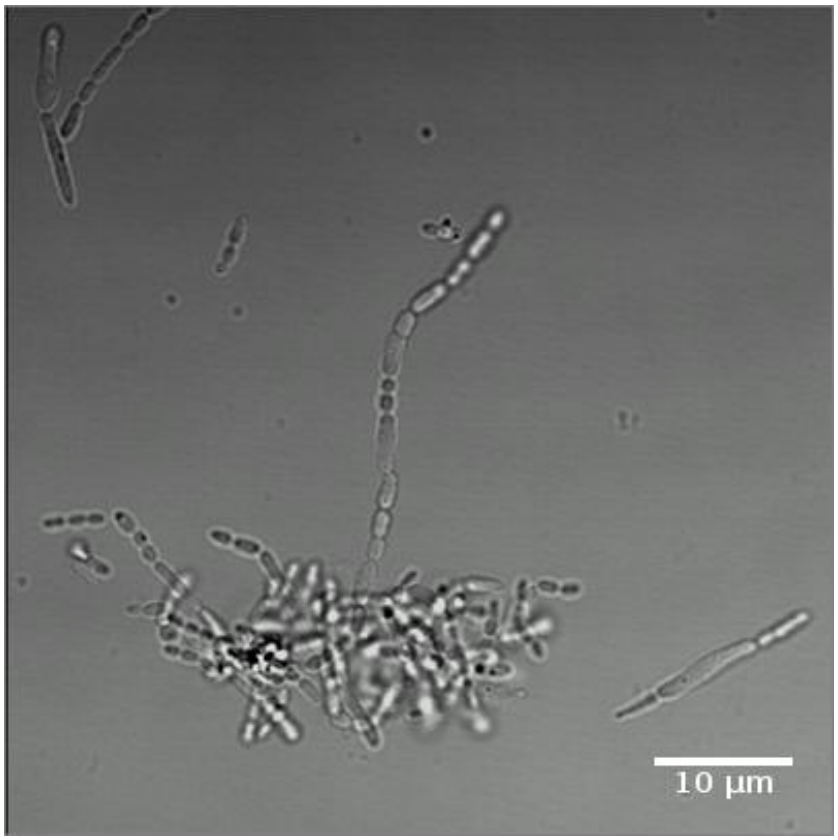


Figure 9.20: A 24 hour *R. sphaeroides* WS8N microcolony composed of of chains of cells.

9.6.3 Do non motile cells form chained cells following surface attachment?

If surface detection was mediated through the flagellum and/or the motor, strains without a functioning flagellum or motor might not form chains, or might form chains inappropriately in planktonic cultures. There is no evidence of chains forming in planktonic cultures for any non-motile strain, and long chains of non-motile and aflagellate strains were seen in competition experiments (Fig. 9.21).

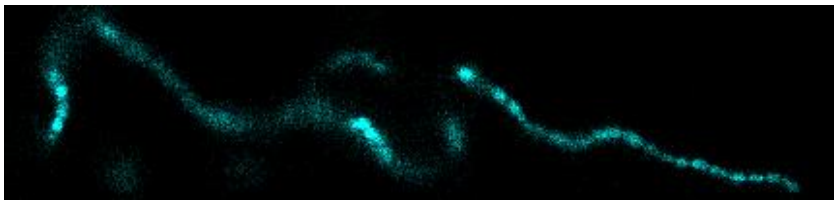


Figure 9.21: A long chain formed by the non-motile aflagellate strain *R. sphaeroides* JPA635

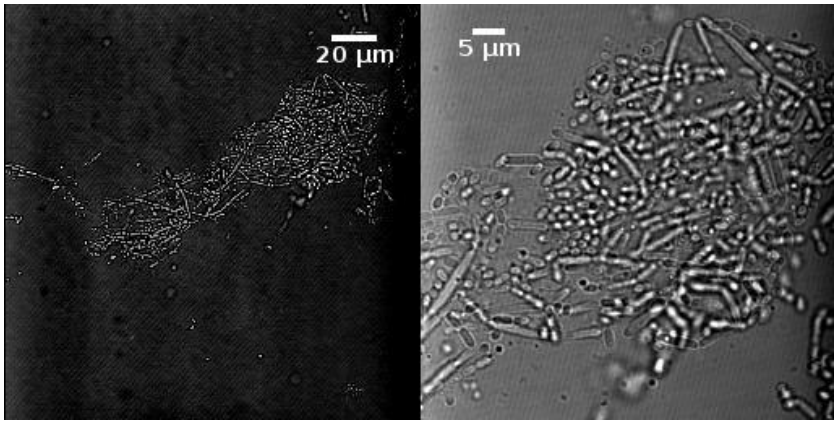


Figure 9.22: A 24 hour microcolony and close up showing some distorted cells, for example the elongated cell on the lower left of the close up image, and chains attaching to the surface.

9.6.4 Electron microscopy of cells attached to a glass surface after one hour

Staining and scanning electron microscopy of recently attached cells shows structures connecting some of the cells. It is not clear what these are, possibly flagella (Fig. 9.23).

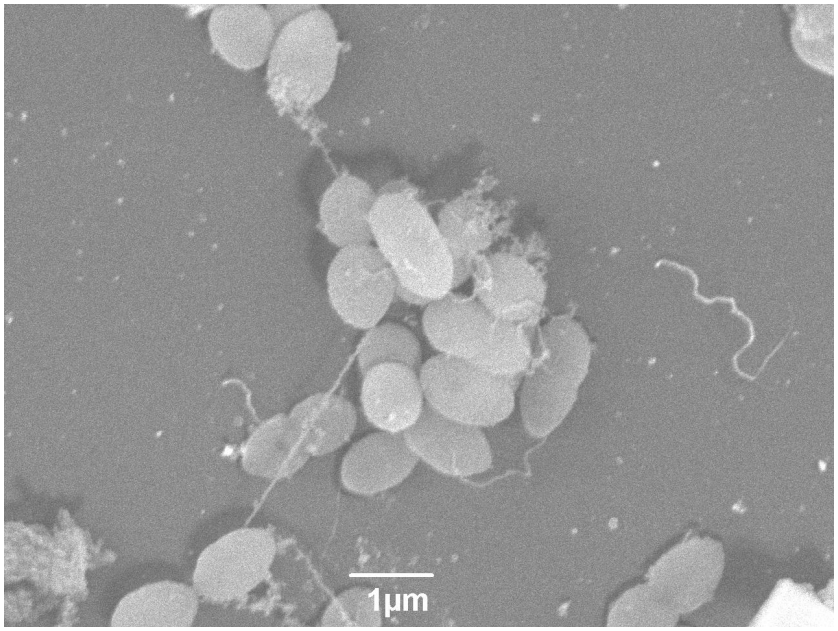


Figure 9.23: EM micrograph showing *R. sphaeroides* cells attached to a surface. Structures linking the cells could be flagella, as could the structure on the middle right of the image They are attached to the cells in a similar position, no cells seen to have more than one, and the dimensions are appropriate. The flagellum can be several microns long and is around 20nm wide (Turner et al., 2000). The fluffy material seen by some of the cells may be EPS, it is also possible it could be due to lysing cells.

9.7 Discussion

The aims of this chapter were to determine whether non-motile cells are defective in surface growth once initial attachment has taken place.

The competition experiments reported in Sections 9.3 and 9.4 show that non-motile cells continue to be less numerous on a surface than motile cells after 24 and 48 hours, but interestingly they are still present and the proportion of motile to non-motile does not seem to have changed compared to the initial half hour reported in Chapter 3, and is not very different inside and outside microcolonies. This strongly supports the hypothesis that a lack of motility adversely affects the ability of *R. sphaeroides* cells to initially reach and attach to a surface, but once cells have attached they can grow and develop

on the surface in the same way as their motile counterparts.

The second part of this chapter is more preliminary and descriptive, and shows that wild-type *R. sphaeroides* WS8N can form chains of cells, suggests that this is likely to be a response to surface attachment, and shows that chain formation occurs in aflagellate strains and is thus not linked to surface detection via the flagellum. This again supports the suggestion that motility in *R. sphaeroides* is only required to increase the number of cells reaching a surface but not for a transition to biofilm growth. Interestingly, preliminary flowcell data suggests a period of acclimatising to the surface before starting to spread (Fig. 9.17). This is also suggested by the delay before developing chains are seen, they usually appear after several hours (unpublished data) or during the second day (Hale, 2009).

Chapter 10

Discussion

Understanding the process of bacterial attachment to surfaces is important as greater understanding could lead to the ability to deter or encourage microbial colonists in situations as different as food preparation, wound healing and bioremediation. It is also interesting theoretically because there are many different surface associated behaviours in different species, and in spite of intensive work over the last 30 years the mechanism of surface sensing is understood in very few cases.

R. sphaeroides motility and chemotaxis are well understood, and *R. sphaeroides* is closely related to environmental primary surface colonisers (Dang et al., 2008; Lee et al., 2005). Several species of bacteria seem to use the apparatus of motility for sensing and attaching to surfaces (Kawagishi et al., 1996; Lauriano et al., 2004; Toutain et al., 2007; Li et al., 2012). For *R. sphaeroides* WS8N, the details of surface attachment and the mechanism for sensing a surface are unknown, though *R. sphaeroides* WS8N can form biofilms on glass and other surfaces, and motility and chemotaxis are involved in the process (Hale, 2009).

The aims of this project were to track swimming changes near surfaces and investigate the first two days of development after attachment and find out whether the effects of motility and chemotaxis seen at 5 days (Hale, 2009)

can be detected at earlier times, and to determine whether the *R. sphaeroides* WS8N uses the flagellum as an adhesin or a surface sensor in initial attachment to a surface.

Comparing the attachment of wild-type and mutant cells with altered motility or chemotaxis showed that in static microcosms non-motile cells attached less than motile cells, with an ratio of very roughly 1:5 at 30 minutes. Some strains of non-motile cells with flagella attached significantly more than aflagellate strains ($p< 0.05$), though the difference was far less than between motile and non-motile. Flagellar staining suggested that non-motile strains with flagella varied, with some strains remaining attached to their flagella and others discarding them, so that in some strains surface conditioning with discarded flagella might affect attachment. Interestingly, initial attachment also varied with swimming behaviour, with strains that swam smoothly with few stops tending to attach more in the first half hour than either wild-type cells, or cells that swam with many stops. This suggested a more subtle relationship between motility and attachment than a simple motile/non-motile split. As cultures reached stationary phase, there was less attachment and some of the cells which had attached detached from the surface. This is consitent with earlier work showing that *R. sphaeroides* WS8N uses quorum sensing to detach from surfaces in crowded conditions (Hale, 2009). Quorum sensing may also explain the lack of attachment at stationary phase, although the reduction of swimming in stationary phase *R. sphaeroides* WS8N may also be relevant.

Having determined that motility affects initial surface colonisation, tracking software was used to calculate speeds and angle changes of wild-type and mutant cells near a capillary glass surface and in the bulk medium. Speeds did not vary significantly for cells near a glass surface, this may be true only for cells swimming roughly parallel to the surface, as these were the ones which were tracked, cells at a steep angle to the surface produced very short tracks which would seem slower since the tracking is in 2D. Angles did change however, with curved paths observed for cells swimming close to the glass surface. The speeds and the proportion of recorded tracks that were stopped

for motile strains which had altered attachment after 30 minutes were also quantified. This confirmed the visual impression that some mutants stopped more or less than wild-type *R. sphaeroides* WS8N.

To determine how cells initially attach to a surface, a library of videos of single cells approaching a surface, attaching and detaching were collected. These showed that roughly half of attaching cells attached first by flagellar tethering, and half showed no evidence of rotation. They also showed that changing from one form of attachment to another was rare in 5 minutes. This suggested that some planktonic *R. sphaeroides* cells are ready to attach to a surface and that the flagellum may not act either as an initial attachment organelle or a surface sensor in *R. sphaeroides* .

To determine whether attachment differences could be explained simply by altered motility affecting the number of cells reaching a surface the predicted diffusion coefficients for non-motile, wild-type and smooth swimming strains were calculated and compared to those found for *E. coli*. It has been shown that bacteria swimming in the absence of a chemical gradient can be modelled as diffusing (Berg, 1993). The different diffusion coefficients were used in a simple model of the 96 well experiments to show that large attachment differences could build up at early timepoints due to motility differences alone. Different cell properties like flagellar sensing were not necessary to account for the differences in attachment. This model could be used with the measured attachment data to make predictions about the probability that a cell will attach, but this was outside the scope of this project. The model would break down after very early timepoints because swimming behaviour changes at surfaces and a simple assumption of diffusion will not be valid. Also gradients of nutrients and wastes will build up and change the random nature of the cell's path. However, diffusion coefficients are a measure of 'amount of movement' of a strain, and this could account for the observed effect on early attachment.

Attempts to alter motility by increasing viscosity and to see whether attachment altered as motility reduced were unsuccessful since attachment was drastically reduced at low levels of viscosity, while swimming was not sig-

nificantly altered until much higher viscosity. Possible explanations are surface conditioning by the viscous agent, Ficoll, or a metabolic effect on *R. sphaeroides* WS8N, which showed reduced growth in Ficoll solutions.

Assuming that the flagellum is not required for surface sensing and the transition to biofilm growth, we examined the development of wild-type and mutant cells on a glass surface over a period of 48 hours. 48 hour microcolonies of fluorescently labelled *R. sphaeroides* wild-type and mutant cells in competition assays showed more motile than non-motile cells, but the proportion had not changed much from the initial ratio of around 1:5, this was also true for cells in random fields of view in slides incubated for 24 and 48 houts. Non-motile cells in competition assays and in flowcells formed chained cells (indicative of biofilm rather than planktonic growth) in the same way as wild-type cells. This suggests that while initial attachment is less for non-motile and aflagellate strains, development on the surface is similar for both. That would imply that the flagellum and motor are not necessary for the transition from reversible to irreversible attachment.

In conclusion, the data from all of these experiments supports the hypothesis that unlike some other species (Introduction 1.8), *R. sphaeroides* WS8N does not use the flagellum either as an attachment organelle or as a surface sensor. Aflagellate strains attach in lower numbers due to lack of motility alone, and once attached all cells seem to develop in the same way as motile strains. It is unclear what *R. sphaeroides* could be using to sense the surface, electron micrographs of recently attached *R. sphaeroides* WS8N cells show no other appendages such as pili, but this is an area for further research.

10.1 Future Work

Experiments on surface conditioning could be undertaken to explain the results of using Ficoll and to see whether preconditioning surfaces with supernatants of log and stationary phase cells alter attachment.

Attachment becomes very variable at later timepoints, and more high through-

put measurements with improved image analysis software could be developed to collect enough data for more robust conclusions. The analysis of the two colour competition experiments could be extended to measure interactions between the strains.

The conclusion that tethering by the flagellum accounts for only half of attachment events was found by tracking the fate of cells that attached by different methods by eye, so the number of cells tracked was limited. If software could be developed to automatically detect rotating cells a very large dataset could be collected and the proportion of tethered cells that eventually detach again could be measured. This should be possible due to the very regular movements of tethered cells, but currently the tracking software tended to allocate tethered cells to tracks unreliably, since it was based on expected motion in bulk fluid. Tethered cells also affect the motion of fluid around them, and swimming cells seem to be attracted towards them, and the path of an approaching cell was often confused with the path of the tethered cell.

The flowcell experiments were preliminary and could be extended to see whether growth in moving fluid with more stable conditions as wastes are removed and nutrients replenished will alter the attachment behaviour of the different strains.

The clearest phenotypic change in attached *R. sphaeroides* WS8N cells over the first hours and days is the formation of chained cells. Further work could establish whether these are formed by alterations in the process of cell division or by cells dividing normally but sticking together after cell division.

All the data so far suggest that *R. sphaeroides* WS8N does not use the flagellum as a surface sensor, leaving the question of how the surface is sensed by this bacterium. It is possible that a subset of cells produce adhesins allowing passive attachment to a nearby surface, but there must still be a point at which the cell changes to a surface attached phenotype. The question 'how does *R. sphaeroides* WS8N know it is at a surface' could be addressed using studies of gene expression changes in attached cells, and by looking for homologues of systems used in related bacteria such as *C. crescentus* .

However, this is an unanswered question for most bacterial species.

Bibliography

M. Alhede, K. N. Kragh, K. Qvortrup, M. Allesen-Holm, M. van Gennip, L. D. Christensen, P. O. Jensen, A. K. Nielsen, M. Parsek, D. Wozniak, S. Molin, T. Tolker-Nielsen, N. Hoiby, M. Givskov, and T. Bjarnsholt. Phenotypes of non-attached *Pseudomonas aeruginosa* aggregates resemble surface attached biofilm. *PloS One*, 6(11), 2011.

B. Alvarez, P. Secades, M. Prieto, M. J. McBride, and J. A. Guijarro. A mutation in *Flavobacterium psychrophilum tlpB* inhibits gliding motility and induces biofilm formation. *Applied and Environmental Microbiology*, 72(6):4044–4053, 2006.

J. P. Armitage. Behavioural responses of bacteria to light and oxygen. *Archives of Microbiology*, 168(4):249–261, 1997.

J. P. Armitage and K. J. Hellingwerf. Light-induced behavioral responses ('phototaxis') in prokaryotes. *Photosynthesis Research*, 76(1-3):145–155, 2003.

J. P. Armitage and R. M. Macnab. Unidirectional, intermittent rotation of the flagellum of *Rhodobacter sphaeroides*. *Journal of Bacteriology*, 169(2): 514–518, 1987.

J. P. Armitage, T. P. Pitta, M. A. S. Vigeant, H. L. Packer, and R. M. Ford. Transformations in flagellar structure of *Rhodobacter sphaeroides* and possible relationship to changes in swimming speed. *Journal of Bacteriology*, 181(16):4825–4833, 1999.

H. J. Bai, Z. M. Zhang, G. E. Yang, and B. Z. Li. Bioremediation of cadmium by growing *Rhodobacter sphaeroides*: kinetic characteristic and mechanism studies. *Bioresource Technology*, 99(16):7716–7722, 2008.

B. L. Bassler, M. Wright, R. E. Showalter, and M. R. Silverman. Intercellular signalling in *Vibrio harveyi*: sequence and function of genes regulating expression of luminescence. *Molecular Microbiology*, 9(4):773–786, 1993.

F. Bastida, M. Rosell, A. G. Franchini, J. Seifert, S. Finsterbusch, N. Jehmlich, S. Jechalke, M. von Bergen, and H. H. Richnow. Elucidating MTBE degradation in a mixed consortium using a multidisciplinary approach. *FEMS Microbiology Ecology*, 73(2):370–384, 2010.

R. Belas and R. Suvanasuthi. The ability of *Proteus mirabilis* to sense surfaces and regulate virulence gene expression involves FliL, a flagellar basal body protein. *Journal of Bacteriology*, 187(19):6789–6803, 2005.

K. Bellenger, X. Ma, W. Shi, and Z. Yang. A CheW homologue is required for *Myxococcus xanthus* fruiting body development, social gliding motility, and fibril biogenesis. *Journal of Bacteriology*, 184(20):5654–5660, 2002.

H. C. Berg. *Random walks in biology*. Princeton University Press, Princeton, N.J. ; Chichester, expanded edition, 1993.

H. C. Berg. The rotary motor of bacterial flagella. *Annual Review of Biochemistry*, 72(1):19–54, 2003.

H. C. Berg and L. Turner. Movement of microorganisms in viscous environments. *Nature*, 278(5702):349–351, 1979.

H. C. Berg and L. Turner. Chemotaxis of bacteria in glass capillary arrays. *Escherichia coli*, motility, microchannel plate, and light scattering. *Biophysical Journal*, 58(4):919–930, 1990.

J. E. Berleman and C. E. Bauer. A Che-like signal transduction cascade involved in controlling flagella biosynthesis in *Rhodospirillum centenum*. *Molecular Microbiology*, 55(5):1390–1402, 2005a.

J. E. Berleman and C. E. Bauer. Involvement of a Che-like signal transduction cascade in regulating cyst cell development in *Rhodospirillum centenum*. *Molecular Microbiology*, 56(6):1457–1466, 2005b.

A. Bible, M. H. Russell, and G. Alexandre. The *Azospirillum brasilense* che1 chemotaxis pathway controls swimming velocity, which affects transient cell-to-cell clumping. *Journal of Bacteriology*, 194(13):3343–3355, 2012.

W. P. Black and Z. Yang. *Myxococcus xanthus* chemotaxis homologs DifD and DifG negatively regulate fibril polysaccharide production. *Journal of Bacteriology*, 186(4):1001–1008, 2004.

W. P. Black, F. D. Schubot, Z. Li, and Z. Yang. Phosphorylation and dephosphorylation among Dif chemosensory proteins essential for exopolysaccharide regulation in *Myxococcus xanthus*. *Journal of Bacteriology*, 192(17): 4267–4274, 2010.

A. Boehm, M. Kaiser, H. Li, C. Spangler, C. A. Kasper, M. Ackermann, V. Kaever, V. Sourjik, V. Roth, and U. Jenal. Second messenger-mediated adjustment of bacterial swimming velocity. *Cell*, 141(1):107–116, 2010.

M. P. Bohrer, W. M. Deen, C. R. Robertson, J. L. Troy, and B. M. Brenner. Influence of molecular configuration on the passage of macromolecules across the glomerular capillary wall. *The Journal of General Physiology*, 74(5):583–593, 1979.

N. P. Boks, W. Norde, H. C. van der Mei, and H. J. Busscher. Forces involved in bacterial adhesion to hydrophilic and hydrophobic surfaces. *Microbiology*, 154(10):3122–3133, 2008.

S. S. Branda, S. Vik, L. Friedman, and R. Kolter. Biofilms: the matrix revisited. *Trends in Microbiology*, 13(1):20–26, 2005.

M. T. Brown. *Control of the unidirectional motor in Rhodobacter sphaeroides*. PhD thesis, University of Oxford, 2009.

J. Bruchmann, S. Kirchen, and T. Schwartz. Sub-inhibitory concentrations of antibiotics and wastewater influencing biofilm formation and gene expression of multi-resistant *Pseudomonas aeruginosa* wastewater isolates. *Environmental Science and Pollution Research International*, 20(6):3539–3549, 2013.

M. Burmolle, L. Hansen, and S. Sorensen. Establishment and early succession of a multispecies biofilm composed of soil bacteria. *Microbial Ecology*, 54 (2):352–362, 2007.

N. C. Caiazza, J. H. Merritt, K. M. Brothers, and G. A. O'Toole. Inverse regulation of biofilm formation and swarming motility by *Pseudomonas aeruginosa* PA14. *Journal of Bacteriology*, 189(9):3603–3612, 2007.

L. S. Cairns, V. L. Marlow, E. Bissett, A. Ostrowski, and N. R. Stanley-Wall. A mechanical signal transmitted by the flagellum controls signalling in *Bacillus subtilis*. *Molecular Microbiology*, 90(1):6–21, 2013.

J. D. Chambless, S. M. Hunt, and P. S. Stewart. A three-dimensional computer model of four hypothetical mechanisms protecting biofilms from antimicrobials. *Applied and Environmental Microbiology*, 72(3):2005–2013, 2006.

I. Chang, E. S. Gilbert, N. Eliashberg, and J. D. Keasling. A three-dimensional, stochastic simulation of biofilm growth and transport-related factors that affect structure. *Microbiology*, 149(10):2859–2871, 2003.

X. Chen and H. C. Berg. Torque-speed relationship of the flagellar rotary motor of *Escherichia coli*. *Biophysical Journal*, 78(2):1036–1041, 2000.

G. S. Chilcott and K. T. Hughes. Coupling of flagellar gene expression to flagellar assembly in *Salmonella enterica* serovar typhimurium and *Escherichia coli*. *Microbiology and Molecular Biology Reviews*, 64(4):694–708, 2000.

M. Choudhary, X. Zanhua, Y. X. Fu, and S. Kaplan. Genome analyses of three strains of *Rhodobacter sphaeroides*: evidence of rapid evolution of chromosome ii. *Journal of Bacteriology*, 189(5):1914–1921, 2007.

M. Clarke, L. Maddera, R. L. Harris, and P. M. Silverman. F-pili dynamics by live-cell imaging. *Proceedings of the National Academy of Sciences USA*, 2008.

S. E. Coetser and T. E. Cloete. Biofouling and biocorrosion in industrial water systems. *Critical Reviews in Microbiology*, 31(4):213–232, 2005.

J. C. Conrad, M. L. Gibiansky, F. Jin, V. D. Gordon, D. A. Motto, M. A. Mathewson, W. G. Stopka, D. C. Zelasko, J. D. Shrout, and G. C. Wong. Flagella and pili-mediated near-surface single-cell motility mechanisms in *P. aeruginosa*. *Biophysical Journal*, 100(7):1608–1616, 2011.

J. W. Costerton, P. S. Stewart, and E. P. Greenberg. Bacterial biofilms: A common cause of persistent infections. *Science*, 284(5418):1318–1322, 1999.

P. Dalgaard. *Introductory statistics with R*. Springer, New York, 2nd ed. edition, 2008.

H. Dang, T. Li, M. Chen, and G. Huang. Cross-ocean distribution of rhodobacterales bacteria as primary surface colonizers in temperate coastal marine waters. *Applied and Environmental Microbiology*, 74(1):52–60, 2008.

T. Danhorn and C. Fuqua. Biofilm formation by plant-associated bacteria. *Annual Review of Microbiology*, 61:401–422, 2007.

N. C. Darnton and H. C. Berg. Force-extension measurements on bacterial flagella: triggering polymorphic transformations. *Biophysical Journal*, 92 (6):2230–2236, 2007.

A. M. del Campo, T. Ballado, L. Camarena, and G. Dreyfus. In *Rhodobacter sphaeroides*, chemotactic operon 1 regulates rotation of the flagellar system 2. *Journal of Bacteriology*, 193(23):6781–6786, 2011.

K. L. V. Dellen, L. Houot, and P. I. Watnick. Genetic analysis of *Vibrio cholerae* monolayer formation reveals a key role for DeltaPsi in the

transition to permanent attachment. *Journal of Bacteriology*, 190(24): 8185–8196, 2008.

A. Ducret, M. P. Valignat, F. Mouhamar, T. Mignot, and O. Theodoly. Wet-surface-enhanced ellipsometric contrast microscopy identifies slime as a major adhesion factor during bacterial surface motility. *Proceedings of the National Academy of Sciences USA*, 109(25):10036–10041, 2012.

D. B. Dusenbery. *Living at micro scale : the unexpected physics of being small*. Harvard University Press, Cambridge, Mass., First Harvard University Press paperback edition, 2009.

A. N. Edwards, P. Siuti, A. N. Bible, G. Alexandre, S. T. Retterer, M. J. Doktycz, and J. L. Morrell-Falvey. Characterization of cell surface and extracellular matrix remodeling of *Azospirillum brasilense* chemotaxis-like 1 signal transduction pathway mutants by atomic force microscopy. *FEMS Microbiology Letters*, 314(2):131–139, 2011.

S. Elias and E. Banin. Multi-species biofilms: living with friendly neighbors. *FEMS Microbiology Reviews*, 2012.

P. Entcheva-Dimitrov and A. M. Spormann. Dynamics and control of biofilms of the oligotrophic bacterium *Caulobacter crescentus*. *Journal of Bacteriology*, 186(24):8254–8266, 2004.

R. Fernandez-Pinar, M. Camara, J. F. Dubern, J. L. Ramos, and M. Espinosa-Urgel. The *Pseudomonas aeruginosa* quinolone quorum sensing signal alters the multicellular behaviour of *Pseudomonas putida* KT2440. *Research in Microbiology*, 162(8):773–781, 2011.

R. A. Fisher. *Statistical methods for research workers*. Oliver and Boyd, Edinburgh ; London, 2d ed. edition, 1928.

H. C. Flemming. The perfect slime. *Colloids and Surfaces. B, Biointerfaces*, 86(2):251–259, 2011.

B. Friedrich. A mesoscopic model for helical bacterial flagella. *Journal of Mathematical Biology*, 53(1):162–178, 2006.

P. D. Frymier and R. M. Ford. Analysis of bacterial swimming speed approaching a solid/liquid interface. *AIChE Journal*, 43(5):1341–1347, 1997.

P. D. Frymier, R. M. Ford, H. C. Berg, and P. T. Cummings. Three-dimensional tracking of motile bacteria near a solid planar surface. *Proceedings of the National Academy of Sciences USA*, 92(13):6195–6199, 1995.

L. D. L. Fuente, E. Montanes, Y. Meng, Y. Li, T. J. Burr, H. C. Hoch, and M. Wu. Assessing adhesion forces of type I and type IV pili of *Xylella fastidiosa* bacteria by use of a microfluidic flow chamber. *Applied and Environmental Microbiology*, 73(8):2690–2696, 2007.

C. Fuqua, M. R. Parsek, and E. P. Greenberg. Regulation of gene expression by cell-to-cell communication: acyl-homoserine lactone quorum sensing. *Annual Review of Genetics*, 35:439–468, 2001.

J. Galloway, F. Dentener, D. Capone, E. Boyer, R. Howarth, S. Seitzinger, G. Asner, C. Cleveland, P. Green, E. Holland, D. Karl, A. Michaels, J. Porter, A. Townsend, and C. Voosmarty. Nitrogen cycles: Past, present, and future. *Biogeochemistry*, 70(2):153–226, 2004.

M. Y. Galperin and A. N. Nikolskaya. Identification of sensory and signal-transducing domains in two-component signaling systems. *Methods in Enzymology*, 422:47–74, 2007.

D. E. Gauden. *Electron Transport Dependent Taxis in in Rhodobacter sphaeroides*. PhD thesis, University of Oxford, 1996.

G. Giuliano, D. Pollock, H. Stapp, and P. Scolnik. A genetic-physical map of the *Rhodobacter capsulatus* carotenoid biosynthesis gene cluster. *Molecular and General Genetics*, 213(1):78–83, 1988.

D. J. Gorth, S. Puckett, B. Ercan, T. J. Webster, M. Rahaman, and B. S. Bal. Decreased bacteria activity on Si(3)N(4) surfaces compared with PEEK or titanium. *International Journal of Nanomedicine*, 7:4829–4840, 2012.

B. Gottenbos, H. C. van der Mei, and H. J. Busscher. Models for studying initial adhesion and surface growth in biofilm formation on surfaces. *Methods in Enzymology*, 310:523–534, 1999.

P. Goymer, S. G. Kahn, J. G. Malone, S. M. Gehrig, A. J. Spiers, and P. B. Rainey. Adaptive divergence in experimental populations of *Pseudomonas fluorescens*. ii. role of the GGDEF regulator WspR in evolution and development of the wrinkly spreader phenotype. *Genetics*, 173(2):515–526, 2006.

E. P. Greenberg and E. Canale-Parola. Motility of flagellated bacteria in viscous environments. *Journal of Bacteriology*, 132(1):356–358, 1977.

L. A. Hale. *The Role of Quorum Sensing in Rhodobacter sphaeroides WS8N*. PhD thesis, Oxford Brookes University, 2009.

L. Hall-Stoodley, J. W. Costerton, and P. Stoodley. Bacterial biofilms: from the natural environment to infectious diseases. *Nature Reviews Microbiology*, 2(2):95–108, 2004.

N. B. Hallam, J. R. West, C. F. Forster, and J. Simms. The potential for biofilm growth in water distribution systems. *Water Research*, 35(17): 4063–4071, 2001.

P. A. Hamblin, B. A. Maguire, R. N. Grishanin, and J. P. Armitage. Evidence for two chemosensory pathways in *Rhodobacter sphaeroides*. *Molecular Microbiology*, 26(5):1083–1096, 1997.

R. Hamer, P. Y. Chen, J. P. Armitage, G. Reinert, and C. M. Deane. Deciphering chemotaxis pathways using cross species comparisons. *BMC Systems Biology*, 4:3, 2010.

D. Hanahan. Studies on transformation of *Escherichia coli* with plasmids. *Journal of Molecular Biology*, 166(4):557–580, 1983.

J. He, G. Zhang, and H. Lu. Treatment of soybean wastewater by a wild strain *Rhodobacter sphaeroides* and to produce protein under natural conditions.

Frontiers of Environmental Science and Engineering in China, 4(3):334–339, 2010.

M. E. Heimbrook, W. L. Wang, and G. Campbell. Staining bacterial flagella easily. *Journal of Clinical Microbiology*, 27(11):2612–2615, 1989.

A. T. Henrici. Studies of freshwater bacteria: I. a direct microscopic technique. *Journal of Bacteriology*, 25(3):277–287, 1933.

M. Hermansson. The DLVO theory in microbial adhesion. *Colloids and Surfaces B: Biointerfaces*, 14(1-4):105–119, 1999.

A. Heydorn, A. T. Nielsen, M. Hentzer, C. Sternberg, M. Givskov, B. K. Ersboll, and S. Molin. Quantification of biofilm structures by the novel computer program comstat. *Microbiology*, 146(10):2395–2407, 2000.

J. W. Hickman, D. F. Tifrea, and C. S. Harwood. A chemosensory system that regulates biofilm formation through modulation of cyclic diguanylate levels. *Proceedings of the National Academy of Sciences USA*, 102(40): 14422–14427, 2005.

R. Higuchi, B. Krummel, and R. K. Saiki. A general method of in vitro preparation and specific mutagenesis of DNA fragments: study of protein and DNA interactions. *Nucleic Acids Research*, 16(15):7351–7367, 1988.

S. M. Hinsa, M. Espinosa-Urgel, J. L. Ramos, and G. A. O'Toole. Transition from reversible to irreversible attachment during biofilm formation by *Pseudomonas fluorescens* WCS365 requires an ABC transporter and a large secreted protein. *Molecular Microbiology*, 49(4):905–918, 2003.

J. A. Hoch and K. I. Varughese. Keeping signals straight in phosphorelay signal transduction. *Journal of Bacteriology*, 183(17):4941–4949, 2001.

L. R. Hoffman, D. A. D'Argenio, M. J. MacCoss, Z. Zhang, R. A. Jones, and S. I. Miller. Aminoglycoside antibiotics induce bacterial biofilm formation. *Nature*, 436(7054):1171–1175, 2005.

S. Holm. A simple sequentially rejective multiple test procedure. *Scandinavian Journal of Statistics*, 6(2):65–70, 1979.

R. M. Horton, Z. L. Cai, S. N. Ho, and L. R. Pease. Gene splicing by overlap extension: tailor-made genes using the polymerase chain reaction. *BioTechniques*, 8(5):528–535, 1990.

A. Houry, R. Briandet, S. Aymerich, and M. Gohar. Involvement of motility and flagella in *Bacillus cereus* biofilm formation. *Microbiology*, 156:1009–1018, 2010.

D. C. Howell. *Fundamental statistics for the behavioral sciences*. Duxbury Press, Belmont, Calif, 3rd edition, 1995.

S. M. Hunt, M. A. Hamilton, J. T. Sears, G. Harkin, and J. Reno. A computer investigation of chemically mediated detachment in bacterial biofilms. *Microbiology*, 149(5):1155–1163, 2003.

S. M. Hunt, E. M. Werner, B. Huang, M. A. Hamilton, and P. S. Stewart. Hypothesis for the role of nutrient starvation in biofilm detachment. *Applied and Environmental Microbiology*, 70(12):7418–7425, 2004.

A. C. Ind, S. L. Porter, M. T. Brown, E. D. Byles, J. A. de Beyer, S. A. Godfrey, and J. P. Armitage. Inducible-expression plasmid for *Rhodobacter sphaeroides* and *Paracoccus denitrificans*. *Applied and Environmental Microbiology*, 75(20):6613–6615, 2009.

K. F. Jarrell and M. J. McBride. The surprisingly diverse ways that prokaryotes move. *Nature Reviews Microbiology*, 6(6):466–476, 2008.

J. F. Jones and D. Velegol. Laser trap studies of end-on *E. coli* adhesion to glass. *Colloids and Surfaces B: Biointerfaces*, 50(1):66–71, 2006.

R. Kamiya and S. Asakura. Helical transformations of salmonella flagella in vitro. *Journal of Molecular Biology*, 106(1):167 – 186, 1976.

E. Karatan and P. Watnick. Signals, regulatory networks, and materials that build and break bacterial biofilms. *Microbiology and Molecular Biology Reviews*, 73(2):310–347, 2009.

I. Kawagishi, M. Imagawa, Y. Imae, L. McCarter, and M. Homma. The sodium-driven polar flagellar motor of marine *Vibrio* as the mechanosensor that regulates lateral flagellar expression. *Molecular Microbiology*, 20(4): 693–699, 1996.

D. B. Kearns. A field guide to bacterial swarming motility. *Nature Reviews Microbiology*, 8(9):634–644, 2010.

M. Kim, S. Lee, H. D. Park, S. I. Choi, and S. Hong. Biofouling control by quorum sensing inhibition and its dependence on membrane surface. *Water Science and Technology*, 66(7):1424–1430, 2012.

S. M. Kirov, M. Castrisios, and J. G. Shaw. *Aeromonas* flagella (polar and lateral) are enterocyte adhesins that contribute to biofilm formation on surfaces. *Infection and Immunity*, 72(4):1939–1945, 2004.

M. Klausen, A. Aaes-Jorgensen, S. Molin, and T. Tolker-Nielsen. Involvement of bacterial migration in the development of complex multicellular structures in *Pseudomonas aeruginosa* biofilms. *Molecular Microbiology*, 50(1):61–68, 2003.

P. Klemm and M. A. Schembri. Bacterial adhesins: function and structure. *International Journal of Medical Microbiology*, 290(1):27–35, 2000.

K. A. Kline, S. Falker, S. Dahlberg, S. Normark, and B. Henriques-Normark. Bacterial adhesins in host-microbe interactions. *Cell Host and Microbe*, 5 (6):580–592, 2009.

K. Kobayashi. *Bacillus subtilis* pellicle formation proceeds through genetically defined morphological changes. *Journal of Bacteriology*, 189(13): 4920–4931, 2007.

M. Kojadinovic, J. P. Armitage, M. J. Tindall, and G. H. Wadhams. Response kinetics in the complex chemotaxis signalling pathway of *Rhodobacter sphaeroides*. *Journal of the Royal Society*, 10(81), 2013.

J.-U. Kreft, C. Picioreanu, J. W. T. Wimpenny, and M. C. M. van Loosdrecht. Individual-based modelling of biofilms. *Microbiology*, 147(11): 2897–2912, 2001.

S. Kudo, N. Imai, M. Nishitoba, S. Sugiyama, and Y. Magariyama. Asymmetric swimming pattern of *Vibrio alginolyticus* cells with single polar flagella. *FEMS Microbiology Letters*, 242(2):221–225, 2005.

L. A. Lardon, B. V. Merkey, S. Martins, A. Dotsch, C. Picioreanu, J.-U. Kreft, and B. F. Smets. idynomics: next-generation individual-based modelling of biofilms. *Environmental Microbiology*, 13(9):2416–2434, 2011.

M. T. Laub and M. Goulian. Specificity in two-component signal transduction pathways. *Annual Review of Genetics*, 41:121–145, 2007.

E. Lauga, W. R. DiLuzio, G. M. Whitesides, and H. A. Stone. Swimming in circles: Motion of bacteria near solid boundaries. *Biophysical Journal*, 90 (2):400–412, 2006.

C. M. Lauriano, C. Ghosh, N. E. Correa, and K. E. Klose. The sodium-driven flagellar motor controls exopolysaccharide expression in *Vibrio cholerae*. *Journal of Bacteriology*, 186(15):4864–4874, 2004.

D.-G. Lee, J.-H. Lee, and S.-J. Kim. Diversity and dynamics of bacterial species in a biofilm at the end of the seoul water distribution system. *World Journal of Microbiology and Biotechnology*, 21(2):155–162, 2005.

Y.-Y. Lee, J. Patellis, and R. Belas. Activity of *Proteus mirabilis* FliL is viscosity dependent and requires extragenic DNA. *Journal of Bacteriology*, 195(4):823–832, 2013.

K. P. Lemon, A. M. Earl, H. C. Vlamakis, C. Aguilar, and R. Kolter. Biofilm development with an emphasis on *Bacillus subtilis*. *Current topics in Microbiology and Immunology*, 322:1–16, 2008.

G. Li and J. X. Tang. Accumulation of microswimmers near a surface mediated by collision and rotational Brownian motion. *Physical Review Letters*, 103(7):078101, 2009.

G. Li, L.-K. Tam, and J. X. Tang. Amplified effect of brownian motion in bacterial near-surface swimming. *Proceedings of the National Academy of Sciences USA*, 2008.

G. Li, J. Bensson, L. Nisimova, D. Munger, P. Mahautmr, J. X. Tang, M. R. Maxey, and Y. V. Brun. Accumulation of swimming bacteria near a solid surface. *Physical Review E*, 84(4):041932, 2011.

G. Li, P. J. B. Brown, J. X. Tang, J. Xu, E. M. Quardokus, C. Fuqua, and Y. V. Brun. Surface contact stimulates the just-in-time deployment of bacterial adhesins. *Molecular Microbiology*, 83(1):41–51, 2012.

S. K. Lim, S. J. Kim, S. H. Cha, Y. K. Oh, H. J. Rhee, M. S. Kim, and J. K. Lee. Complete genome sequence of *Rhodobacter sphaeroides* kd131. *Journal of Bacteriology*, 191(3):1118–1119, 2009.

F. Lindberg, B. Lund, L. Johansson, and S. Normark. Localization of the receptor-binding protein adhesin at the tip of the bacterial pilus. *Nature*, 328(6125):84–87, 1987.

M. Linkert, C. T. Rueden, C. Allan, J. M. Burel, W. Moore, A. Patterson, B. Loranger, J. Moore, C. Neves, D. Macdonald, A. Tarkowska, C. Sticco, E. Hill, M. Rossner, K. W. Eliceiri, and J. R. Swedlow. Metadata matters: access to image data in the real world. *The Journal of Cell Biology*, 189 (5):777–782, 2010.

D. Lopez, H. Vlamakis, and R. Kolter. Biofilms. *Cold Spring Harbor Perspectives in Biology*, 2(7), 2010.

P. S. Lovely and F. W. Dahlquist. Statistical measures of bacterial motility and chemotaxis. *Journal of Theoretical Biology*, 50(2):477–496, 1975.

G. S. Lukat and J. B. Stock. Response regulation in bacterial chemotaxis. *Journal of Cellular Biochemistry*, 51(1):41–46, 1993.

C. Mackenzie, J. M. Eraso, M. Choudhary, J. H. Roh, X. Zeng, P. Bruscella, A. Puskas, and S. Kaplan. Postgenomic adventures with *Rhodobacter sphaeroides*. *Annual Review of Microbiology*, 61(1):283–307, 2007.

M. T. Madigan and J. M. Martinko. *Brock biology of microorganisms*. Pearson Prentice Hall, Upper Saddle River, NJ, 11th edition, 2006.

J. S. Madsen, M. Burmolle, L. H. Hansen, and S. J. Sorensen. The interconnection between biofilm formation and horizontal gene transfer. *FEMS Immunology and Medical Microbiology*, 65(2):183–195, 2012.

E. I. Madukasi, X. Dai, C. He, and J. Zhou. Potentials of phototrophic bacteria in treating pharmaceutical wastewater. *International Journal of Environmental Science and Technology*, 7(1):165–174, 2010.

P. C. Marijuan, J. Navarro, and R. del Moral. On prokaryotic intelligence: strategies for sensing the environment. *Bio Systems*, 99(2):94–103, 2010.

A. C. Martin, G. H. Wadhams, D. S. H. Shah, S. L. Porter, J. C. Mantotta, T. J. Craig, P. H. Verdult, H. Jones, and J. P. Armitage. CheR- and cheB-dependent chemosensory adaptation system of *Rhodobacter sphaeroides*. *Journal of Bacteriology*, 183(24):7135–7144, 2001.

A. C. Martin, M. Gould, E. Byles, M. A. Roberts, and J. P. Armitage. Two chemosensory operons of rhodobacter sphaeroides are regulated independently by sigma 28 and sigma 54. *Journal of Bacteriology*, 188(22): 7932–7940, 2006.

J. S. Mattick. Type IV pili and twitching motility. *Annual Review of Microbiology*, 56:289–314, 2002.

T. J. McGenity, B. D. Folwell, B. A. McKew, and G. O. Sanni. Marine crude-oil biodegradation: a central role for interspecies interactions. *Aquatic Biosystems*, 8(1):10–9063–8–10, 2012.

B. V. Merkey, L. A. Lardon, J. M. Seoane, J.-U. Kreft, and B. F. Smets. Growth dependence of conjugation explains limited plasmid invasion in

biofilms: an individual-based modelling study. *Environmental Microbiology*, 13(9):2435–2452, 2011.

J. H. Merritt, D. E. Kadouri, and G. A. O'Toole. Growing and analyzing static biofilms. *Current Protocols in Microbiology*, Chapter 1:Unit 1B.1, 2005.

P. M. Merritt, T. Danhorn, and C. Fuqua. Motility and chemotaxis in *Agrobacterium tumefaciens* surface attachment and biofilm formation. *Journal of Bacteriology*, 189(22):8005–8014, 2007.

H. Mikkelsen, M. Sivaneson, and A. Filloux. Key two-component regulatory systems that control biofilm formation in *Pseudomonas aeruginosa*. *Environmental Microbiology*, 13(7):1666–1681, 2011.

M. B. Miller and B. L. Bassler. Quorum sensing in bacteria. *Annual Review of Microbiology*, 55:165–199, 2001.

G. Mino, T. E. Mallouk, T. Darnige, M. Hoyos, J. Dauchet, J. Dunstan, R. Soto, Y. Wang, A. Rousselet, and E. Clement. Enhanced diffusion due to active swimmers at a solid surface. *Phys. Rev. Lett.*, 106:048102, 2011.

S. Moller, C. Sternberg, J. B. Andersen, B. B. Christensen, J. L. Ramos, M. Givskov, and S. Molin. In situ gene expression in mixed-culture biofilms: evidence of metabolic interactions between community members. *Applied and Environmental Microbiology*, 64(2):721–732, 1998.

R. D. Monds and G. A. O'Toole. The developmental model of microbial biofilms: ten years of a paradigm up for review. *Trends in Microbiology*, 17(2):73–87, 2009.

R. D. Monds, P. D. Newell, R. H. Gross, and G. A. O'Toole. Phosphate-dependent modulation of c-di-GMP levels regulates *Pseudomonas fluorescens* Pf0-1 biofilm formation by controlling secretion of the adhesin LapA. *Molecular Microbiology*, 63(3):656–679, 2007.

D. Monroe. Looking for chinks in the armor of bacterial biofilms. *PLoS Biology*, 5(11), 2007.

C. D. Nadell, J. B. Xavier, and K. R. Foster. The sociobiology of biofilms. *FEMS Microbiology Reviews*, 33(1):206–224, 2009.

P. D. Newell, C. D. Boyd, H. Sondermann, and G. A. O'Toole. A c-di-GMP effector system controls cell adhesion by inside-out signaling and surface protein cleavage. *Plos Biology*, 9(2), 2011.

H. S. O'Neil and H. Marquis. *Listeria monocytogenes* flagella are used for motility, not as adhesins, to increase host cell invasion. *Infection and Immunity*, 74(12):6675–6681, 2006.

G. O'Toole, H. B. Kaplan, and R. Kolter. Biofilm formation as microbial development. *Annual Review of Microbiology*, 54:49–79, 2000.

G. A. O'Toole and R. Kolter. Flagellar and twitching motility are necessary for *Pseudomonas aeruginosa* biofilm development. *Molecular Microbiology*, 30(2):295–304, 1998.

N. Otsu. A threshold selection method from gray-level histograms. *IEEE Transactions on Systems, Man and Cybernetics*, 9(1):62–66, 1979.

S. J. Pamp, C. Sternberg, and T. Tolker-Nielsen. Insight into the microbial multicellular lifestyle via flow-cell technology and confocal microscopy. *Cytometry*, 75A(2):90–103, 2009.

R. J. Penfold and J. M. Pemberton. An improved suicide vector for construction of chromosomal insertion mutations in bacteria. *Gene*, 118(1): 145–146, 1992.

M. G. Petrino and R. N. Doetsch. 'viscotaxis', a new behavioural response of leptospira interrogans (biflexa) strain b16. *Journal of General Microbiology*, 109(1):113–117, 1978.

O. E. Petrova and K. Sauer. A novel signaling network essential for regulating *Pseudomonas aeruginosa* biofilm development. *PLoS Pathogens*, 5(11), 2009.

O. E. Petrova and K. Sauer. The novel two-component regulatory system BfiSR regulates biofilm development by controlling the small RNA rsmZ through CafA. *Journal of Bacteriology*, 192(20):5275–5288, 2010.

O. E. Petrova and K. Sauer. SagS contributes to the motile-sessile switch and acts in concert with bfisr to enable *Pseudomonas aeruginosa* biofilm formation. *Journal of Bacteriology*, 193(23):6614–6628, 2011.

C. Picioreanu, M. C. M. van Loosdrecht, and J. J. Heijnen. Two-dimensional model of biofilm detachment caused by internal stress from liquid flow. *Biotechnology and Bioengineering*, 72(2):205–218, 2001.

C. Picioreanu, J. U. Kreft, M. Klausen, J. A. Haagensen, T. Tolker-Nielsen, and S. Molin. Microbial motility involvement in biofilm structure formation–a 3d modelling study. *Water Science and Technology*, 55(8-9): 337–343, 2007.

G. Pizarro, D. Griffeath, and D. R. Noguera. Quantitative cellular automaton model for biofilms. *Journal of Environmental Engineering*, 127(9):782–789, 2001.

S. Poggio, C. Abreu-Goodger, S. Fabela, A. Osorio, G. Dreyfus, P. Vinuesa, and L. Camarena. A complete set of flagellar genes acquired by horizontal transfer coexists with the endogenous flagellar system in *Rhodobacter sphaeroides*. *Journal of Bacteriology*, 189(8):3208–3216, 2007.

P. S. Poole, S. Brown, D. Counsell, and J. P. Armitage. The effect of phosphate on the motility of *Rhodobacter sphaeroides*. *FEMS Microbiology Letters*, 79(1):1–4, 1991.

J. R. Porter. Antony van Leeuwenhoek: Tercentenary of his discovery of bacteria. *Bacteriological Reviews*, 40(2):260–269, 1976.

S. L. Porter. *The Chemotaxis Proteins of Rhodobacter sphaeroides*. PhD thesis, University of Oxford, 2002.

S. L. Porter, A. V. Warren, A. C. Martin, and J. P. Armitage. The third chemotaxis locus of *Rhodobacter sphaeroides* is essential for chemotaxis. *Molecular Microbiology*, 46(4):1081–1094, 2002.

S. L. Porter, G. H. Wadhams, A. C. Martin, E. D. Byles, D. E. Lancaster, and J. P. Armitage. The CheYs of *Rhodobacter sphaeroides*. *The Journal of Biological Chemistry*, 281(43):32694–32704, 2006.

S. L. Porter, G. H. Wadhams, and J. P. Armitage. *In vivo* and *in vitro* analysis of the *Rhodobacter sphaeroides* chemotaxis signaling complexes. *Methods in Enzymology*, 423:392–413, 2007.

S. L. Porter, G. H. Wadhams, and J. P. Armitage. *Rhodobacter sphaeroides*: complexity in chemotactic signalling. *Trends in Microbiology*, 16(6):251–260, 2008.

S. L. Porter, D. A. Wilkinson, E. D. Byles, G. H. Wadhams, S. Taylor, N. J. Saunders, and J. P. Armitage. Genome sequence of *Rhodobacter sphaeroides* strain WS8N. *Journal of Bacteriology*, 193(15):4027–4028, 2011.

L. A. Pratt and R. Kolter. Genetic analysis of *Escherichia coli* biofilm formation: roles of flagella, motility, chemotaxis and type I pili. *Molecular Microbiology*, 30(2):285–293, 1998.

T. Proft and E. N. Baker. Pili in gram-negative and gram-positive bacteria - structure, assembly and their role in disease. *Cellular and Molecular Life Sciences*, 66(4):613–635, 2009.

B. M. Pruss, K. Verma, P. Samanta, P. Sule, S. Kumar, J. Wu, D. Christianson, S. M. Horne, S. J. Stafslien, A. J. Wolfe, and A. Denton. Environmental and genetic factors that contribute to *Escherichia coli* K-12 biofilm formation. *Archives of Microbiology*, 192(9):715–728, 2010.

S. D. Puckett, E. Taylor, T. Raimondo, and T. J. Webster. The relationship between the nanostructure of titanium surfaces and bacterial attachment. *Biomaterials*, 31(4):706–713, 2010.

E. B. Purcell, D. Siegal-Gaskins, D. C. Rawling, A. Fiebig, and S. Crosson. A photosensory two-component system regulates bacterial cell attachment. *Proceedings of the National Academy of Sciences USA*, 2007.

E. M. Purcell. Life at low Reynolds number. *American Journal of Physics*, 45(1):3–11, 1977.

A. Puskas, E. P. Greenberg, S. Kaplan, and A. L. Schaefer. A quorum-sensing system in the free-living photosynthetic bacterium *Rhodobacter sphaeroides*. *Journal of Bacteriology*, 179(23):7530–7537, 1997.

R Core Team. *R: A Language and Environment for Statistical Computing*. R Foundation for Statistical Computing, Vienna, Austria, 2013.

V. A. Ray, A. R. Morris, and K. L. Visick. A semi-quantitative approach to assess biofilm formation using wrinkled colony development. *Journal of visualized experiments : JoVE*, (64):e4035. doi(64):e4035, 2012.

N. C. Reading and V. Sperandio. Quorum sensing: the many languages of bacteria. *FEMS Microbiology Letters*, 254(1):1–11, 2006.

R. J. Redfield. Is quorum sensing a side effect of diffusion sensing? *Trends in Microbiology*, 10(8):365–370, 2002.

A. Reisner, J. A. J. Haagensen, M. A. Schembri, E. L. Zechner, and S. Molin. Development and maturation of *Escherichia coli* K-12 biofilms. *Molecular Microbiology*, 48(4):933–946, 2003.

O. Rendueles and J. M. Ghigo. Multi-species biofilms: how to avoid unfriendly neighbors. *FEMS Microbiology Reviews*, 2012.

H. H. Rijnaarts, W. Norde, E. J. Bouwer, J. Lyklema, and A. J. Zehnder. Bacterial adhesion under static and dynamic conditions. *Applied and Environmental Microbiology*, 59(10):3255–3265, 1993.

M. Roberts, E. August, A. Hamadeh, P. Maini, P. McSharry, J. Armitage, and A. Papachristodoulou. A model invalidation-based approach for eluci-

dating biological signalling pathways, applied to the chemotaxis pathway in *R. sphaeroides*. *BMC Systems Biology*, 3(1):105, 2009.

M. A. Roberts, G. H. Wadhams, K. A. Hadfield, S. Tickner, and J. P. Armitage. Para-like protein uses nonspecific chromosomal DNA binding to partition protein complexes. *Proceedings of the National Academy of Sciences USA*, 109(17):6698–6703, 2012.

D. N. Rodriguez-Navarro, M. S. Dardanelli, and J. E. Ruiz-Sainz. Attachment of bacteria to the roots of higher plants. *FEMS Microbiology Letters*, 272(2):127–136, 2007.

E. Rosenberg and Y. Ben-Haim. Microbial diseases of corals and global warming. *Environmental Microbiology*, 4(6):318–326, 2002.

G. Rosser, A. G. Fletcher, D. A. Wilkinson, J. A. de Beyer, C. A. Yates, J. P. Armitage, P. K. Maini, and R. E. Baker. Novel methods for analysing bacterial tracks reveal persistence in *Rhodobacter sphaeroides*. *PLoS Computational Biology*, 9(10):e1003276, 2013.

V. Roy, M. T. Meyer, J. A. Smith, S. Gamby, H. O. Sintim, R. Ghodssi, and W. E. Bentley. AI-2 analogs and antibiotics: a synergistic approach to reduce bacterial biofilms. *Applied Microbiology and Biotechnology*, 97(6): 2627–2638, 2013.

T. Rudrappa, K. J. Czymmek, P. W. Pare, and H. P. Bais. Root-secreted malic acid recruits beneficial soil bacteria. *Plant Physiology*, 148(3):1547–1556, 2008.

R. P. Ryan, T. Tolker-Nielsen, and J. M. Dow. When the PilZ don't work: effectors for cyclic di-GMP action in bacteria. *Trends in Microbiology*, 20 (5):235–242, 2012.

E. Ryu. A simple method of staining bacterial flagella. *Kitasato Archives of Experimental Medicine*, 14:218–219, 1937.

P. G. Santos, P. A. Santos, A. R. Bello, and A. C. Freitas-Almeida. Association of *Aeromonas caviae* polar and lateral flagella with biofilm formation. *Letters in Applied Microbiology*, 52(1):49–55, 2011.

A. Schafer, A. Tauch, W. Jager, J. Kalinowski, G. Thierbach, and A. Puhler. Small mobilizable multi-purpose cloning vectors derived from the *Escherichia coli* plasmids pk18 and pk19: selection of defined deletions in the chromosome of corynebacterium glutamicum. *Gene*, 145(1):69–73, 1994.

G. Schaller, S.-H. Shiu, and J. Armitage. Two-component systems and their co-option for eukaryotic signal transduction. *Current Biology*, 21(9):R320 – R330, 2011.

M. A. Schembri, K. Kjaergaard, and P. Klemm. Global gene expression in *Escherichia coli* biofilms. *Molecular Microbiology*, 48(1):253–267, 2003.

J. Schluter and K. R. Foster. The evolution of mutualism in gut microbiota via host epithelial selection. *PLoS Biology*, 10(11), 2012.

C. A. Schneider, W. S. Rasband, and K. W. Eliceiri. Nih image to imagej: 25 years of image analysis. *Nature Methods*, 9(7):671–675, 2012.

W. R. Schneider and R. N. Doetsch. Effect of viscosity on bacterial motility. *Journal of Bacteriology*, 117(2):696–701, 1974.

K. A. Scott, S. L. Porter, E. A. L. Bagg, R. Hamer, J. L. Hill, D. A. Wilkinson, and J. P. Armitage. Specificity of localization and phosphotransfer in the CheA proteins of *Rhodobacter sphaeroides*. *Molecular Microbiology*, 76(2): 318–330, 2010.

D. O. Serra, A. M. Richter, G. Klauck, F. Mika, and R. Hengge. Microanatomy at cellular resolution and spatial order of physiological differentiation in a bacterial biofilm. *mBio*, 4(2), 2013.

D. S. Shah, S. L. Porter, A. C. Martin, P. A. Hamblin, and J. P. Armitage. Fine tuning bacterial chemotaxis: analysis of *Rhodobacter sphaeroides* behaviour under aerobic and anaerobic conditions by mutation of the major

chemotaxis operons and *cheY* genes. *The EMBO Journal*, 19(17):4601–4613, 2000.

J. G. Shoesmith. The measurement of bacterial motility. *Journal of General Microbiology*, 22(2):528–535, 1960.

A. Shrivastava, J. J. Johnston, J. M. van Baaren, and M. J. McBride. *Flavobacterium johnsoniae* GldK, GldL, GldM, and SprA are required for secretion of the cell surface gliding motility adhesins SprB and RemA. *Journal of Bacteriology*, 195(14):3201–3212, 2013.

J. D. Shrout, D. L. Chopp, C. L. Just, M. Hentzer, M. Givskov, and M. R. Parsek. The impact of quorum sensing and swarming motility on *Pseudomonas aeruginosa* biofilm formation is nutritionally conditional. *Molecular Microbiology*, 62(5):1264–1277, 2006.

J. D. Shrout, T. Tolker-Nielsen, M. Givskov, and M. R. Parsek. The contribution of cell-cell signaling and motility to bacterial biofilm formation. *Materials Research Society Bulletin*, 36(5):367–373, 2011.

H. Shum, E. A. Gaffney, and D. J. Smith. Modelling bacterial behaviour close to a no-slip plane boundary: the influence of bacterial geometry. *Proceedings of the Royal Society A: Mathematical, Physical and Engineering Science*, 466(2118):1725–1748, 2010.

A. Siggins. Exploring mixed microbial community functioning: recent advances in metaproteomics. *FEMS Microbiology ecology*, 80(2):265–280, 2012.

R. Singh, D. Paul, and R. K. Jain. Biofilms: implications in bioremediation. *Trends in Microbiology*, 14(9):389–397, 2006.

P. Siuti, C. Green, A. N. Edwards, M. J. Doktycz, and G. Alexandre. The chemotaxis-like Che1 pathway has an indirect role in adhesive cell properties of *Azospirillum brasilense*. *FEMS Microbiology Letters*, 323(2):105–112, 2011.

J. Skerker and H. Berg. Direct observation of extension and retraction of type IV pili. *Proceedings of the National Academy of Sciences USA*, 98 (12):6901–6904, 2001.

R. E. Sockett and J. P. Armitage. Isolation, characterization, and complementation of a paralyzed flagellar mutant of *Rhodobacter sphaeroides* ws8. *Journal of Bacteriology*, 173(9):2786–2790, 1991.

H. Sondermann, N. J. Shikuma, and F. H. Yildiz. You've come a long way: c-di-GMP signaling. *Current Opinion in Microbiology*, 15(2):140–146, 2012.

V. Sourjik and J. P. Armitage. Spatial organization in bacterial chemotaxis. *The EMBO Journal*, 29(16):2724–2733, 2010.

V. Sourjik and N. S. Wingreen. Responding to chemical gradients: bacterial chemotaxis. *Current Opinion in Cell Biology*, 24(2):262–268, 2012.

Y. Sowa and R. M. Berry. Bacterial flagellar motor. *Quarterly Reviews of biophysics*, 41(2):103–132, 2008.

A. J. Spiers and P. B. Rainey. The *Pseudomonas fluorescens* SBW25 wrinkly spreader biofilm requires attachment factor, cellulose fibre and LPS interactions to maintain strength and integrity. *Microbiology*, 151(9):2829–2839, 2005.

S. Sternberg. Biomedical image processing. *Computer*, 16.

A. M. Stock, V. L. Robinson, and P. N. Goudreau. Two-component signal transduction. *Annual Review of Biochemistry*, 69(1):183–215, 2000.

J. B. Stock, A. J. Ninfa, and A. M. Stock. Protein phosphorylation and regulation of adaptive responses in bacteria. *Microbiological Reviews*, 53 (4):450–490, 1989.

J. B. Stock, A. M. Stock, and J. M. Mottonen. Signal transduction in bacteria. *Nature*, 344(6265):395–400, 1990.

N. Sudarsan, E. R. Lee, Z. Weinberg, R. H. Moy, J. N. Kim, K. H. Link, and R. R. Breaker. Riboswitches in eubacteria sense the second messenger cyclic di-GMP. *Science*, 321(5887):411–413, 2008.

H. Sun, D. R. Zusman, and W. Shi. Type IV pilus of *Myxococcus xanthus* is a motility apparatus controlled by the frz chemosensory system. *Current Biology : CB*, 10(18):1143–1146, 2000.

J. Taktikos, H. Stark, and V. Zaburdaev. How the motility pattern of bacteria affects their dispersal and chemotaxis. *PLoS One*, 8(12), 2013.

A. Tasteyre, T. Karjalainen, V. Avesani, M. Delmée, A. Collignon, P. Bourlioux, and M.-C. Barc. Phenotypic and genotypic diversity of the flagellin gene (*fliC*) among *Clostridium difficile* isolates from different serogroups. *Journal of Clinical Microbiology*, 38(9):3179–3186, 2000.

C. L. Tavano and T. J. Donohue. Development of the bacterial photosynthetic apparatus. *Current Opinion in Microbiology*, 9(6):625–631, 2006.

I. The MathWorks. Matlab, image analysis toolbox, parallel processing toolbox and statistics toolbox, 2009.

K. M. Thormann, R. M. Saville, S. Shukla, D. A. Pelletier, and A. M. Spormann. Initial phases of biofilm formation in *Shewanella oneidensis* mr-1. *Journal of Bacteriology*, 186(23):8096–8104, 2004.

C. M. Toutain, M. E. Zegans, and G. A. O'Toole. Evidence for two flagellar stators and their role in the motility of *Pseudomonas aeruginosa*. *Journal of Bacteriology*, 187(2):771–777, 2005.

C. M. Toutain, N. C. Caizza, M. E. Zegans, and G. A. O'Toole. Roles for flagellar stators in biofilm formation by *Pseudomonas aeruginosa*. *Research in Microbiology*, 158(5):471–477, 2007.

L. Turner, W. S. Ryu, and H. C. Berg. Real-time imaging of fluorescent flagellar filaments. *Journal of Bacteriology*, 182(10):2793–2801, 2000.

W. B. Valderrama and C. N. Cutter. An ecological perspective of *Listeria monocytogenes* biofilms in food processing facilities. *Critical Reviews in Food Science and Nutrition*, 53(8):801–817, 2013.

van der Woude and I. R. Henderson. Regulation and function of Ag43 (Flu). *Annual Review of Microbiology*, 62(1):153–169, 2008.

M. C. van Loosdrecht, J. J. Heijnen, H. Eberl, J. Kreft, and C. Picioreanu. Mathematical modelling of biofilm structures. *Antonie van Leeuwenhoek*, 81(1-4):245–256, 2002.

S. Vatanyoopaisarn, A. Nazli, C. E. Dodd, C. E. Rees, and W. M. Waites. Effect of flagella on initial attachment of *Listeria monocytogenes* to stainless steel. *Applied and Environmental Microbiology*, 66(2):860–863, 2000.

R. M. Vejborg and P. Klemm. Cellular chain formation in *Escherichia coli* biofilms. *Microbiology*, 155(Pt 5):1407–1417, 2009.

G. H. Wadhams and J. P. Armitage. Making sense of it all: bacterial chemotaxis. *Nature Reviews Molecular Cell Biology*, 5(12):1024–1037, 2004.

G. H. Wadhams and Y. Sowa. *Bacterial Flagella: Flagellar Motor*. eLS. John Wiley and Sons, Ltd, 2001.

P. Watnick and R. Kolter. Biofilm, city of microbes. *Journal of Bacteriology*, 182(10):2675–2679, 2000.

P. I. Watnick, C. M. Lauriano, K. E. Klose, L. Croal, and R. Kolter. The absence of a flagellum leads to altered colony morphology, biofilm development and virulence in *Vibrio cholerae* O139. *Molecular Microbiology*, 39 (2):223–235, 2001.

N. S. Webster and M. W. Taylor. Marine sponges and their microbial symbionts: love and other relationships. *Environmental Microbiology*, 14(2): 335–346, 2012.

B. L. Welch. On the comparison of several mean values: An alternative approach. *Biometrika*, 38(3-4):330–336, 1951.

C. B. Whitchurch, A. J. Leech, M. D. Young, D. Kennedy, J. L. Sargent, J. J. Bertrand, A. B. Semmler, A. S. Mellick, P. R. Martin, R. A. Alm, M. Hobbs, S. A. Beatson, B. Huang, L. Nguyen, J. C. Commolli, J. N. Engel, A. Darzins, and J. S. Mattick. Characterization of a complex chemosensory signal transduction system which controls twitching motility in *Pseudomonas aeruginosa*. *Molecular Microbiology*, 52(3):873–893, 2004.

M. Whiteley, M. G. Bangera, R. E. Bumgarner, M. R. Parsek, G. M. Teitzel, S. Lory, and E. P. Greenberg. Gene expression in *Pseudomonas aeruginosa* biofilms. *Nature*, 413(6858):860–864, 2001.

W. B. Whitman, D. C. Coleman, and W. J. Wiebe. Prokaryotes: The unseen majority. *Proceedings of the National Academy of Sciences USA*, 1998.

J. W. T. Wimpenny and R. Colasanti. A unifying hypothesis for the structure of microbial biofilms based on cellular automaton models. *FEMS Microbiology Ecology*, 22(1):1–16, 1997.

P. M. Wolanin, P. A. Thomason, and J. B. Stock. Histidine protein kinases: key signal transducers outside the animal kingdom. *Genome biology*, 3 (10), 2002.

A. J. Wolfe and H. C. Berg. Migration of bacteria in semisolid agar. *Proceedings of the National Academy of Sciences USA*, 86(18):6973–6977, 1989.

A. C. Wong. Biofilms in food processing environments. *Journal of Dairy Science*, 81(10):2765–2770, 1998.

T. Wood, C. A. Yates, D. Wilkinson, and G. Rosser. Simplified multitarget tracking using the PHD filter for microscopic video data. *IEEE Transactions on Circuits and Systems for Video Technology*, 22(5):702–713, 2012.

T. K. Wood, A. F. G. Barrios, M. Herzberg, and J. Lee. Motility influences biofilm architecture in *Escherichia coli*. *Applied Microbiology and Biotechnology*, 72(2):361–367, 2006.

K. B. Xavier and B. L. Bassler. Interference with AI-2-mediated bacterial cell-cell communication. *Nature*, 437(7059):750–753, 2005.

J. Xu, T. G. Platt, and C. Fuqua. Regulatory linkages between flagella and surfactant during swarming behavior: Lubricating the flagellar propeller? *Journal of Bacteriology*, 194(6):1283–1286, 2012.

S. Yamada and Y. Shiro. Structural basis of the signal transduction in the two-component system. *Advances in Experimental Medicine and Biology*, 631:22–39, 2008.

J. Zan, E. M. Cicirelli, N. M. Mohamed, H. Sibhatu, S. Kroll, O. Choi, C. L. Uhlson, C. L. Wysoczynski, R. C. Murphy, M. E. Churchill, R. T. Hill, and C. Fuqua. A complex luxR-luxI type quorum sensing network in a roseobacterial marine sponge symbiont activates flagellar motility and inhibits biofilm formation. *Molecular Microbiology*, 85(5):916–933, 2012.

K. Zhao, B. S. Tseng, B. Beckerman, F. Jin, M. L. Gibiansky, J. J. Harrison, E. Luijten, M. R. Parsek, and G. C. Wong. Psl trails guide exploration and microcolony formation in *Pseudomonas aeruginosa* biofilms. *Nature*, 497(7449):388–391, 2013.

E. A. Zottola and K. C. Sasahara. Microbial biofilms in the food processing industry–should they be a concern? *International Journal of Food Microbiology*, 23(2):125–148, 1994.

R. Zuo. Biofilms: strategies for metal corrosion inhibition employing microorganisms. *Applied Microbiology and Biotechnology*, 76(6):1245–1253, 2007.

D. R. Zusman, A. E. Scott, Z. Yang, and J. R. Kirby. Chemosensory pathways, motility and development in *Myxococcus xanthus*. *Nature Reviews Microbiology*, 5(11):862–872, 2007.

Chapter 11

Appendix A - Media recipes and reagents

11.0.1 LB Medium

Bacto-tryptone 10g/l
Yeast extract 5g/l
NaCl 5g/l
pH 7.0

11.0.2 M22 Minimal Medium

1M Phosphate buffer 20ml (refphos)
Concentrated Base 20ml (refbase)
Ammonium Sulphate 0.5g
Growth Factors 2ml (refgf)
NaCl 0.5g
Made up to 1l with distilled water, pH adjusted to 7.2 with KOH

11.0.3 Succinate medium

1M Phosphate buffer 20ml (refphos)
Concentrated Base 20ml (refbase)
Ammonium Sulphate 0.5g
Growth Factors 2ml (refgf)
NaCl 0.5g
Sodium Succinate 2g
Casamino acids 1g
Made up to 1l with distilled water, pH adjusted to 7.2 with KOH

11.0.4 Concentrated Base

Nitriloacetic acid (disodium salt) 5.94g
Metals 44 solution 25ml
$MgSO_4.7H_2O$ 14.5g
$CaCL_2.6H_2O$ 2.5g
$FeSO_4.7H_2O$ 50mg
Ammonium molybdate ($4H_2O$) 4.6mg
Made up to 1l with distilled water and filter sterilised, stored at 4^oC.

11.0.5 Metals 44 Solution

EDTA 2.5g $ZnSO_4.7H_2O$ 11g
$FeSO_4.7H_2O$ 5g
$MnSO_4.4H_2O$ 2g
$CuSO_4.5H_2O$ 0.39g
$CoCl_2.6H_2O$ 0.2g
H_3BO_3 (Boric acid) 0.12g
Sulphuric acid 1.5ml
Made up to 1l with distilled water and filter sterilised, stored at 4^oC.

11.0.6 Growth Factors

$NaHCO_3$ 50mg
Biotin 2mg
Niacin 100mg
Thiamine 50mg
Made up to 100ml with distilled water and filter sterilised, stored at 4^oC.

11.0.7 1M Phosphate Buffer

Buffer A 136.8g $K_2HP)_4.3H_2O$ in 600ml water
Buffer B 68g $KH_2P)_4$ in 500ml water
Mix 61.5ml Buffer A with 38.5ml BufferB, adjusted to pH 7.0, stored at 4^oC.

11.0.8 HEPES Motility Buffer

4-(2-hydroxyethyl)-1-piperazineethanesulfonic acid 2.38g in 1l distilled water, adjusted to pH 7.2 with KOH, stored at room temperature.

Chapter 12

Appendix B - Primers

Table 12.1: Primers for genomic fluorescence

Name	**Sequence (enzyme sites in red, overlaps in blue)**
Left flank forward	5'-CTAGCGAATTCAGCGCGGCCGCACCGG
Left flank reverse	5'-CAATCGGTACCCCGCCTGCGGCTCCAAC
Right flank forward	5'-CTGGCTCTAGACAAGGAGGAGAAGGCCCGC
Right flank reverse	5'-CGATGAAGCTTGACCGCACTGGCCGGCGCCTC
GFP/mCherry forward	5'-AACAATTTCACACATATGGTGAGCAAGGGC
GFP/mCherry reverse	5'-CTAGCTCTAGATTACTTGTACAGCTCGTCCATGC
Promoter forward	5'-CTAGCGGTACCTTTATCAAAAAGAGTGTTGACTTGTG
Promoter reverse	5'-GCCCTTGCTCACCATATGTGTGAAATTGTTATCCGC
Checking forward	5'-CCATCGTGGAACAGTACGAG
Checking reverse	5'-GCGAGCGACGGCGAAGCCTGAGAC

Chapter 13

Appendix C - Software

13.1 CountCells MATLAB code

```
 %
%
%  MATLAB program with user interface for examining the channels of
%  an image from the Nikon A! confocal microscope, .nd2 format, and for
%  saving files for later processing. The threshold can be changed, and
%  object centroids, counts and sizes saved. This can be done image by
%  image or for a whole set of images. The images can also be saved as
%  a movie (AVI).
%  The images are despeckled to remove noise and very small objects
%  and initially thresholded by Otsu's method (MATLAB routine).
%
%  Data files are saved to the same folder as the original image files.
%
%  Sarah Chacko 2010
%
%
function varargout = countCells(varargin)
% COUNTCELLS MATLAB code for countCells.fig
```

```
%      COUNTCELLS, by itself, creates a new COUNTCELLS or raises the existing
%      singleton*.
%
%      H = COUNTCELLS returns the handle to a new COUNTCELLS or the handle to
%      the existing singleton*.
%
%      COUNTCELLS('CALLBACK',hObject,eventData,handles,...) calls the local
%      function named CALLBACK in COUNTCELLS.M with the given input arguments.
%
%      COUNTCELLS('Property','Value',...) creates a new COUNTCELLS or raises the
%      existing singleton*.  Starting from the left, property value pairs are
%      applied to the GUI before countCells_OpeningFcn gets called.  An
%      unrecognized property name or invalid value makes property application
%      stop.  All inputs are passed to countCells_OpeningFcn via varargin.
%
%      *See GUI Options on GUIDE's Tools menu.  Choose "GUI allows only one
%      instance to run (singleton)".
%
% See also: GUIDE, GUIDATA, GUIHANDLES

% Edit the above text to modify the response to help countCells

% Last Modified by GUIDE v2.5 25-Jul-2012 15:54:31

% Begin initialization code - DO NOT EDIT
gui_Singleton = 1;
gui_State = struct('gui_Name',       mfilename, ...
                   'gui_Singleton',  gui_Singleton, ...
                   'gui_OpeningFcn', @countCells_OpeningFcn, ...
                   'gui_OutputFcn',  @countCells_OutputFcn, ...
                   'gui_LayoutFcn',  [] , ...
                   'gui_Callback',   []);
if nargin && ischar(varargin{1})
```

```
    gui_State.gui_Callback = str2func(varargin{1});
end

if nargout
    [varargout{1:nargout}] = gui_mainfcn(gui_State, varargin{:});
else
    gui_mainfcn(gui_State, varargin{:});
end
% End initialization code - DO NOT EDIT


% --- Executes just before countCells is made visible.
function countCells_OpeningFcn(hObject, eventdata, handles, varargin)
% This function has no output args, see OutputFcn.
% hObject    handle to figure
% eventdata  reserved - to be defined in a future version of MATLAB
% handles    structure with handles and user data (see GUIDATA)
% varargin   command line arguments to countCells (see VARARGIN)

% Choose default command line output for countCells
handles.output = hObject;

% Update handles structure
guidata(hObject, handles);

% UIWAIT makes countCells wait for user response (see UIRESUME)
% uiwait(handles.figure1);


% --- Outputs from this function are returned to the command line.
function varargout = countCells_OutputFcn(hObject, eventdata, handles)
% varargout  cell array for returning output args (see VARARGOUT);
% hObject    handle to figure
```

```
% eventdata  reserved - to be defined in a future version of MATLAB
% handles    structure with handles and user data (see GUIDATA)

% Get default command line output from handles structure
varargout{1} = handles.output;


%%%%%%%%%%%%%%%%%%%%%%%%%%%%%%%%%%%%%%%%%%%%%%%%%%%%%%%%%%%%%%%%%%%%%%%%%%%%
%
% Change threshold for CFP channel (channel 1)
%
%%%%%%%%%%%%%%%%%%%%%%%%%%%%%%%%%%%%%%%%%%%%%%%%%%%%%%%%%%%%%%%%%%%%%%%%%%%%
function cfpSlider_Callback(hObject, eventdata, handles)
% hObject    handle to cfpSlider (see GCBO)
% eventdata  reserved - to be defined in a future version of MATLAB
% handles    structure with handles and user data (see GUIDATA)

% Hints: get(hObject,'Value') returns position of slider
%        get(hObject,'Min') and get(hObject,'Max') to determine range of slider
cfpThreshold = get(hObject,'Value');
set(handles.cfpThreshtxt,'String',num2str(cfpThreshold));
displayCFPImage(handles);

% --- Executes during object creation, after setting all properties.
function cfpSlider_CreateFcn(hObject, eventdata, handles)
% hObject    handle to cfpSlider (see GCBO)
% eventdata  reserved - to be defined in a future version of MATLAB
% handles    empty - handles not created until after all CreateFcns called

% Hint: slider controls usually have a light gray background.
if isequal(get(hObject,'BackgroundColor'), get(0,'defaultUicontrolBackgroundColo
    set(hObject,'BackgroundColor',[.9 .9 .9]);
    set(hObject,'Min',0);
```

```
    set(hObject,'Max',1);
end




%%%%%%%%%%%%%%%%%%%%%%%%%%%%%%%%%%%%%%%%%%%%%%%%%%%%%%%%%%%%%%%%%%%%%%%%%%%%
%
% Load a set of image files (.nd2, Nikon proprietory format)
%
%%%%%%%%%%%%%%%%%%%%%%%%%%%%%%%%%%%%%%%%%%%%%%%%%%%%%%%%%%%%%%%%%%%%%%%%%%%%
% --- Executes on button press in filesBtn.
function filesBtn_Callback(hObject, eventdata, handles)
% hObject    handle to filesBtn (see GCBO)
% eventdata  reserved - to be defined in a future version of MATLAB
% handles    structure with handles and user data (see GUIDATA)

clear theFiles thePath numFiles
[theFiles thePath] = uigetfile('*.nd2*','MultiSelect','on');
if(ischar(theFiles))
    numFiles = 1;
else
    numFiles = length(theFiles);
end
set(handles.openFilestxt,'String',num2str(numFiles));
currentFile = 1;
set(handles.currentFiletxt,'String',num2str(currentFile));
setappdata(handles.openFilestxt,'allFiles',theFiles) ;
setappdata(handles.openFilestxt,'thePath',thePath) ;
setappdata(handles.openFilestxt,'currentCFPCentroids', []);
setappdata(handles.openFilestxt,'currentYFPCentroids', []);

getCurrentFile(handles);
```

```
%%%%%%%%%%%%%%%%%%%%%%%%%%%%%%%%%%%%%%%%%%%%%%%%%%%%%%%%%%%%%%%%%%%%%%%%%%%%
%
% Change threshold for YFP channel (channel 2)
%
%%%%%%%%%%%%%%%%%%%%%%%%%%%%%%%%%%%%%%%%%%%%%%%%%%%%%%%%%%%%%%%%%%%%%%%%%%%%
function yfpSlider_Callback(hObject, eventdata, handles)
% hObject    handle to yfpSlider (see GCBO)
% eventdata  reserved - to be defined in a future version of MATLAB
% handles    structure with handles and user data (see GUIDATA)

% Hints: get(hObject,'Value') returns position of slider
%        get(hObject,'Min') and get(hObject,'Max') to determine range of slider
thePath = getappdata(handles.openFilestxt,'thePath');
theFiles = getappdata(handles.openFilestxt,'allFiles');
yfpThreshold = get(hObject,'Value');
set(handles.yfpThreshtxt,'String',num2str(yfpThreshold));
displayYFPImage(handles);

% --- Executes during object creation, after setting all properties.
function yfpSlider_CreateFcn(hObject, eventdata, handles)
% hObject    handle to yfpSlider (see GCBO)
% eventdata  reserved - to be defined in a future version of MATLAB
% handles    empty - handles not created until after all CreateFcns called

% Hint: slider controls usually have a light gray background.
if isequal(get(hObject,'BackgroundColor'), get(0,'defaultUicontrolBackgroundColo
    set(hObject,'BackgroundColor',[.9 .9 .9]);

end
```

```
%%%%%%%%%%%%%%%%%%%%%%%%%%%%%%%%%%%%%%%%%%%%%%%%%%%%%%%%%%%%%%%%%%%%%%%%%%%%
%
% Get images of both channels from the current file.
% Called at the start, and after a change of file.
% Save the current image and details to variables.
%
% This uses the function bfopen and the routines from
% loci.jar, from bioformats to access ,nd2 files (Nikon)
% nd2 files can have complex structure with timeseries, zstacks etc.
% The ones here are just single plane, 2 or 3 channels. If there
% are three channels the third is DIC. (1 is CFP and 2 is YFP)
%
%%%%%%%%%%%%%%%%%%%%%%%%%%%%%%%%%%%%%%%%%%%%%%%%%%%%%%%%%%%%%%%%%%%%%%%%%%%%
function  getCurrentFile(handles)
%
% Get the image data and separate into channel 1 CFP and channel 2 YFP
%
thePath = getappdata(handles.openFilestxt,'thePath');
theFiles = getappdata(handles.openFilestxt,'allFiles');
% default to showing centroids
setappdata(handles.openFilestxt,'showCentroids',1);
%
i = eval(get(handles.currentFiletxt,'String'));
numFiles = eval(get(handles.openFilestxt,'String'));

 if(numFiles > 1)
     currentFile = theFiles{i}
        data = bfopen([thePath theFiles{i}]);
 else
        data = bfopen([thePath theFiles]);
 end
 series1 = data{1, 1};
```

```
 numChannels = size(series1, 1);

 % channel 1 is CFP
 cfpImage(:,:) = series1{1, 1};
 nextTitle = series1{1, 2};
 axes(handles.cfpAxes);
 % imshow(cfpImage(1:512,1:512), []);
 % despeckle (a lot of background especially in CFP.)
 % remove small things, salt and pepper noise
 cfpImage = immultiply(cfpImage,16);
 cfpImage = imopen(cfpImage,strel('disk',2));
% imshow(cfpImage);
 set(handles.cfpTitletxt,'String',nextTitle);
 setappdata(handles.openFilestxt,'currentCFPImage',cfpImage);



 % Initialise threshold to Otsu graythresh level
 CFPlevel = graythresh(cfpImage);
 set(handles.cfpThreshtxt,'String',num2str(CFPlevel));
 set(handles.cfpSlider,'Value',CFPlevel);

% channel 2 is YFP
 yfpImage(:,:) = series1{2, 1};
 nextTitle = series1{2, 2};
 axes(handles.yfpAxes);
 %imshow(cfpImage(1:512,1:512), []);
 % despeckle (a lot of background especially in CFP.)
 % remove small things, salt and pepper noise
  yfpImage = immultiply(yfpImage,16);
 yfpImage = imopen(yfpImage,strel('disk',2));
% imshow(yfpImage);
 set(handles.yfpTitletxt,'String',nextTitle);
```

```
 setappdata(handles.openFilestxt,'currentYFPImage',yfpImage);
 % Initialise threshold to Ostu graythresh level
 YFPlevel = graythresh(yfpImage);
 set(handles.yfpThreshtxt,'String',num2str(YFPlevel));
 set(handles.yfpSlider,'Value',YFPlevel);

 % if there is a channel 3 it is DIC (transmitted light)
     DICImage(:,:) = zeros(size(cfpImage));
     try
       DICImage(:,:) = series1{3, 1};
     catch
     end
  setappdata(handles.openFilestxt,'currentDICImage',DICImage);
  showCurrentImages(handles);


%%%%%%%%%%%%%%%%%%%%%%%%%%%%%%%%%%%%%%%%%%%%%%%%%%%%%%%%%%%%%%%%%%%%%%%%%%%%
%
% Display both images
%
%%%%%%%%%%%%%%%%%%%%%%%%%%%%%%%%%%%%%%%%%%%%%%%%%%%%%%%%%%%%%%%%%%%%%%%%%%%%

function showCurrentImages(handles)
set(handles.outputtxt,'String','Working');
displayCFPImage(handles);
displayYFPImage(handles);
pause(.01);
set(handles.outputtxt,'String','Ready');

function displayCFPImage(handles)
%%%%%%%%%%%%%%%%%%%%%%%%%%%%%%%%%%%%%%%%%%%%%%%%%%%%%%%%%%%%%%%%%%%%%%%%%%%%
%
% Show current CFP channel image with centroids of objects defined by the curren
```

```
%
%%%%%%%%%%%%%%%%%%%%%%%%%%%%%%%%%%%%%%%%%%%%%%%%%%%%%%%%%%%%%%%%%%%%%%%%%%%%%%%
cfpImage = getappdata(handles.openFilestxt,'currentCFPImage');
thePath = getappdata(handles.openFilestxt,'thePath');
theFiles = getappdata(handles.openFilestxt,'allFiles');
CFPthresh = eval(get(handles.cfpThreshtxt,'String'));
CFPMask(:,:) = im2bw(cfpImage,CFPthresh);

axes(handles.cfpAxes);
%bw = im2bw(I,level);
 %   bw = imopen(bw,strel('disk',2));
cc = bwconncomp(CFPMask);
stats = regionprops(cc,'Centroid','Area' );
allCFPCentroids = cat(1, stats.Centroid);
allCFPAreas  = cat(1, stats.Area);
setappdata(handles.openFilestxt,'currentCFPCentroids', allCFPCentroids)
setappdata(handles.openFilestxt,'currentCFPAreas', allCFPAreas)


hold off
imshow(cfpImage);
try
    if(getappdata(handles.openFilestxt,'showCentroids') == 1)
       hold on
       plot(allCFPCentroids(:,1), allCFPCentroids(:,2), 'c+')
    end
catch
end


function displayYFPImage(handles)
%%%%%%%%%%%%%%%%%%%%%%%%%%%%%%%%%%%%%%%%%%%%%%%%%%%%%%%%%%%%%%%%%%%%%%%%%%%%%%%
%
```

```
% Show current YFP channel image with centroids of objects defined by the curren
%
%%%%%%%%%%%%%%%%%%%%%%%%%%%%%%%%%%%%%%%%%%%%%%%%%%%%%%%%%%%%%%%%%%%%%%%%%%%%%%%
yfpImage = getappdata(handles.openFilestxt,'currentYFPImage');
thePath = getappdata(handles.openFilestxt,'thePath');
theFiles = getappdata(handles.openFilestxt,'allFiles');
YFPthresh = get(handles.yfpSlider,'Value');
%
% Apply threshold
%
YFPMask = im2bw(yfpImage,YFPthresh);
axes(handles.yfpAxes);
cc = bwconncomp(YFPMask);
stats = regionprops(cc,'Centroid','Area' );
allYFPCentroids = cat(1, stats.Centroid);
allYFPAreas = cat(1, stats.Area);

hold off
imshow(yfpImage);
setappdata(handles.openFilestxt,'currentYFPCentroids', allYFPCentroids)
hold on
try
    if(getappdata(handles.openFilestxt,'showCentroids')==1)
       plot(allYFPCentroids(:,1), allYFPCentroids(:,2), 'y+')
    end
catch
end


%%%%%%%%%%%%%%%%%%%%%%%%%%%%%%%%%%%%%%%%%%%%%%%%%%%%%%%%%%%%%%%%%%%%%%%%%%%%%%%
%
% Writes the open files to avi movies, each channel separately.
% This can be useful to pass them through to another analysis
```

```
% program, for example Gabriel Rosser's local thresholding
%%%%%%%%%%%%%%%%%%%%%%%%%%%%%%%%%%%%%%%%%%%%%%%%%%%%%%%%%%%%%%%%%%%%%%%%%%%%
% --- Executes on button press in movieBtn.
%%%%%%%%%%%%%%%%%%%%%%%%%%%%%%%%%%%%%%%%%%%%%%%%%%%%%%%%%%%%%%%%%%%%%%%%%%%%
function movieBtn_Callback(hObject, eventdata, handles)
% hObject    handle to movieBtn (see GCBO)
% eventdata  reserved - to be defined in a future version of MATLAB
% handles    structure with handles and user data (see GUIDATA)
thePath = getappdata(handles.openFilestxt,'thePath');
theFiles = getappdata(handles.openFilestxt,'allFiles');
set(handles.outputtxt,'String',['C:\\channel1.avi']);
% aviFile1 = avifile('C:\Users\linc2474\Documents\channel1.avi');
% aviFile2 = avifile('C:\Users\linc2474\Documents\channel2.avi');
numFiles = eval(get(handles.openFilestxt,'String'));
for j = 1:numFiles
     if(numFiles > 1)
            data = bfopen([thePath theFiles{j}]);
     else
            data = bfopen([thePath theFiles]);
     end
     set(handles.outputtxt,'String','Starting movies');
     series1 = data{1, 1};
     numChannels = size(series1, 1);

     % channel 1 is CFP
     cfpImage(:,:) = series1{1, 1};
     nextTitle = series1{1, 2};
     axes(handles.cfpAxes);
     imshow(cfpImage(:,:), []);
     set(handles.cfpTitletxt,'String',nextTitle);
     F1(j) = getframe

    % channel 2 is YFP
```

```
    yfpImage(:,:) = series1{2, 1};
    nextTitle = series1{2, 2};
    axes(handles.yfpAxes);
    imshow(yfpImage(:,:), []);
    set(handles.yfpTitletxt,'String',nextTitle);
    F2(j) = getframe



end
movie2avi(F1, 'C:\Channel1.avi', 'compression', 'None');
movie2avi(F2, 'C:\Channel2.avi', 'compression', 'None');
set(handles.outputtxt,'String','Finished movies');

%%%%%%%%%%%%%%%%%%%%%%%%%%%%%%%%%%%%%%%%%%%%%%%%%%%%%%%%%%%%%%%%%%%%%%%%%%%%
%
% Move to the next file, if there is one, and reset variables
%
%%%%%%%%%%%%%%%%%%%%%%%%%%%%%%%%%%%%%%%%%%%%%%%%%%%%%%%%%%%%%%%%%%%%%%%%%%%%
% --- Executes on button press in nextBtn.
function nextBtn_Callback(hObject, eventdata, handles)
% hObject    handle to nextBtn (see GCBO)
% eventdata  reserved - to be defined in a future version of MATLAB
% handles    structure with handles and user data (see GUIDATA)
i = eval(get(handles.currentFiletxt,'String'));
numFiles = eval(get(handles.openFilestxt,'String'));
if(i<numFiles)
    i = i + 1;

    setappdata(handles.openFilestxt,'currentCFPCentroids', []);
    setappdata(handles.openFilestxt,'currentYFPCentroids', []);
    setappdata(handles.openFilestxt,'currentCFPAreas', []);
    setappdata(handles.openFilestxt,'currentYFPAreas', []);
```

```
    set(handles.currentFiletxt,'String',i);
    getCurrentFile(handles);
end


%%%%%%%%%%%%%%%%%%%%%%%%%%%%%%%%%%%%%%%%%%%%%%%%%%%%%%%%%%%%%%%%%%%%%%%%%%%%
%
% Move to the previous file, if there is one, and reset variables
%
%%%%%%%%%%%%%%%%%%%%%%%%%%%%%%%%%%%%%%%%%%%%%%%%%%%%%%%%%%%%%%%%%%%%%%%%%%%%
% --- Executes on button press in prevBtn.
function prevBtn_Callback(hObject, eventdata, handles)
% hObject    handle to prevBtn (see GCBO)
% eventdata  reserved - to be defined in a future version of MATLAB
% handles    structure with handles and user data (see GUIDATA)
i = eval(get(handles.currentFiletxt,'String'));
numFiles = eval(get(handles.openFilestxt,'String'));
if(i>1)
    i = i - 1
    setappdata(handles.openFilestxt,'currentCFPCentroids', []);
    setappdata(handles.openFilestxt,'currentYFPCentroids', []);
    setappdata(handles.openFilestxt,'currentCFPAreas', []);
    setappdata(handles.openFilestxt,'currentYFPAreas', []);


    set(handles.currentFiletxt,'String',i);

    getCurrentFile(handles);

end
%%%%%%%%%%%%%%%%%%%%%%%%%%%%%%%%%%%%%%%%%%%%%%%%%%%%%%%%%%%%%%%%%%%%%%%%%%%%
```

```
% --- Executes on button press in exitBtn.
%     Clears variables and shuts windows and program
%%%%%%%%%%%%%%%%%%%%%%%%%%%%%%%%%%%%%%%%%%%%%%%%%%%%%%%%%%%%%%%%%%%%%%%%%%%%
function exitBtn_Callback(hObject, eventdata, handles)
% hObject    handle to exitBtn (see GCBO)
% eventdata  reserved - to be defined in a future version of MATLAB
% handles    structure with handles and user data (see GUIDATA)
clear all;
close all;
exit

%%%%%%%%%%%%%%%%%%%%%%%%%%%%%%%%%%%%%%%%%%%%%%%%%%%%%%%%%%%%%%%%%%%%%%%%%%%%
% --- Executes on button press in saveCentroidsBtn.
%     Writes files for later processing
%
%%%%%%%%%%%%%%%%%%%%%%%%%%%%%%%%%%%%%%%%%%%%%%%%%%%%%%%%%%%%%%%%%%%%%%%%%%%%
function saveCentroidsBtn_Callback(hObject, eventdata, handles)
% hObject    handle to saveCentroidsBtn (see GCBO)
% eventdata  reserved - to be defined in a future version of MATLAB
% handles    structure with handles and user data (see GUIDATA)
set(handles.outputtxt,'String','Working');
theFiles = getappdata(handles.openFilestxt,'allFiles');
thePath = getappdata(handles.openFilestxt,'thePath');
if(ischar(theFiles))
    numFiles = 1;
else
    numFiles = length(theFiles);
end
i = eval(get(handles.currentFiletxt,'String'));
set(handles.outputtxt,'String',['Working on file no ' num2str(i) ' of' num2str(n
if(numFiles > 1)
     currentFile = theFiles{i};
```

```
 else
     currentFile = theFiles;
 end
centroidsFile = [currentFile(1:length(currentFile)-4) '_centroids'];
centroidFileCSV = [centroidsFile '.csv'] ; % best format for analysis in R
allCFPCentroids = getappdata(handles.openFilestxt,'currentCFPCentroids');
allYFPCentroids = getappdata(handles.openFilestxt,'currentYFPCentroids');
allCFPAreas = getappdata(handles.openFilestxt,'currentCFPCentroids');
allYFPAreas = getappdata(handles.openFilestxt,'currentYFPCentroids');
YFPthresh = get(handles.yfpSlider,'Value');
CFPthresh = get(handles.cfpSlider,'Value');
ImageSize = size(getappdata(handles.openFilestxt,'currentYFPImage')); % CFP will
%
% write comma separated text file
%

fid = fopen([thePath centroidFileCSV], 'w');
titleString = 'Filename,Channel,xPos,yPos,area'
fprintf(fid, '%s\n', titleString);
for centroidCount = 1:size(allCFPCentroids,1);
    dataString = [currentFile ',' 'CFP' ',' num2str(allCFPCentroids(centroidCoun
    num2str(allCFPCentroids(centroidCount,2)) ',',num2str(allCFPAreas(centroidCo
fprintf(fid, '%s\n', dataString);
dataString = '';
end
for centroidCount = 1:size(allYFPCentroids,1);
        dataString = [currentFile ',' 'YFP' ',' num2str(allYFPCentroids(centroid
        num2str(allYFPCentroids(centroidCount,2)) ',' num2str(allYFPAreas(centro

fprintf(fid, '%s\n', dataString);
dataString = '';
end
fclose(fid);
```

```
%
% Save MATLAB data file, including threshold settings
%
save([thePath centroidsFile],'allCFPCentroids','allYFPCentroids','YFPthresh','CF
set(handles.outputtxt,'String',['Saved file ' thePath centroidsFile]);
%%%%%%%%%%%%%%%%%%%%%%%%%%%%%%%%%%%%%%%%%%%%%%%%%%%%%%%%%%%%%%%%%%%%%%%%%%%%
% --- Executes on button press in showCentroidsBtn.
%     Toggles the display of centroids.
%%%%%%%%%%%%%%%%%%%%%%%%%%%%%%%%%%%%%%%%%%%%%%%%%%%%%%%%%%%%%%%%%%%%%%%%%%%%
function showCentroidsBtn_Callback(hObject, eventdata, handles)
% hObject    handle to showCentroidsBtn (see GCBO)
% eventdata  reserved - to be defined in a future version of MATLAB
% handles    structure with handles and user data (see GUIDATA)
showCentroids = getappdata(handles.openFilestxt,'showCentroids');
if(showCentroids == 1)
    setappdata(handles.openFilestxt,'showCentroids',0);
else
    setappdata(handles.openFilestxt,'showCentroids',1);
end
showCurrentImages(handles);

%%%%%%%%%%%%%%%%%%%%%%%%%%%%%%%%%%%%%%%%%%%%%%%%%%%%%%%%%%%%%%%%%%%%%%%%%%%%
% --- Executes on button press in overlayBtn.
%     Displays all centroids, with blue or yellow crosses, overlaid on the
%     transmitted light image if one exists, otherwise together on a black
%     background. This allows checking that cells are not picked up in both
%     channels, or (if there is a transmitted light image) not in either channel
%%%%%%%%%%%%%%%%%%%%%%%%%%%%%%%%%%%%%%%%%%%%%%%%%%%%%%%%%%%%%%%%%%%%%%%%%%%%
function overlayBtn_Callback(hObject, eventdata, handles)
% hObject    handle to overlayBtn (see GCBO)
% eventdata  reserved - to be defined in a future version of MATLAB
% handles    structure with handles and user data (see GUIDATA)
dicImage = getappdata(handles.openFilestxt,'currentDICImage');
```

```
figure
imshow(dicImage,[]);
figure
imshow(dicImage,[]);
hold on
CFP = getappdata(handles.openFilestxt,'currentCFPCentroids');
YFP = getappdata(handles.openFilestxt,'currentYFPCentroids');
plot(CFP(:,1), CFP(:,2), 'c+')
plot(YFP(:,1), YFP(:,2), 'y+')
```

13.2 3D cylinder PDE code

The Matlab PDE toolkit deals with equations with two spatial dimensions. It can be used for this three dimensional problem because it is symmetrical and can be reduced to two dimensions by using cylindical co-ordinates. It allows the geometry to be specified and a mesh generated and refined. There are methods for setting boundary conditions and for specifying and solving PDEs on the chosen geometry. The PDE solver expects an equation expressed in the specific form:

$$du' - \nabla.(c\nabla(u) + au = f \tag{13.1}$$

where d, c, a and f can be functions of u and u'.

To express equation 5.26 in this format, with time variable t and space variables R and Z, we need to choose the multiplying functions. Calling the concentration u as above,

$$\nabla.(c\nabla(u) = \frac{\partial c}{\partial R}\frac{\partial u}{\partial R} + c\frac{\partial^2 u}{\partial R^2} + \frac{\partial c}{\partial Z}\frac{\partial u}{\partial Z} + c\frac{\partial^2 u}{\partial Z^2} \tag{13.2}$$

comparing this to equation 5.26, multiply through by R to get

$$R\frac{\partial u}{\partial T} = R\frac{\partial^2 u}{\partial R^2} + \frac{\partial u}{\partial R} + R\frac{\partial^2 u}{\partial Z^2} \tag{13.3}$$

which gives the correct format with $d = R$, $c = R$, $a = 0$ and $f = 0$.